Contrôle de la stabilité du message génétique au cours de l'infection et de l'oncogenèse : fonctions et régulation du nonsense mediated mRNA decay

Vincent Mocquet

Mémoire d'habilitation à diriger des recherches

Contrôle de la stabilité du message génétique au cours de l'infection et de l'oncogenèse : fonctions et régulation du nonsense mediated mRNA decay.

Vincent Mocquet

CRCN Inserm

Laboratoire de Biologie et de Modélisation de la Cellule

UMR5239 U1293 / ENS de Lyon/ Université de Lyon

Jury

Dr Claudine Pique (pré-rapporteur)

Dr Fabrice Lejeune (pré-rapporteur)

Dr Emiliano Ricci (pré-rapporteur)

Dr Chloé Journo

Pr Patrice Gouet

Pr Bertrand Mollereau

Table des matières

CV

- MOCQUET, Vincent 20/06/1981
- Laboratoire de Biologie et Modélisation de la Cellule (LBMC) / ENS LYON
  46 allée d'Italie
  69364 LYON Cedex 07

SITUATION ACTUELLE

- Chercheur CRCN, INSERM
- Dirige l'équipe « Post-transcriptional Regulation in Infection and Oncogenesis » (PRIO), LBMC, U1293, UMR5239, ENS de Lyon, Université de Lyon.

CURSUS

- Diplômes

2004-2007 **Doctorat**. *Aspect moléculaires et cellulaires de la biologie*
Université Louis Pasteur, Strasbourg, France.
Institut de Génétique et de Biologie Moléculaire et Cellulaire (IGBMC). Dr J.M. Egly

2003 **Master**. *Procédés Biotechnologiques et Alimentaires.* (Mention Bien) INPL

2000-2003 **Ingénieur agronome** (ENSAIA), INPL, Nancy, France.

- Formations professionnelles complémentaires

2022 **Formation à l'utilisation de GitHub** *(pôle bioinformatique, LBMC)*
2021 **Formation à l'utilisation de R** *(pôle de bioinformatique, LBMC)*
2017 **Expérimentation animale de niveau 1** *(Université Claude Bernard, Lyon I)*
2013 **Analyse des données RNA-SEQ et CHIP-SEQ**, *(PRABI, Lyon)*

- Expériences professionnelles académiques

Depuis 2021 *Dirige l'équipe PRIO, LBMC, ENS de Lyon, U1293, UMR5239.* http://www.ens-lyon.fr/LBMC/equipes/controle-de-l2019expression-genetique-et-oncogenese-virale

Depuis 2013 *Chercheur INSERM équipe CEGOV*
-Regulation du NMD dans des contextes d'infection et d'oncogenèse

2008-2013 *Post-doctorat- équipe CEGOV, LBMC, ENS Lyon, UMR5239. Dr Pierre Jalinot*
-Etude de la dégradation des ARNm viraux (HTLV) et de l'hôte par la voie NMD

-Etude du rôle d'INT6 dans la traduction des ARN histones

-Etude de l'impact d'INT6 dans la régulation des ARN télomériques TERRA et la stabilité des télomères

2003-2007 *Doctorat- U964, UMR7104, IGBMC, Dr Jean-Marc Egly*
-Description moléculaire du mécanisme de réparation de l'ADN par la voie NER

2003 *Master- U964, UMR7104, IGBMC, Dr Jean-Marc Egly*
-Etude du rôle d'XPE dans la réparation de l'ADN par la voie NER.

2002 *Stage d'ingénieur (2 mois)-* Université de Leeds, UK ; *Pr. Hanma. Zhang*
-Identification de marqueurs d'une mutation inhibant la croissance racinaire chez Arabidopsis T.

PUBLICATIONS

ORCID 0000-0002-2089-6727

1-*The fluorescent protein stability assay: an efficient method for monitoring intracellular protein stability.*

Roisin A, Buchsbaum S, Mocquet V, Jalinot P.

***BIOTECHNIQUES** Volume:70 Issue 6 Pages : 336-344 Published MAI 25 2021*

2-*The Complex Relationship between HTLV-1 and Nonsense-Mediated mRNA Decay (NMD).*

Prochasson, L. ; Jalinot P. et Mocquet Vincent.

PATHOGENS Volume: 9 Article Number: E287 Published: AVR 15 2020

3-*HTLV-1 Tax plugs and freezes UPF1 helicase leading to nonsense-mediated mRNA decay inhibition*

Fiorini, F.; Robin, J.P.; Kanaan, J.; LeHir, H.; Croquette V.; Jalinot P. et Mocquet Vincent.

NATURE COMMUNICATIONS Volume: 9 Article Number: 431 Published: JAN 30 2018

4-The proto-oncogenic protein TAL1 controls TGF-β1 signaling through interaction with SMAD3.

Terme JM, Lemaire S, Auboeuf D, Mocquet V, Jalinot P.

BIOCHIM OPEN 2016 May 14;2:69-78. doi: 10.1016/j.biopen.2016.05.001. eCollection 2016 Jun.

5-How Retroviruses Escape the Nonsense-Mediated mRNA Decay

Mocquet Vincent; Durand, S.; Jalinot, P.

AIDS RESEARCH AND HUMAN RETROVIRUSES Volume: 31 Issue: 10 Pages: 948-958 Published: OCT 1 2015

6-The Human T-Lymphotropic Virus Type 1 Tax Protein Inhibits Nonsense-Mediated mRNA Decay by Interacting with INT6/EIF3E and UPF1

Mocquet Vincent; Neusiedler, J.; Rende, F.; et al.

JOURNAL OF VIROLOGY Volume: 86 Issue: 14 Pages: 7530-7543 Published: JUL 2012

7-INT6 interacts with MIF4GD/SLIP1 and is necessary for efficient histone mRNA translation

Neusiedler, J*.; Mocquet Vincent*; Limousin, T.; et al.

RNA Volume: 18 Issue: 6 Pages: 1163-1177 Published: JUN 2012

8 -Inhibition of the hTERT promoter by the proto-oncogenic protein TAL1

Terme, J-M; Mocquet, V.; Kuhlmann, A-S; et al.

LEUKEMIA Volume: 23 Issue: 11 Pages: 2081-2089 Published: NOV 2009

9-Nucleotide excision repair driven by the dissociation of CAK from TFIIH

Coin, F.; Oksenych, V.; Mocquet Vincent; et al.

MOLECULAR CELL Volume: 31 Issue: 1 Pages: 9-20 Published: JUL 11 2008

10-Sequential recruitment of the repair factors during NER: the role of XPG in initiating the resynthesis step

Mocquet Vincent; Laine, J. P.; Riedl, T.; et al.

EMBO JOURNAL Volume: 27 Issue: 1 Pages: 155-167 Published: JAN 9 2008

11-The human DNA repair factor XPC-HR23B distinguishes stereoisomeric benzo[a]pyrenyl-DNA lesions

Mocquet Vincent; Kropachev, K.; Kolbanovskiy, M.; et al.

EMBO JOURNAL Volume: 26 Issue: 12 Pages: 2923-2932 Published: JUN 20 2007

12-[A cigarette, an aromatic...and a cancer].

Mocquet V, Egly JM, Geacintov N.

Med Sci (Paris). 2008 Mar;24(3):233-4. doi: 10.1051/medsci/2008243233.

13-Common XPD (ERCC2) polymorphisms have no measurable effect on nucleotide excision repair and basal transcription.

Lainé JP, Mocquet V, Bonfanti M, Braun C, Egly JM, Brousset P.

DNA Repair (Amst). 2007 Sep 1;6(9):1264-70. doi: 10.1016/j.dnarep.2007.02.010. Epub 2007 Apr 2.

14-DNA repair and transcriptional deficiencies caused by mutations in the Drosophila p52 subunit of TFIIH generate developmental defects and chromosome fragility.

Fregoso M, Lainé JP, Aguilar-Fuentes J, Mocquet V, Reynaud E, Coin F, Egly JM, Zurita M.

Mol Cell Biol. 2007 May;27(10):3640-50. doi: 10.1128/MCB.00030-07. Epub 2007 Mar 5.

15-TFIIH enzymatic activities in transcription and nucleotide excision repair.

Lainé JP, Mocquet V, Egly JM.

Methods Enzymol. 2006;408:246-63. doi: 10.1016/S0076-6879(06)08015-3.

FINANCEMENTS

-2022-2023 FINOVI (***Study on the mechanism of SARS-CoV-2 Nucleocapsid and cellular Nonsense-mediated mRNA Decay interplay) AO15****;*18k€; collaboration

- 2018-2022 ANRS (***Dérégulation du NMD lors de l'infection par HIV et impact cellulaire***); **ECTZ75066;** 80 k€; PI & coordinateur: V. Mocquet

- 2018-2022 ARC (***Impact des dérégulations postranscriptionnelles et traductionnelles associées à l'inhibition du NMD dans les processus oncogéniques*****); PJA 20181207764;** 50 k€; PI & coordinateur: V. Mocquet

- 2015-2017 Ligue contre le cancer (***Inhibition du Nonsense Mediated mRNA Decay (NMD), son impact sur la tumorigenèse in vivo***); **R15MOCQUET;** 40 k€; PI & coordinateur: V. Mocquet

- 2014-2016 ARC (***Implication de la voie "Nonsense-Mediated mRNA Decay'' (NMD) dans l'instabilité génétique induite par le retrovirus HLTV-1*****); PJA 20131200186 ;** 25 k€; PI & coordinateur: V. Mocquet

ENCADREMENT

- Stagiaires M1-M2 *A. Duissembekova 2015, A. Queffelou 2016 P.Tripathi 2017, M.Mouehli 2017, K.Corbin 2018, C.Folliet 2019, I.Chaabani 2020, G.Lamiral 2021, M.MGhezzi* Habella *2022…*

- Doctorants *M.Beynelles 2012-2015, L.Prochasson 2019*-2022, M. Mghezzi Habella 2022-…

- Evaluation *: -membre de Comité de suivi de thèse (LBMC, CIRI, IGBMC)*
*-jurys de M2 et de thèse (exa**m**inateur)*

INFORMATIONS COMPLEMENTAIRES

***-**Responsable des pièces de culture cellulaire (organisation, entretien et équipement). Mise en place d'un système de culture en conditions contrôlées en O2 (choix du système, micro implantation et responsable utilisateurs)*

- depuis 2010 élu au conseil de laboratoire (représentant post-doctorat puis chargé de recherche)

- 2014-2019 conseil scientifique du PSF (Protein Science Facility), SFR biosciences, Lyon Gerland

-Depuis 2019 membre de l'éditorial Board de la revue Biology (MDPI)

-Reviewing *pour RNA, Science Reports, Cancers, Biology, Genes, Journal of Cancer, Biomolecules, Frontiers*, IJMS

-Network *: SFBBM (Societe Française de Biochimie et de Biologie Moléculaire),*
IRVA (International RetroVirology Association),
SFV (Société Francophone de Virologie)

PARCOURS SYNTHETIQUE

Mon parcours scientifique s'organise autour de l'étude des systèmes de contrôle de l'intégrité du message génétique et de l'analyse des impacts associés à leur dérégulation.

Le message génétique s'exprime dans les cellules sous différents états : l'ADN, l'ARN et la protéine. Alors que la multiplication de ces supports assure une grande finesse dans la modulation de l'expression, cela augmente également le risque de diminuer la fidélité de l'information exprimée. L'intégrité du message génétique est effectivement constamment mise à mal par l'influence directe d'agents exogènes et par des erreurs ponctuelles des systèmes cellulaires. Contrôler l'intégrité d'un message génétique est alors indispensable au maintien de l'homéostasie cellulaire et à plus grande échelle au fonctionnement adéquat d'un tissu et d'un organisme. Des évènements de contrôle qualité opèrent ainsi régulièrement sur chaque support de l'expression du message génétique. Dans les cas où une erreur serait détectée, ces processus sont couplés à des phénomènes de restauration de l'information d'origine ou de dégradation du support défectueux.

-Au niveau de l'ADN, les dommages sont perçus grâce aux checkpoints du dommage et réparés par les 4 grandes voies de réparation de l'ADN. L'une d'entre elles est la réparation par excision de nucléotides (NER) sur laquelle j'ai travaillé durant mon DEA et ma thèse dans l'équipe de JM. EGLY à l'IGBMC. Mes différents travaux ont ainsi permis d'apporter un éclairage nouveau sur certaines étapes critiques de cette voie de réparation. J'ai notamment travaillé sur la reconnaissance initiale du dommage, la coordination entre la reconnaissance du dommage et la double incision de part et d'autre du dommage ainsi que sur la transition vers l'étape finale de resynthèse d'un nouveau brin d'ADN après l'excision de l'ADN endommagé.

-Au niveau de l'ARN ce contrôle s'opère en partie via les voies de contrôle qualité de l'ARN dont la voie de dégradation des ARN nonsense (NMD) est le mécanisme le plus étudié. C'est autour de ce mécanisme co-traductionnel que s'est concentré mon post-doc dans l'équipe de P. JALINOT au LBMC. Mon projet initial visait à démontrer que la protéine Tax du rétrovirus HTLV-1 est capable d'inhiber le NMD. Avec ces résultats nous avons établi la preuve de concept que le NMD constitue une menace pour les ARN viraux et qu'il peut contrôler leur niveau d'expression. Pour la première fois, nous suggérions que le NMD peut avoir une fonction antivirale dans les cellules humaines. Ayant obtenu un poste de chargé de Recherche à l'INSERM dans l'équipe de P. JALINOT pour approfondir ces questions, nous avons ensuite caractérisé comment Tax est capable d'inhiber le fonctionnement de l'ARN/ADN hélicase UPF1 à 2 étapes différentes du NMD. L'idée que le NMD constitue une menace critique pour la réplication virale est renforcée par l'existence d'une seconde protéine virale impactant le NMD, le transporteur d'ARN viral non/partiellement épissé Rex. Identifiée par une équipe concurrente, nous avons entrepris d'en expliquer le mécanisme d'action par

une approche comparative avec l'autre rétrovirus pathogène humain, HIV, qui code un homologue fonctionnel : Rev. Ce travail, en cours, est porté par une étudiante dont j'encadre la thèse. Désormais co-directeur de l'équipe PRIO avec P. JALINOT, nos projets consistent à comprendre l'impact de l'inhibition du NMD par les facteurs viraux sur l'expression de transcrits productifs ou non et d'en évaluer la part dans les pathologies associées à l'infection par HTLV. Nous nous employons également à comprendre si la fonction antivirale du NMD s'applique à d'autres virus tels que le SARS-Cov2. Finalement, sur la base de nos observations avec Rex et Rev, nous recherchons comment la modulation de l'export nucléaire CRM1 dépendent peut réguler le NMD et si ces observations peuvent se retrouver hors contexte viral. Un nouvel étudiant vient de commencer sa thèse sur ce projet.

Contrôle de la stabilité de l'ADN par la voie NER. Description d'un mécanisme moléculaire. *Doctorat (2003-2007)*

INTRODUCTION

Sur les $3x10^9$ bases du génome, on estime qu'entre 25000 et 50000 bases sont endommagées par cellule et par jour [1]. Notre organisme est effectivement exposé à de multiples agents génotoxiques exogènes ainsi que des facteurs endogènes qui induisent une grande diversité de dommages. Il existe une forte spécificité entre l'agent génotoxique et la lésion induite. Une des principales réponses biologiques à l'émergence de ces dommages est alors l'activation de mécanismes de réparation de l'ADN. Il en existe 4 principaux : la réparation des cassures double brin (DSB), la réparation des mésappariements (MMR), la réparation par excision de bases (BER) et la réparation par excision de nucléotides (NER) [2].

La NER est le mécanisme de réparation le plus polyvalent : il s'attache à l'élimination des lésions générées par différents agents tels que les UV (cyclobutane pyrimidine dimers CPD, pyrimidines 6-4 pyrimidones 6-4PP), les composés aromatiques polycycliques (benzo[a]pyrènes (B[a]P)) ou même des agents pontant utilisés en chimiothérapie (cisplatine) . Certaines lésions de type oxydatif ont aussi été identifiées comme substrats de la NER (cyclodA, cyclodG). Ces processus font intervenir plus de 30 protéines [3]. Des mutations dans certains des facteurs impliqués provoquent un défaut de réparation et sont responsables de maladies génétiques rares : le Xeroderma Pigmentosum (XP), le syndrome de Cockayne (CS) ou la Trichothiodystrophie (TTD)[4]. Ces trois maladies sont génétiquement hétérogènes et il est remarquable que des mutations différentes dans les mêmes gènes soient associées à des phénotypes très différents [4,5].

Les patients XP sont caractérisés par leur peau parcheminée (xeroderma) et une pigmentation anormale (pigmentosum) au niveau des zones exposées au soleil. Leur risque de développer des cancers de la peau est augmenté de 1000 fois. Le Syndrome de Cockayne (CS) est une maladie génétique rare associée à des retards de croissance et mentaux. Bien que CS se caractérise aussi par une sensibilité aux UV ainsi qu'à de nombreux autres agents génotoxiques, les patients CS, contrairement aux XP, ne sont pas prédisposés à développer des cancers de la peau. La Trichothiodystrophie (TTD) se caractérise principalement par des phanères cassants dues à un défaut dans la synthèse des protéines soufrées. Des retards de croissance et mentaux sévères sont très semblables à ceux des patients CS. Les patients TTD, bien que photosensibles avec des défauts de NER ne développent pas de cancer de la peau comme les XP.
Il est globalement établi que ce que l'on appelle la NER comprend en fait 2 voies :

- La réparation couplée à la transcription (TCR) : c'est le blocage de l'ARN Pol II par la modification structurale induite par le dommage qui initie la réparation. Les dommages présents sur le brin codant des gènes activement transcrits, sont plus rapidement réparés. Les syndromes CS et TTD sont spécifiques de défauts de la TCR c'est pourquoi il est souvent considéré qu'il s'agit de syndromes de type transcriptionnels [6].

- La « Global Genome NER » (GG-NER). Contrairement à la TCR, la GG-NER s'applique à l'ensemble du génome. La reconnaissance des dommages s'effectue par des complexes protéiques spécifiques (UV-DDB et XPC-HR23B) qui scannent l'ADN. Les autres protéines de réparation impliquées sont communes aux 2 voies : XPA, TFIIH, RPA, XPF, XPG ainsi que les facteurs dits de resynthèse (PCNA, RF-C, les ADN polymérase (δ, ε, η essentiellement) et les systèmes de ligation (Ligase 1 et FEN1 et/ou XRCC1 et Ligase3)). Les symptômes de type XP sont dus à des défauts de la GG-NER. La GG-NER est généralement décrite en trois étapes : la reconnaissance du dommage [7,8], la double incision permettant l'excision d'un fragment d'ADN contenant la lésion [9] et la resynthèse/ligation qui assure le remplacement du fragment d'ADN endommagé par un brin néo-synthétisé [10,11].

Au cours de ma thèse, afin de mieux comprendre le fonctionnement de la NER et les conséquences de ses défauts, j'ai étudié la nature et le rôle des sous-complexes protéiques impliqués dans ces différentes étapes. A l'aide d'un système de réparation reconstitué in vitro j'en ai notamment décrit l'enchainement et la coordination.

RESULTATS

1) De la reconnaissance du dommage à l'initiation de la NER.

La diversité de substrats de la NER a longtemps compliqué la compréhension des mécanismes de discrimination du dommage et les caractéristiques de l'initiation de la GG NER par XPC. J'ai donc travaillé sur un dérivé de benzo[a]pyrène qui se lie covalemment avec les guanines de l'ADN et génère un adduit déformant de l'ADN sous trois formes stéréoisomèriques différentes : (+)-trans-BPDE-dG, (-)-trans-BPDE-dG et (+)-cis-BPDE-dG [12]. Ce travail a été effectué en collaboration avec le Dr N.Geacintov du laboratoire de physico-chimie de l'Université de New York .

Malgré la composition chimique identique de ces 3 ADN endommagés, les conformations de la double hélice générées par chaque stéréoisomère sont relativement différentes. Cette approche permet de déterminer le rôle exact de la distorsion de l'ADN dans l'initiation de la NER et la reconnaissance par XPC/hR23B.

En utilisant des protéines recombinantes et des extraits cellulaires dans des tests de réparation in vitro, j'ai démontré que chacun des 3 types de dommage est réparé par la voie NER. En quantifiant les niveau d'XPC se fixant sur un ADN immobilisé, j'ai pu préciser que l'efficacité de réparation est directement corrélée à

l'efficacité de recrutement d'XPC/hR23B au dommage. Des empreintes au KMNO4- ont cependant montré que le recrutement d'XPC/hR23B au dommage est lui-même dépendant de la distorsion initiale générée par le stéréoisomère. Ainsi le (+)-trans-BPDE (majoritairement présent dans la fumée de cigarette) qui se loge dans le sillon de la double hélice et n'affecte que faiblement l'appariement des bases et la distorsion de l'ADN, est difficilement reconnu par XPC/HR23B ce qui peut expliquer son très fort pouvoir cancérigène : l'ADN subit une déstabilisation suffisante pour générer des mutations réplicationnelles mais insuffisante pour que la lésion soit efficacement reconnue par la machinerie de réparation.

(**The human DNA repair factor XPC-HR23B distinguishes stereoisomeric benzo[a]pyrenyl-DNA lesions; Mocquet** et al, Vol: 26 Issue: 12 Pages: 2923-2932)

2) TFIIH au cours de la double incision.

Après l'ancrage d'XPC sur le dommage, le complexe multiprotéique TFIIH (10 sous-unités) est recruté [13]. TFIIH est un complexe impliqué à la fois dans la transcription et la réparation. Ce complexe est composé d'un « core » (6 sous unités dont l'hélicase XPB), d'un « CAK » (complex activating kinase, 3 sous unités) et de l'hélicase XPD [14]. Contrairement aux hélicases, le CAK n'est pas indispensable pour l'activité de réparation [15]. Grâce l'activité ATPase d'XPB et l'activité hélicase d'XPD, TFIIH ouvre l'ADN de part et d'autre du dommage, afin de permettre son excision. Le blocage de l'adduit au cœur d'XPB au cours de la déshybridation du brin endommagé constituerait la dernière vérification de présence d'un dommage. Les protéines XPA et XPG qui stimulent les activités enzymatiques de TFIIH sont également présentes à ce moment [16,17]. Pour mieux comprendre la régulation de l'activité de TFIIH pendant la NER, nous avons suivi sa composition au cours de la réparation.

En utilisant une approche d'imunoprécipitation d'XPB sur des extraits cellulaires crosslinkés au formaldéhyde suivis d'une révélation par western blot, nous avons montré qu'après irradiation, le CAK se dissociait de la fraction de TFIIH associée à la chromatine. En reproduisant cette situation de réparation in vitro, en utilisant un ADN endommagé et immobilisé par des billes magnétiques et différentes combinaisons d'extraits cellulaires ou de facteurs recombinants purifiés, j'ai identifié que la dissociation du CAK de TFIIH est nécessaire et dépendante du recrutement du facteur XPA. Ce travail démontre donc l'importance d'une modulation de la composition de TFIIH au cours de la réparation.

(**Nucleotide excision repair driven by the dissociation of CAK from TFIIH** Coin, F.; Oksenych, V.;**Mocquet V**; et al. **MOLECULAR CELL 2008** Volume: 31 Issue: 1 Pages: 9-20)

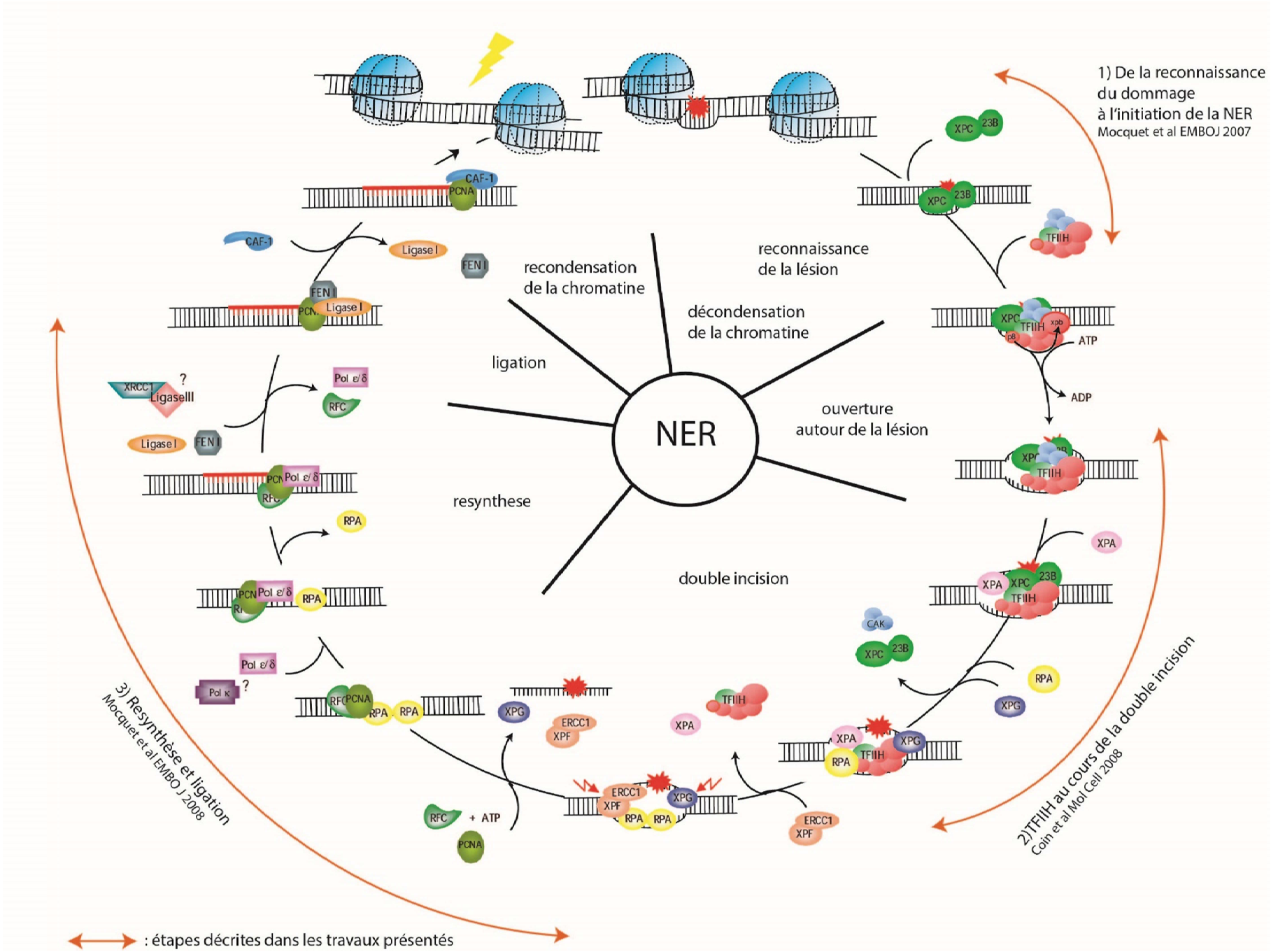
1) De la reconnaissance
du dommage
à l'initiation de la NER
Mocquet et al EMBOJ 2007
NER
reconnaissance
de la lésion
décondensation
de la chromatine
ouverture
autour de la lésion
double incision
resynthese
ligation
recondensation
de la chromatine
2)TFIIH au cours de la double incision
Coin et al Mol Cell 2008
3) Resynthèse et ligation
Mocquet et al EMBO J 2008
: étapes décrites dans les travaux présentés
XPC
23B
TFIIH
ATP
ADP
XPA
XPG
ERCC1
XPF
RPA
CAK
CAF-1
PCNA
FEN I
Ligase I
XRCC1
LigaseIII
Pol ε/δ
RFC
Pol κ
+ ATP

3) Resynthèse et ligation.

Après la déshybridation locale de l'ADN, les endonucléases XPG et ERCC1-XPF assurent l'incision d'un fragment d'environ 25 nucléotides contenant la lésion. Ce fragment est finalement remplacé au cours d'un épisode de synthèse d'ADN puis ligué à l'ADN préexistant. Les facteurs minimums impliqués dans ces étapes finales sont connus depuis longtemps : il s'agit des facteurs réplicatifs RF-C et PCNA, stimulant l'ADN polymérase delta. La ligation est ensuite assurée par les couples FEN-1/ligaseI ou XRCC1/ligaseIII [18,19]. Depuis 2010, d'autres combinaisons de facteurs réplicatifs ont été identifiées (DNA Polε/PCNA/modified RFC et pol k/ubiquitinated PCNA/XRCC1) ; leur implication dépendrait du cycle cellulaire [20]. Peu de données sont disponibles sur la coordination des étapes de double incision et de resynthèse. Pourtant ces deux étapes sont nécessairement finement coordonnées afin de réguler au mieux leur enchainement et d'éviter l'accumulation d'intermédiaires de réparation plus sensibles aux cassures d'ADN.

Afin de comprendre les évènements ayant lieu au cours de cette transition, un ADN mono-lésé et immobilisé a été incubé avec les 11 facteurs recombinants de la NER. J'ai observé le recrutement séquentiel de ces facteurs par western blot. L'analyse de ces cinétiques a permis de disséquer la chronologie des évènements et le rôle joué par chaque facteur au sein du complexe de réparation. J'ai ainsi démontré que les facteurs XPG et RPA permettent la coordination entre les étapes de double incision et de resynthèse en stabilisant le recrutement de PCNA et RFC respectivement. J'ai donc pu mettre en exergue un rôle nouveau pour XPG dans un processus réplicatif. Finalement, cette étude a permis de préciser la cinétique de la ligation et de suggérer la spécificité du couple ligase I/FEN-1 avec la polymérase delta plutôt que la ligase III/XRCC1.

(**Sequential recruitment of the repair factors during NER: the role of XPG in initiating the resynthesis step, Mocquet et al EMBO JOURNAL 2008** Vol: 27 Issue: 1 Pages: 155-167)

Figure 1 : Schéma bilan récapitulant le mécanisme global de la NER à la fin de ma thèse. Les étapes caractérisées par les travaux présentés sont indiquées avec la flèche.

Contrôle de la stabilité de l'ARN par la voie NMD dans un contexte d'infection virale. *Postdoctorat (2008-2013) / Chargé de Recherche INSERM (depuis 2013)*

CONTEXTE

Comme pour l'ADN, la qualité de l'ARN est étroitement contrôlée. Ces mécanismes de surveillance/dégradation sont en continuelle compétition avec les procédés cellulaires assurant normalement les différentes étapes de la vie de l'ARN : transcription, capping, épissage, export nucléaire, traduction, etc…[21] Ces mécanismes ciblent l'ARN dont l'accumulation reflète l'absence d'une ou plusieurs protéines chaperonne (RBP pour RNA Binding Protein) ou la formation d'un complexe ribonucleoprotéique (RNP) incorrect. Par exemple, quand l'extrémité 5' de l'ARN nascent n'est pas protégée par le complexe CBP (Cap Binding Complex), l'enzyme DXO initie le decapping de l'ARN et sa dégradation par l'exonucléase 5'-3' XRN2 [22]. Le dépôt de l'Exon Junction Complex (EJC) est également un checkpoint important qui valide l'épissage. L'EJC est impliqué, plus tard, dans les étapes d'export et de traduction et notamment dans la dégradation de l'ARN si ces étapes sont défectueuses [23,24].

Dans le cytoplasme, la qualité des ARN traduits est contrôlée par 3 mécanismes principaux :

- Le NoGo Decay (NGD) cible les ARN dont l'élongation de la traduction est bloquée par ses propres structures secondaires ou des structures secondaires du peptide nascent. Une quantité suboptimale de tRNA peut aussi être à l'origine de son initiation [25].
- Le NonStop Decay (NSD) cible les ARN sans codon STOP provenant de cassures de l'ARN ou de polyadenylation erronée ayant lieu dans l'ORF. Notre connaissance du NGD et du NSD est encore incomplète mais il semble que ces 2 voies soient mécanistiquement liées [26,27] : le blocage du ribosome induit des collisions de ribosomes : la zone de contact entre ribosomes permet le recrutement de l'ubiquitine ligase ZNF598 impliquée dans la dégradation de l'ARN avec l'endonucléase N4BP2 et le recyclage des ribosomes avec les protéines HBS1 et Pelota (2 paralogues d'eRF1 et eRF3).
- Le Nonsense mediated MRNA Decay (NMD), qui cible les ARN présentant un codon stop considéré par la cellule comme prématuré. Le NMD est le mieux décrit de ces mécanismes de contrôle qualité de l'ARN.

Depuis 2008 je cherche à comprendre comment le NMD est régulé dans un contexte d'infection par le virus HTLV-1 : après avoir introduit le NMD puis le virus HTLV-1, je présenterai les hypothèses et objectifs puis les résultats de mes travaux à l'interface entre ces 2 thématiques. Finalement j'aborderai les 3 projets vers lesquels nous nous orientons.

INTRODUCTION

1) Le mécanisme du NMD

1.1 De la terminaison de la traduction à l'initiation du NMD

Le NMD est une voie de dégradation de l'ARNm co-traductionnelle conservée au cours de l'évolution. Elle est déclenchée lorsque la traduction se termine dans un environnement spécifique et défavorable. En conditions normales, la terminaison de la traduction s'initie par la lecture du premier codon stop rencontré par le ribosome. Ce dernier conduit au recrutement du facteur de décrochage eRF1 au niveau du site A du ribosome. Par hydrolyse de GTP, eRF1 est stimulé par eRF3 et provoque la libération du peptide synthétisé [28]. Enfin, le recrutement du facteur ABCE1 conduit à la dissociation des sous-unités ribosomales [29,30].

La terminaison de la traduction est alors un point de régulation critique où une décision doit être prise entre dissociation/recyclage du ribosome et initiation du NMD. Par exemple, la protéine PABPC qui se lie spécifiquement à la queue polyA de l'ARNm, interagit avec eRF3 et eIF4G. PABPC joue un rôle important dans la circularisation de l'ARNm, facilitant ainsi la terminaison et la réinitiation de la traduction de cet ARN. Certaines études proposent un modèle dans lequel PABPC et UPF1, un facteur central de NMD, sont en compétition pour l'interaction avec eRF3. Ceci converge avec d'autres études qui démontrent que plus la distance entre le codon stop et la queue polyA associée à PABPC est importante, plus le NMD a de chance de s'initier car cela favorise la stabilisation d'UPF1 et son réseau d'interactions [31–35]. De plus, plusieurs facteurs du complexe d'initiation de la traduction dont eIF3 (avec la sous-unité eIF3E/INT6) ont été identifiées comme interagissant avec des protéines du NMD. UPF1 est une hélicase qui se lie à l'ARN sans spécificité de séquence. Elle peut se transloquer de 5' en 3' d'un ARN simple brin et deshybrider des structures d'acides nucléiques double brin [36]. Au cours de la traduction, UPF1 semble être décrochée par le ribosome ce qui provoque son accumulation sur le 3'UTR de l'ARNm[37,38]. Le ralentissement des étapes de terminaison de la traduction dû à la séquence d'ARNm, à l'organisation tridimensionnelle (en particulier la distance avec la queue polyA) et/ou à la composition du mRNP, pourraient donc favoriser la rétention du facteur central du NMD UPF1 au niveau du codon stop avec le ribosome immobilisé et conduire à l'activation du NMD. Il n'est pas encore clairement défini si UPF1 joue directement un rôle dans la terminaison de la traduction malgré ses liens avec eRF1 et eRF3, mais c'est un facteur indispensable de l'initiation du NMD. Des études récentes ont montré qu'un autre facteur du NMD, UPF3B, peut inhiber la terminaison de la traduction (sans UPF1) et favoriser la dissociation des complexes post-terminaison in vitro [71]. UPF1 et UPF3B interagissent également, augmentant mutuellement leur stabilité au niveau du codon stop. UPF3B peut être associé à l'EJC. Enfin, une interaction transitoire entre UPF1 et la protéine CBP80 pourrait également augmenter la stabilité de l'hélicase au niveau du ribosome arrêté.

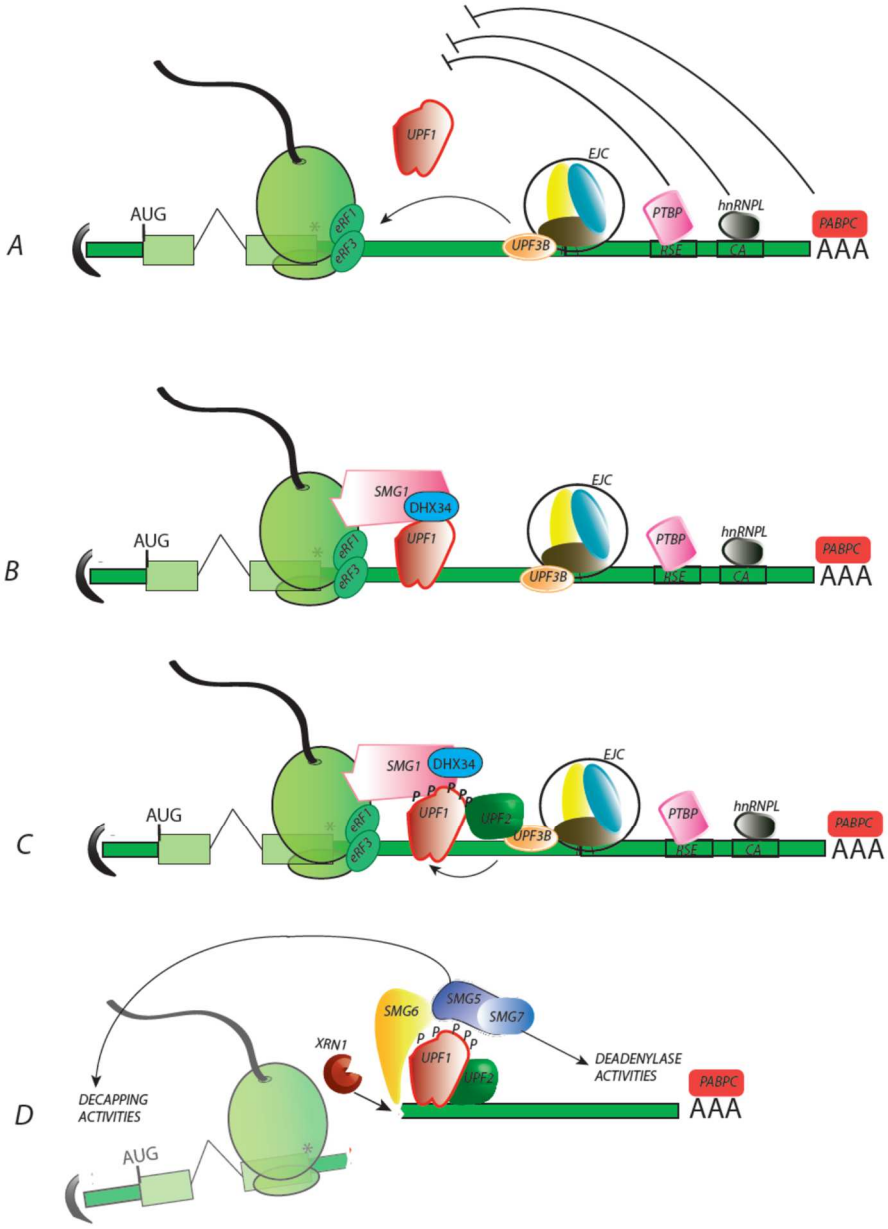

Figure 2 : le NMD en 4 étapes. A) La stabilisation d'UPF1 en aval d'un ribosome arrêté sur un codon stop est une étape critique de l'initiation du NMD. Elle est contrôlée par l'organisation et la composition du 3'UTR. B) Formation du complexe SURF. C) Le « decay induicing complexe » (DECID) promeut la phosphoyrlation d'UPF1. D) pUP1 sert de plateforme pour le recrutement des ribonucleases.

1.2 De la formation d'un complexe NMD à la dégradation de l'ARN.

L'interaction d'UPF1 avec la kinase PI3K SMG1 au niveau du codon stop complète le complexe d'initiation du NMD nommé SURF (SMG1-UPF1- release factors). Elle pourrait aussi jouer un rôle dans le retardement de la terminaison de la traduction. SMG1 phosphoryle UPF1 sur les résidus S/TQ et est régulé par SMG8 et SMG9 [39–42]. La phosphorylation d'UPF1 est également stimulée par le recrutement d'UPF2 et/ou de DHX34 [43,44]. UFP2 se lie à UPF1 (le plus souvent via UPF3B), induisant un

changement conformationnel nécessaire au déclenchement de l'activité ATPase et hélicase d'UPF1 [45]. L'hyperphosphorylation d'UPF1 (pUPF1) au niveau de ses extrémités Nter et Cter (domaines CH et SQ respectivement) agit comme une plateforme pour recruter des enzymes de dégradation telles que l'endonucléase SMG6 [46]. SMG6 clive l'ARN au voisinage du codon stop conduisant à des fragments d'ARN non protégés en 5 'et 3' qui sont ensuite dégradés par XRN1 et l'exosome [47]. pUPF1 peut également recruter l'hétérodimère SMG5-SMG7. Ce dernier permet le recrutement d'enzymes de déadénylation (CNOT8 de CCR4-NOT) ou de décapping (avec DCP1a et DCP2) [48–50]. Bien que les activités enzymatiques d'UPF1 soient indispensables et bien caractérisées in vitro [51,52], les étapes du NMD nécessitant ces activités enzymatiques in vivo ne sont pas encore clairement élucidées. L'activité hélicase d'UPF1 pourrait jouer un rôle dans l'élimination des structures secondaires et des protéines associées aux produits de clivage 3' pour permettre l'activité exonucléase XRN1. L'activité ATPase peut également être impliquée dans le remodelage des sous-complexes, contrôlant ainsi la séquence des étapes conduisant à la dégradation de l'ARN [53,54]. Au cours de la dernière étape, UPF1 est déphosphorylée par la phosphatase PP2A et dissociée du mRNP cible.

La localisation cellulaire du processus de NMD a longtemps été un sujet de questionnement. En tant que processus co-traductionnel, le NMD s'initie dans le cytoplasme sur les sites de traduction. Pendant longtemps, on a pensé que les étapes finales de dégradation de l'ARN avaient lieu dans les Processing Bodies (PB) en raison de l'augmentation de leur taille et de leur nombre lorsque le NMD est inhibé [55]. Dans ces conditions, les PB sont également enrichis en facteurs NMD et en intermédiaires de dégradation de l'ARNm. Les PB sont des granules cytoplasmiques composés d'ARNm condensés avec des facteurs associés à la dégradation de l'ARNm. Cependant, il est maintenant suggéré que l'accumulation de composants NMD dans le PB est une conséquence du blocage du NMD avant son achèvement et que les PB sont plus probablement des granules de stockage d'ARNm dans un état de répression traductionnel [56]. Déterminer si les étapes de dégradation se produisent à l'extérieur ou à l'intérieur de granules cytoplasmiques spécifiques est toujours à l'étude.

1.3 Régulation du NMD.

Étroitement liée à la terminaison de la traduction, l'efficacité du NMD est naturellement modulée par l'organisation de l'ARNm et la composition du mRNP. Comme décrit précédemment, éloigner physiquement la queue polyA liée à PABPC1 du codon de terminaison favorise l'accumulation l'UPF1 et le déclenchement du NMD. Lorsqu'elle est associée à l'ARN en aval d'un codon stop, la polypyrimide Track Binding Protein1 (PTBP1) inhibe le NMD en empêchant le recrutement de l'UPF1 [57]. Il se lie à une séquence spécifique connue sous le nom d'élément de stabilité de l'ARN (RSE), identifiée dans l'ARN du virus du sarcome de Rous et plus récemment dans de nombreux 3'UTR cellulaires proches du codon de terminaison. Le recrutement d'hNRNPL sur un ARNm permet aussi d'échapper au NMD [58]. De plus la présence

d'un EJC est un paramètre critique : lorsqu'il est situé en aval du codon stop (au moins à 55nt pour permettre la lecture du codon de terminaison par le ribosome sans être éliminé), l'EJC favorise l'enrichissement du 3'UTR en facteurs NMD tels qu'UPF3B et UPF2, stimulant le NMD (revu dans [59,60]). De plus, différentes compositions de l'EJC ont été observées et associées à la modulation du NMD. Par exemple, le remplacement de RNPS1 par MLN51/Barentz /CASC3 entraîne une réduction de l'efficacité du NMD. RNPS1 peut assurer l'activation du NMD de façon UPF3b indépendante tandis que le paralogue UPF3A a été décrit comme inhibiteur d'UPF3B [61,62]. Récemment, la kinase AKT1, acteur central de la voie de signalisation PI3K/AKT/mTOR, a été décrite comme une kinase supplémentaire d'UPF1 au cours du NMD. Elle est recrutée par la protéine UPF3b au niveau de l'EJC et permettrait l'activation d'une voie alternative du NMD indépendante d'UPF2. [63,64]. Plusieurs ARNm peuvent néanmoins subir un NMD de manière indépendante de l'EJC [65].
A l'ensemble de ces déclinaisons possibles du mécanisme de NMD permettant une régulation physiologique fine, s'ajoutent des interférences exogènes : plusieurs cribles chimiques ont identifié des molécules capables d'inhiber/d'activer le NMD [55,63,66]. Parmi les composés chimiques inhibiteurs se trouvent des inducteurs de l'apoptose qui provoquent la dégradation d'UPF1 (doxorubicin) ou des inhibiteurs de la traduction. Des activateurs de la translecture du codon stop comme l'Amlexanox et les inhibiteurs du cytosquelette Cytochalasin D et jasplakinolide (JPK) provoquent également l'inhibition du NMD. L'activité kinase de SMG1 et les interactions d'UPF1 avec ses partenaires sont aussi ciblées par d'autres composés [67–70].
Finalement, plusieurs protéines virales sont capables d'inhiber le NMD. Les mécanismes sont très variables et peuvent être associés à la dégradation de facteurs NMD, leur séquestration ou le blocage d'une étape (voir après).

1.4 Substrats et fonctions du NMD

1.4.1 Contrôle de la qualité de l'ARNm par le NMD

Comme son nom l'indique, les substrats NMD sont des transcrits présentant un codon stop prématuré (PTC). Les PTC peuvent apparaitre suite à divers évènements :

- mutations génomiques : mutations non-sens ou indel/insertions entraînant un décalage du cadre de lecture et la survenue de PTC.

- épissage défectueux/épissage alternatif, ARNm chimérique : environ 30% des événements d'épissage conduisent à une modification de l'ORF avec des occurrences de PTC ou l'incorporation d'intron dans la séquence 3'UTR.

Les PTC ainsi décrits sont présents à l'intérieur de l'ORF, souvent en amont d'un EJC, ou créant un 3'UTR plus long. Dans les deux cas, le ribosome s'arrête à distance du codon d'arrêt physiologique et de son environnement optimal de terminaison. Comme décrit ci-dessus, ces paramètres favorisent grandement le déclenchement du NMD et l'élimination de l'ARNm.

Traduire un ARNm portant un PTC conduit à des protéines tronquées, délétères pour la cellule, car non fonctionnelles voire présentant un effet dominant négatif. Le NMD prévient ces événements : c'est la fonction de contrôle de la qualité qui lui a été historiquement attribuée. Par exemple plusieurs maladies génétiques telles que la béta thalassémie, sont causées par des mutations génomiques non-sens. Des phénotypes légers sont observés lorsque les PTC sont sensibles au NMD (sans protéines tronquées exprimées) tandis que des phénotypes agressifs sont observés lorsque les PTC échappent au NMD (avec une protéine tronquée exprimée)[71,72]. Il est intéressant de noter que les ARNm contenant des PTC et qui évitent le NMD seraient impliqués dans plus de 30% des cancers [73–75]. À titre d'exemple, il a été récemment montré que l'inhibition du NMD est impliquée dans la stabilisation et la traduction de l'ARNm de fusion BCL2-IGH, favorisant l'expression du facteur anti-apoptotique BCL2 et dont résulte une forme de lymphome diffus à grandes cellules B [58]
On estime que 5 à 30 % des transcrits humains présentent un codon de terminaison prématurée (PTC).

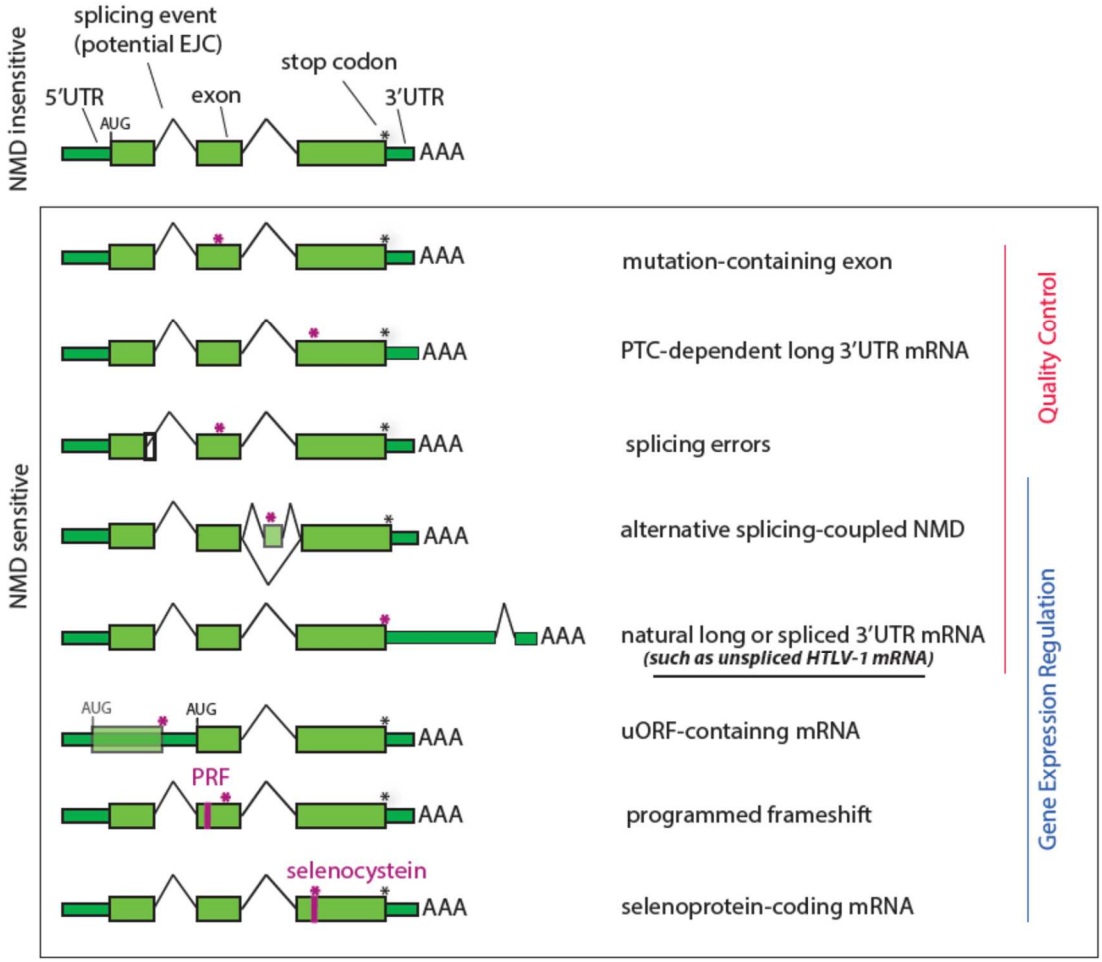

Figure 3 : Représentation des différentes conformations d'ARN ciblés par le NMD

1.4.2 Contrôle de l'expression des gènes au niveau post-transcriptionnel par le NMD.

Contrairement à sa fonction de contrôle qualité, qui dégrade systématiquement les ARNm « aberrants », le NMD peut également réguler les niveaux d'ARNm « non aberrants ». Ainsi, ~ 15% des ARNm physiologiques sont ciblés par le NMD. Il a été suggéré que cette fonction du NMD pourrait jouer un rôle sur le contrôle du bruit transcriptomique, les mécanismes de rétroaction positive ou négative (lorsqu'ils sont couplés à l'épissage) ou sur la régulation l'expression de gènes du développement, de l'équilibre prolifération/différenciation, de la réponse au stress et de la réponse immunitaire (revue dans [76,77]). Cinq « familles » d'ARNm sont représentatives de ces événements :

- ARNm avec uORF : l'uORF, présent dans ~50% des transcrits humains, peut être traduit en fonction de la densité ribosomique. La terminaison initiée par le codon stop de l'uORF déclencherait alors le NMD en raison d'EJC en aval placés sur l'ORF principal. L'ARNm de CREB-2/ATF4 est un exemple bien documenté [78].

- ARNm avec 3'UTR long et ARNm avec EJC dans le 3'UTR. L'organisation du 3'UTR d'un ARNm est finement contrôlée. Elle peut être allongée ou un raccourcie par rétention d'intron ou polyadénylation alternative. Ceci modifie sa taille, sa composition en RBP et sa structure secondaire qui sont des éléments majeurs du déclenchant le NMD comme évoqué plus haut. De même, des événements d'épissage alternatif se produisant en aval du codon stop peuvent conduire au dépôt d'un EJC dans le 3'UTR stimulant fortement le NMD [79]. Dans ces cas, c'est le codon stop normal qui déclenche le NMD.

- Isoformes d'ARNm issues d'un saut ou d'une rétention d'intro/exon. L'épissage alternatif (AS) et le NMD sont étroitement liés : en plus de la mise en forme de l'extrémité 3', il peut également modifier périodiquement le corps de l'ORF en produisant des isoformes alternatives avec des PTC. De multiples transcrits de ce type sont identifiées avec les approches de séquençage à haut débit et documentées dans des bases de données. Plusieurs types de facteurs de réparation de l'ADN ou d'épissage tels que les protéines SR sont régulées par cette voie AS/NMD, élargissant l'impact indirect du NMD sur la régulation post-transcriptionnelle [80–82]

- ARNm avec des décalages de ribosomes programmés (Programed Ribosomic Frameshits, PRF) : les PRF sont des repositionnements spécifiques du ribosome d'un cadre de lecture à un autre avec une efficacité variable. Dans plus de 95% des cas, le nouveau cadre de lecture redirige le ribosome vers un PTC (par rapport à l'ORF d'origine) conduisant au NMD. Par exemple, la traduction de l'ARNm du récepteur de chimiokine CCR5 ainsi que de plusieurs interleukines sont soumises au PRF. Le PRF est fortement favorisé par la liaison de micro ARN, conduisant à une répression de l'expression de ces ARNm dépendante du NMD [83].

- ARNm codant pour la sélénocystéine. La sélénocystéine est codée par un codon UGA. Sous une faible concentration de sélénocystéine, ce codon est lu comme un codon stop induisant le NMD [84].

2) L'infection par HTLV-1 comme modèle pour étudier le NMD

Le modèle utilisé dans mes travaux de recherche sur le NMD est l'infection par le virus du lymphome/leucémie à cellules T humaines de type 1 (HTLV-1).

HTLV-1 est un deltarétrovirus qui infecte environ 10 millions de personnes dans le monde par le biais de fluides corporels infectés, notamment le sang et le lait [1]. Seuls 2 à 5 % des porteurs de HTLV-1 évoluent vers la maladie : la leucémie/lymphome T adulte (ATLL), une forme agressive de leucémie caractérisée par la prolifération des cellules T CD4+. Cette pathologie apparaît généralement après une période asymptomatique de plusieurs décennies post-infection [85,86]. HTLV-1 est également l'agent étiologique de la HAM/TSP, une maladie inflammatoire associée à la démyélinisation de la moelle épinière et à l'accumulation de cellules infectées par HTLV-1 et de cellules CD8+ dirigées contre HTLV-1 dans le système nerveux central [87]. D'autres syndromes non prolifératifs sont associés au HTLV-1 : lésion pulmonaire (bronchopneumopathie interstitielle lymphoïde), arthropathie, polymyosite, dermatite et uvéite [88–90]

2.1 Organisation du génome et protéines d'HTLV-1

Le génome d'HLTV-1 est composé d'une séquence polycistronique d'environ 8,5 kB codant plus de 10 protéines. 2 longues séquences répétées terminales (LTR) flanquent la région codante virale une fois intégrée dans le génome de l'hôte. Ils présentent des promoteurs conduisant à la transcription sens et antisens par l'ARN polII de l'hôte. Pour maximiser sa capacité de codage, le virus s'appuie sur des cadres de lecture qui se chevauchent, des décalages du cadre de lecture programmés, des séquences Kozac sous-optimales et des évènements d'épissage alternatif (revue dans [91]).

3 classes d'ARNm sont exportées vers le cytoplasme (Figure 4):

Les ARNm codant les protéines structurales

-L'ARN non épissé correspond à une copie complète du génome viral. Il est exporté pour être empaqueté dans de nouveaux virions ou traduit en protéines structurales GAG, GAG-PRO et GAG-PRO-POL. La protéine GAG est composée de 3 domaines : la matrice (MA), la capside (CA) et la nucléaocapside (NC). 10 à 40 nucléotides avant le codon stop GAG, une séquence homopolymérique dite "slippery sequence" et un pseudonœud (PK) spécifique en aval du codon stop provoquent une translocation du ribosome avec un décalage du cadre de lecture d'1 codon (-1FS) conduisant au repositionnement de ce ribosome sur l'ORF de la protéase (PRO) pour traduire une protéine de fusion composée de GAG et de la protéase virale. Cette aspartyl protéase forme un dimère et est impliquée dans la maturation des particules virales par le clivage des 3 domaines de GAG. Un deuxième décalage du cadre de lecture programmé à la fin de la protéase conduit à la synthèse de la protéine POL fusionnée

à GAG et PRO. POL présente 2 domaines enzymatiques qui portent l'activité de réverse transcriptase et l'activité intégrase, respectivement. Ces fonctions sont également activées après le clivage protéolytique. Alors que pour le VIH l'efficacité du -1FS est d'environ ~ 5%, pour HTLV-1, seul le -1FS pro-pol a été quantifié autour de 20% [92].

- L'ARN épissé simplement code la protéine structurale ENV. ENV est traduit sous la forme d'un précurseur de polyprotéine ensuite glycosylé et clivé en gp46 (SU) et gp21 transmembranaire (TM). SU et TM s'assemblent hétérodimères à la surface des virions et sont responsables de l'initiation de la liaison avec la cellule cible, de la fusion des membranes et de l'entrée virale[93].

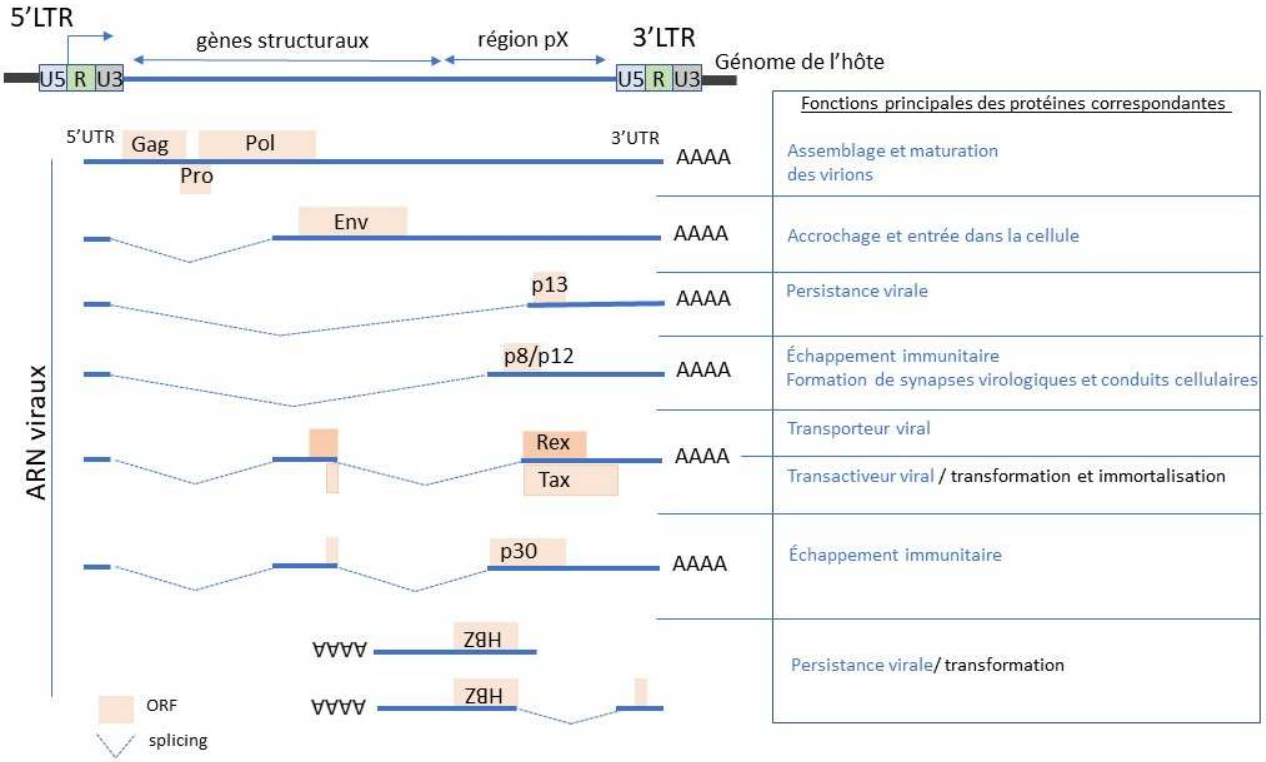

Figure 4 : Les différents ARNm d'HTLV.

Les ARNm codant les protéines auxiliaires et régulatrices (région pX)

Les protéines auxiliaires et régulatrices proviennent de gènes à l'extrémité 3' du génome dans la région pX. Les ARNm correspondants sont épissés simplement ou doublement. On notera en particulier :

- L'ARNm doublement épissé code p30 qui séquestre l'ARNm tax/rex dans le noyau et lie directement Rex pour réprimer leur activité.

- Les ARNm doublement épissés codent également les protéines TAX et REX (p21 et p27Rex). Rex est responsable de l'export nucléaire des ARNm gag/pol non épissés et env simplement épissés dans le cytoplasme, assurant la traduction des protéines structurales et la présence cytoplasmique d'ARNv non épissé pour l'assemblage de

particules virales matures. Tax est le transactivateur viral. Plusieurs interactomes ont identifié une myriade de protéines cellulaires interagissant avec Tax. [94]. L'importance de cet interactome est certainement due à la nature intrinsèquement désordonnée de sa structure.

- les transcrits antisens (non épissés et épissés simplement) codant HBZ. HBZ agit souvent dans des directions opposées à Tax afin de contrôler la réponse immunitaire de l'hôte et de soutenir la transformation maligne à long terme [95]. Contrairement à Tax, dont la perte d'expression fréquente dans les cellules de patients ATL suggère l'implication principale dans les phénomènes initiaux de la transformation leucémique, HBZ est exprimé de manière ubiquitaire, jouant un rôle crucial dans le maintien du processus oncogène et la progression de la maladie. De façon intéressante, l'ARN hbz joue des rôles spécifiques dans la prolifération, différemment de la protéine HBZ [96]

2.2 Cycle viral d'HTLV-1.

HTLV-1 infecte une grande variété de cellules : CD8+, lymphocytes B, cellules myéloïdes, cellules endothéliales, fibroblastes, neutrophiles, monocytes, cellules dendritiques myéloïdes et plasmacytoïdes [97–99]. Les précurseurs lymphoïdes peuvent également être un réservoir d'infection latente. Les particules virales, bourgeonnant à partir de la membrane plasmique, sont composées d'un assemblage complexe de protéines ENV et GAG. Les 2 copies de l'ARN viral non épissé sont recouvertes de NC et emballées dans la capside avec l'intégrase et la reverse transcriptase. Les virions HTLV-1 libres sont peu infectieux. Il a été établi que la transmission du virus repose essentiellement sur des contacts de cellule à cellule [100–103]:

- Le biofilm viral produit à la surface des cellules infectées joue un rôle critique en favorisant la rétention des particules virales à proximité de la surface des cellules et leur transmission lors d'un contact entre la cellule infectée et la cellule non infectée.

- Des conduits cellulaires agissent comme des tunnels pour transférer le matériel viral.

- La synapse virologique est un réarrangement spécifique du cytosquelette conduisant à la production locale de particules virales dans une zone réduite au niveau du site de contact entre les cellules.

Alors que HTLV s'appuie sur des particules virales pour infecter de nouvelles cellules, certains clones peuvent entrer en expansion. Ce comportement oncogène provient de la modulation de multiples processus cellulaires et aboutit à l'ATL; Tax joue notamment un rôle essentiel dans la transformation cellulaire en générant une instabilité génomique et un contournement des points de contrôle cellulaires : il inhibe la réparation de l'ADN, perturbe la progression du cycle cellulaire et affecte l'autophagie. Il module également la transcription en modifiant le contexte épigénétique et la composition des complexes de transcription. Il dérégule notamment les voies de signalisation dont la voie NF-□B (induisant son activation constitutive). Tax réprime également l'immunité innée de la cellule infectée (avec un effet immunosuppresseur). Cependant, bien qu'il soit largement admis que l'infection par HTLV-1 entraîne une

prolifération cellulaire, il a également été observé qu'elle provoque fréquemment l'apoptose et la sénescence des cellules lymphoïdes ou non lymphoïdes de manière Tax-dépendante. Contrairement à HBZ, l'expression de Tax est progressivement inhibée (par hyperméthylation du promoteur, rétroaction négative via le recrutement d'inhibiteurs de la transactivation virale via Tax (bcl3, HBZ…), délétion ou mutations non-sens dans la séquence de Tax) ou ne se produit que par « bursts » de transcription occasionnelle dans les cellules leucémiques[104,105]. L'infection persistante à HTLV-1 est probablement associée à la sélection de clones capables d'échapper au système immunitaire de l'hôte. Sachant qu'une forte réponse des lymphocytes T cytotoxiques est dirigée contre Tax, ces clones sont naturellement ceux dont l'expression de Tax est mesurée (notamment grâce à HBZ) ou nulle (revu dans [106,107]).

2.3 Impact d'HTLV-1 sur les processus post-transcriptionnels.

Alors que de grands efforts ont été faits depuis la découverte d'HTLV-1 en 1980 pour déchiffrer l'impact de l'infection virale sur la transcription de l'hôte, moins d'études ont été menées pour en évaluer l'impact viral sur les processus post-transcriptionnels. (figure5).

Épissage de l'ARN

L'épissage de l'ARN est étroitement coordonné au fitness transcriptionnel du gène qui contrôle le recrutement de certains éléments du spliceosome. L'épissage est également un carrefour important des processus post-transcriptionnels.

Thenoz et al[108] a été le premier article à révéler qu'HTLV-1 altère de manière significative la structure des transcrits cellulaires en modifiant l'utilisation des exons alternatifs. Une étude complémentaire a démontré que l'expression de Tax régule l'épissage de façon DDX5/17 dépendante, favorisant la formation d'un complexe RELA/DDX5/17 intragénique. HTLV-1 pourrait ainsi avoir un impact sur l'épissage en modulant la transcription ainsi qu'en interférant directement avec le mécanisme d'épissage [109]. Cette implication directe de Tax dans les mécanismes post-transcriptionnels a ensuite été confirmée par Vandermeulen et al [110], et Shallack et al [111], dans des analyses d'interactome des protéines oncovirales Tax et HBZ. Un large ensemble d'interactions avec les protéines de liaison à l'ARN, y compris U2AF2, un régulateur cellulaire clé de l'épissage du pré-ARNm a été découvert. Il a également été démontré que HBZ perturbe l'épissage en altérant la composition en exons. Dans cette étude, Tax et HBZ agissent de manière opposée, Tax induisant l'inclusion d'exons tandis que HBZ semble induire l'exclusion d'exons.

Récemment, une analyse par spectrométrie de masse des partenaires Rex a révélé des interactions avec d'autres facteurs d'épissage tels que NONO et SFPQ, en relation avec l'export de l'ARNv. Dans la même étude, les interactions avec hnRNPL et l'ARN U5 du spliceosome supportent un impact direct de Rex sur le processus d'épissage de l'hôte dans les cellules T. Appuyant ces observations, le profil d'épissage de plus de 600 transcrits hôtes a été modifié après la seule expression de Rex [112].

Ces altérations de l'épissage ont été observées dans des cellules transfectées, des lymphocytes infectés chroniquement par HTLV-1 ou dans des cellules de patients de cohortes infectées par HTLV-1.

Voie des micro ARN

L'infection par HTLV-1 est associée à une dérégulation massive de l'expression des miARN. La plupart des études ont porté sur le contrôle transcriptionnel de l'expression des miARN par les protéines virales Tax et HBZ [113,114].

De façon intéressante, 2 rapports ont étudié l'influence directe de Rex et Tax sur le mécanisme de la voie des miARN. Premièrement, Rex inhiberait la voie des ARN interférents en interagissant avec Dicer, la nucléase impliquée dans la conversion du dsARN en siARN afin d'activer le complexe RISC [115]. Deuxièmement, il a été constaté que Tax interagit in vitro et colocalise dans le noyau avec Drosha. Il a été suggéré que Tax pourrait rediriger Drosha vers le protéasome, empêchant le clivage primaire des miARN[116]. De plus, Tax peut également interagir avec TRBP, un partenaire moléculaire de Drosha. Cependant, les conséquences de cette interaction n'ont été analysées qu'à la lumière des activités transactivatrices de Tax[117].

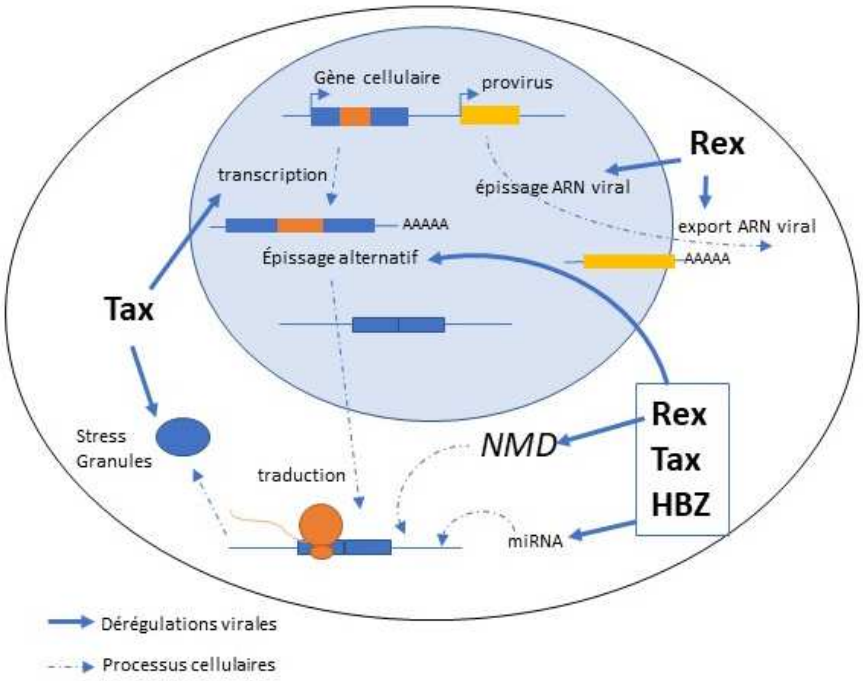

Figure 5 : Schéma récapitulatif des dérégulations post-transcriptionnelles induites par HTLV-1

Régulation de la traduction

L'implication directe de Tax dans les processus post-transcriptionnels est également soutenue par Legros et al, dont le travail a montré son impact sur la formation de granules de stress (SG). Comme les PBodies, les SG sont des structures cytoplasmiques composées essentiellement d'agrégats de mRNP. On peut aussi y retrouver des facteurs non liés au processing de l'ARN tels que HDAC6. Leur formation est une réponse adaptative aux stimuli de stress (oxydatif, osmotique, hypoxique, choc thermique, UV, …) qui conduit à l'inhibition de la traduction des ARNm de gènes de

ménage tout en favorisant la traduction des protéines critiques pour la réponse au stress telles que les chaperonnes et les enzymes impliquées dans la réparation des dommages à l'ADN [118,119]. Dans ce contexte, il a été montré que dans les lymphocytes T infectés par HTLV-1, la formation de SG après un traitement à l'arsénite est altérée et dépendante d'une interaction Tax HDAC6. Le blocage traductionnel induit par l'arsénite serait alors partiellement levé[120].

Il a aussi été observé que Tax interagit avec eIF3e/INT6, une sous-unité du facteur d'initiation de la traduction eIF3. Suite à leur interaction, INT6 est déplacé du noyau vers le cytoplasme. L'importance de cette relocalisation sur la traduction reste à démontrer [121].

Enfin, Tax interagit avec la tristetrapoline (TTP). La TTP est une protéine de liaison aux éléments AU-rich de l'ARN, qui favorise la dégradation rapide de l'ARNm, notamment l'ARNm du TNFa. Tax provoque la relocalisation nucléaire de la TTP, protégeant indirectement l'ARNm du TNFa et favorisant l'expression de la protéine TNFa [122].

Transfert cytoplasmique de l'ARNv

Comme indiqué précédemment, Rex a d'abord été décrit comme un transporteur de l'ARNv, homologue fonctionnel de HIV Rev. Il exporte sélectivement l'ARNv non épissé ou simplement épissé via le RxRE (Rex responsive element) situé entre les régions U3 et R du LTR. Rex y reconnait une séquence d'ARN structurée de 12 nt avec une affinité et une spécificité élevées [123,124]. En parallèle, hnRNPA1 est inhibé, empêchant l'utilisation de sites accepteurs d'épissage de la région pX [125,126]. L'export dépendant de Rex se produit via CRM1/XPO1 (chromosome maintenance region 1/ exportin1) : Rex associé à l'ARNv interagit avec CRM1 via son domaine NES et est exporté à travers les pores nucléaires sous un gradient GTP [127,128]. Dans le cytoplasme, Rex contacte l'importB (indépendamment de l'importa) avec son domaine NLS, permettant son retour dans le noyau. Sachant que le domaine de liaison à l'ARN et le domaine NLS de Rex se chevauchent partiellement, il a été suggéré que la liaison à ImportB est responsable du déchargement de l'ARNv par Rex[129]**.**

NMD

En 2013, l'étude de Nakano et al, confirme l'inhibition du NMD préalablement démontrée par notre travail (voir après). Néanmoins, elle y caractérise Rex comme protéine inhibitrice [130]. Récemment, les mêmes auteurs ont démontré que l'état de phosphorylation de Rex contrôle son activité inhibitrice et que c'est son extrémité Nter qui interagit avec UPF1. De plus ils retrouvent aussi Rex associé aux facteurs SMG5/SMG7 et UPF3B ; Ils suggèrent alors que Rex favorise l'intégration d'UPF3A dans le complexe NMD, ce qui participerait à son inhibition [131]. Par une approche de séquençage haut débit, ils illustrent finalement que Rex promeut l'expression d'une forme anormale de l'ARNm PD-L1/CD247 avec inclusion d'un PTC, due à une modification du splicing alternatif couplée à l'inhibition du NMD. Une protéine PD-L1 tronquée de son domaine transmembranaire est produite, favorisant sa sécrétion [112].

HYPOTHESES ET OBJECTIFS

D'une part, l'infection par HTLV-1 est associée à la dérégulation de multiples voies cellulaires telles que : la réparation de l'ADN, l'épissage de l'ARN, l'autophagie, la voie des miARN, la réponse au stress, la réplication et bien sûr la transcription. En conséquence, les cellules/tissus infectés par HTLV-1 présentent une instabilité génétique, une altération de l'apoptose et la prolifération, une réponse immunitaire défectueuse, des phénotypes pro-inflammatoires, etc. (revu dans [132])

D'autre part, il a été démontré que des processus post-transcriptionnels tels que le NMD interviennent dans la régulation des mêmes processus ; le NMD est fonctionnellement lié à la réponse immunitaire et à l'inflammation : par exemple, chez Arabidopsis, une inhibition prolongée du NMD en éteignant les composants du NMD amène à un phénotype d'auto-immunité caractérisé par un retard de croissance, la formation spontanée de lésions nécrotiques et un niveau élevé d'acide salicylique [133]. Un fonctionnement altéré du NMD dans le cerveau de la souris déclenche une activation de la réponse immunitaire et entraîne une neuro-inflammation exacerbée [134]. De plus, plusieurs ARNm codant pour des interleukines, des chimiokines ainsi que pour leurs récepteurs respectifs sont régulés de manière UPF1 dépendante (liste non exhaustive : IL-12, IL-6, IL-2, IL-1b, récepteur 2 du facteur de nécrose tumorale (TNFR2), CXCL2, CCL5, CXCL16, CXCR2…). Le NMD participe à la maturation des thymocytes ainsi qu'à la production d'antigènes pour la présentation du MHCI [135,136]. Le NMD contribue également à la stabilité génétique en raison de sa fonction de contrôle/qualité et de la régulation de l'expression de certains facteurs de réparation de l'ADN. En condition hypoxique ou de stress oxydant ainsi qu'en condition de déficit en acides aminés, il a été démontré que l'inhibition du NMD joue un rôle dans l'adaptation au stress, favorisant la tumorigenèse [137] [138,139]

En plus de ces convergences, notre intérêt à étudier l'efficacité du NMD lors de l'infection par HTLV-1 reposait sur 2 observations supplémentaires :

-Tout d'abord, en effectuant un criblage double hybride dans le passé, eIF3E/INT6 a été identifié comme un puissant interacteur de Tax [121]. À l'origine, le gène INT6 avait été identifié chez la souris comme étant le site d'insertion du MMTV dans les lésions néoplasiques des glandes mammaires. Étant une sous-unité du facteur d'initiation de la traduction eIF3, INT6 a été davantage caractérisée comme un acteur important de la voie NMD. INT6 peut interagir avec les domaines MIF4G notamment UPF2 et CPB80 et son extinction provoque une inhibition de NMD. Le rôle exact d'INT6 est toujours à l'étude [140]. En interagissant avec elle, Tax induit une relocalisation d'INT6. Nous avons alors émis l'hypothèse que cela pourrait avoir un impact sur plusieurs fonctions d'INT6, y compris au cours du NMD.

-Deuxièmement, l'organisation génétique spécifique des rétrovirus nous a fait rapidement suspecter que l'ARN rétroviral pourrait être sensible au NMD. Comme indiqué précédemment, la taille et l'organisation de la région 3'UTR est une caractéristique importante du déclenchement du NMD. Alors que la taille médiane des 3'UTR humaines est d'environ 750 nt [79], le 3'UTR de l'ARNm gag est d'environ 4000 nt. Un autre paramètre de l'ARNm non épissé du HTLV et de celui d'autres rétrovirus

est le décalage de cadre de lecture (–1FS). Pour maintenir le bon rapport entre les 3 protéines structurales (GAG PRO et POL), le -1FS ralentit la lecture des ribosomes et empêche la terminaison de la traduction ce qui pourrait favoriser le NMD.

Au final, ces observations ont soulevé plusieurs questions (Figure 6):

1) L'ARNv est-il un substrat NMD ?

L'ARNv est-il directement ciblé par le NMD ou certains facteurs impliqués dans la transactivation virale peuvent-ils être régulés par le NMD ? Dans le cas d'une sensibilité directe au NMD, quels sont les déterminants du NMD et où sont-ils localisés ? Est-ce que tous les ARN viraux sont sensibles ou juste un sous-ensemble d'entre eux ?

2) Le NMD est-elle une barrière contre l'infection virale ?

Le NMD est-il un nouvel acteur de la réponse intrinsèque antivirale de l'hôte ? La modulation de NMD impacte-t-elle la réplication virale ?

3) Quelles sont les stratégies d'HTLV-1 pour contourner cette menace ?

Considérant que l'ARNv et le fitness réplicatif d'HTLV-1 sont sensibles au NMD, nous nous demandons comment le virus a réussi à contourner cette sensibilité ? Existe-t-il une inhibition du NMD dans les cellules infectées ? Des protéines virales sont-elles impliquées ? Quels sont leurs mécanismes d'action ?

4) L'inhibition du NMD par voie virale joue-t-elle un rôle dans les pathologies associées à l'infection par HTLV-1 ?

Quelle part des dérégulations transcriptomiques induites par l'expression virale sont dues à l'inhibition du NMD ? Quelles sont les conséquences de l'inhibition du NMD pour l'hôte ? Qu'elles sont les voies de signalisation affectées ?

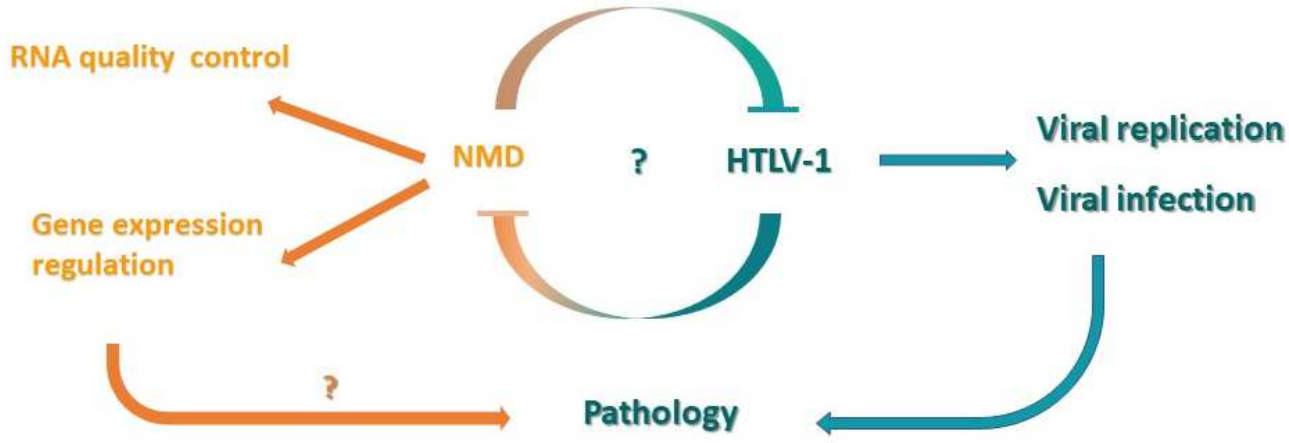

Figure 6 : schéma récapitulatif des hypothèses et objectifs

RESULTATS

1. *The Human T-Lymphotropic Virus Type 1 Tax Protein Inhibits Nonsense-Mediated mRNA Decay by Interacting with INT6/EIF3E and UPF1*

En analysant la stabilité d'un ARN rapporteur présentant un codon Stop prématuré, j'ai découvert que des cellules infectées chroniquement par HTLV-1 ou exprimant uniquement Tax étaient capables d'inhiber le NMD. Par co-immunoprécipitation j'ai également décrypté un réseau d'interactions mutuellement exclusives entre Tax, INT6, UPF1 et UPF2. De plus, des expériences de microscopie confocale ont confirmé que Tax peut titrer INT6 pour le délocaliser hors de portée de UPF1 et UPF2. L'utilisation de mutants de Tax démontre qu'une partie de l'inhibition de NMD dépend de l'interaction entre Tax et INT6. A l'appui de ces observations, Tax provoque l'accumulation de formes hyperphosphorylées d'UPF1 (actives dans le processus de NMD) et la modification des PB en nombre et en taille. Nous avons analysé l'effet de l'expression de Tax sur une sélection d'ARNm connus pour être sensibles au NMD, tels que Gadd45a : ils ont été stabilisés comme attendu. Enfin, nous avons vérifié si les ARN viraux sont sensibles au NMD : des cellules transfectées avec un clone moléculaire HTLV-1 ont été traitées avec des siRNA contrôle ou dirigés contre UPF1. La quantification par RTqPCR a révélé que tous les ARNv étaient régulés positivement en l'absence d'UPF1, y compris l'ARNm de HBZ.

En conclusion, ce travail a démontré pour la première fois que le NMD est inhibée dans une cellule infectée. De plus, nous avons montré que dans le cas d'une infection par HTLV-1, cette trans-inhibition est (au moins) dépendante de la protéine virale Tax. Enfin, ces résultats soutiennent que parmi toutes les dérégulations transcriptomiques induites par Tax, un impact direct au niveau post-transcriptionnel doit être considéré.

JVI Journals.ASM.org

The Human T-Lymphotropic Virus Type 1 Tax Protein Inhibits Nonsense-Mediated mRNA Decay by Interacting with INT6/EIF3E and UPF1

Vincent Mocquet,[a] Julia Neusiedler,[a]* Francesca Rende,[b] David Cluet,[a] Jean-Philippe Robin,[a] Jean-Michel Terme,[a]* Madeleine Duc Dodon,[a] Jürgen Wittmann,[c] Christelle Morris,[a] Hervé Le Hir,[d] Vincenzo Ciminale,[b] and Pierre Jalinot[a]

Laboratoire de Biologie Moléculaire de la Cellule, Unité Mixte de Recherche 5239, Centre National de la Recherche Scientifique, Ecole Normale Supérieure de Lyon, Lyon, France[a]; Department of Oncology and Surgical Sciences, Institute of Neuroscience at the Department of Biomedical Sciences, Università di Padova, Padua, Italy[b]; Division of Molecular Immunology, Department of Internal Medicine III, Nikolaus Fiebiger Center, University of Erlangen-Nürnberg, Erlangen, Germany[c]; and Institut de Biologie de l'Ecole Normale Supérieure, Unité Mixte de Recherche 8197, Centre National de la Recherche Scientifique UMR8197, Paris, France[d]

In this report, we analyzed whether the degradation of mRNAs by the nonsense-mediated mRNA decay (NMD) pathway was affected in human T-lymphotropic virus type 1 (HTLV-1)-infected cells. This pathway was indeed strongly inhibited in C91PL, HUT102, and MT2 cells, and such an effect was also observed by the sole expression of the Tax protein in Jurkat and HeLa cells. In line with this activity, Tax binds INT6/EIF3E (here called INT6), which is a subunit of the translation initiation factor eukaryotic initiation factor 3 (eIF3) required for efficient NMD, as well as the NMD core factor upstream frameshift protein 1 (UPF1). It was also observed that Tax expression alters the morphology of processing bodies (P-bodies), the cytoplasmic structures which concentrate RNA degradation factors. The presence of UPF1 in these subcellular compartments was increased by Tax, whereas that of INT6 was decreased. In line with these effects, the level of the phosphorylated form of UPF1 was increased in the presence of Tax. Analysis of several mutants of the viral protein showed that the interaction with INT6 is necessary for NMD inhibition. The alteration of mRNA stability was observed to affect viral transcripts, such as that coding for the HTLV-1 basic leucine zipper factor (HBZ), and also several cellular mRNAs sensitive to the NMD pathway. Our data indicate that the effect of Tax on viral and cellular gene expression is not restricted to transcriptional control but can also involve posttranscriptional regulation.

Human T-lymphotropic virus type 1 (HTLV-1) infection is associated with the onset of severe diseases, mainly adult T-cell leukemia (ATL) and tropical spastic paraparesis, also named HTLV-1-associated myelopathy, in 2 to 5% of patients (for a review, see reference 44). These conditions are characterized by a long latency, with infection often occurring in childhood and disease development at an adult age. Accordingly, it is estimated that the development of ATL involves several phases, ending in the acute proliferation of monoclonal ATL cells. At the initial stage, lymphocytes are infected by viral particles, leading to provirus integration and the expression of various viral proteins. Among them, Tax plays an important role both by inducing the transcription of the provirus and by stimulating the proliferation of the host cell. Tax, which is present in both the nucleus and the cytoplasm, exerts these functions by directly binding or by modulating the expression of several key cellular proteins involved in transcriptional control, cell cycle progression, genomic stability, cell adherence and migration, protein degradation, and RNA metabolism (7).

Among these various cellular proteins bound by Tax, we have previously characterized INT6, also known as EIF3E, one the 13 subunits of the translation initiation factor eukaryotic initiation factor 3 (eIF3) (16). The complex between both proteins was found to be cytoplasmic, whereas in normal cells, INT6 is present in both the cytoplasm and the nucleus (16, 27, 64). In mammalian cells, the silencing of INT6 seems to marginally affect general translation, but evidence for a role of INT6 in the translation of specific genes was recently obtained (26, 67). Regarding its role in association with eIF3, we have previously shown that INT6 was important for the degradation of cellular mRNAs by nonsense-mediated mRNA decay (NMD) (47). The latter is a quality control process leading to the degradation of mRNAs, including a premature stop codon (PTC), which can arise from mutation or aberrant alternative splicing and eventually prevents the synthesis of a truncated protein, which could serve as a dominant negative protein against an intact protein (3). NMD also regulates the expression of mRNA with upstream open reading frame (ORF) (uORF) or long 3′-untranslated (3′UTR) sequences. After a first round of translation (12, 30), the presence of a PTC more than 50 nucleotides upstream of an exon-exon junction leads to the association of the SMG1-eRF1-eRF3-UPF1 complex (SURF) with the mRNA. Upstream frameshift protein 1 (UPF1) then interacts with the UPF2 and UPF3 proteins present in the nearby exon junction complex (EJC) (11, 33). These interactions lead to the phosphorylation of UPF1 by SMG1 and the routing of the mRNA toward degradation (31), which presumably occurs in cytoplasmic compartments known as processing bodies (P-bodies) (49, 57). P-bodies are cytoplasmic foci that contain proteins involved in different aspects

Received 7 December 2011 Accepted 20 April 2012
Published ahead of print 2 May 2012
Address correspondence to Pierre Jalinot, pjalinot@ens-lyon.fr.
* Present address: Julia Neusiedler, Wellcome Trust Centre for Gene Regulation and Expression, University of Dundee, Dundee, United Kingdom; Jean-Michel Terme, Molecular Biology Institute of Barcelona (IBMB), CSIC, Barcelona, Spain.
V.M. and J.N. equally contributed to this work.
Supplemental material for this article may be found at http://jvi.asm.org/.

doi:10.1128/JVI.07021-11

of mRNA turnover, such as the decapping enzyme DCP1 and the XRN1 exonuclease, also including NMD factors (14, 53). Concomitantly with degradation, UPF1, which is also present in P-bodies, is dephosphorylated by SMG5 and PP2A and can then be recycled to bind novel mRNAs (51).

It was shown previously that the deregulation of gene expression in stressed cells was due in part to the modification of mRNA stability (20). Moreover, while previous works associated the presence of a PTC in tumor suppressor genes (such as WT1, p53, and BRCA1) with the development of cancers (19, 34, 36, 52), recent data demonstrated that NMD inhibition plays an important role in the initiation of tumorigenesis (1, 5, 18, 28, 52, 63) and the potential expression of truncated tumor suppressor factors (3). By considering the multifactorial process of leukemogenesis in HTLV-1 cells, the role of INT6 in the NMD pathway, and the effect of Tax on INT6, we asked whether Tax was able to modulate the NMD process. By using functional assays, we observed that this mRNA surveillance pathway was effectively downregulated in Tax-expressing cells. In line with this activity, Tax binds both INT6 and UPF1 and inhibits interactions between these two NMD factors. In agreement with these abilities, Tax expression alters the morphology of P-bodies and stabilizes cellular and viral RNAs prone to NMD degradation by acting at the posttranscriptional level.

MATERIALS AND METHODS

Constructs, cell culture, and transfection. The following plasmids used in NMD assays were previously described: globin NS39 (GlNS39) and wild-type (WT) globin (GlWT) (47) and wild-type and mutated β-globin fused to *Renilla* luciferase (6). The HTLV-1 basic leucine zipper factor (HBZ), expression vector was generated from the *HBZ* ORF including the 3′ long terminal repeat (LTR) of plasmid pCSHTLV-I (15) by using oligonucleotides A and B. In parallel, the pUC 19 backbone from pCSHTLV-I was amplified by using primers C and D. After digestion by EcoRV and EcoRI, both the vector and insert were ligated, creating pCS-HBZ. Sequences of the primers are as follows: 5′-AACTTGATATCGCCTCTCCAGCGCCCG-3′ for primer A, 5′-AACTTGAATTCCACTTGGCCGTGGGCCAAG-3′ for primer B, 5′-AACTTGAATTCACTGGCCGTCGTTTTACAACGTCG-3′ for primer C, and 5′-AACTTGATATCAAGCTTGGCGTAATCATGGTCATAGC-3′ for primer D.

All T-cell lines (Jurkat, JPX9, TL-OmI, C91PL, HUT102, and MT2) were transfected by using Fugene 6 (Promega). For JPX9 cells, Tax expression was induced by the addition of 150 μM $ZnCl_2$ for various times. The cell culture medium was changed, and 24 h later, reporter constructs were transfected. 293T cells were transfected by a calcium phosphate procedure described previously (62). In the case of DNA and small interfering RNA (siRNA) cotransfection, 293T cells were first transfected with the siRNAs by using Lipofectamine 2000 (Invitrogen) reagent according to the manufacturer's instructions. After 24 h, the medium was changed, and the transfection of DNA vectors was done by the calcium phosphate procedure. For viral mRNA analysis, 48 h after the transfection of siRNAs with Lipofectamine 2000, cells were transfected with 2 μg of the HTLV-1 molecular clone pACH by using GeneJuice reagent (Novagen) for 20 to 24 h.

NMD assays and qRT-PCR. NMD assays with HeLa cells with the GlNS39 and GlWT constructs were performed as described previously (47), and mRNAs were measured by quantitative reverse transcription-PCR (qRT-PCR) using the QuantiTect SYBR green qRT-PCR kit (Qiagen) and β-globin primers. Similarly, for the analysis of *GADD45*α, *SLIT2*, *BAG1*, *ATF4*, and *MAP3K14* mRNA half-lives, total RNA was extracted by using the Nucleospin RNA kit (Macherey-Nagel). One-step qRT-PCR (QuantiTect SYBR green qRT-PCR kit) was further performed by using appropriate primers with normalization with respect to glyceraldehyde-3-phosphate dehydrogenase (GAPDH) mRNA (47).

In T cells, 2 μg of the WT or NS39 globin-*Renilla* luciferase construct was transfected together with 1 μg of firefly luciferase reporter plasmid, which was used for normalization. The NMD assay was carried out according to a dual-luciferase assay procedure reported previously (6). mRNAs were measured by qRT-PCR using the QuantiTect SYBR green qRT-PCR kit (Qiagen) and appropriate primers, as previously described (47). The values presented in the graphs correspond to the means of data from at least three independent measures, with error bars corresponding to standard deviations. The asterisks in the figures correspond to the results of Student's *t* test (two tailed and unpaired).

For the analysis of HTLV-1 RNA primer/probe sequences, cycling profiles and absolute quantitations of transcripts were carried out as previously described (54). The $\Delta\Delta C_T$ method was applied to verify the silencing of *UPF1*. The data presented are the means of data from six independent measurements. For *HBZ* mRNA analysis, 8 μg of pCS-HBZ and 1 μg of a *Renilla* luciferase expression vector plasmid were transfected into HeLa cells with Lipofectamine 2000 together with or without pSG-Tax (1 μg). The *HBZ sp1* mRNA was reverse transcribed by using the High Capacity cDNA reverse transcription kit (Roche Applied Science) by using primer 5′-AACTGTCTAGTATAGCCATCA-3′ and then PCR amplified with the following oligonucleotides: 5′-GCCGATCACGATGCGTTTCCC-3′ and 5′-GGCAGAACGCGACTCAACCG-3′.

Protein production, purification, and GST pulldown. Glutathione *S*-transferase (GST), GST-Tax, His-GST-INT6, and His-UPF1 were produced in BL21 Codon+ *Escherichia coli* cells. INT6 was produced and purified according to a protocol reported previously (60). The His-GST tag was removed after proteolysis overnight by use of a His-GST-tobacco etch virus (TEV) protease while dialyzing the eluted INT6 with buffer (50 mM NaH_2PO_4 [pH 8], 300 mM NaCl, 1 mM dithiothreitol [DTT], 5% glycerol), followed by an additional purification on Ni-nitrilotriacetic acid (NTA) resin. His-UPF1 was produced as previously reported (11). GST and GST-Tax proteins were produced as previously described (9). Briefly, bacteria were induced with isopropyl-β-D-thiogalactopyranoside (IPTG) at 28°C for 3 h. The bacteria were then resuspended in MTBS (150 mM NaCl, 12.5 mM Na_2HPO_4, 2.5 mM KH_2PO_4, 100 mM EDTA [pH 7.3], 10% glycerol), lysed by sonication (4 times for 30 s), and centrifuged at 10,000 rpm for 1 h. The lysate was incubated with glutathione-agarose beads in the presence of 1% Triton X-100. The beads were washed in DE80 buffer (20 mM Tris [pH 7.9], 5% glycerol, 80 mM KC1, 1 mM $MgC1_2$, 0.2 mM EDTA, 10 μM $ZnCl_2$, 0.5 mM DTT, 0.5 mM phenylmethylsulfonyl fluoride [PMSF]) plus 1% Triton X-100 and either eluted with elution buffer (20 mM reduced glutathione, 20 mM Tris-HCl [pH 7.9]) or incubated with purified UPF1 (11) or purified INT6 (60) in DE80 buffer plus 0.1% Triton and 5 mg/ml bovine serum albumin (BSA). After 3 washes, proteins were eluted from the beads and analyzed by immunoblotting.

Immunofluorescence. A total of 0.05×10^6 HeLa cells were transfected by the calcium phosphate procedure. Cells were fixed for 20 min with fresh 4% paraformaldehyde, washed 3 times, and incubated with phosphate-buffered saline (PBS)–1% BSA. Cells were incubated with the primary antibody for 1.5 h at room temperature, washed 3 times, and further incubated for 1 h with the secondary antibody. Finally, cells were mounted in 10 μl of Vectashield 4′,6-diamidino-2-phenylindole (DAPI) (1.5 μg/ml) (Vector Laboratories). Slides were observed with an LSM 510 confocal microscope (Zeiss). For quantification, fluorescence intensity was analyzed by using the ImageJ program (National Institutes of Health).

Immunoprecipitation. Immunoprecipitations were conducted as described previously (62), using the following antibodies: rabbit antisera to INT6 (C-20, N-19, or C-169, as indicated in the figures) (46, 48); rabbit polyclonal antibodies to UPF1 and UPF2 (65); mouse monoclonal antibody to phospho-UPF1, which was kindly provided by A. Yamashita (clone 8E6) (66); rabbit polyclonal antibody to phospho-Ser/Thr ATM/ATR substrate (catalog number 2851; Cell Signaling Technology); mouse monoclonal antibody to Tax (clone 474); and mouse monoclonal antibodies to the FLAG (clone M2; Sigma) and hemagglutinin (HA) (clone 7; Sigma) epitopes.

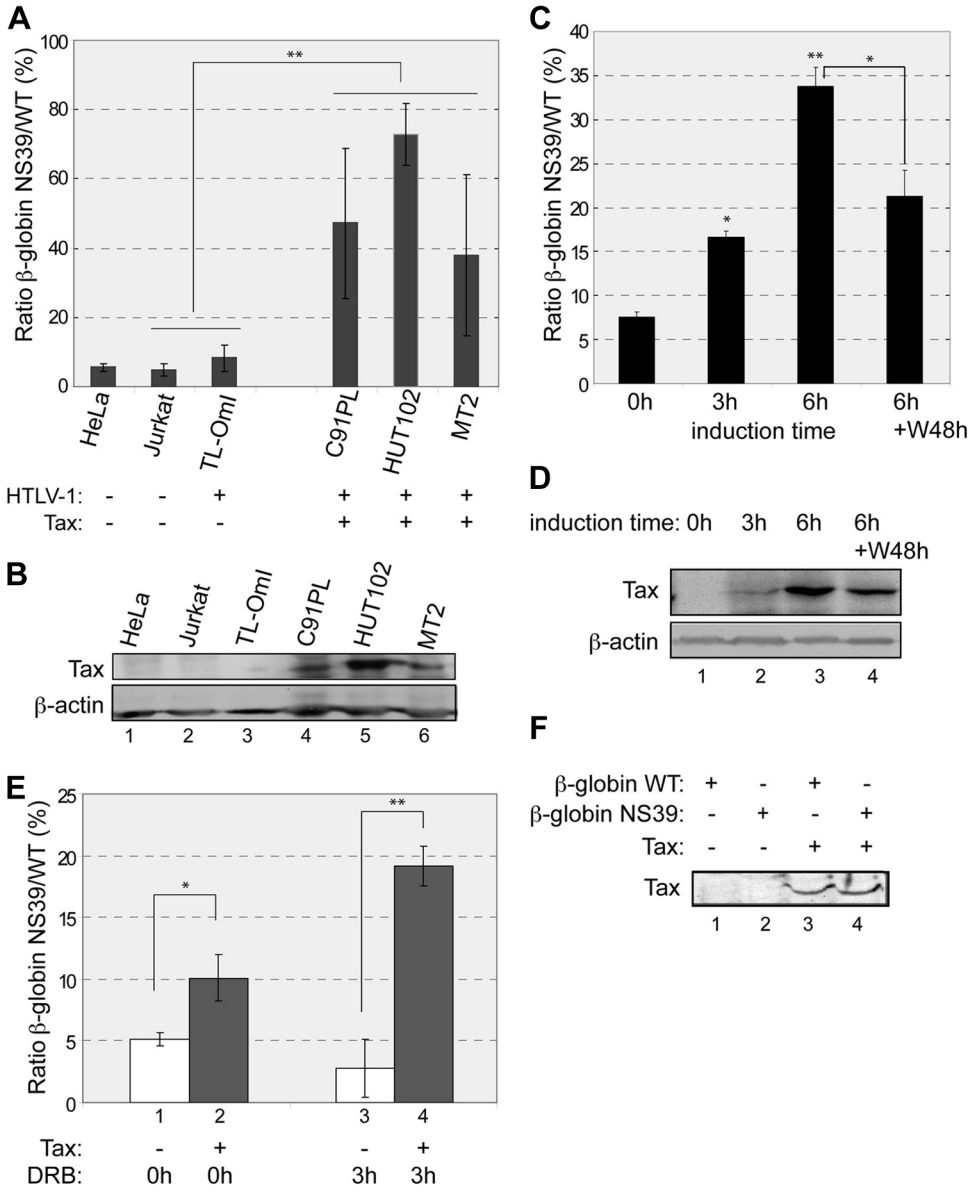

FIG 1 Effect of Tax on stability of NMD-prone mRNA. (A) NMD assays were performed with the indicated cell lines. The *Renilla* luciferase activity from the GlNS39 plasmid was normalized and expressed as a percentage of that from the GlWT plasmid. The bar graph represents mean values, with error bars corresponding to standard deviations. The Student *t* test corresponds to Tax-expressing cell lines versus non-Tax-expressing cell lines, as indicated (**, $P < 0.01$). (B) Extracts from panel A were analyzed by immunoblotting with antibodies to Tax (top) and to β-actin (bottom). (C) NMD assays were performed with JPX9 cells without (0 h) or with Tax induction for 3 h or 6 h. The 6 h+W48h bar corresponds to cells washed and further cultured for 48 h after 6 h of induction (*, $P < 0.05$; **, $P < 0.01$ [Student's *t* test results refer to the 0-h conditions, except for 6 h+W48 {6 h of induction}]). (D) Extracts used in panel C were analyzed by immunoblotting with antibodies to Tax and to β-actin. (E) NMD assays were performed with HeLa cells in the absence (lanes 1 and 3) or in the presence (lanes 2 and 4) of Tax expression, without (lanes 1 and 2) or with (lanes 3 and 4) the addition of 100 μg/ml DRB for 3 h. The percentage of GlNS39 mRNA with respect to GlWT mRNA is represented as described above for panel A. (F) Extracts used in panel E were analyzed by immunoblotting with an antibody to Tax.

RESULTS

HTLV-1 Tax inhibits mRNA degradation via the NMD pathway. We first evaluated whether the NMD pathway is downregulated in HTLV-1-infected cells. This evaluation was carried out by performing NMD assays using reporter plasmids including either wild-type β-globin (GlWT) or a PTC at position 39 (GlNS39) fused to the *Renilla* luciferase coding sequence (6). Control or HTLV-1-infected cell lines (HeLa, Jurkat, TL-OmI, C91PL, HUT102, and MT2 cells) were transfected with these reporter plasmids, and the levels of luciferase activities corresponding to wild-type and NS39-mutated β-globin sequences were quantified. As expected, in the HeLa and Jurkat cell lines, the GlNS39-associated activity represented only a small percentage of the activity associated with wild-type β-globin (Fig. 1A). In contrast, in the cell lines expressing the complete provirus with an active 5′ LTR (C91PL, HUT102, and MT2), the levels of GlNS39-associated activity were increased and much closer to that corresponding to wild-type β-globin (Fig. 1A). The strongest effect was observed on

HUT102 cells, which express a higher amount of Tax than do C91PL and MT2 cells (Fig. 1B, compare lane 5 to lanes 4 and 6). Interestingly, in the TL-OmI cells, which include the HTLV-1 sequence but which do not express Tax (Fig. 1B, lane 3), the NMD activity evaluated by this assay was very similar to that observed for the control HeLa and Jurkat cell lines. These results suggested that the NMD activity is downregulated in HTLV-1-expressing cells and that Tax was possibly involved in this effect.

To address the role of Tax more directly, we carried out assays with JPX9 cells, which are Jurkat cell derivatives expressing Tax under the control of a metallothionein promoter which can be induced by the addition of Zn^{2+} cations in the culture medium (61). Depending on the duration of induction, we observed increasing Tax expression levels (Fig. 1D), which correlated with a significant increase in the level of activity of the GlNS39 reporter, with the ratio with respect to the wild type increasing from 7% in the absence of Tax to 34% at 6 h postinduction (Fig. 1C). We also carried out a reversal of Tax induction by washing the cells after a 6-h induction and culturing them for 48 h in the absence of Zn^{2+} cations. Under these conditions, the intracellular concentration of Tax decreased (Fig. 1D, compare lanes 3 and 4), and this correlated with a significant drop of the GlNS39/GlWT ratio from 34% to 21% (Fig. 1C). We also analyzed the decay of the mRNAs after a transcription blockade by the addition of the RNA polymerase II (Pol II) elongation inhibitor 5,6-dichloro-1-β-D-ribofuranosylbenzimidazole (DRB). In agreement with the luciferase activity measurements, a specific stabilization of the mRNA including the NS39 mutation in the presence of Tax was observed (see Fig. S1A in the supplemental material).

This NMD inhibition was also analyzed with HeLa cells, which were transfected with vectors expressing wild-type and NS39-mutated β-globin mRNAs without fusion to the *Renilla* luciferase coding sequence, and both mRNAs were quantified by qRT-PCR. According to previously reported observations (43), in the absence of Tax coexpression, the amount of GlNS39 mRNA was only 5% of that of GlWT (Fig. 1E, lane 1). In the presence of Tax, we observed a 2-fold increase in the GlNS39/GlWT ratio (Fig. 1E, lane 2, and F, lane 3). Moreover, when analyzed 3 h after the addition of DRB, this GlNS39/GlWT ratio dropped from 5% to 2.5% in the absence of Tax (Fig. 1E, lane 3), while this ratio increased from 10% to 18% in the presence of the viral protein (Fig. 1E, compare lanes 2 and 4, and see Fig. S1B in the supplemental material). This indicated a specific posttranscriptional effect of Tax on GlNS39 mRNA stability. Collectively, these observations indicated that Tax is able to stabilize an NMD-sensitive transcript.

Tax binding to INT6 and to the UPF1-UPF2 complex. We then analyzed the association of Tax with the NMD core factors. First, an immunoprecipitation directed against Tax in HUT102 cells was performed, and the presence of UPF1, UPF2, and INT6 was checked by immunoblotting. Jurkat cell extracts were used as a control. The intracellular concentrations of UPF1, UPF2, and INT6 were similar in both extracts (Fig. 2A, lanes 1 and 2). We found that Tax associates with these 3 factors in the HTLV-1-infected cell line HUT102 (Fig. 2A, lanes 3 and 4). Similar immunoprecipitations were done with antibodies to UPF1, UPF2, or INT6 by using RNase A-treated extracts from C8166 cells (see Fig. S2A in the supplemental material), and a Tax signal was detected specifically after immunoprecipitation with all three antibodies (see Fig. S2B, lane 1, in the supplemental material). In order to determine whether these interactions were direct, recombinant, highly purified INT6, GST-Tax, and His-UPF1 were produced (see Fig. S2C in the supplemental material). GST pulldown assays showed that Tax is able to interact with UPF1 as well as INT6 (Fig. 2B and C, lane 1). In contrast, purified INT6 and UPF1 were unable to interact directly together (Fig. 2D), in agreement with our previously reported observations indicating that the INT6-UPF1 interaction was dependent on RNA (47).

We further analyzed this network of interactions and how the presence of Tax affects the composition of the NMD complex. To this end, 293T cells were transfected with different combinations of vectors expressing Tax, INT6-FLAG, HA-UPF1, and HA-UPF2. Immunoprecipitations were carried out by using and antibody to the HA epitope, and immunoprecipitated proteins were analyzed by immunoblotting with antibodies to the HA epitope,

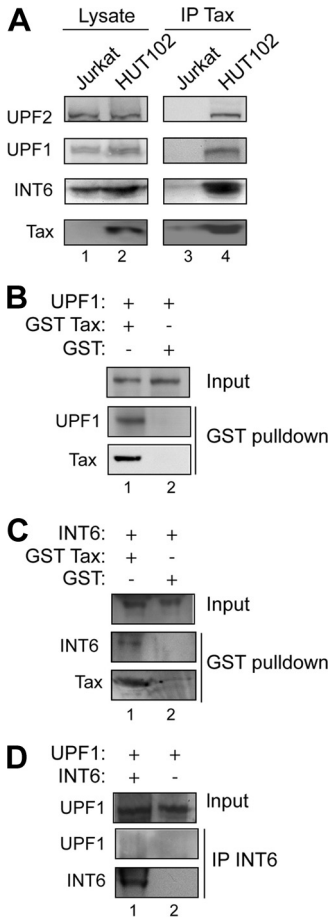

FIG 2 Interaction of Tax with NMD factors. (A) Extracts of Jurkat (lane 1) and HUT102 (lane 2) cells treated with RNase A were analyzed by immunoblotting with antibodies to UPF2, UPF1, INT6, and Tax. Using these Jurkat (lane 3) and HUT102 (lane 4) cell extracts, immunoprecipitation (IP) with an antibody to Tax was carried out, and the immunoprecipitates were analyzed by immunoblotting with the same set of antibodies. (B) GST, GST-Tax, and UPF1 were produced in bacteria and purified. UPF1 was mixed with GST-Tax (lane 1) or GST (lane 2), and a GST pulldown was carried out. The presence of UPF1 (middle) and Tax (bottom) in the eluates was assessed by immunoblotting. The top panel corresponds to 2% of the input. (C) Same as B, with purified INT6 instead of UPF1. (D) Purified INT6 and UPF1 were mixed, and immunoprecipitation was carried out with the N-19 antibody to INT6 (lane 1). The immunoprecipitate was analyzed by immunoblotting with antibodies to UPF1 (middle) and to INT6 (bottom). As a control, the same experiment was done in the absence of purified INT6 (lane 2).

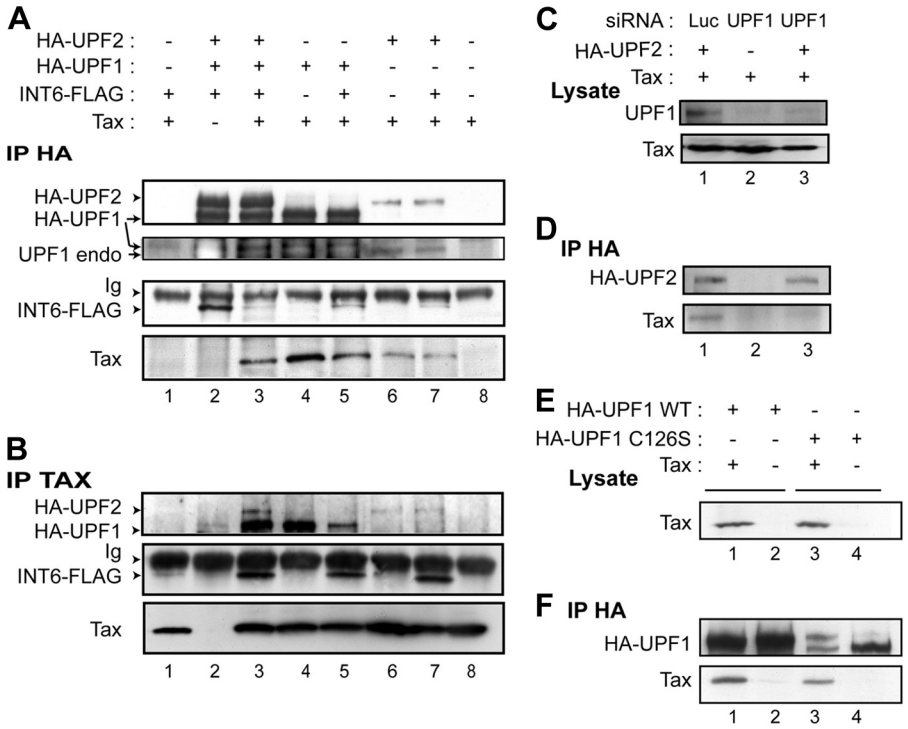

FIG 3 Network of interactions between Tax, INT6, UPF1, and UPF2. (A) Extracts of 293T cells transfected with Tax, INT6-FLAG, HA-UPF1, and HA-UPF2 expression vectors, as indicated, were used for immunoprecipitations using the antibody to the HA epitope. Immunoprecipitates were analyzed by immunoblotting using antibodies to HA (top), UPF1 (top middle), FLAG (bottom middle), and Tax (bottom). Ig marks the signal of the immunoglobulin heavy chain. (B) The same extracts were also immunoprecipitated with an antibody to Tax, and immunoprecipitates were analyzed by immunoblotting with antibodies to HA (top), FLAG (middle), and Tax (bottom). (C) 293T cells were transfected with either control (luciferase) (lane 1) or anti-UPF1 (lanes 2 and 3) siRNA duplexes as well as with vectors expressing Tax (lanes 1 to 3) and HA-UPF2 (lanes 1 and 3). Protein levels of endogenous UPF1 (top) and Tax (bottom) were monitored by immunoblotting. (D) Extracts of these transfected cells were used for immunoprecipitations carried out with the antibody to HA, and immunoprecipitates were analyzed by immunoblotting with antibodies to HA (top) and to Tax (bottom). (E) 293T cells were transfected with vectors expressing HA-UPF1, either the wild type (lanes 1 and 2) or including the C126S mutation (lanes 3 and 4) and Tax (lanes 1 and 3). Tax expression in the cell extracts was monitored by immunoblotting. (F) Extracts of these transfected cells were used for immunoprecipitations using the antibody to HA, and coimmunoprecipitated proteins were analyzed by immunoblotting with antibodies to HA (top) and to Tax (bottom).

UPF1, the FLAG epitope, and Tax (Fig. 3A). In agreement with data from the experiments described above, the immunoprecipitations of both UPF1 and UPF2 led to a clear Tax signal (Fig. 3A, bottom, lane 3). Similar results were obtained when HA-UPF1 and HA-UPF2 were transfected and immunoprecipitated separately (Fig. 3A, lanes 4 and 6, respectively); however, in the latter case, the HA-UPF2 and Tax signals were markedly weaker. This is likely due to a stabilizing effect of UPF1 on UPF2 expression under these conditions. By precipitating Tax, we confirmed its association with HA-UPF1, HA-UPF2, and INT6-FLAG (Fig. 3B, lanes 1, 3, 4, and 6). As a control for the specificity of Tax binding to these factors, we checked that Tax does not bind to coexpressed FLAG-green fluorescent protein (GFP) under these conditions (see Fig. S3B and S3C in the supplemental material). In these experiments, the association of Tax with HA-UPF2 was possibly mediated by endogenous UPF1. In this regard, a weak endogenous UPF1 signal was detected after the immunoprecipitation of HA-UPF2 alone (Fig. 3A, top middle, lanes 6 and 7). In order to clarify this point, we silenced UPF1 by RNA interference while transiently expressing Tax and HA-UPF2 (Fig. 3C). The level of Tax associated with HA-UPF2 was then reduced to a background level (Fig. 3D, bottom, compare lanes 1 and 3), indicating that UPF1 is likely to bridge Tax and UPF2. In this regard, by using the UPF1 C126S mutant, a mutant that does not bind UPF2 (33), it was observed that the binding of Tax to UPF1 was independent of its association with UPF2 (Fig. 3E and F). Collectively, these experiments confirmed that Tax associates with INT6 (16) and showed the binding of Tax to the core NMD complex through an interaction with UPF1.

Displacement of INT6 from UPF1 by Tax binding. In the same experiment, it was also observed that Tax expression decreased the amount of INT6 immunoprecipitated by UPF1 and UPF2, suggesting that Tax prevents the association of INT6 with these NMD factors (Fig. 3A, bottom middle, compare lanes 2 and 3). This observation was not related to a weaker expression of FLAG-INT6 (see Fig. S3A in the supplemental material). Similarly, while a clear association of Tax with HA-UPF1 was observed after the immunoprecipitation of HA-UPF1 or Tax, this level of binding was decreased when INT6 was coexpressed (Fig. 3A and B, compare lanes 4 and 5). These data suggested that Tax binds INT6, forming a complex that cannot associate with the upstream frameshifts (UPFs). We confirmed this with endogenous NMD proteins in HeLa cells, where INT6 coimmunoprecipitated much less endogenous UPF1 in the presence of Tax (compare lanes 1 and 2 in Fig. S3E, top, in the supplemental material). These observations support the notion that Tax competes for the binding of INT6 to an NMD complex including UPF1. This point was also addressed by performing confocal microscopy analyses to observe

the subcellular localizations of these proteins. We observed that in the absence of Tax, approximately 80% of the rare HA-UPF1 cytoplasmic foci were also stained by the antibody to INT6, while in the presence of Tax, no more than 20% of UPF1 spots colocalized with INT6 (see Fig. S4A and S4B in the supplemental material). These combined results led us to conclude that Tax, by interacting with both UPF1 and INT6, impairs their association.

Tax leads to the accumulation of UPF1 in P-bodies. In order to better understand the effect of Tax binding on the functioning of UPF1, we further analyzed how Tax modifies the subcellular localization of UPF1. It was previously reported that UPF1 is partially localized in P-bodies and that the inhibition of mRNA degradation increases this localization (57). For these analyses, HeLa cells were transfected with vectors expressing HA-UPF1, DCP1-red fluorescent protein (RFP) (a component of the P-bodies), and either a control or a Tax expression vector (Fig. 4A). In the absence of Tax, and in agreement with previous reports, DCP1 fluorescence was observed mainly in a limited number (3 to 9) of small cytoplasmic foci corresponding to the P-bodies (35) (Fig. 4Ac). UPF1 was homogeneously distributed in the cytoplasm, with rare small foci which often colocalized with DCP1 (Fig. 4Ab, and see Fig. S4C in the supplemental material). In the presence of Tax, numerous and larger cytoplasmic foci of UPF1 appeared (Fig. 4Ag). This point was confirmed by quantifying the number of UPF1 foci and the UPF1 fluorescence present in three cellular compartments (the cytoplasm, cytoplasmic foci, and nucleus). This analysis confirmed the increase in the number of UPF1 foci and showed that the presence of Tax leads to a significant decrease in the diffuse cytoplasmic staining of UPF1 (−17%) to the benefit of cytoplasmic foci (10-fold increase) (Fig. 4B and C). Similarly, the DCP1 foci were much larger than those in the absence of Tax (compare Fig. 4Ac and h, and see Fig. S4C, S5A, and S5B in the supplemental material). UPF1 and DCP1 still colocalized in the presence of Tax (Fig. 4Ai and j, and see Fig. S4C in the supplemental material). We were also able to identify other known components of the P-bodies, Ago2 and p54, in these DCP1 cytoplasmic foci, suggesting that Tax increases the storage of UPF1 in P-bodies and causes their enlargement (Fig. 4D, and see Fig. S5A in the supplemental material). In the absence of Tax, INT6 similarly showed discrete cytoplasmic foci that colocalized with those corresponding to DCP1 fluorescence, which is in agreement with a role of INT6 in NMD (see Fig. S6 in the supplemental material). In the presence of Tax, the sizes of the INT6 foci did not increase as for UPF1 and marginally colocalized with the enlarged P-bodies (see Fig. S4A, S4B, and S6 in the supplemental material). In agreement with the notion that Tax causes a disruption of UPF1/INT6 binding, these observations clearly show that the viral protein affects the subcellular localizations of INT6 and UPF1 differently. In order to correlate the accumulation of UPF1 in P-bodies with its interaction with Tax, we first looked at the localization of the viral protein in cells expressing DCP1-RFP and p54-GFP. In the absence of Tax, DCP1 and p54 displayed the usual pattern for P-bodies, while Tax led to the formation of DCP1 and p54 cytoplasmic foci with unusual sizes and numbers (Fig. 4Db, c, g, and h, and see Fig. S4C in the supplemental material). This effect was dependent on the amount of Tax (data not shown). Moreover, we were able to identify a colocalization of Tax with these unusual P-bodies (Fig. 4D). In addition, in HA-UPF1-transfected cells, we observed an increased presence of Tax in the cytoplasm and several foci exhibiting Tax, UPF1, and DCP1 costaining (Fig. 4A). These observations are in agreement with the interaction of Tax with UPF1 during RNA processing and suggest that Tax might play a direct role in the alteration of the P-bodies.

In P-bodies, UPF1 is dephosphorylated by the phosphatase PP2A, which is recruited via the SMG5-SMG7 complex (51) and then leaves the P-bodies to possibly reenter a novel round of RNA processing (17). Accordingly, we further tested whether the accumulation of UPF1 in P-bodies was linked to an alteration of this dephosphorylation step. To address this point, cells were transfected with the HA-UPF1 vector together with either a control or a Tax expression vector (Fig. 5A). Extracts were analyzed with an antibody raised against phosphorylated UPF1 (66) and another one which recognizes the S/TQ motifs phosphorylated by phosphatidylinositol 3-kinase kinases (PI3KKs) such as SMG1, the NMD UPF1 kinase. The expression of Tax increased the intensity of the signal detected with both antibodies (Fig. 5A, middle and bottom, compare lanes 1 and 2), while the total amount of HA-UPF1 was unchanged (Fig. 5A, top). A densitometric analysis of the blot showed a >2-fold increase in the phosphorylated form after normalization to the total amount of UPF1. An immunoprecipitation of Tax was also performed with these extracts and revealed that Tax associates with phosphorylated UPF1 (Fig. 5B, middle and bottom). We further analyzed the association of these phosphorylated forms of UPF1 with SMG5, which is part of the NMD dephosphorylation complex. Cells were transfected with different combinations of Tax, HA-SMG5, and UPF1 (without the HA tag) expression plasmids. Immunoprecipitations were carried out against the HA tag of SMG5, and the presence of UPF1 in the immunoprecipitates was analyzed by immunoblotting. In the absence of Tax, UPF1-SMG5 complexes could not be detected, presumably due to UPF1 dephosphorylation in the presence of overexpressed SMG5 (Fig. 5C and D, lane 1). In the presence of Tax and with similar levels of immunoprecipitated HA-SMG5, UPF1 was clearly detected (Fig. 5D, lane 2). Collectively, these data suggest that Tax is able to inhibit NMD-dependent UPF1 dephosphorylation, leading to the stabilization of the SMG5-UPF1 association.

Inhibition of NMD by Tax depends on its interaction with INT6. In order to better understand how Tax inhibits NMD, we tested the effects of three different Tax mutants: Tax M22, which is inactive for NF-κB activation (58); Tax M47, which is inefficient in transactivating CREB-responsive promoters (32); and Tax K1-10R, in which all lysines potentially modified by ubiquitination were mutated to arginines. The latter mutant is defective with respect to both the NF-κB and CREB pathways (13, 50). The effects of these Tax mutants were assessed by using the NMD assay. In agreement with the results shown in Fig. 1A, the level of expression of wild-type Tax in HeLa cells increased the GlNS39/GlWT ratio to approximately 9%. The expression of Tax M22 and Tax K1-10R led to a stronger increase (20% and 18%, respectively). In contrast, with the Tax M47 mutant, the GlNS39/GlWT ratio was unchanged with respect to that observed in the absence of Tax, indicating a complete lack of activity of this mutant (Fig. 6A). We further tested whether this inactivity was due to a protein-protein interaction defect. Cells were transfected with vectors expressing HA-UPF1 and INT6-FLAG together with a control plasmid or the different Tax expression vectors (Fig. 6B to D). Tax immunoprecipitations were carried out, and the presence of HA-UPF1 and INT6-FLAG in the immunoprecipitates was analyzed by immunoblotting. Interestingly, the binding of M47 to HA-UPF1 was slightly increased (1.5-fold), but the interaction with INT6-FLAG

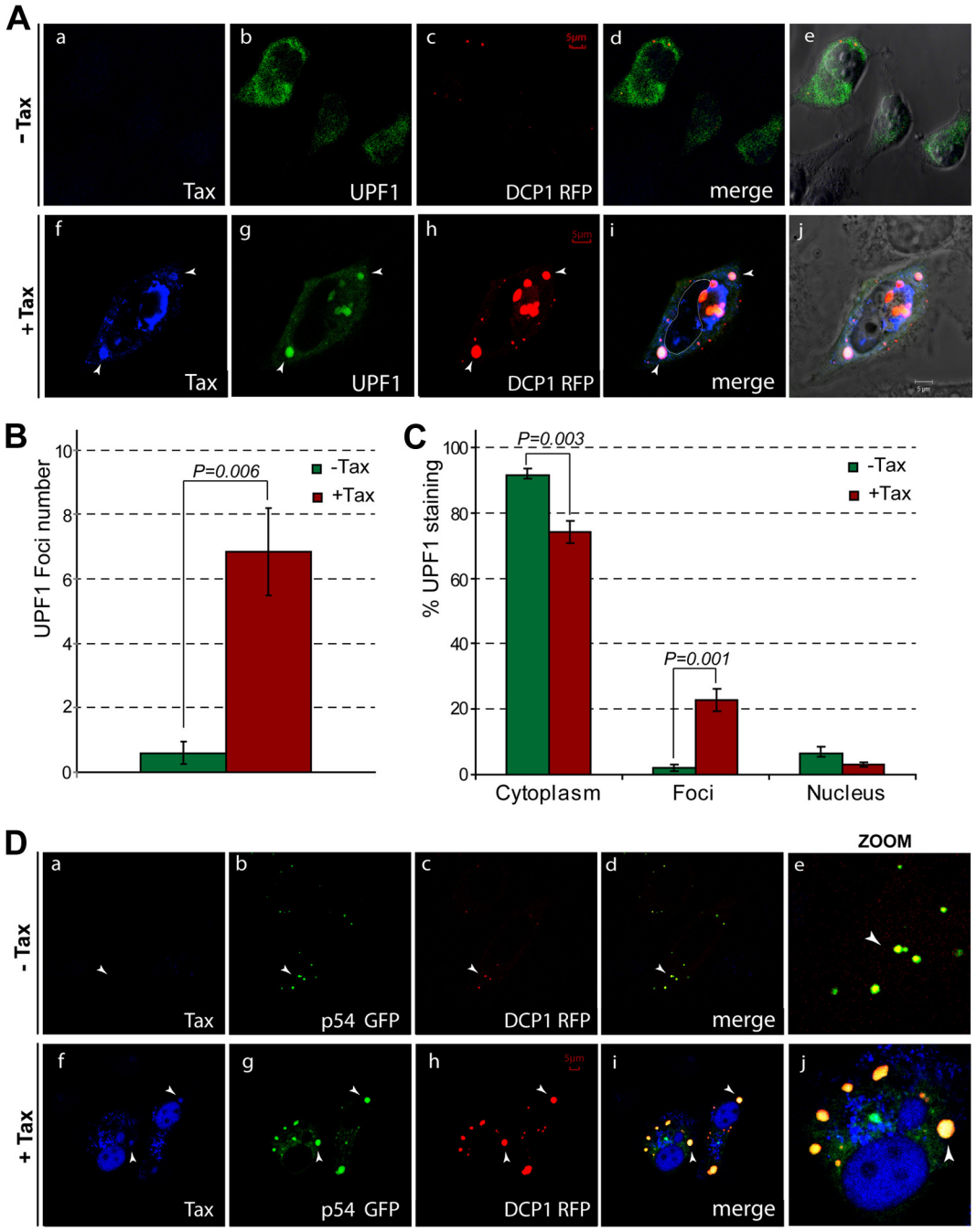

FIG 4 Colocalization of Tax and NMD factors with P-bodies. (A) Confocal microscopy analysis of HeLa cells transfected with HA-UPF1 and DCP1-RFP expression vectors together with a control (a to e) or Tax (f to j) expression vector. Immunostaining was done with antibodies to Tax (blue) (a and f) and to HA (green) (b and g). The DCP1-RFP fluorescence was also analyzed (red) (c and h). Panels d and i correspond to the superposition of the three fluorescences, with the nucleus limits identified from the transmission view, highlighted with a white line. Panels e and j correspond to the superposition of all three fluorescences with the transmission view. (B) Quantification of the UPF1 foci observed in the absence or presence of Tax. The numbers of UPF1 foci in several cells ($n = 10$) were determined, and the mean number of foci under both conditions is represented (green, without Tax; red, with Tax), with error bars corresponding to standard deviations. The statistical significance of the difference between both conditions was calculated with Welch's *t* test and is indicated on the graph. (C) Similarly to panel B, the UPF1 fluorescence in the cytoplasm outside the foci, in the cytoplasmic foci, and in the nucleus in the absence or the presence of Tax was quantified and is represented in a bar graph. (D) Confocal microscopy analysis of HeLa cells transfected with vectors coding for the P-body components p54-GFP and DCP1-RFP without or with 0.1 μg of the Tax-expressing plasmid. Immunostaining of Tax appears in blue (a and f), along with p54-GFP fluorescence (green) (b and g) and DCP1-RFP fluorescence (red) (c and h). Panels d and i correspond to a superposition of the three fluorescences, and panels e and j correspond to an enlargement of this image.

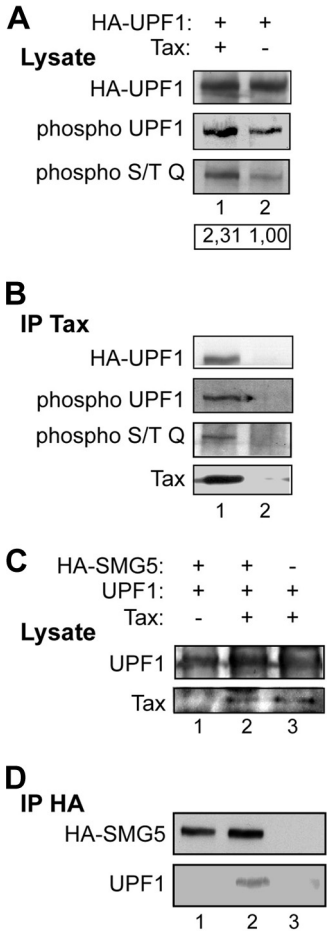

FIG 5 Tax stabilizes the phosphorylated forms of UPF1. (A) 293T cells were transfected with Tax and HA-UPF1 expression vectors, as indicated. Cell extracts were analyzed by immunoblotting with an antibody to HA (top), phosphorylated UPF1 (middle), or phosphorylated S/TQ motifs (bottom). The signals of phosphorylated UPF1 were quantified by densitometric analysis and normalized to those corresponding to total UPF1. The ratios of phosphorylated UPF1/total UPF1 are indicated below the blot images. (B) Extracts from panel A were immunoprecipitated with an antibody to Tax, and immunoprecipitates were analyzed by immunoblotting with the indicated antibodies. (C) 293T cells were transfected with HA-SMG5, UPF1, and Tax expression vectors, as indicated. Cell extracts were analyzed by immunoblotting using antibodies to UPF1 (top) and to Tax (bottom). (D) Extracts from panel C were immunoprecipitated with the antibody to HA, and immunoprecipitates were analyzed with antibodies to HA (top) and to UPF1 (bottom).

was markedly reduced (4-fold less) (Fig. 6D). In this experiment, equal quantities of Tax protein were precipitated (Fig. 6C). This observation indicates that Tax residues L319 and L320 are necessary for the association with INT6. We also observed that Tax M22 and Tax K1-10R bound more strongly to both INT6-FLAG (2-fold) and HA-UPF1 (3-fold) than did WT Tax. In these cases, it seems likely that the stronger interactions with INT6 and UPF1 resulted from an increased availability of Tax due to its loss of interactions with other partners, in particular those belonging to the NF-κB pathway. Hence, the interaction with INT6 appears to be essential for the inhibitory effect of Tax on NMD: Tax M22 and K1-10R, which bind INT6 more efficiently than the wild type, are more active in inhibiting the NMD, whereas Tax M47, which interacts poorly with this protein, is inactive. In induced JPX9 cells, it was also observed by performing an NMD assay that the overexpression of INT6 caused a significant decrease (39%) in the inhibition of NMD, likely due to Tax titration (see Fig. S7 in the supplemental material). A similar effect was observed with the overexpression of UPF1 (see Fig. S7 in the supplemental material).

We also analyzed the effects of the M22 and M47 Tax mutants on the P-body aspect. As expected, Tax M22 was able to increase the number and size of DCP1-RFP foci similarly to WT Tax (in both cases, approximately 80% of the cells exhibited abnormal P-bodies), while only a limited number of unusual DCP1-RFP foci were observed with Tax M47 (11% of the cells) (Fig. 6E). These data show a correlation between the abilities of Tax to functionally inhibit NMD and to modify the aspect of P-bodies. Moreover, a comparative analysis of P-body profiles and interaction efficiencies with the M47 mutant suggested that the Tax-INT6 association is a prerequisite for P-body deformation by UPF1 sequestration.

HTLV-1 mRNAs are sensitive to NMD. The identification of NMD inhibition in HTLV-1-expressing cells raised the question of the sensitivity of the various viral mRNAs to this process. To address this question, we transfected plasmid pACH, which includes the entire HTLV-1 provirus, into cells that were previously treated with either control or UPF1 siRNAs. Twenty-four hours after provirus transfection, RNAs were prepared from these cells and analyzed by qRT-PCR (54). Under these conditions, the level of UPF1 mRNA was reduced to approximately 20% of its level in control cells, indicating effective silencing (Fig. 7A). Although the sensitivities of the viral mRNAs to UPF1 silencing were variable, a significant increase was seen for all of them (Fig. 7B). This analysis suggested that viral RNAs are prone to UPF1-mediated degradation. Since we previously demonstrated that Tax was an important player in HTLV-1-associated NMD inhibition, we further tested whether it can stabilize such viral RNAs. To do so, we analyzed the *HBZ* transcript, which was selected because its transcription is much less sensitive to Tax than the other sense transcripts (V. Mocquet, unpublished data). *HBZ* mRNA is produced by the transcription of the antisense strand from the 3′ LTR and is expressed with or without alternative splicing. Here, HeLa cells were transfected with a provirus similar to the ACH used in Fig. 7B but lacking its 5′ LTR as well as the first 4 kb of coding sequence. Thus, this plasmid expresses *HBZ* mRNAs only under the control of the 3′ LTR. The alternatively spliced isoform of HBZ (sp1) is the main expressed isoform in ATL cells (10). Hence, we analyzed by qRT-PCR the decay of *HBZ sp1* mRNA, after the addition of DRB, in the presence or absence of Tax. This experiment showed that Tax increases the half-life of the *HBZ sp1* mRNA 2.6 times (Fig. 7C). Collectively, these data support the notion that Tax enhances the amount of some viral mRNAs by also acting at the posttranscriptional level through the inhibition of the NMD pathway.

Stability of NMD-prone cellular mRNA is modified in the presence of Tax. By testing a series of NMD-prone mRNAs, we previously observed that INT6 was required for the degradation of a subgroup of them, including *GADD45*α, *SLIT2*, *BAG1*, and *ATF4/CREB-2* but not *MAP3K14* (47). To further evaluate the consequences of NMD inhibition by Tax, we analyzed the half-lives of these five endogenous mRNAs in JPX9 cells with or without Tax induction. Cells were harvested at 0 h, 1.5 h, and 4 h after the addition of DRB, and these mRNAs were quantified by qRT-PCR, while Tax levels were monitored by immunoblotting (Fig. 8F). Interestingly, the *GADD45*α, *SLIT2*, and *ATF4/CREB-2*

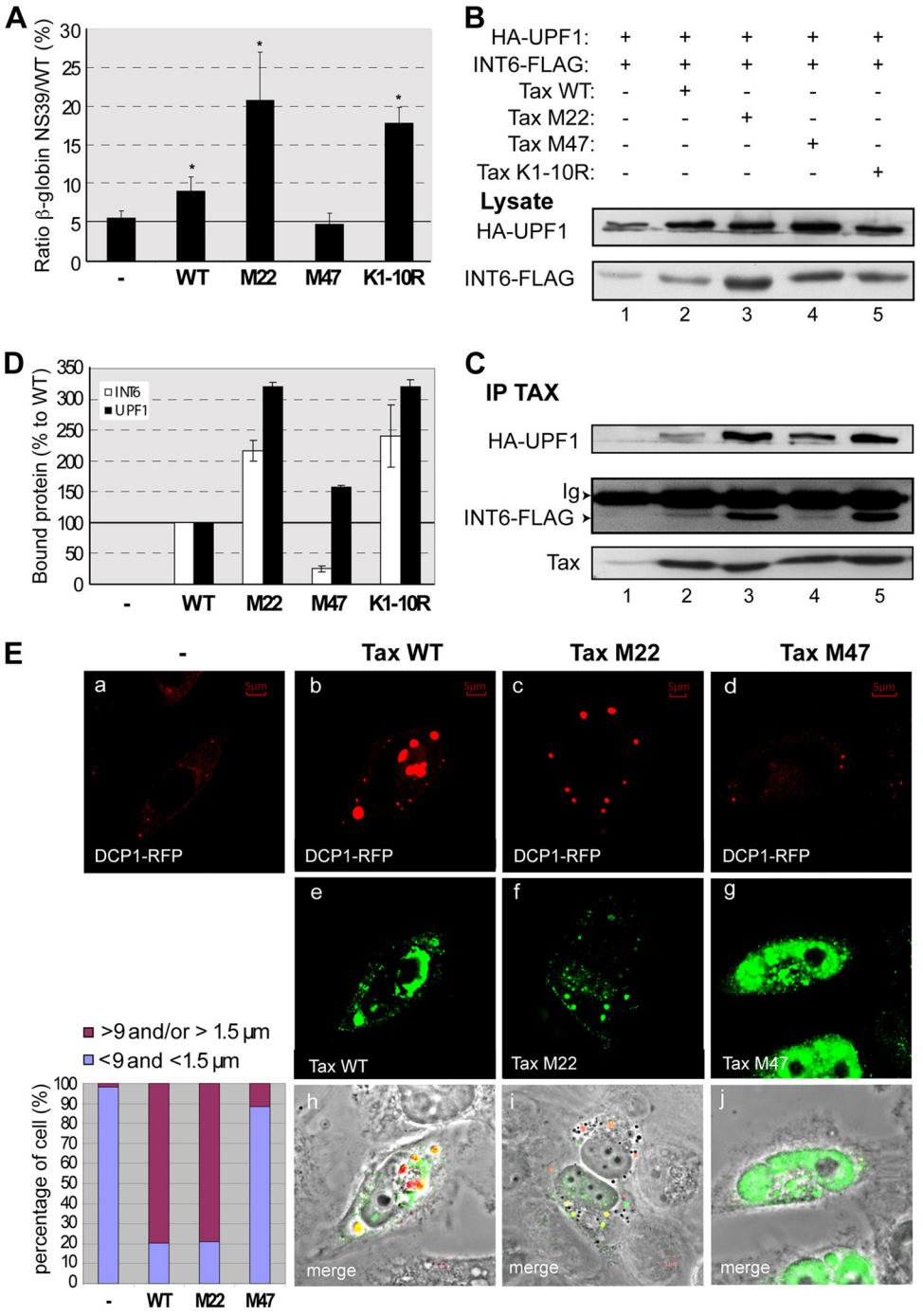

FIG 6 Tax mutants affect NMD efficiencies differently. (A) NMD assays were carried out, as described in the legend of Fig. 1A, with the cotransfection of control (−), wild-type (WT) Tax, Tax M22, Tax M47, and Tax K1-10R expression vectors (*, $P < 0.05$ [Student's *t* test *P* values refer to the control point {−}]). (B) Cells were transfected with the HA-UPF1, INT6-FLAG, and Tax expression vectors, as indicated. Extracts from these cells were analyzed by immunoblotting with antibodies to HA (top) and to FLAG (bottom). (C) Extracts from panel B were immunoprecipitated by using an antibody to Tax, and immunoprecipitates were analyzed with antibodies to HA (top), FLAG (middle), and Tax (bottom). Ig marks the immunoglobulin heavy chain. (D) Signals corresponding to HA-UPF1 and to INT6-FLAG in the immunoprecipitates from panel C were quantified and normalized to the signals detected in the extracts. The mean values obtained from three experiments are represented in a bar graph, with error bars corresponding to standard deviations. (E) Confocal microscopy analysis of HeLa cells transfected with constructs expressing DCP1-RFP together with a control (a) or vectors expressing either WT Tax (b and e), Tax M22 (c and f), or Tax M47 (d and g). The fluorescence from DCP1-RFP (red) and Tax immunostaining (green) is shown. The proportions of normal P-bodies ($n < 9$ and a diameter of <1.5 μm) and unusual P-bodies ($n > 9$ and/or a diameter of >1.5 μm) are presented in a bar graph.

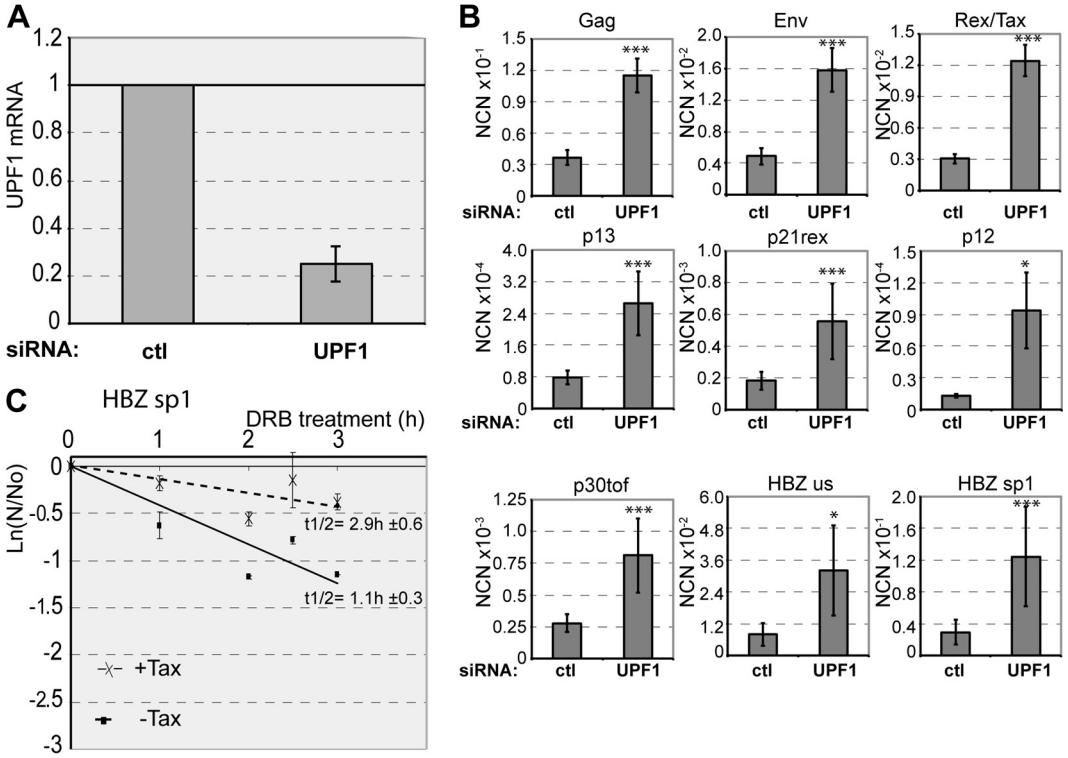

FIG 7 HTLV-1 mRNAs are sensitive to NMD. (A) HeLa cells were transfected first with 20 pmol of a control or UPF1 siRNA and 48 h later with the HTLV-1 molecular clone construct pACH. UPF1 mRNA from these cells was quantified to control the silencing efficiency. (B) Using these cells, the normalized copy number (NCN) of the various HTLV-1 transcripts in control and UPF1-silenced cells was determined by qRT-PCR. The mean values obtained from six experimental points are presented in the bar graphs for each viral transcript, with error bars corresponding to standard deviations. The results of Student's *t* tests are also indicated (∗, $P < 0.05$; ∗∗∗, $P < 0.001$). (C) The half-life of the *HBZ sp1* mRNA was measured in HeLa cells transfected with or without Tax. The amounts of *HBZ* mRNA were measured by qRT-PCR at each time point after the addition of DRB and normalized to *Renilla* mRNA levels, and the natural logarithm of the values, expressed as fractions to time zero, were plotted against time.

mRNA half-lives were significantly increased in the presence of Tax (3.4-, 4.1-, and 3.9-fold, respectively). The *BAG1* mRNA half-life increased 1.9-fold (Fig. 8A to D). This was not the case for the *MAP3K14* mRNA (Fig. 8E). These observations confirmed that by acting on INT6, Tax is also able to increase the stability of various cellular NMD-sensitive mRNAs.

DISCUSSION

By analyzing the inhibitory effect of HTLV-1 factors on the NMD pathway, our results point to an important action of Tax through interactions with the INT6 and UPF1 cellular proteins. Our observations also add evidence for an important role of INT6 in mRNA degradation by the NMD pathway. While UPF1 inhibits translation by associating with eIF3 (31), our data suggest that INT6 participates in this eIF3-UPF1 complex. An issue which will require further evaluation is the dynamics of the process. Indeed, some considerations indicate that INT6 might be present at early as well as at late steps of the processing of an mRNA targeted for degradation (4, 47, 67). Interestingly, it was reported previously that a fraction of INT6 was associated with chromatin (8), and purification experiments have shown its presence in the RNA Pol II holoenzyme (P. Jalinot and J.-M. Egly, unpublished data). Together with our previous characterization of an interaction of INT6 with the CBP80 subunit of the cap binding complex (47), these observations indicate that INT6 might be loaded onto mRNA at an early step of its processing. Once the pioneer round of translation is completed, the mRNP is reconfigured (39) and routed toward active translation, with the presence of INT6 in the eIF3 complex then being necessary or not (26, 67). Alternatively, when the mRNA includes a PTC or another feature favoring NMD, UPF1 is phosphorylated, inhibits translation through interactions with eIF3, and triggers mRNA degradation (31, 40). The presence of INT6 in P-bodies, which concentrate NMD factors and degradative enzymatic activities, indicates that this protein is likely to stick to the mRNP until its degradation, as UPF1 does. This is not the case for other eIF3 subunits (26), which are likely removed at an earlier step.

The HTLV-1 Tax protein has been described as a potent transactivator of provirus expression but also as an immortalizing protein with pleiotropic activities. In this report, we show a novel effect of Tax: the inhibition of the NMD pathway. We observed that Tax binds both INT6 and UPF1 but inhibits the presence of both proteins in the same complex. The analysis of Tax mutants indicated that the Tax-INT6 association is necessary for NMD inhibition, and our data suggest that Tax sequesters INT6 out of reach from UPF1. Tax also binds to UPF1 and causes an increase in the amount of phospho-UPF1. These activities coincide with an enhanced localization of UPF1 in the P-bodies, in which Tax was also partially detected. Tax-expressing cells also showed an increase in the number and size of the P-bodies. In agreement with previous studies performed in particular with a chemical inhibitor of NMD (17), this effect is likely due to the inhibition of mRNA

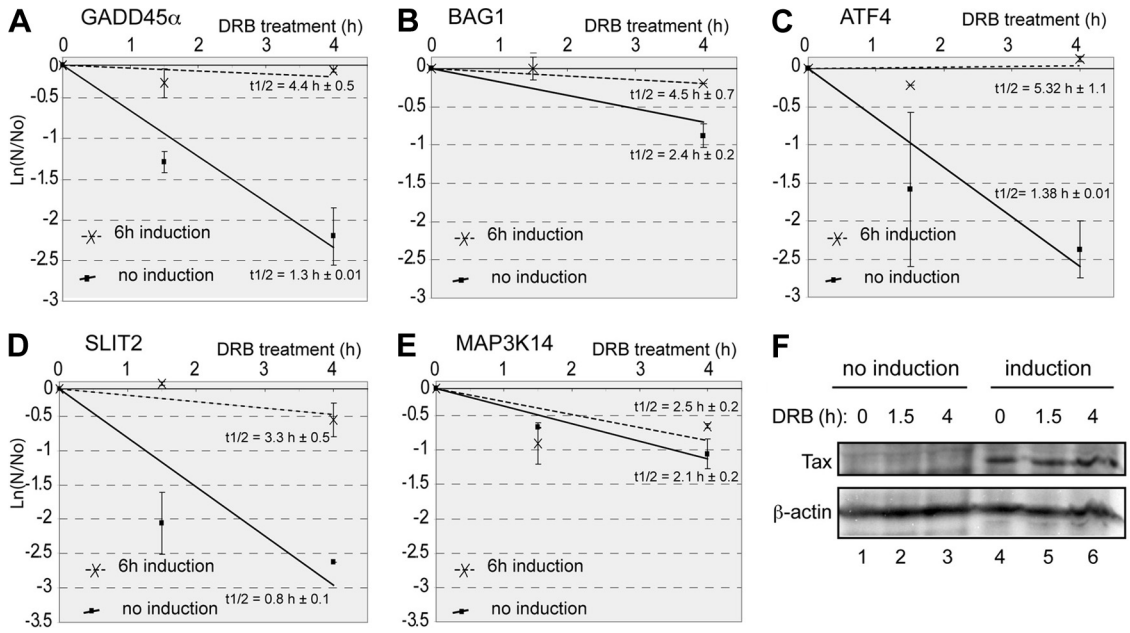

FIG 8 (A) The half-life of the *GADD45*α mRNA was measured in noninduced (squares and full line) and 6-h-induced (crosses and dotted line) JPX9 cells. The amounts of *GADD45*α mRNA were measured by qRT-PCR at each time point after the addition of DRB and normalized to GAPDH mRNA levels, and the natural logarithms of the values, expressed as fractions to time zero, were plotted against time. Each point corresponds to the mean of data from three independent measurements, and error bars indicate standard deviations. The half-life of the mRNA under both conditions was calculated and is indicated in the graph. (B to E) Same as in panel A but for *BAG1* (B), *ATF4/CREB-2* (C), *SLIT2* (D), and *MAP3K14* mRNAs (E). (F) Zero hours, 1.5 h, and 4 h after the addition of DRB, extracts of noninduced (lanes 1 to 3) or 6-h-induced (lanes 4 to 6) JPX9 cells were prepared and analyzed by immunoblotting using antibodies to Tax (top) and to β-actin (bottom).

degradation. The colocalization of Tax within the P-bodies revealed a new cytoplasmic localization of this viral protein. Interestingly, the modification by Tax of other cytoplasmic granules known to be involved in mRNA processing was recently documented (38). Moreover, through the SMG5 and SMG7 proteins, UPF1 was shown to be dephosphorylated by PP2A, thereby allowing its recycling (41). Knowing that Tax is able to maintain IKKγ in an active state by inhibiting its dephosphorylation by PP2A (22, 29), it is likely that Tax impedes the dephosphorylation of UPF1 by inhibiting this phosphatase in a similar manner. As a consequence, the Tax-UPF1 complexes would accumulate in the P-bodies, preventing the recycling of this core NMD factor and thereby interfering with complete mRNA degradation and inhibiting NMD (21) (Fig. 9).

It was recently reported that the inhibition of NMD is an important part of the development of tumorigenesis (63). Moreover, approximately 30% of cancers are considered to result from premature stop codons in tumor suppressor genes, which then escape NMD and lead to truncated dominant negative mutants. The Tax-dependent NMD inhibition that we observed might extend such an effect to an in-frame PTC due to mutations or alternative splicing events, which frequently occur in T cells (42). Considering our observation that NMD is globally downregulated in HTLV-1 cells expressing Tax, it can be speculated that this inhibition plays a role in the transformation of infected cells. Here, we limited our analysis of the impact of Tax on cellular mRNAs to those previously described to be stabilized after the silencing of UPF1, UPF2, or INT6 (45, 47, 65). Among these cellular genes, ATF4/CREB-2, for instance, which is regulated by NMD due to the presence of three uORFs (25), plays a role in HTLV-1 pathogenicity by heterodimerizing with AP-1 family transcription factors and has been associated with T-cell transformation through AP-1-responsive genes (23). Moreover, with the knowledge that modifications in RNA stability are an important source of gene expression alterations in stressed cells (20), future systematic studies of NMD-sensitive transcripts increased by Tax should help to define more precisely how this activity of Tax contributes to cell transformation. Among the viral genes, the expression of the antisense gene *HBZ* is clearly detectable throughout infection at the RNA level (56, 59). The current hypothesis is that the *HBZ* gene has a dual functionality: the *HBZ* mRNA promotes T-cell proliferation (55), while the HBZ protein suppresses Tax-mediated viral transcription (41). In line with its sensitivity to UPF1-mediated degradation, our data show that Tax significantly stabilizes *HBZ* mRNA. This observation illustrates the complexity of the cross talk between both viral proteins. By affecting both cellular and *HBZ* mRNAs, this inhibition of NMD by Tax is likely to contribute to cell transformation and the emergence of a leukemic clone of T lymphocytes. The inhibition of NMD can also be considered a potent means to significantly facilitate the expression of the HTLV-1 genome. In particular, ATF4/CREB-2 was reported previously to be involved in HTLV-1 LTR transactivation (24). This effect of Tax might then participate in the transcriptional induction of HTLV-1 provirus, since the increase of ATF4/CREB-2 protein levels by NMD inhibition is a well-described effect (25). Our data also show that some HTLV-1 mRNAs are sensitive to UPF1-mediated degradation. This suggests that viral mRNA expression downstream of activated transcription is also regulated at the posttranscriptional level. Thus, it is likely that in addition to its important effect on transcription, Tax would also intervene by

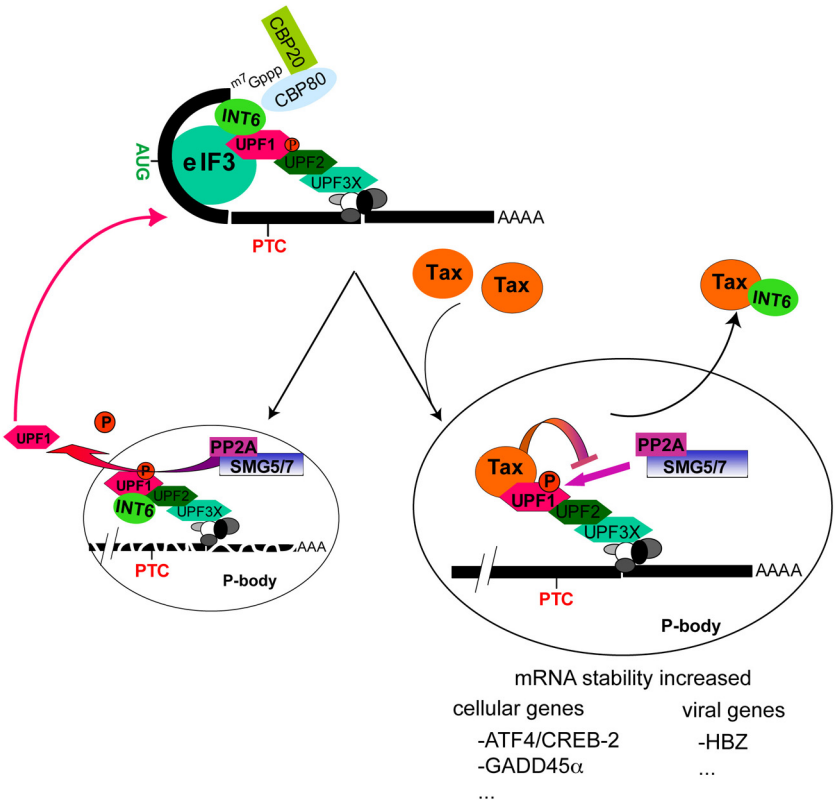

FIG 9 Summary scheme of the effect of Tax on the NMD pathway. In the case of an NMD-prone mRNA, UPF1 is phosphorylated by the SMG1 kinase and associates with UPF2 and UPF3. Under these conditions, UPF1 represses translation initiation by interacting with eIF3. Phosphorylated UPF1 also triggers an association with mRNA decay factors such as DCP1, XRN1, and the exosome component EXOSC2. After mRNA routing toward P-bodies, it is considered that UPF1 is dephosphorylated by the SMG5/7-PP2A complex and recycled (left bottom part of the scheme). In Tax-expressing cells, from the data presented in this report, Tax binds INT6, thereby impairing the INT6-UPF1 association. Tax also binds phospho-UPF1 and presumably prevents its normal dephosphorylation by PP2A, thus causing an accumulation of phospho-UPF1 in the P-bodies (right bottom part of the scheme). These combined effects lead to the stabilization of cellular as well as viral mRNAs by inhibiting their degradation.

allowing the escape of the RNAs from degradation. While NMD could be an effective protective mechanism against viral infection, Tax allows an escape from it, favoring the expression and persistence of the virus.

In conclusion, although NMD has already been associated with host-pathogen biology (2, 37), we report here for the first time that an HTLV-1 regulatory protein actively interferes with this pathway. While our observations establish that Tax is a major player in this inhibition, other viral proteins might also play a role. In this regard, it is worth mention that the NMD inhibition observed in HTLV-1-infected cell lines such as HUT102 was more potent than that observed in HeLa or Jurkat cells by expressing Tax alone. Whatever the contribution of other viral factors, our results show that Tax not only controls the transcription of viral and cellular genes but also acts on the posttranscriptional outcome of the corresponding mRNAs. Thus, it will be important in the future to consider this NMD effect to reach a complete understanding of the oncogenic effects of HTLV-1.

ACKNOWLEDGMENTS

We are grateful to L. Gazzolo and F. Mortreux for critical reading of the manuscript; A. Yamashita, S. Ohno, and H.-M. Jäck for providing us with antibodies; and N. Kedersha, A. Kulozik, C. Sun, and J. Cate for plasmids. We also thank A. Roisin for help with cell culture and C. Lionnet and F. Simian-Lermé for their assistance with microscopes.

This work was supported by a fellowship (V.M.) and a grant from the Association pour la Recherche sur le Cancer and by a fellowship (J.N.) from the Ligue Nationale contre le Cancer.

REFERENCES

1. **Abbas S, Erpelinck-Verschueren CA, Goudswaard CS, Lowenberg B, Valk PJ.** 2010. Mutant Wilms' tumor 1 (WT1) mRNA with premature termination codons in acute myeloid leukemia (AML) is sensitive to nonsense-mediated RNA decay (NMD). Leukemia **24**:660–663.
2. **Amor S, et al.** 2010. Alternative splicing and nonsense-mediated decay regulate telomerase reverse transcriptase (TERT) expression during virus-induced lymphomagenesis in vivo. BMC Cancer **10**:571. doi:10.1186/1471-2407-10-571.
3. **Anczukow O, et al.** 2008. Does the nonsense-mediated mRNA decay mechanism prevent the synthesis of truncated BRCA1, CHK2, and p53 proteins? Hum. Mutat. **29**:65–73.
4. **Asano K, Phan L, Anderson J, Hinnebusch AG.** 1998. Complex formation by all five homologues of mammalian translation initiation factor 3 subunits from yeast Saccharomyces cerevisiae. J. Biol. Chem. **273**:18573–18585.
5. **Barbier J, et al.** 2007. Regulation of H-ras splice variant expression by cross talk between the p53 and nonsense-mediated mRNA decay pathways. Mol. Cell. Biol. **27**:7315–7333.
6. **Boelz S, Neu-Yilik G, Gehring NH, Hentze MW, Kulozik AE.** 2006. A chemiluminescence-based reporter system to monitor nonsense-mediated mRNA decay. Biochem. Biophys. Res. Commun. **349**:186–191.
7. **Boxus M, et al.** 2008. The HTLV-1 Tax interactome. Retrovirology **5**:76. doi:10.1186/1742-4690-5-76.
8. **Buchsbaum S, Morris C, Bochard V, Jalinot P.** 2007. Human INT6

interacts with MCM7 and regulates its stability during S phase of the cell cycle. Oncogene **26**:5132–5144.
9. **Caron C, et al.** 1993. Functional and biochemical interaction of the HTLV-I Tax1 transactivator with TBP. EMBO J. **12**:4269–4278.
10. **Cavanagh MH, et al.** 2006. HTLV-I antisense transcripts initiating in the 3′LTR are alternatively spliced and polyadenylated. Retrovirology **3**:15. doi:10.1186/1742-4690-3-15.
11. **Chamieh H, Ballut L, Bonneau F, Le Hir H.** 2008. NMD factors UPF2 and UPF3 bridge UPF1 to the exon junction complex and stimulate its RNA helicase activity. Nat. Struct. Mol. Biol. **15**:85–93.
12. **Chang YF, Imam JS, Wilkinson MF.** 2007. The nonsense-mediated decay RNA surveillance pathway. Annu. Rev. Biochem. **76**:51–74.
13. **Chiari E, et al.** 2004. Stable ubiquitination of human T-cell leukemia virus type 1 tax is required for proteasome binding. J. Virol. **78**:11823–11832.
14. **Couttet P, Grange T.** 2004. Premature termination codons enhance mRNA decapping in human cells. Nucleic Acids Res. **32**:488–494.
15. **Derse D, Mikovits J, Polianova M, Felber BK, Ruscetti F.** 1995. Virions released from cells transfected with a molecular clone of human T-cell leukemia virus type I give rise to primary and secondary infections of T cells. J. Virol. **69**:1907–1912.
16. **Desbois C, Rousset R, Bantignies F, Jalinot P.** 1996. Exclusion of Int-6 from PML nuclear bodies by binding to the HTLV-I Tax oncoprotein. Science **273**:951–953.
17. **Durand S, et al.** 2007. Inhibition of nonsense-mediated mRNA decay (NMD) by a new chemical molecule reveals the dynamic of NMD factors in P-bodies. J. Cell Biol. **178**:1145–1160.
18. **El-Bchiri J, et al.** 2005. Differential nonsense mediated decay of mutated mRNAs in mismatch repair deficient colorectal cancers. Hum. Mol. Genet. **14**:2435–2442.
19. **Englert C, et al.** 1995. Truncated WT1 mutants alter the subnuclear localization of the wild-type protein. Proc. Natl. Acad. Sci. U. S. A. **92**:11960–11964.
20. **Fan J, et al.** 2002. Global analysis of stress-regulated mRNA turnover by using cDNA arrays. Proc. Natl. Acad. Sci. U. S. A. **99**:10611–10616.
21. **Franks TM, Singh G, Lykke-Andersen J.** 2010. Upf1 ATPase-dependent mRNP disassembly is required for completion of nonsense-mediated mRNA decay. Cell **143**:938–950.
22. **Fu DX, Kuo YL, Liu BY, Jeang KT, Giam CZ.** 2003. Human T-lymphotropic virus type I tax activates I-kappa B kinase by inhibiting I-kappa B kinase-associated serine/threonine protein phosphatase 2A. J. Biol. Chem. **278**:1487–1493.
23. **Fujii M, et al.** 2000. Activation of oncogenic transcription factor AP-1 in T cells infected with human T cell leukemia virus type 1. AIDS Res. Hum. Retroviruses **16**:1603–1606.
24. **Gachon F, Devaux C, Mesnard JM.** 2002. Activation of HTLV-I transcription in the presence of Tax is independent of the acetylation of CREB-2 (ATF-4). Virology **299**:271–278.
25. **Gardner LB.** 2008. Hypoxic inhibition of nonsense-mediated RNA decay regulates gene expression and the integrated stress response. Mol. Cell. Biol. **28**:3729–3741.
26. **Grzmil M, et al.** 2010. An oncogenic role of eIF3e/INT6 in human breast cancer. Oncogene **29**:4080–4089.
27. **Guo J, Sen GC.** 2000. Characterization of the interaction between the interferon-induced protein P56 and the Int6 protein encoded by a locus of insertion of the mouse mammary tumor virus. J. Virol. **74**:1892–1899.
28. **Holbrook JA, Neu-Yilik G, Hentze MW, Kulozik AE.** 2004. Nonsense-mediated decay approaches the clinic. Nat. Genet. **36**:801–808.
29. **Hong S, et al.** 2007. Heptad repeats regulate protein phosphatase 2a recruitment to I-kappaB kinase gamma/NF-kappaB essential modulator and are targeted by human T-lymphotropic virus type 1 tax. J. Biol. Chem. **282**:12119–12126.
30. **Ishigaki Y, Li X, Serin G, Maquat LE.** 2001. Evidence for a pioneer round of mRNA translation: mRNAs subject to nonsense-mediated decay in mammalian cells are bound by CBP80 and CBP20. Cell **106**:607–617.
31. **Isken O, et al.** 2008. Upf1 phosphorylation triggers translational repression during nonsense-mediated mRNA decay. Cell **133**:314–327.
32. **Jiang H, et al.** 1999. PCAF interacts with tax and stimulates tax transactivation in a histone acetyltransferase-independent manner. Mol. Cell. Biol. **19**:8136–8145.
33. **Kashima I, et al.** 2006. Binding of a novel SMG-1-Upf1-eRF1-eRF3 complex (SURF) to the exon junction complex triggers Upf1 phosphorylation and nonsense-mediated mRNA decay. Genes Dev. **20**:355–367.
34. **Kawasaki T, et al.** 1994. mRNA and protein expression of p53 mutations in human bladder cancer cell lines. Cancer Lett. **82**:113–121.
35. **Kedersha N, et al.** 2005. Stress granules and processing bodies are dynamically linked sites of mRNP remodeling. J. Cell Biol. **169**:871–884.
36. **King-Underwood L, Renshaw J, Pritchard-Jones K.** 1996. Mutations in the Wilms' tumor gene WT1 in leukemias. Blood **87**:2171–2179.
37. **LeBlanc JJ, Beemon KL.** 2004. Unspliced Rous sarcoma virus genomic RNAs are translated and subjected to nonsense-mediated mRNA decay before packaging. J. Virol. **78**:5139–5146.
38. **Legros S, et al.** 2011. The HTLV-1 Tax protein inhibits formation of stress granules by interacting with histone deacetylase 6. Oncogene **30**:4050–4062.
39. **Lejeune F, Ishigaki Y, Li X, Maquat LE.** 2002. The exon junction complex is detected on CBP80-bound but not eIF4E-bound mRNA in mammalian cells: dynamics of mRNP remodeling. EMBO J. **21**:3536–3545.
40. **Lejeune F, Li X, Maquat LE.** 2003. Nonsense-mediated mRNA decay in mammalian cells involves decapping, deadenylating, and exonucleolytic activities. Mol. Cell **12**:675–687.
41. **Lemasson I, et al.** 2007. Human T-cell leukemia virus type 1 (HTLV-1) bZIP protein interacts with the cellular transcription factor CREB to inhibit HTLV-1 transcription. J. Virol. **81**:1543–1553.
42. **Li S, Wilkinson MF.** 1998. Nonsense surveillance in lymphocytes? Immunity **8**:135–141.
43. **Matsuda D, Sato H, Maquat LE.** 2008. Studying nonsense-mediated mRNA decay in mammalian cells. Methods Enzymol. **449**:177–201.
44. **Matsuoka M, Jeang KT.** 2011. Human T-cell leukemia virus type 1 (HTLV-1) and leukemic transformation: viral infectivity, Tax, HBZ and therapy. Oncogene **30**:1379–1389.
45. **Mendell JT, Sharifi NA, Meyers JL, Martinez-Murillo F, Dietz HC.** 2004. Nonsense surveillance regulates expression of diverse classes of mammalian transcripts and mutes genomic noise. Nat. Genet. **36**:1073–1078.
46. **Morris C, Jalinot P.** 2005. Silencing of human Int-6 impairs mitosis progression and inhibits cyclin B-Cdk1 activation. Oncogene **24**:1203–1211.
47. **Morris C, Wittmann J, Jack HM, Jalinot P.** 2007. Human INT6/eIF3e is required for nonsense-mediated mRNA decay. EMBO Rep. **8**:596–602.
48. **Morris-Desbois C, Bochard V, Reynaud C, Jalinot P.** 1999. Interaction between the Ret finger protein and the Int-6 gene product and co-localisation into nuclear bodies. J. Cell Sci. **112**(Pt 19):3331–3342.
49. **Muhlemann O, Lykke-Andersen J.** 2010. How and where are nonsense mRNAs degraded in mammalian cells? RNA Biol. **7**:28–32.
50. **Nasr R, et al.** 2006. Tax ubiquitylation and sumoylation control critical cytoplasmic and nuclear steps of NF-kappaB activation. Blood **107**:4021–4029.
51. **Ohnishi T, et al.** 2003. Phosphorylation of hUPF1 induces formation of mRNA surveillance complexes containing hSMG-5 and hSMG-7. Mol. Cell **12**:1187–1200.
52. **Perrin-Vidoz L, Sinilnikova OM, Stoppa-Lyonnet D, Lenoir GM, Mazoyer S.** 2002. The nonsense-mediated mRNA decay pathway triggers degradation of most BRCA1 mRNAs bearing premature termination codons. Hum. Mol. Genet. **11**:2805–2814.
53. **Rehwinkel J, Behm-Ansmant I, Gatfield D, Izaurralde E.** 2005. A crucial role for GW182 and the DCP1:DCP2 decapping complex in miRNA-mediated gene silencing. RNA **11**:1640–1647.
54. **Rende F, et al.** 2011. Kinetics and intracellular compartmentalization of HTLV-1 gene expression: nuclear retention of HBZ mRNAs. Blood **117**:4855–4859.
55. **Satou Y, Matsuoka M.** 2007. Implication of the HTLV-I bZIP factor gene in the leukemogenesis of adult T-cell leukemia. Int. J. Hematol. **86**:107–112.
56. **Satou Y, Yasunaga J, Yoshida M, Matsuoka M.** 2006. HTLV-I basic leucine zipper factor gene mRNA supports proliferation of adult T cell leukemia cells. Proc. Natl. Acad. Sci. U. S. A. **103**:720–725.
57. **Sheth U, Parker R.** 2006. Targeting of aberrant mRNAs to cytoplasmic processing bodies. Cell **125**:1095–1109.
58. **Smith MR, Greene WC.** 1990. Identification of HTLV-I tax trans-activator mutants exhibiting novel transcriptional phenotypes. Genes Dev. **4**:1875–1885.
59. **Suemori K, et al.** 2009. HBZ is an immunogenic protein, but not a target antigen for human T-cell leukemia virus type 1-specific cytotoxic T lymphocytes. J. Gen. Virol. **90**:1806–1811.
60. **Sun C, et al.** 2011. Functional reconstitution of human eukaryotic trans-

lation initiation factor 3 (eIF3). Proc. Natl. Acad. Sci. U. S. A. **108**:20473–20478.
61. **Tatewaki M, et al.** 1995. Constitutive overexpression of the L-selectin gene in fresh leukemic cells of adult T-cell leukemia that can be transactivated by human T-cell lymphotropic virus type 1 Tax. Blood **86**:3109–3117.
62. **Terme JM, et al.** 2008. Cross talk between expression of the human T-cell leukemia virus type 1 Tax transactivator and the oncogenic bHLH transcription factor TAL1. J. Virol. **82**:7913–7922.
63. **Wang D, et al.** 2011. Inhibition of nonsense-mediated RNA decay by the tumor microenvironment promotes tumorigenesis. Mol. Cell. Biol. **31**: 3670–3680.
64. **Watkins SJ, Norbury CJ.** 2004. Cell cycle-related variation in subcellular localization of eIF3e/INT6 in human fibroblasts. Cell Prolif. **37**:149–160.
65. **Wittmann J, Hol EM, Jack HM.** 2006. hUPF2 silencing identifies physiologic substrates of mammalian nonsense-mediated mRNA decay. Mol. Cell. Biol. **26**:1272–1287.
66. **Yamashita A, et al.** 2009. SMG-8 and SMG-9, two novel subunits of the SMG-1 complex, regulate remodeling of the mRNA surveillance complex during nonsense-mediated mRNA decay. Genes Dev. **23**:1091–1105.
67. **Zhou C, et al.** 2005. PCI proteins eIF3e and eIF3m define distinct translation initiation factor 3 complexes. BMC Biol. **3**:14. doi:10.1186/1741-7007-3-14.

2. *HTLV-1 Tax plugs and freezes UPF1 helicase leading to nonsense-mediated mRNA decay inhibition*

Après avoir établi la preuve de concept de l'inhibition de NMD par Tax, j'ai décidé de concentrer mon intérêt sur l'interaction entre Tax et UPF1. Dans ce travail, nous avons caractérisé cette interaction au niveau moléculaire. Nous avons effectué des GST pulldowns pour délimiter les domaines d'interaction entre Tax et UPF1 et établi des tests fonctionnels pour évaluer l'activité enzymatique d'UPF1. Nous avons constaté que Tax interagit au moins avec le domaine hélicase d'UPF1 et inhibe son activité ATPase. Nous avons trouvé deux explications ; premièrement, sachant que, l'activité ATPase des hélicases est dépendante de leur association à l'ARN, nous avons démontré que la liaison de Tax au domaine hélicase empêche l'association ultérieure de l'UPF1 avec l'ARN. Pour cela, nous avons utilisé des approches d'EMSA, des mesures de constantes cinétiques (koff, kon) ainsi que des expériences d'immunoprecipitation d'ARN dans des cellules exprimant soit Tax soit le virus complet. Deuxièmement, nous avons constaté que Tax peut également interagir avec UPF1 séquentiellement après que ce dernier soit chargé sur l'ARN. Dans ce cas, l'affinité du domaine hélicase à l'ARN est moins sensible à l'hydrolyse de l'ATP. L'analyse en molécule unique à l'aide de pinces magnétiques a confirmé que l'ajout séquentiel de Tax sur le domaine de l'hélicase en cours de translocation peut conduire au blocage d'UPF1 sur le substrat avant que des forces opposées ne le déstabilisent.

En conclusion nous avons donc montré dans cette étude que la protéine virale Tax peut directement inhiber les activités enzymatiques de l'hélicase d'UPF1, induisant la répression du NMD. Cette inhibition s'opère à travers 2 voies : soit en empêchant son recrutement sur l'ARN, en amont de l'initiation du NMD, soit après l'association d'UPF1 à l'ARN en la figeant sur son substrat bloquant le NMD en cours de réaction.

nature COMMUNICATIONS

ARTICLE

DOI: 10.1038/s41467-017-02793-6 OPEN

HTLV-1 Tax plugs and freezes UPF1 helicase leading to nonsense-mediated mRNA decay inhibition

Francesca Fiorini[1,2,3], Jean-Philippe Robin[2], Joanne Kanaan[3], Malgorzata Borowiak[2,4], Vincent Croquette[5], Hervé Le Hir[3], Pierre Jalinot[2] & Vincent Mocquet[2]

Up-Frameshift Suppressor 1 Homolog (UPF1) is a key factor for nonsense-mediated mRNA decay (NMD), a cellular process that can actively degrade mRNAs. Here, we study NMD inhibition during infection by human T-cell lymphotropic virus type I (HTLV-1) and characterise the influence of the retroviral Tax factor on UPF1 activity. Tax interacts with the central helicase core domain of UPF1 and might plug the RNA channel of UPF1, reducing its affinity for nucleic acids. Furthermore, using a single-molecule approach, we show that the sequential interaction of Tax with a RNA-bound UPF1 freezes UPF1: this latter is less sensitive to the presence of ATP and shows translocation defects, highlighting the importance of this feature for NMD. These mechanistic insights reveal how HTLV-1 hijacks the central component of NMD to ensure expression of its own genome.

[1] Molecular Microbiology and Structural Biochemistry, MMSB-IBCP UMR5086 CNRS, Univ Lyon1, 7 passage du Vercors, 69367 Lyon Cedex 7, France. [2] Laboratory of Biology and Modelling of the Cell, ENS de Lyon, Univ Claude Bernard Lyon 1, CNRS UMR 5239, INSERM U1210, 46 allée d'Italie, 69364 Lyon, France. [3] Institut de Biologie de l'Ecole Normale Supérieure, CNRS UMR8197, Inserm, Ecole Normale Supérieure, PSL Research University, 46 rue d'Ulm, 75005 Paris, France. [4] Department of Chemistry and Pharmacy and Centre for Integrated Protein Science, Ludwig-Maximilians-University Munich, 5-13 Butenandtstrasse, 81377 Munich, Germany. [5] Laboratoire de Physique Statistique, École Normale Supérieure, PSL Research University, Univ Paris Diderot Sorbonne Paris-Cité, Sorbonne Univ UPMC Univ Paris 06, CNRS, 24 rue Lhomond, 75005 Paris, France. Francesca Fiorini and Jean-Philippe Robin contributed equally to this work. Correspondence and requests for materials should be addressed to P.J. (email: pjalinot@ens-lyon.fr) or to V.M. (email: vincent.mocquet@ens-lyon.fr)

Up-Frameshift Suppressor 1 Homolog (UPF1) is a DNA/RNA helicase at the crossroads of many critical cellular pathways for RNA and DNA maintenance, as well as for post-transcriptional regulation of gene expression. UPF1 is the central factor in nonsense-mediated mRNA decay (NMD) and is also directly involved in telomere homeostasis, DNA replication, histone mRNA degradation and staufen-mediated mRNA decay[1–4].

Our understanding of UPF1 action and regulation comes from the progressive elucidation of the molecular mechanisms involved in NMD. Despite the identification of several physiological and aberrant substrates, the mRNA features that trigger NMD are still elusive (reviewed in ref. [5]). A common working model for mammalian cells states that NMD is a process of targeting and degrading mRNA, depending on the composition of the RNP around the translation-terminating ribosome. Instead of contacting PABP1 for proper translation termination, the translation termination factors eRF1-3 associate with UPF1, which binds to RNA nonspecifically and accumulates downstream of the first stop codon to encounter the translating ribosome[6–11]. Hence, NMD initiates the decay of mRNA with a premature termination codon (PTC; induced by mutation, alternative splicing or frameshift); NMD also regulates the stability of non-mutated RNA, depending on the size and organisation of their 3′ untranslated region (3′UTR)[12–19]. Recently, NMD has been shown to have an important role in the pervasive and cryptic decay of transcripts in yeast, appearing as the major factor to remove spurious transcripts that have escaped degradation in the nucleus.

Stabilised at the stop codon, UPF1 then successfully activates its essential ATPase activity after contact with UPF2 and most likely other molecular partners[20–23]. Before decay occurs, UPF1 undergoes multiple SMG1-mediated phosphorylation events stimulated by UPF2 and UPF3[20,24,25]. These events lead to efficient recruitment of the endonuclease SMG6, as well as the adaptors SMG5, SMG7 and PNRC2, which are connected to general decapping, deadenylation and exonucleolytic activities, including XRN1[26–29]. It has been suggested that RNP remodelling during these late phases of the process most likely requires UPF1 translocation[30]. In mammals, NMD is enhanced by the 3′ presence of an exon junction complex (EJC) that facilitates UPF1 activation by its UPF2 and UPF3 components[20,23,31].

UPF1 is a modular enzyme that contains a conserved helicase core (helicase domain—HD) formed by two RecA lobes that are able to progressively unwind double-stranded nucleic acids through an inchworm mechanism of translocation[20,32,33]. The HD of the human protein is surrounded by two terminal domains: the N-terminal CH domain, which is enriched with cysteine and histidine residues, and the C-terminal SQ domain, which is enriched with clusters of serine–glutamine residues. Both domains tightly repress the ATPase and helicase activities of UPF1, raising the possibility of enzymatic activation during NMD[20–22]. Indeed, the RNA-dependent ATPase activity is required for NMD target selectivity and is essential for 3′mRNP remodelling and decay completion[30,34,35]. Structural and functional information describes how the CH domain, localised above the RecA2 domains, induces clamping of the enzyme on its RNA substrate by inhibiting its helicase and ATPase activities[20,21]. Binding of the UPF2 cofactor displaces the CH domain from its original position, thereby releasing UPF1 enzymatic activity[21,36]. An inhibitory function is also exerted by the SQ domain, regardless of its phosphorylation state[22]. Once triggered, the exact activity exerted by UPF1 on the RNA and the importance of its translocation during NMD are actually unknown.

There is now much evidence demonstrating the antiviral functions of NMD and the viral means to escape this cellular control (reviewed in refs. [37,38]). Plant and animal positive-strand RNA viruses, as well as retroviruses, use different mechanisms to fully express their compact genome that generate mRNA with NMD-inducing features[39–43]. A well-characterised example is exhibited by the RNA stability elements (RSEs) downstream of the translation termination codon of avian retrovirus Rous sarcoma virus, which stabilises its *gag* RNA[44–46]. These RSEs recruit polypyrimidine tract binding protein 1 (PTBP1), thereby reducing UPF1 binding to the 3′UTR[47]. During human immunodeficiency virus infection, NMD inhibition might occur by a tethering mechanism in which UPF1 is hijacked to promote the nucleocytoplasmic export of vRNAs that enhance their stability[42,48,49]. Interestingly, in Moloney murine leukaemia virus, reverse transcriptase binds to eRF1 at the translation-terminating ribosome to prevent the binding of eRF3 and UPF1, thereby promoting read-through of the stop codon and preventing NMD[50].

In HTLV-1, the viral proteins Tax and Rex exhibit a NMD inhibitory effect[5,6], and we correlated Tax-mediated inhibition to a direct interaction with UPF1[41]. In the present study, we use a combination of ex vivo and in vitro bulk and single-molecule assays to demonstrate how Tax directly affects UPF1 function. We describe a two-level regulation of UPF1 function demonstrating a Tax effect (1) prior to the binding of UPF1 to RNA and (2) on an actively unwinding enzyme. We show a regulatory host/pathogen mechanism, in which an exogenous factor is able to affect UPF1 translocation, highlighting the importance of this mechanical feature for the NMD process.

Results

HTLV-1 Tax inhibits NMD. In a previous report, we showed that, during HTLV-1 infection, viral RNAs are sensitive to NMD and that retroviral Tax protein can inhibit this important cellular mRNA surveillance pathway[41]. Here we analysed the stability of reporter and several endogenous NMD substrates in ex vivo experimental conditions simulating physiological HTLV-1 infection of the cell.

The decay assays were performed monitoring the mRNA levels by carrying out qRT-PCR analyses at the indicated time points after transcription inhibition induced by 100 μg.ml^{-1} of 5,6-dichloro-1-D-ribofuranosylbenzimidazole (DRB). Using this assay the stability of mRNAs transcribed from transfected β-globin minigenes, WT or with a PTC in the second exon (hereafter called Gl-WT and Gl-PTC, respectively) showed a clear destabilization effect of the PTC (Fig. 1a) that was impaired by coexpression of Tax as previously reported (Supplementary Fig. 1a). In order to validate this PCR assay, the half-life of the PTC β-globin mRNA without and with Tax coexpression was also measured by performing a northern blot analysis. This approach led to a similar result that confirmed the Tax-stabilising effect (Supplementary Fig. 1b, c). This NMD impairment was similarly observed when cells were co-transfected with the plasmid pCMVHTLV1-WT that expresses the entire HTLV-1 genome instead of solely the Tax protein (Fig. 1b). The HTLV-1 genome possesses a region termed pX, located between the *env* gene and the 3′ LTR, which contains all the genes coding for regulatory viral factors including the Tax and Rex proteins[51]. While previous studies have shown that HTLV-1 Rex protein may also play a critical role in the suppression of host NMD activity[52], we engineered a molecular clone deleted of ~1 kb of the pX region coding the major part of the second exon of Tax and Rex (ΔpX molecular clone). In these conditions, Tax and Rex expression are abolished. Consistently with previous results, the mRNA decay assay and a P-bodies analysis showed that NMD efficiency was not affected in ΔpX-transfected cells (Fig. 1c and Supplementary Fig. 1d, e). To further assess the role of Tax, a rescue experiment

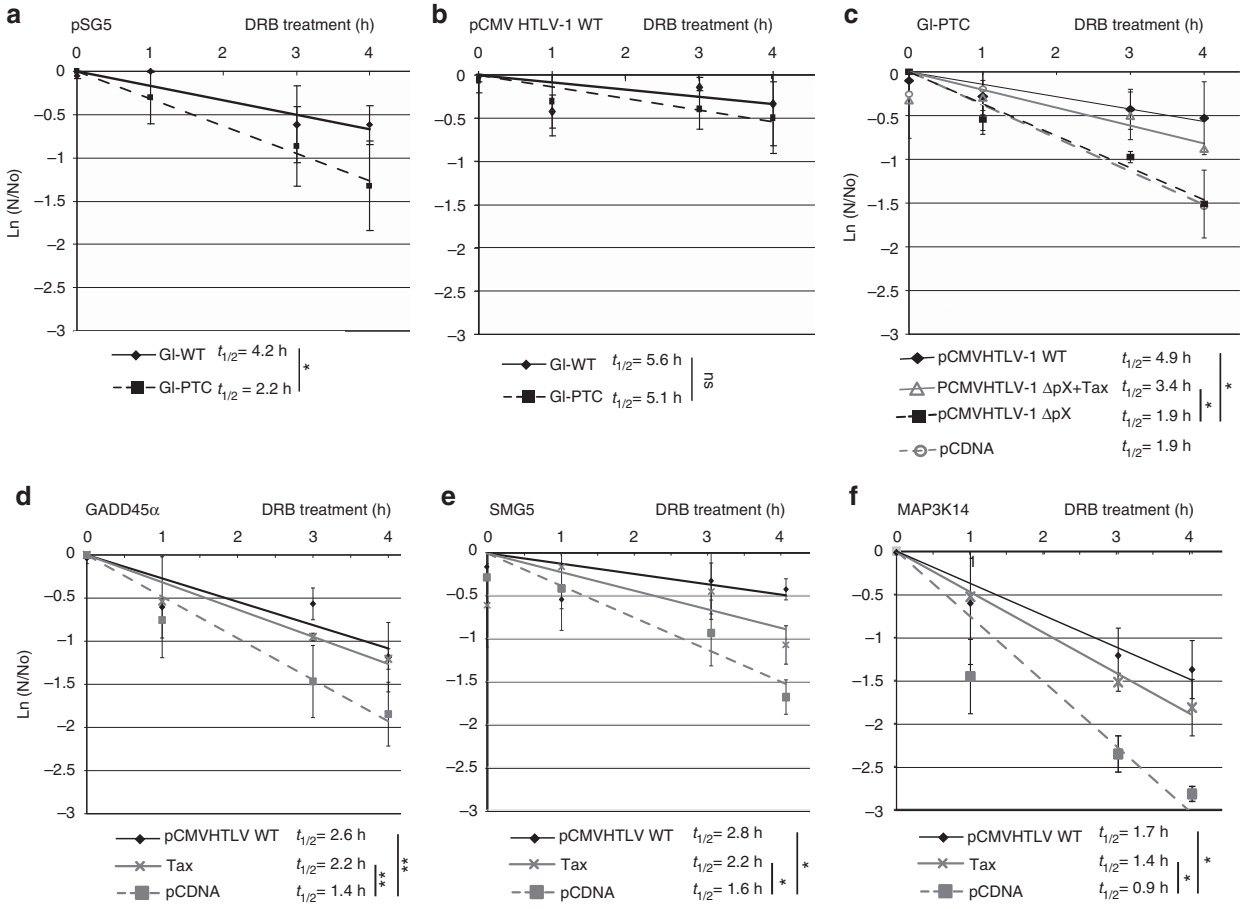

Fig. 1 HTLV-1 Tax protects reporter and endogenous mRNAs from NMD in mammalian cells. **a** RNA decay assays were carried out in HeLa cells. The stability of Gl-PTC and Gl-WT mRNA was analysed after RNA quantification by qRT-PCR. mRNA half-lives ($t_{1/2} = \ln(2)/\lambda$ with λ the time constant of the decay curves) are indicated in front of their respective conditions. **b** Same as **a** except that HeLa cells were co-transfected with HTLV-1 molecular clone. **c** RNA decay assays of Gl-PTC mRNA in the presence of WT HTLV-1 molecular clone (continuous line, diamonds), truncated ΔpX HTLV-1 molecular clone complemented with Tax protein (continuous line, triangle), truncated ΔpX HTLV-1 molecular clone alone (dashed line, square) and empty vector (dashed line, circle). **d** RNA decay assays examining the stability of endogenous *GADD45α* mRNA in the presence of an empty vector (dashed line, square), Tax (continuous line, cross) or a WT HTLV-1 molecular clone (continuous line, diamond; **e**), **f** Same as **d** with *SMG5* and *MAP3K14* endogenous mRNA. The values represented in each graph correspond to the mean of at least three biological replicates, and the error bars correspond to the SD. Half-lives were calculated for each replicate, and *P* values were calculated by performing a Student's *t*-test (unpaired, two-tailed) ns: $P > 0.05$; $^{*}P < 0.05$; $^{**}P < 0.01$

was performed by coexpressing Tax concomitantly to pCMVHTLV-1 ΔpX transfection. The presence of Tax almost completely rescued stabilisation of the Gl-PTC mRNA and thus restored NMD inhibition (Fig. 1c). In addition, we confirmed that this effect is not due to an inhibition of the translation since the protein neo-synthesis was not significantly modified under Tax expression (Supplementary Fig. 1f).

Then, under the same conditions, we analysed the stability of several NMD-prone endogenous mRNAs: GADD45α, SMG5 and MAP3K14 (Figs. 1d–f). GADD45α includes a 5′uORF and is one critical target of NMD in both *Drosophila* and mammalian cells[53,54]. SMG5 has been previously demonstrated to be NMD-sensitive due to its long 3′UTR, while the sensitivity of MAP3K14 is likely due to alternative splicing of exon11 in HeLa cells that leads to out-of-frame translation and occurrence of a PTC located more than 55nt- upstream of EJC (Genebank: CR749592.1 from clone DKFZp686J04131, cDNA sequencing consortium of the German Genome Project). The stability of these three endogenous NMD-prone mRNAs were increased by expression of Tax alone or transfection of the HTLV-1 molecular clone (Figs. 1d–f).

Taken together, these results confirm the direct role of Tax in NMD inhibition when the provirus is expressed and suggest a more general role of this factor in host gene expression.

Tax directly binds UPF1-HD and inhibits its ATPase activity. In a previous work, we showed that Tax co-immunoprecipitated with several NMD factors, including the RNA helicase UPF1[41]. This result suggested that Tax-mediated inhibition of NMD could be related to its interaction with UPF1. To further test this hypothesis, we studied the Tax–UPF1 interaction using purified recombinant proteins and protein fragments (Fig. 2a). Concerning UPF1 recombinant proteins, the boundaries between the N-terminal (CH) domain, the central HD and the C-terminal (SQ) domain were defined according to previous structural studies[21,55]. We produced UPF1 full-length (UPF1-FL; amino acids (aa) 1–1118); a protein containing the CH domain of UPF1 (UPF1-CH; aa 115–294); UPF1 helicase core domain (UPF1-HD; aa 295–914); a protein fragment containing both the CH and HD domains (UPF1-CH-HD; aa 115–914); and a protein containing both the HD and the SQ domains (UPF1-HD-SQ; 295–1118 aa).

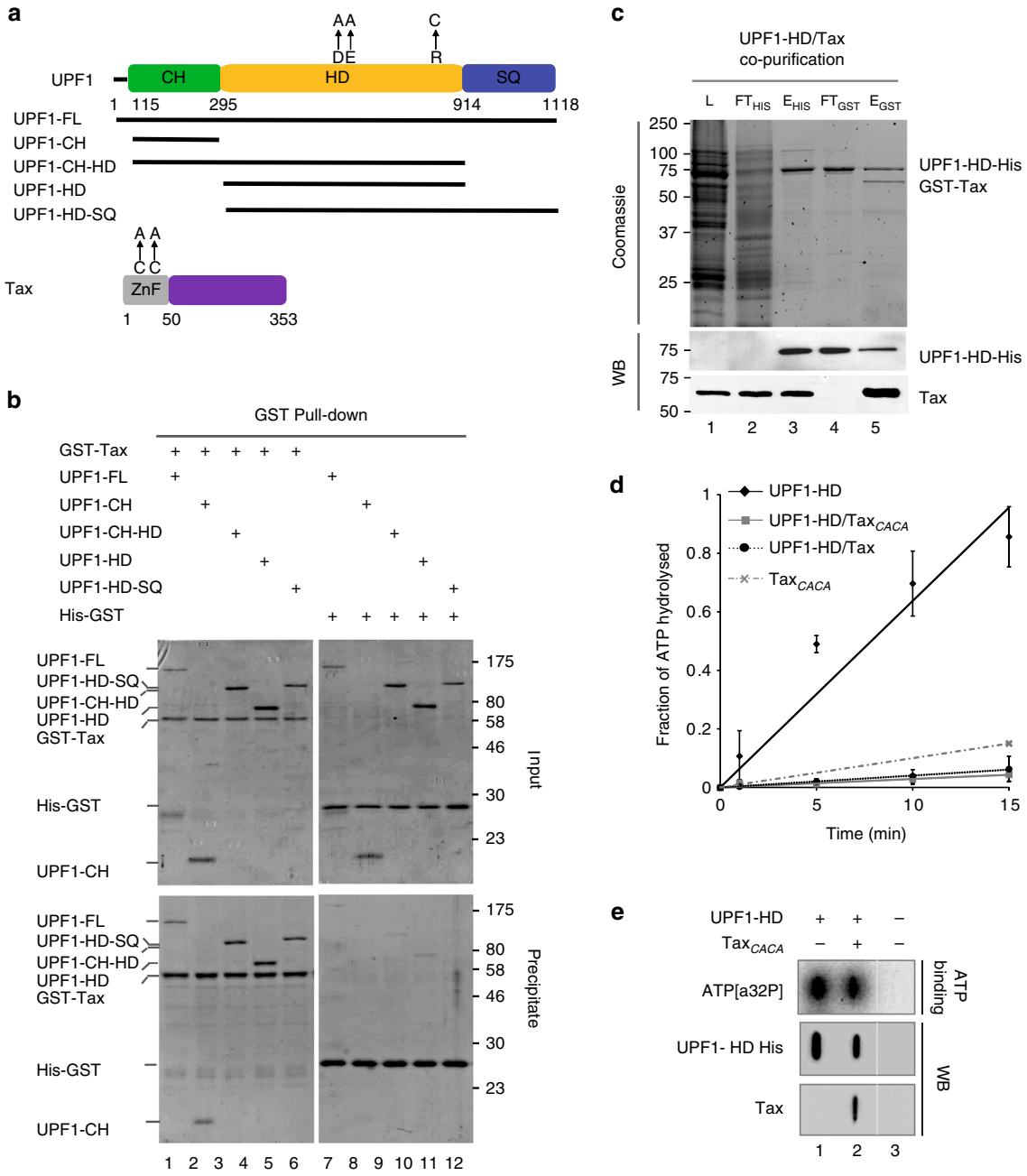

Fig. 2 HTLV-1 Tax interacts directly with UPF1-HD and inhibits its ATPase activity. **a** Schematic diagram showing the UPF1 and Tax domains and sites of mutant derivatives used for this study. Structural domains are represented by rectangles and the protein truncations used by black lines. **b** Pulldown experiment using GST-Tax (lanes 1–6) or GST-His tag (lanes 7–12) as bait. After incubation, protein mixtures before (input 20% of total) or after precipitation (precipitate) were separated on a 10% SDS-PAGE gel and visualised by coomassie staining. **c** A SDS-PAGE gel illustrating the co-purification of human UPF1-HD-His and HTLV-1 GST-Tax proteins by two sequential affinity purifications (Nickel and Glutathione columns). Samples from the *Escherichia coli* lysate (lane 1: L), flow through (lanes 2 and 4: FTHIS and FTGST) and eluate (lanes 3 and 5: EHIS and EGST) fractions were loaded on the gel. The purity of the fractions was evaluated by coomassie staining (upper panel). The proteins were visualised by western blot analysis using anti-His and anti-Tax antibodies targeting UPF1 HD-His and GST-Tax, respectively (lower panels). **d** Graph showing the percentage of [α-^{32}P]ATP hydrolysed as a function of time by UPF1-HD (continuous line, diamond), UPF1-HD/Tax$_{CACA}$ (continuous line, square), UPF1-HD/Tax (dotted line, circle) and Tax$_{CACA}$ (dashed lane, cross) under conditions of steady-state ATPase turnover. Aliquots from the reaction mixture were quenched 0, 1, 5, 10 and 15 min before TLC chromatography (see Methods). The values are the mean of at least three biological replicates, and the error bars correspond to the SD. **e** UPF1-HD, UPF1-HD/Tax$_{CACA}$ complex and BSA proteins were spotted onto a nitrocellulose membrane and exposed to [α-^{32}P]ATP (top panel). The levels of the proteins used were also analysed by slot-blot on a different membrane. The membrane was incubated with anti-His and anti-Tax antibodies (middle and lower). Nonsignificant lanes were removed as indicated by the vertical white line. Uncropped scans related to Fig. 2 are available in Supplementary Fig. 6

Several point mutations, the position of which are indicated in Fig. 2a, were also produced for the purposes described thereafter. HTLV-1 Tax is a 353-amino-acid protein containing cysteine and histidine-rich regions at its N terminus (aa 22–53). UPF1 proteins were fused to a calmodulin-binding peptide at the N terminus and/or to a hexahistidine tag at the C terminus and were purified by successive affinity steps with nickel and calmodulin resin columns[22,56]. Analogously, N-terminal glutathione S-transferase (GST)-fused Tax was purified from a Glutathione Sepharose column as described elsewhere[57]. To assess the direct interaction of Tax with UPF1 and to map the eventual Tax-binding site in UPF1, we incubated the different UPF1 fragments with Tax and performed GST pulldown (Fig. 2b). After extensive washes with 0.3 M NaCl, input and eluted protein(s) were fractionated by sodium dodecyl sulphate-polyacrylamide gel electrophoresis (SDS-PAGE) and visualised by coomassie staining. UPF1-FL, UPF1-CH-HD, UPF1-HD and UPF1-HD-SQ were efficiently co-precipitated when GST-Tax was used as bait (lanes 1, 3–6) and compared to GST alone (lanes 7, 9–12). UPF1-CH interacted to a reduced extent compared with HD-containing proteins (lanes 2, 8 and Supplementary Fig. 2a). These data suggest that the Tax-binding site on UPF1 is most likely multipartite but clearly includes HD.

The effects of Tax on the NMD process together with its direct interaction with the UPF1 enzymatic core suggested possible inhibition of UPF1 activity. To prevent the nonspecific binding of Tax_{WT} to RNA observed in RNA pull-down experiments, we engineered a double mutated version of Tax by changing C23 and C29 to alanine (mutant called Tax_{CACA}, Fig. 2a). We reasoned that disruption of the Zinc Finger (ZnF) domain in the Tax N-terminal region[58] should interfere with its nucleic acid binding. First, we controlled that this mutation is not altering Tax ability to inhibit NMD ex vivo (Supplementary Fig. 2c). In addition, overexpression of Tax protein in *E.coli* led to the formation of inclusion bodies. We speculated that the co-purification of UPF1-HD and Tax proteins might help to solubilise Tax. Indeed, using C-terminal hexahistidine-fused UPF1-HD and N-terminal GST-tagged Tax, we obtained the bimolecular complex after sequential Histidine and Glutathione affinity chromatography under stringent conditions (0.3 M NaCl; Fig. 2c, lane 5). The presence of both partners was confirmed by western blot analysis using anti-Histidine and anti-Tax antibodies (Fig. 2c, bottom panels). Analogously to UPF1-HD/Tax_{CACA} complex, we were able to co-purify UPF1-HD with Tax_{WT} as described before (Supplementary Fig. 2b).

The enzymatic activity of UPF1-HD was then measured by following the steady-state ATP hydrolysis rates of UPF1-HD, UPF1-HD/Tax_{CACA} and UPF1-HD/Tax preformed complexes, as well as Tax_{CACA} alone (Fig. 2d). The purified proteins and complexes (Supplementary Fig. 2b) were pre-incubated with RNA substrate (polyU), and the reaction was initiated by addition of ATP. The amount of ADP released was analysed by thin layer chromatography (TLC), and the ATPase efficiencies were deduced from the proportion of ATP and ADP over time (Fig. 2d). Under these conditions, all UPF1–HD/Tax complexes showed very weak ATPase activity compared with UPF1-HD. To assess the ability of UPF1-HD to bind ATP in the presence of Tax, we performed an ATP-binding assay. We incubated the proteins spotted on nitrocellulose membrane with [α-^{32}P]ATP (Fig. 2e). The results showed that both UPF1-HD and UPF1-HD/Tax_{CACA} complexes could bind ATP (lanes 1 and 2).

These results show a strong inhibitory effect of Tax on UPF1 ATPase activity without affecting ATP binding.

Tax decreases UPF1-HD binding to RNA. The ATPase activity of UPF1 and its affinity for the nucleic-acid substrate were linked to classify UPF1 as an RNA/DNA-dependent ATPase. Thus, we wondered whether the effect of Tax on decreasing UPF1 ATPase activity was due to a Tax-mediated RNA-binding defect. First, we analysed the RNA association of UPF1 ex vivo by performing RNA immunoprecipitation (RIP) experiments using HeLa cells transiently co-transfected with the Gl-PTC and HTLV-1 molecular clones or Tax expression plasmid. After immunoprecipitation of endogenous UPF1, the amount of Gl-PTC mRNA was quantified by qRT-PCR with two different oligonucleotide couples specific either of full-length or only the 3′ portion downstream of PTC. Transfection of the NMD-inhibiting HTLV-1 molecular clone was correlated with a drastic loss of Gl-PTC mRNA associated with UPF1 in comparison to its derivative lacking the ΔpX region (Fig. 3a). The expression of Tax alone also caused a significant decrease in Gl-PTC mRNA amount bound to UPF1 (Fig. 3a). Moreover, since UPF1 nonspecifically binds RNA, the same experiment was carried out using Gl-WT instead of Gl-PTC as the reporter mRNA. Tax was also able to decrease the affinity of UPF1 for Gl-WT mRNA (Supplementary Fig. 3a).

To gain molecular insights into this effect, we performed a series of in vitro tests. First, we performed electrophoretic mobility shift assays (EMSA) by incubating 30-mer radiolabelled single-stranded RNA (ssRNA) with increasing concentrations of purified UPF1-HD in the presence or absence of Tax_{CACA}. The presence of Tax markedly reduced the affinity of UPF1 for the ssRNA (Fig. 3b, lanes 6–10) compared with UPF1 alone (Fig. 3b, lanes 1–5). As expected, Tax_{CACA} did not bind the RNA substrate (Fig. 3b, lane 6). To measure the rate constants of the UPF1-HD/RNA interaction in the presence of Tax, we used Bio-Layer Interferometry (BLItz, ForteBio). We immobilised a 5′-biotinylated RNA or DNA 30-mer on a streptavidin-coated biosensor and incubated it with 10 nM of UPF1-HD or UPF1-HD/Tax_{CACA} complex (Supplementary Fig. 3b, c). The biosensor was further washed without protein to monitor passive dissociation. Consistent with previous results, Tax_{CACA} mutant did not bind to the substrates. The obtained sensorgrams showed that the real-time association kinetics (upward slope) of UPF1-HD markedly decreased in the presence of Tax for both substrates (Supplementary Fig. 3b, c), suggesting that Tax prevents the association of UPF1 with nucleic acids. To extrapolate the association (k_{on}) and dissociation constants (k_{off}) to calculate K_D, we performed a BLItz assay using increasing amounts of the UPF1-HD or UPF1-HD/Tax_{CACA} preformed complex (Supplementary Fig. 3d, e). Because of the lower affinity of the complex for DNA compared with UPF1-HD alone, the association time was extended to 600 s. The collected data are summarised in the table of Fig. 3c. As expected, the presence of Tax increased by approximately five times the K_D of UPF1-HD from 8.25 to 40.6 nM. Interestingly, the analysis of k_{on} and k_{off} revealed that, while the k_{on} showed a 10-fold decrease in the presence of Tax (31.6×10^4 for HD to 3.05×10^4 M^{-1} s^{-1} for HD/Tax_{CACA}), k_{off} slightly decreased (2.6×10^{-3} for HD to 1.24×10^{-3} s^{-1} for HD/Tax_{CACA}). Hence, Tax reduced UPF1-HD affinity for its nucleic acid substrate, mainly by preventing its association with nucleic acids.

Finally, to identify the residues critical for Tax binding, we analysed several UPF1-HD mutants. We focused on two of them that were extensively used in the literature and that were associated with RNA affinity and ATP hydrolysis defects: R843C and DE636AA, respectively. R843 is localised just below the CH domain at the RNA entry site and contacts the RNA phosphate backbone[21] (Fig. 3d). The R843C mutation of human UPF1, together with the corresponding yeast R779C mutation, has been shown to confer the strongest NMD inhibition effect in vivo[35,59]. Conversely, the DE636 residues are localised within the ATP

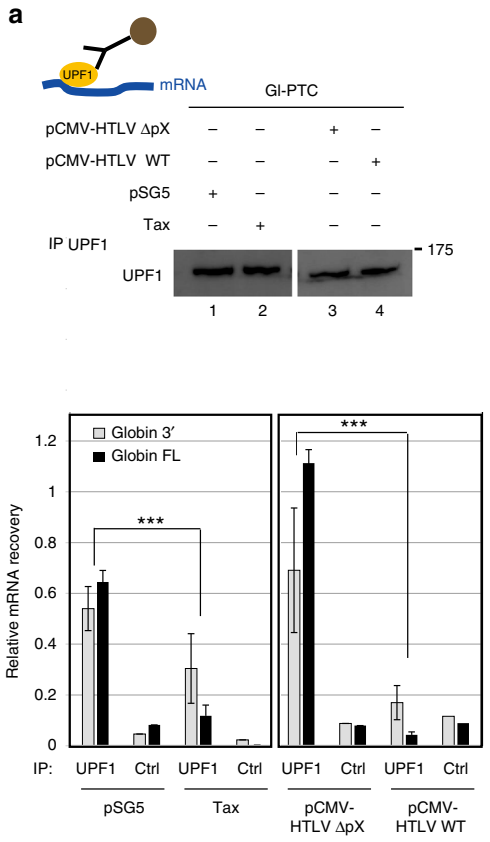

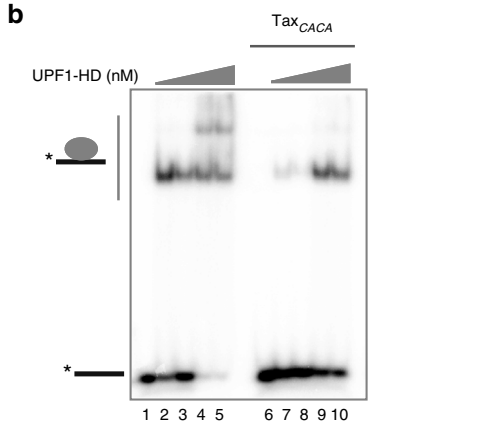

c

Substrate affinity

	K_D (M)	kon (1/Ms)	koff (1/s)
UPF1-HD	8.25×10^{-9}	$31.6\times10^{4} \pm 1.96\times10^{4}$	$2.60\times10^{-3} \pm 1.37\times10^{-4}$
UPF1-HD/Tax	40.6×10^{-9}	$3.05\times10^{4} \pm 0.30\times10^{4}$	$1.24\times10^{-3} \pm 4.60\times10^{-5}$

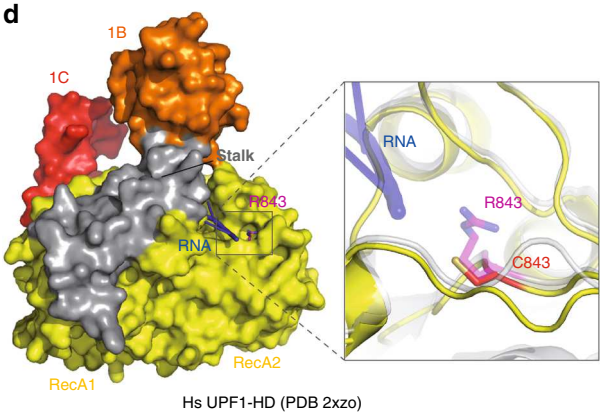

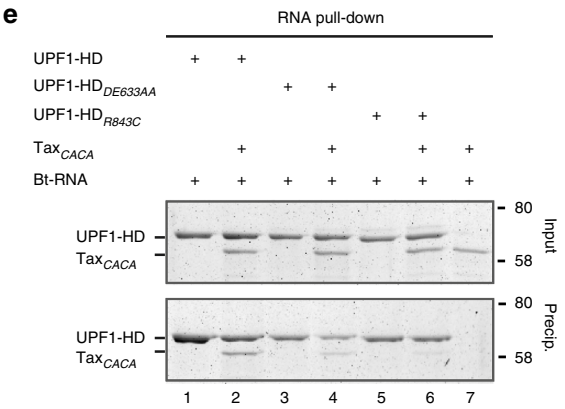

f

Tax affinity

	K_D (M)	kon (1/Ms)	koff (1/s)
UPF1-HD	1.66×10^{-8}	$2.29\times10^{4} \pm 1.06\times10^{2}$	$3.80\times10^{-4} \pm 2.04\times10^{-5}$
UPF1-HD *DE633AA*	3.14×10^{-8}	$9.03\times10^{3} \pm 1.26\times10^{2}$	$2.83\times10^{-4} \pm 5.52\times10^{-5}$
UPF1-HD *R843C*	5.38×10^{-8}	$8.12\times10^{3} \pm 1.12\times10^{2}$	$4.37\times10^{-4} \pm 5.59\times10^{-5}$
UPF1-HD *R843S*	6.66×10^{-8}	$1.32\times10^{4} \pm 2.26\times10^{2}$	$8.77\times10^{-4} \pm 8.09\times10^{-5}$

binding and hydrolysis cleft. The DE636AA mutant has been shown to affect the ATPase activity of UPF1 despite its ability to bind ATP[55]. We produced histidine-tagged UPF1-HD$_{R843C}$ and UPF1-HD$_{DE636AA}$, and we performed an RNA pull-down assay to qualitatively estimate their RNA-binding affinity in the presence of Tax. As expected, the binding of Tax to UPF1-HD induced a reduction of its RNA affinity (Fig. 3e, lanes 1 and 2). The same effect was observed using UPF1-HD$_{DE636AA}$ mutant (Fig. 3e, lanes 3 and 4). Interestingly, UPF1$_{R843C}$ did not interact with Tax in this assay. As a consequence, it did not either show decreased binding to RNA (Fig. 3e, lanes 5 and 6). The interaction between UPF1-HD$_{R843C}$ and RNA was likely due to the numerous residues involved in the RNA interaction within the channel[21]. We performed BLItz assays to quantitatively assess the Tax-UPF1 affinity using a highly sensitive technique. We immobilised GST-tagged Tax$_{CACA}$ on the sensor and measured the binding parameters of UPF1 WT and mutants (Supplementary Fig. 3f–h).

Consistent with RNA pull-down results, the R843C mutation decreased the dissociation constant (K_D) for Tax protein ~3.2 times compared with WT (Fig. 3f and Supplementary Fig. 3f and h). The DE636AA mutant of UPF1 showed slightly affected binding by ~1.8 times compared with WT (Fig. 3f and Supplementary Fig. 3f, g). Unfortunately, we could not affirm that the R843 residue of UPF1 was directly contacted by Tax because C843 possibly formed a disulphide bond with other cysteines affecting the global folding of the HD. To assess whether

Tax bound directly to the R843 residue, we produced histidine-tagged UPF1-HD$_{R843S}$ and performed a BLItz assay to test the interaction with Tax (Supplementary Fig. 3f and i).The UPF1-HD$_{R843S}$ mutant showed four times less affinity for Tax compared with WT. That finding is consistent with the hypothesis of a direct interaction of Tax with R843 of the HD.

Considering the position of the R843 residue (Fig. 3d), these results strongly suggest that Tax may interfere with the entry of RNA into the binding channel of UPF1, preventing its association with, rather than dissociation from, the substrate.

Tax binds UPF1 containing RNP and modifies UPF1 behaviour. However, as observed in Fig. 3c, the in vitro analysis showed that the K_D of the UPF1-HD/Tax complex, although higher than that of UPF1-HD alone, was still rather low, suggesting that a significant portion of the UPF1/Tax complex was nonetheless associated to the substrate. This was supported by RNA pull-down experiments' observation (Fig. 3e, lane 2).

To verify the existence of a UPF1/Tax complex bound to NMD substrates and to assess its physiological relevance and whether UPF1 was still active under these circumstances, we immunoprecipitated transiently expressed Tax protein in HeLa cells and quantified the associated β-globin mRNA as described previously (Fig. 4a). The antibody against Tax was able to precipitate approximately ten times and five times more Gl-PTC mRNA compared with the control immunoglobulin and Tax-free samples, respectively. The association of Tax with Gl-PTC mRNA was also four times stronger than Gl-WT. Interestingly, after treatment of HeLa cells with UPF1 siRNAs, three times less Gl-PTC mRNA was co-immunoprecipitated with Tax compared with the control (Fig. 4a). These data were in agreement with the visualisation of semiquantitative RT-PCR amplicons after migration through an agarose gel (Supplementary Fig. 4a). Similar experiments were carried out with the HTLV-1 molecular clones WT and ΔpX, and showed the same trend (Supplementary Fig. 4b). To confirm the concomitant presence of UPF1 and Tax on NMD substrates, we transfected HeLa cells with HA-UPF1 together with Tax expression plasmids to perform a double-RIP experiment (Fig. 4b). The hemagglutinin (HA) tag was used as bait to immunoprecipitate UPF1 (Fig. 4c, lane 6). The precipitate was incubated with an anti-Tax antibody to further pull down the UPF1-HD/Tax$_{CACA}$ complexes. The western blot showed the presence of both Tax and UPF1 in the sample after the second immunoprecipitation (Fig. 4c, lane 7). Concomitantly, mRNAs were extracted from fractions of the immunoprecipitates, and the presence of Gl-PTC mRNA was analysed by semiquantitative RT-PCR (Fig. 4d, lanes 4 and 5). Notably, the amount of Gl-PTC mRNA in the second immunoprecipitate represented a fraction of the total transcript associated with UPF1. Taken together, these data demonstrated that, although to a lesser extent, UPF1 was still able to bind NMD targets in the presence of Tax ex vivo.

With the aim to confirm these data, we monitored Tax binding to UPF1-HD already associated with the DNA substrate by using the BLItz assay (Fig. 4e). We first measured the association of UPF1-HD to a biotinylated 30-mer DNA oligonucleotide bound to the sensor tip (Fig. 4e, both curves up to 300 s), and then we added or did not add Tax$_{CACA}$ in *trans* at 330 s (Fig. 4e, continuous blue line and red dashed line, respectively). The increasing BLI signal in the sensorgram indicated the association kinetics of Tax on UPF1-HD instead of the dissociation of the UPF1-HD/Tax complex. Next, we wondered whether Tax could modify the UPF1-HD behaviour on its substrate. It has been shown that the binding of ATP or its non-hydrolysable analogue (ADPNP) within the active site modulates the nucleic-acid affinity of UPF1, most likely at the base of enzyme translocation[20,21,33,55]. In general, the presence of ATP or ADPNP decreases UPF1 affinity for the substrate. Hence, we performed a BLItz assay using the UPF1-HD and UPF1-HD/Tax$_{CACA}$ preformed complex to test the effect of the nucleotide presence. According to the observed k_{on} (Fig. 3c), we used seven times more complex than UPF1 protein alone. The presence of ATP or ADPNP strongly reduced UPF1-HD affinity for the ligand, while a weaker effect was observed using the UPF1-HD/TAX$_{CACA}$ complex (Fig. 4f).

These results demonstrate that Tax can be embedded within UPF1-containing RNP and that, under these conditions, UPF1-HD is less sensitive to the presence of ATP.

UPF1 translocation is inhibited by Tax binding. Finally, we used magnetic tweezers (MT, Picotwist®) to determine the real-time effect of Tax on UPF1-HD protein actively running on DNA. The experimental configuration is a 1200-base pair (bp) DNA hairpin tethered between a glass surface and a magnetic bead[33,60]. The biotinylated 5′ end of DNA binds the streptavidin-coated bead, while the digoxygenated 3′ end interacts with the antidigoxygenin antibody attached to a glass surface. A controlled force was applied to the ends of the hairpin using two magnets (Fig. 5a), and Z(t) was measured by tracking the position of the

Fig. 3 Tax binding near the entry site of RNA decreases UPF1 affinity for its substrate. **a** The upper panel shows the levels of endogenous UPF1 immunoprecipitation (IP) from mock (lane 1), Tax (lane 2), pCMV- HTLV-1 ΔpX (lane 3) and pCMV- HTLV-1 WT (lane 4)-transfected HeLa cells. The lower panel represents the relative quantification of Gl-PTC RNA recovery upon UPF1 RIP. The ΔΔCt method of mRNA quantification was applied to each experimental condition. The control sample (Ctrl) derived from IP using immunoglobulin G (IgG) antibody. The values represented in each graph correspond to the mean of at least three biological replicates, and the error bars correspond to the SD. ***$P < 0.005$ with Student's t-test (two-tailed, unpaired). **b** Representative native 8% polyacrylamide gel illustrating the interaction of UPF1-HD protein with a 30mer-ssRNA (grey line) labelled with ^{32}P (black star) with or without Tax$_{CACA}$ factor. The RNA substrate (1 nM) was incubated with increasing concentrations of UPF1-HD (0, 1, 3, 5 and 10 nM) alone or with 300 nM of Tax$_{CACA}$. The absence of an interaction between Tax$_{CACA}$ and the substrate was also verified (lane 6). **c** Recapitulative tables of Bio-Layer Interferometry experiments listing K_D, k_{on} and k_{off} in real-time measurements of UPF1-HD and UPF1-HD/Tax complex binding to 5′ biotinylated 30mer-ssDNA. These data were obtained using the BLItz® System instrument and BLItz ®Pro 1.2 software (ForteBio). **d** Crystal structure of human UPF1-HD complexed with RNA substrate showing the position of the R843 residue[21]. The magnification shows the structural model of the R843C mutant produced using I-Tasser software. **e** Protein co-precipitation with 3′ end-biotinylated 30-mer ssRNA (Bt-RNA). Combinations of UPF1-HD (lanes 1 and 2), UPF1-HD$_{DE633AA}$ (lanes 3 and 4) or UPF1-HD$_{R843C}$ (lanes 5 and 6) were mixed with Tax$_{CACA}$ (lanes 2, 4 and 6) and incubated in a buffer containing 200 mM NaCl before co-precipitation. Tax$_{CACA}$ was incubated with Bt-RNA alone as a control for aspecific binding (lane 7). Input (20% of total) and pull-down fractions were analysed by 12% SDS-PAGE followed by coomassie blue staining. **f** Recapitulative tables of BLItz listing K_D, k_{on} and k_{off} in real-time measurements for UPF1-HD$_{WT}$, UPF1-HD$_{DE633AA}$, UPF1-HD$_{R843C}$ and UPF1-HD$_{R843S}$ binding to Tax. Uncropped scans related to Fig. 3 are available in Supplementary Fig. 7

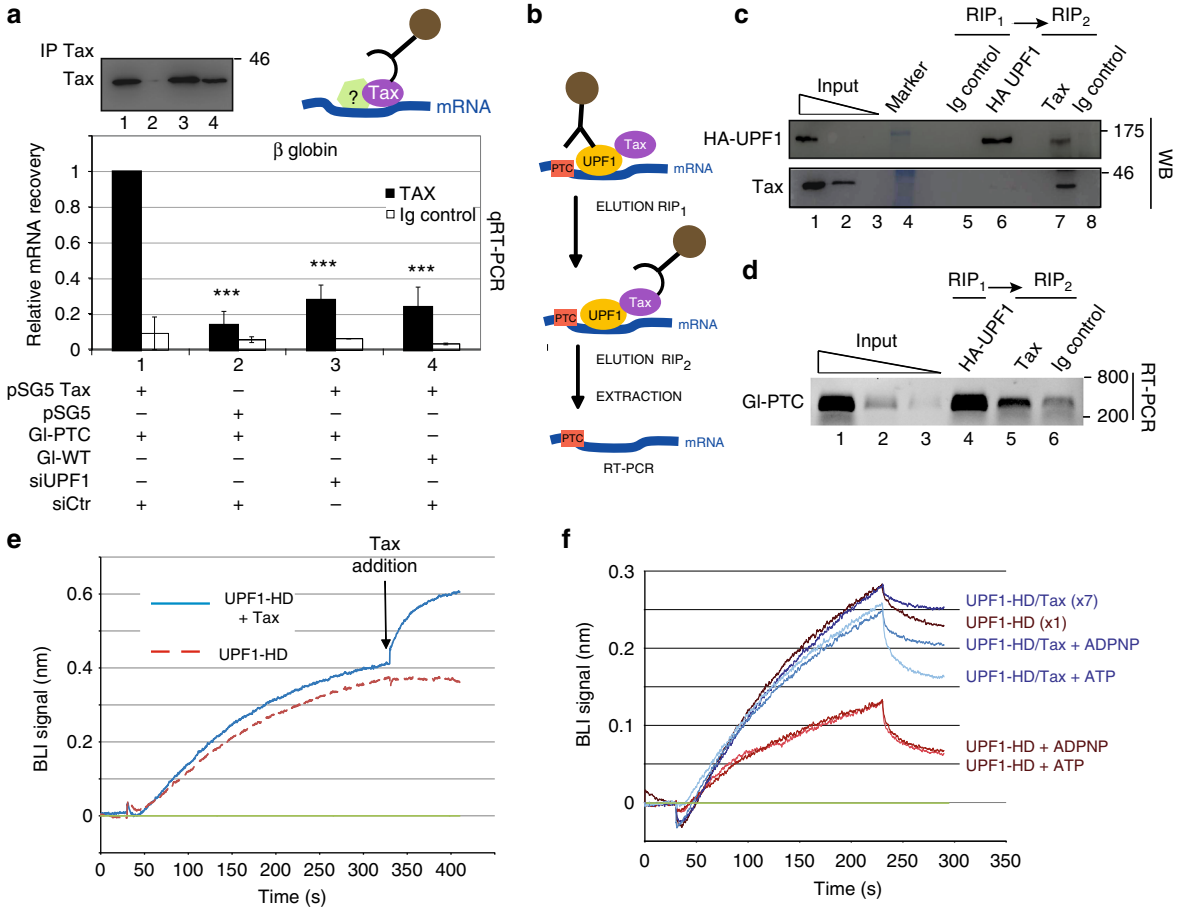

Fig. 4 The UPF1-HD/Tax complex shows residual RNA-binding ability. **a** Quantification of precipitated Gl-PTC from Tax immunoprecipitation (black bars) vs. IgG immunoprecipitation control (white bars) using the globin 3′ oligos. The histogram represents the quantification of relative RNA recovery upon normalisation to input RNA under condition 1 that was set to 1. The ΔΔCt method of mRNA quantification was applied to each experimental condition. The construct encoding Tax (conditions 1, 3 and 4) or empty vector (lane 2) were co-transfected with reporter plasmids expressing Gl-PTC (lanes 1–3) or Gl-WT (lane 4). The cells were treated with non-targeting siRNA (siCtr; lanes 1, 2 and 4) or UPF1 siRNA (siUPF1; lane 3). The values represented in each graph correspond to the mean of at least three biological replicates, and the error bars correspond to the SD. ***$P < 0.005$ with Student's t-test (two-tailed, unpaired). Immunoprecipitated Tax was analysed by western blotting using anti-Tax antibody (upper left panel). **b** Schematic representation of the double-RIP workflow. **c** Western blot analysis monitoring the presence of both UPF1 and Tax in each fraction. **d** Agarose gel showing the products of RT-PCR using globin 3′ oligonucleotides with input and immunoprecipitated RNA samples. **e** Real-time sensorgram of the Bio-Layer interferometry experiment showing UPF1-HD binding to 5′-biotinylated 30mer-DNA (red dashed line), and the interaction of UPF1-HD with Tax_{CACA} when Tax_{CACA} was added at 330 s (blue line). **f** Association and dissociation curves of UPF1-HD (10 nM) and UPF1-HD/Tax (70 nM) preformed complex to the DNA-coated sensor with or without ATP or ADPNP. Given that the k_{on} of the UPF1-HD/Tax_{CACA} complex is one order of magnitude lower than that UPF1-HD, the concentration of the protein complex was adjusted to have almost the same association kinetics with DNA than the enzyme alone. Biosensor DNA tips were loaded with: UPF1-HD (brown), UPF1-HD supplemented with 2 mM of ADPNP (red) or 2 mM of ATP (orange), UPF1-HD/Tax (dark blue), UPF1-HD/Tax supplemented with 2 mM of ADPNP (middle blue) or 2 mM of ATP (light blue). Uncropped scans related to Fig. 4 are available in Supplementary Fig. 8

magnetic bead in real-time. During the helicase MT assay, the unwinding activity of UPF1-HD was deduced from changes in the extension of the DNA molecule. As expected, we observed a saw-tooth track of unwound bases as a function of time. The rising edge corresponds to the hairpin unwinding by UPF1-HD. The falling edge represents hairpin refolding immediately behind UPF1-HD that is translocating on single-stranded (ss) DNA (Fig. 5b; Supplementary Fig. 5a and ref. [33]). Consistently with the previously published data, the average unwinding and ss-translocation rates of UPF1-HD were 0.58 and 1.40 bp.s^{-1}, respectively, for this experiment[33]. To assess the effect of Tax binding, we performed a MT assay in which actively unwinding/translocating UPF1 was identified and monitored before addition of Tax into the reaction chamber. During the helicase MT assay, two injections of Tax_{CACA} were performed between 1150–1325 and 3100–3275 s in the experiment presented in Fig. 5c. We observed 51 unwinding events out of 63 in which the UPF1-HD activity was affected. Among a whole series of unwinding events affected by Tax, we observed instantaneous refolding of the hairpin, indicating the dissociation of UPF1-HD from the substrate (Fig. 5c, upper track at 3625 s; Supplementary Fig. 5e, f). When Tax interacts with UPF1-HD that is undergoing active ss-translocation, the effect is more complex, as shown in Fig. 5c, lower track and Supplementary Fig. 5b–d. In these panels, the recorded tracks illustrate all three types of inhibiting events affecting the UPF1 translocation. They present a characteristic burst shape with a normal rising edge compared with the UPF1-HD recorded track (Fig. 5b and Supplementary Fig. 5a). However,

their falling edge is interrupted in almost 44% of the total Tax interacting events, and the activity of ss-translocation of UPF1 is blocked (Fig. 5c, lower track, from 1920 to 2370 s and from 2414 to 3660 s). In 41% of the events, the hairpin instantaneously refolds (Fig. 5c, lower track, at 3660 s), indicating that Tax induces the dissociation of UPF1-HD from its substrate. In 15% of the inhibited events, we observed a rapid refolding of the hairpin that we call sliding, followed by a blocking event (Fig. 5c, lower track, between 2372 and 2417 s; Supplementary Fig. 5b). This temporary sliding of the UPF1/Tax complex was likely boosted by the hairpin rezipping behind UPF1. These data demonstrate that Tax destabilises UPF1 during both unwinding and translocation, leading to its dissociation from the substrate.

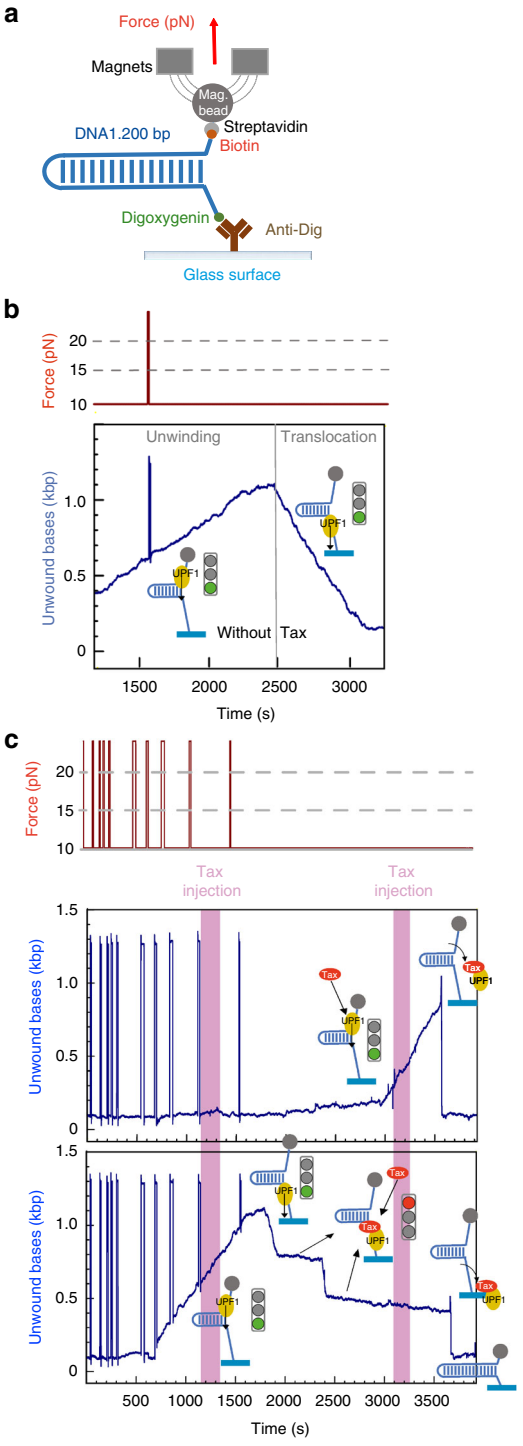

Discussion

UPF1 ATPase activity plays a key role during NMD, while the biological meaning of UPF1 translocation remains unclear. The helicase and ATP binding and hydrolysis activities were linked to a selective association with NMD targets[34,61], as well as to the proper translation termination at PTC and overall nonsense mRNP remodelling[30,34,62]. In this study, we describe how the HTLV-1 Tax factor inhibits NMD during retroviral infection by affecting UPF1 activity at several levels, disturbing substrate binding and translocation.

Our earlier work showed that the viral protein Tax interacts with NMD components, including UPF1, UPF2 and the translation initiation factor INT6/eIF3E, inhibiting the degradation of some cellular and viral mRNAs by NMD[41,63]. Here, we strengthened those results by analysing the effect of Tax on several host-endogenous NMD targets presenting different NMD-triggering features and in the context of an HTLV-1 molecular clone mimicking HTLV-1 infection (Figs. 1a–f). On the basis of these results, Tax should be considered a regulator of global host gene expression during HTLV-1 infection.

We established the direct interaction of Tax with UPF1, through its helicase core and, to a lesser extent, the N-terminal CH domain (Figs. 2b, c). Since UPF1 is a very tightly regulated enzyme[20–22,33], we investigated the possible Tax-mediated modulation of its activities. While UPF1 is a nucleic-acid-dependent hydrolase, we characterised two different ways in which Tax deregulates UPF1 functioning, depending on when their interaction takes place.

The first level of regulation involves the interaction with Tax before UPF1 binding to the nucleic-acid substrate. We found that the presence of Tax was associated with a 10 times lower affinity of UPF1 for nucleic acids (Figs. 3a–c). Measurement of the UPF1/Tax complex affinity (k_{on} and k_{off}) showed that the UPF1 association with RNA, instead of its dissociation, is affected. This Tax-mediated loss of RNA affinity is most likely the cause of the low ATP hydrolysis rate of the enzyme (Figs. 2d, e). We observed that UPF1 mutations of the R843 residue (R843C or R843S) decrease the Tax interaction (Figs. 3e, f). On the basis of the structural information, R843 has been observed to interact with the phosphate backbone of the RNA 5′ extremity and is localised within the nucleic-acid-binding channel in an external region exposed to the solvent[21] (Fig. 3d). In our hands, the R843C mutation only slightly decreased the affinity of UPF1-HD for RNA in vitro, most likely due to compensatory effects exerted by other residues of the channel. The localisation of R843 strongly suggests that the RNA

Fig. 5 Tax blocks UPF1 translocation. **a** Schematic representation of the DNA substrate used for the magnetic tweezers' set-up. **b** Experimental magnetic tweezer traces showing the activity of UPF1-HD under a saturating concentration of ATP (blue line). The trace showing the force monitoring (red line) is shown above the recorded track. The number of unwound bases is deduced from the molecular extension $Z(t)$ obtained at $F = 10$ piconewton (pN). From 1000 to 2500 s, the helicase unwound the ~1200 bp DNA hairpin. From 2500 to 3200 s, the DNA hairpin refolded while the UPF1-HD translocated on the ss-DNA. **c** The upper and lower panels show two types of enzymatic activity detected for UPF1-HD in the presence of Tax. On the upper panel, UPF1-HD is unwinding the DNA hairpin between 3000 and 3625 s before dissociation induced by Tax binding. On the lower panel, UPF1-HD is unwinding the whole DNA hairpin between 500 and 1750 s and translocating between 1750 and 1920 s on the ss-DNA. Tax blocks UPF1-HD translocation twice between 1920 and 2370 s and 2414 and 3660 s. A sliding event and the final dissociation of UPF1-HD can be observed at 2372 and 3660 s, respectively

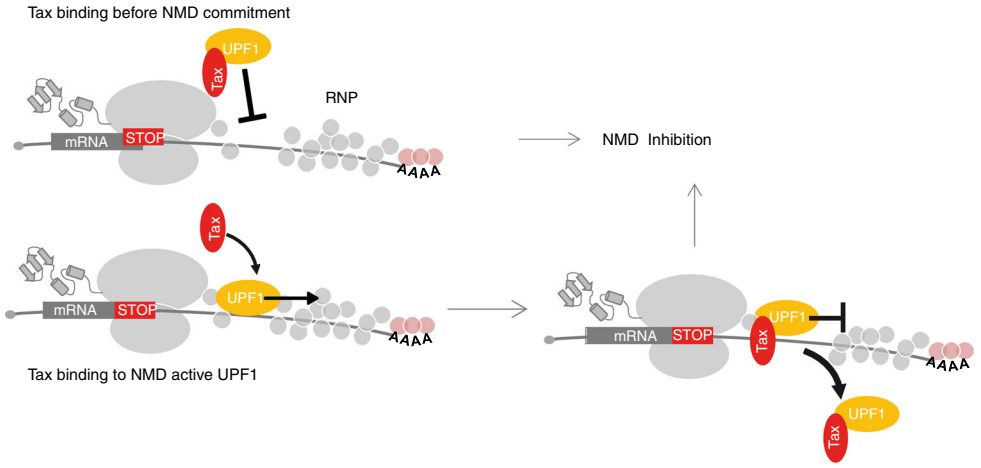

Fig. 6 Model proposed for Tax-mediated inhibition of UPF1 activity. The fate of UPF1 depends on the time frame of interaction with Tax that occurs during HTLV-1 infection. Tax can prevent the recruitment of UPF1 to the RNA substrate. Alternately, Tax can affect the activity of previously bound RNA and NMD-engaged UPF1: the translocation activities of UPF1 can be blocked by Tax binding. The UPF1/Tax complex then dissociates from the RNA substrate or remains stuck in P-bodies

entry site is sterically hindered by Tax bound to the UPF1 helicase core domain.

The second level of UPF1 enzymatic activity inhibition involves the interaction with Tax in a sequential manner, after UPF1 is already bound to its nucleic-acid substrate. Our results showed that a significant fraction of the UPF1/Tax complex is associated with nucleic acids in vitro and ex vivo, supporting the relevance of this complex to RNA (Figs. 3 and 4). To understand the impact of Tax in this configuration of events, we monitored an actively running UPF1 at the single-molecule level (Fig. 5). Recently, the striking processivity and single-stranded translocation activity of UPF1 were formally demonstrated[33] (Fig. 5a and Supplementary Fig. 5a). The enzymatic features of UPF1 are strongly linked ex vivo to mRNP disassembly, a mandatory step for mRNA degradation during NMD[7]. Translocation ability may also be included in these essential UPF1 activities. In vitro, the affinity of UPF1 for nucleic acids is so high that under conditions that dissociate proteins strongly bound to DNA, UPF1 still translocates[33]. Surprisingly, Tax was able to induce UPF1 dissociation during double-stranded DNA unwinding (Fig. 5c and Supplementary Fig. 5e–f). Moreover, the effect of Tax differed on UPF1 that was actively translocating on single-stranded DNA. It mainly blocked UPF1 translocation for a while before inducing its dissociation from the substrate under the pressure of hairpin refolding (Fig. 5c and Supplementary Fig. 5b–d). This Tax-mediated effect should also be related to the accessibility of the Tax-binding site. In fact, during UPF1 translocation from the 5′ to 3′ end of DNA, the refolding hairpin is likely localised on its backside close to R843 (Fig. 3d). The access of Tax may be sterically hindered by DNA, and it may pass through a blocked UPF1 conformation before reaching a dissociation conformation. Moreover, interferometry observations showing that the UPF1/Tax complex was insensitive to the presence of ATP or ATP analogues in the binding site (Figs. 4f and 2e), combined with the blocking effect observed at a single-molecule level (Fig. 5c and Supplementary Fig. 5b–d), suggest that Tax likely stabilises a “closed” conformation of UPF1 that is reminiscence of the CH-domain effect. In fact, structural analysis showed that the CH domain stabilises a clamping conformation of UPF1-HD by narrowing the groove around RNA and by preventing translocation of the enzyme[21,33]. Furthermore, the slight interaction of Tax with the CH domain (Fig. 1b) might suggest a possible concerted inhibition mechanism of UPF1 enzymatic activity.

In our model, HTLV-1 Tax showed two mechanisms of action, depending on whether UPF1 was already bound to mRNA substrate (Fig. 6). Physiologically, this dual inhibition mechanism suggests that Tax may inhibit NMD during early steps before UPF1 is engaged with the substrate, as well as in later steps once UPF1 translocation is triggered. In the latter case, analogously to UPF1 ATP binding and hydrolysis mutations[7], Tax might prevent mRNP disassembly and completion of NMD factor turnover necessary for correct mRNA decay. Consistently, in the presence of Tax, aberrant P-body profiles and higher levels of phosphorylated UPF1 were also observed (Supplementary Fig. 1 and ref. [41]). As a consequence, the activity of Tax may be widespread by regulating the expression of several host and pathogen mRNAs that are usually degraded by the NMD machinery, including cellular mRNA, such as GADD45α and viral mRNAs (Fig. 1f and refs. [5,6]). Tax-mediated regulation may offer advantages to HTLV-1, not only by ensuring the expression of its own genome but also by controlling several cellular functions that potentially participate in leukemogenesis. Thus, as Tax is known to have a mutagenic effect, blocking of NMD is likely to facilitate expression of truncated or mutated proteins that exert deleterious effects.

In conclusion, we establish that UPF1 translocation jamming correlates with strong NMD inhibition, supporting the notion that UPF1 translocation plays a key role during NMD. Analysis of specific UPF1 mutants in the absence of an exogenous factor will be suitable to identify a more direct relationship between translocation and NMD. Moreover, it will also be interesting to further describe the interplay of Tax with other NMD factors that contribute to the complex intramolecular regulation of UPF1.

Methods

Plasmids. All directed mutagenesis experiments were carried out by a 20-cycle PCR using Phusion polymerase (Thermo Fisher Scientific), a pair of reverse complementary primers (2 µM) and 50 ng of parental plasmid. PCR products were digested with DpnI restriction enzyme and used for XL1blue transformation. The pGEX2T-Tax_{WT}[57] was mutated into pGEX2T-Tax_{CACA} using 5′-GTTTGGA-GACgctGTACAAGGCGACTGGgccCCCATCTCTGGG-3′ oligonucleotide. UPF1 full-length and domains were produced with the pHL UPF1-FL, pHL UPF1-HD, pHL UPF1-CH-HD and pHL UPF1-HD-SQ constructs previously described[22]. UPF1-HD_{DEAA} and UPF1-HD_{R843C} were modified using primers 5′-GCTCCATTTTAATCGcCGcA AGCACCCAGGCCACC-3′ and 5′-

CTGTCCTGTGTGtGcGCCAACGAGCACCAAG-3′, respectively. Viral molecular pCMV HTLV-1 WT[64] was modified into pCMV HTLV ΔpX by digestion/religation of the two BlpI sites within the Tax/Rex-coding sequence.

Antibodies. The antibodies used were mouse monoclonal antibody against Tax (clone 474, Covalab, 1:1000), mouse monoclonal antibodies against HA (monoclonal clone 7, Sigma-Aldrich, 1:1000), rabbit polyclonal against UPF1 (rabbit polyconal clone A301-902A, Bethyl, 1:20,000), Anti α-His (polyclonal, Abcam ab18184, 1:1000) and anti β-beta actin (monoclonal AC15, Sigma-Aldrich, 1:5000).

Protein expression and purification. GST-Tax proteins were produced from BL21-DE3 bacteria (Novagen) induced with 0.1 mM IPTG at 25 °C during 1 h. After sonication in MTPBS (150 mM NaCl, 12.5 mM Na_2HPO_4, 2.5 mM KH_2PO_4, 100 mM EDTA pH 7.3, 0.05% Triton,10% glycerol), the lysate was incubated for 3 h at 4 °C with glutathione magnetic beads (Promega). The beads were washed three times, and Tax was further eluted in three fractions with MTPBS supplemented with 10 mM reduced glutathione at 4 °C. HisUPF1 proteins were produced and purified as previously described[22]. Briefly, BL21 DE3 bacteria were transformed and induced overnight at 16 °C in 1 l of LB. Lysis was carried by sonication in 1.5× phosphate-buffered saline (PBS), 0.1% NP40, 20 mM imidazole, 1 mM magnesium acetate and 10% glycerol with lysozyme. Soluble lysate was applied to 1 ml of NiNTA beads (Macherey-Nagel) for 3 h at 4 °C. The NiNTA resin was washed three times, and UPF1 proteins were eluted in three fractions with lysis buffer supplemented with 150 mM imidazole. The Tax/UPF1-HD complex was purified with a NGS HPLC system (Bio-Rad) after co-lysis of 200 ml of HisUPF1-HD and 1 l of Tax-expressing bacteria pellets. Lysis was performed in MTPBS with lysosyme and 5 mM imidazole. The co-lysate was first applied to a HisTrap column. The eluate (250 mM Imidazole) was dialysed in buffer PBS (1 × PBS, 10 % glycerol, 4 µM $MgCl_2$, 6 µM $ZnCl_2$, 0.1% NP40) and further purified with a GST-Trap column. The Tax/UPF1-HD complex was finally eluted with PBS buffer supplemented with 10 mM reduced glutathione and dialysed against PBS buffer.

RNA and protein co-precipitation. The RNA co-precipitation and GST pulldown were performed as described previously[20,22,41,65]. Briefly, in the RNA co-precipitation assay, proteins or preformed protein complex (2 µg) were mixed with 70 pmoles of 3′ end-biotinylated ssRNA (CGUCCAUCUGGUCAUCUAGUGAUAUCAUCG[BtnTg]) in binding buffer (20 mM HEPES pH 7.5, 150 mM potassium acetate, 2 mM magnesium acetate, 1 mM dithiothreitol (DTT), 6.3% (v/v) glycerol and 0.1% (w/v) NP-40). The reactions were performed in a final volume of 30 µl and incubated for 20 min at 30 °C. Then, 5 µl of pre-coated streptavidin-coupled magnetic beads (Dynabeads, Life Technologies) were added before further incubation for 1 h at 4 °C. Unless indicated otherwise, the beads were washed with binding buffer containing 200 mM NaCl. Proteins were eluted by addition of 7.5 µl of SDS loading buffer directly to the beads. The various fractions were subsequently analysed by 12% SDS-PAGE. For precipitation of protein complexes by GST-bait protein, the magnetic beads were replaced with 12 µl of GST resin (50% slurry, Promega). The resin was washed three times with 500 µl of binding buffer containing 200 mM NaCl and eluted with SDS loading buffer. Eluates were separated by 10% SDS-PAGE and visualised by coomassie staining.

ATP binding. Equilibrated amounts of proteins were applied to a nitrocellulose membrane with a slotblot apparatus. The membrane was soaked in blocking buffer (20 mM HEPES pH 7.0, 50 mM potassium acetate, 2.5 mM magnesium acetate, 2 mM DTT, 3% BSA (w/v), 10% (v/v) glycerol) and incubated on a rocking platform for 1 h at room temperature. The blocking buffer was then replaced with binding buffer (20 mM HEPES pH 7.0, 50 mM potassium acetate, 2.5 mM magnesium acetate, 2 mM DTT, 1.5% (w/v) BSA, 10% (v/v) glycerol) supplemented with 30 mCi of [α-^{32}P]-ATP (Perkin Elmer) before further incubation for 20 min at room temperature. The membrane was washed twice with blocking buffer before being dried and analysed by phosphorimaging.

ATP hydrolysis. ATPase assays were carried out as described in ref. [22]. Briefly, 10 pmol of UPF1 protein and UPF1/Tax preformed complex were incubated at 30 °C in a 10-µl reaction mixture containing 20 mM MES pH 6.0, 100 mM potassium acetate, 1 mM DTT, 0.1 mM EDTA, 1 mM magnesium acetate, 1 mM zinc sulphate, 5% (v/v) glycerol, 2 µCi of [α-^{32}P]-ATP (800 Ci.mmol^{-1}, Perkin Elmer), 25 mM cold ATP and 20 µg.ml^{-1} tRNA. At the indicated times, 2 µl reaction aliquots were withdrawn and quenched with 10 mM EDTA and 0.5% (v/v) SDS. Samples were analysed by phosphorimaging after TLC on polyethyleneimine cellulose plates (Merck) with 0.35 M potassium phosphate (pH 7.5) as migration buffer.

Electrophoretic mobility shift assay. The EMSA was performed as described in Fiorini et al[22]. Samples were prepared by mixing a radiolabelled 30-mer oligoribonucleotide (1 nM; CGUCCAUCUGGUCAUCUAGUGAUAUCAUCG) with UPF1 protein (0, 1, 3, 5, 10 nM) with or without Tax_{CACA} (300 nM) in a buffer containing 20 mM MES pH 6.0, 150 mM potassium acetate, 2 mM DTT, 0.2 µg.µl^{-1} BSA and 6% (v/v) glycerol. The samples were incubated at 30 °C for 20 min before being resolved by native 6.5% polyacrylamide (19:1) gel electrophoresis and analysed by phosphorimaging.

RNA decay assays and qRT-PCR/RT-PCR. RNA decay assays were performed to assess the stability of mRNA expressed from a β-globin reporter minigene that was either WT (Gl-WT) or with a PTC in the second exon (Gl-PTC)[41]. For this procedure, 0.5 µg of Gl-PTC or 0.05 µg of Gl-WT constructs were co-transfected as indicated with 0.5 µg of renilla-expressing vector in 0.7×10^6 HeLa cells with jetprime reagent (polyplus transfection). Additional plasmids were co-transfected as indicated in the figures. The medium was changed after 12 h, and cells were further cultivated for 24 additional hours. Then, following RNA decay, the cells were cultivated for 0, 1, 3 or 4 h under DRB treatment (100 µg.ml^{-1}) to block transcription. Total mRNAs were extracted using the Macherey-Nagel RNA easy extraction kit and quantified by qRT-PCR using the QuantiTect SYBR Green qRT-PCR kit (Qiagen) and appropriate primers:

GLOBIN (Globin 3′ forward 5′-TTGGGGATCTGTCCACTCC-3′, Globin 3′ reverse 5′-CACACCAGCCACCACTTTC-3′, Globin full-length forward 5′-GATGAAGTTGGTGGTGAGGC-3′, Globin full-length reverse 5′-AGTGATACTTGTGGGCCAGG-3′), *GADD45*α (forward 5′-ACGAGGACGACGACAGAGAT-3′, reverse 5′-GCAGGATCCTTCCATTGAGA-3′), MAP3K14 (forward 5′-TCAGTGCAGAACCAGGTCAG-3′, reverse (5′-GGGGACTGAGAACCACTTCA-3′) and SMG5 (forward (5′-ACAGAATGGGATGCCAGGAA-3′, reverse 5′-TCAACACTCCAAAAGCCAGC-3′). Normalisation was carried out with respect to renilla mRNA (renilla forward primer 5′-CTAACCTCGCCCTTCTCCTT-3′, renilla reverse 5′-TCGTCCATGCTGAGAGTGTC-3′). The values represented in the graphs correspond to the mean of at least three biological replicates, and the error bars correspond to the SD. Half-lives were calculated for each replicate, and *P* values were calculated by performing a Student's *t*-test (unpaired, two-tailed) ns: $P > 0.05$; $^*P < 0.05$; $^{**}P < 0.01$.

RNA immunoprecipitation. For UPF1 RIP, ~2×10^6 HeLa cells were transfected as described in the figures, harvested and resuspended in lysis buffer (50 mM Tris–Cl, pH 7.5, 1% NP-40, 0.5% sodium deoxycholate, 0.05% SDS, 1 mM EDTA, 150 mM NaCl, protease inhibitor (Roche) and RNAsin (Promega)). Extracts obtained after centrifugation at 12,000*g* for 15 min were incubated with primary antibody overnight at 4 °C. Protein A and G magnetic beads (dynabeads, Life Technology; 5 µl each) were mixed and coated with PBS + 5% BSA, supplemented with tRNA and RNasin overnight. After re-equilibration in lysis buffer (supplemented with tRNA), the beads were added to the lysate for 2 h at 4 °C before extensive washing in lysis buffer. The beads were resuspended in elution buffer (50 mM Tris–HCl, pH 7.0. 1 mM EDTA, 10 mM DTT and 1% SDS).

For RIP Tax, we followed the protocol described by Niranjanakumari et al.[66] to perform reversible crosslinking combined with RIP. For each RIP condition, ~2×10^6 HeLa cells were transfected as described in the figures, harvested and fixed with 0.05% formaldehyde for 20 min at room temperature. Then, 0.25 M glycine was added for 5 min before PBS washing. The cell pellet was resuspended in 2 ml of lysis buffer, and the lysate was sonicated (bioruptor, diagenode). The immunoprecipitation steps were carried out as described for UPF1 RIP, except that extensive washings were performed with 50 mM Tris–Cl, pH 7.5, 1% NP-40, 0.5% sodium deoxycholate, 0.05% SDS, 1 mM EDTA, 500 mM NaCl and 1 M urea. The beads were resuspended in elution buffer and incubated at 70 °C for 45 min for reverse-crosslinking. In the case of the double-RIP experiment, ~9×10^6 HeLa cells were transfected with 10 µg of Tax and 15 µg of the HA-UPF1 expression plasmids[41], as well as 10 µg of Gl-PTC construct. The cells were treated using similar conditions as described for Tax RIP. First, the HA tag was immunoprecipitated. Elution was carried out at 4 °C in 10 µl of 50 mM Tris HCl, 1 mM EDTA, RNAsin and 20 mM DTT for 1 h, plus one additional hour in 150 µl of 50 mM Tris HCl, 1 mM EDTA complemented with 100 µg.ml^{-1} HA elution peptide. Finally, the elution volume was increased to 500 µl (50 mM Tris–Cl, pH 7.5, 1% NP-40, 0.5% sodium deoxycholate, 0.05% SDS, 1 mM EDTA, 150 mM NaCl, protease inhibitor (Roche) and RNAsin), and Tax immunoprecipitation was performed. After extensive washing, the beads were resuspended in elution buffer and incubated at 70 °C for 45 min for reverse-crosslinking.

For all RIP, RIP and double-RIP experiments, the precipitated RNA was further extracted with RNAzolRT reagent (MRC) and subjected to qRT-PCR.

DNA and siRNA transfection. DNA and short interfering RNA (siRNA) co-transfection in HeLa cells was carried out using jetprime® reagent according to the manufacturer's instructions (Polyplus transfection SA). The siCtrl (MISSION siRNA Universal negative control, SIGMA) and siUPF1 (5′-GAUGCAGUUCCGCUCCAUUGAUGCAGUUCCGCUCCAUU-3′) were used at a final concentration of 10 nM. Twenty-four hours later, the cells were washed with PBS and reincubated in fresh medium for 48 h before harvest.

Biolayer interferometry. Biolayer interferometry experiments were carried out using a BLItz apparatus (ForteBio). The affinity of UPF1 HD for its substrate was analysed with a SAX biosensor. First, the absence of aspecific binding of each of the analysed proteins on the biosensor was verified. Next, a 90 µg.ml^{-1} solution of random 30-mer DNA oligonucleotides with Biotin TEG at its 5′ extremity was

immobilised on the streptavidin SAX biosensor in 1 × PBS buffer. The biosensor was further equilibrated in 20 mM HEPES pH 7.5, 150 mM potassium acetate, 2 mM magnesium acetate, 1 mM DTT, 6.3% (v/v) glycerol and 0.1% (w/v) NP-40. For the association curve, the ligand proteins were diluted at the indicated concentrations in 20 mM HEPES pH 7.5, 150 mM potassium acetate, 2 mM magnesium acetate, 1 mM DTT, 6.3% (v/v) glycerol and 0.1% (w/v) NP-40 and further incubated with the SAX biosensor. The following dissociation curve was obtained by incubating the biosensor in 20 mM HEPES pH 7.5, 150 mM potassium acetate, 2 mM magnesium acetate, 1 mM DTT, 6.3% (v/v) glycerol and 0.1% (w/v) NP-40) without ligand. The biosensor was regenerated with buffer containing 150 mM NaCl, 1.25 mM EDTA and 0.125% SDS. The k_{on}, k_{off} and K_D were calculated using the manufacturer's software (BLItz Pro 1.2). Each experiment was conducted at least in triplicate.

The affinity of UPF1-HD WT and mutant proteins for GST-Tax was analysed with an AR2G sensor (ForteBio). First, GST-Tax was covalently bound to the biosensor following the manufacturer's procedure: the biosensor was activated for 300 s with 20 mM EDC, 10 mM NHS and 10 mM sodium acetate pH 5. Next, 20 nM of Tax diluted in 100 mM sodium acetate pH 4 were linked for 500 s before quenching with 1 M ethanolamine pH 8.5. The baseline was acquired after 120 s of incubation in the manufacturer's running buffer (300 mM NaCl, 20 mM phosphate, 0.02% Tween 20, 0.1% albumin, 0.05% ProClin300) before 250 s of incubation with UPF1 His-HD protein diluted in the running buffer. Finally, the dissociation step was acquired after 60 s of incubation of the sensor with running buffer without protein.

Experiment with magnetic tweezers. The DNA hairpin used for single-molecule experiments was performed as described by Fiorini et al.[33]. The 1.2-kbp DNA substrate is a 1239-bp hairpin with a 4-nt loop, a 76-nt 5′-biotinylated ssDNA tail and a 146 bp 3′-digoxigenin-labelled dsDNA (sequence available in supplementary methods). We used a PicoTwist magnetic tweezers instrument (www.picotwist.com) to manipulate individual DNA. The DNA hairpins were attached by the 5′-biotinylated extremity to streptavidin-coated magnetic beads (Dynabeads MyOne streptavidin T1, Life Technology) and by a 3′-digoxigenin-modified extremity to an anti-Dig-coated glass surface. The glass coverslip had been previously treated with anti-digoxigenin antibody (Roche) and passivated with 1 × PBS Buffer (1 × PBS pH 7.5, 0.2% pluronic surfactant, 5 mM EDTA, 10 mM sodium azide and 0.2% BSA (Sigma-Aldrich)). Experiments were conducted at 37 °C in helicase buffer (20 mM Tris-HCl pH 7.5, 75 mM potassium acetate, 3 mM magnesium chloride, 2% BSA, 0.5 mM DTT and 2 mM ATP). The indicated UPF1 concentration was the lowest possible concentration to observe helicase activity under single-molecule conditions (between 1 and 20 nM depending on the protein batch). Tax_{CACA} was used at a 5 nM final concentration.

Data availability. All relevant data are available from the authors.

Received: 25 June 2017 Accepted: 28 December 2017
Published online: 30 January 2018

References

1. Kim, Y. K., Furic, L., Desgroseillers, L. & Maquat, L. E. Mammalian Staufen1 recruits Upf1 to specific mRNA 3'UTRs so as to elicit mRNA decay. *Cell* **120**, 195–208 (2005).
2. Azzalin, C. M. & Lingner, J. The human RNA surveillance factor UPF1 is required for S phase progression and genome stability. *Curr. Biol.* **16**, 433–439 (2006).
3. Chawla, R. et al. Human UPF1 interacts with TPP1 and telomerase and sustains telomere leading-strand replication. *EMBO J.* **30**, 4047–4058 (2011).
4. Kaygun, H. & Marzluff, W. F. Regulated degradation of replication-dependent histone mRNAs requires both ATR and Upf1. *Nat. Struct. Mol. Biol.* **12**, 794–800 (2005).
5. Karousis, E. D., Nasif, S. & Mühlemann, O. Nonsense-mediated mRNA decay: novel mechanistic insights and biological impact. *Wiley Interdiscip. Rev. RNA* **7**, 661–682 (2016).
6. Zund, D., Gruber, A. R., Zavolan, M. & Muhlemann, O. Translation-dependent displacement of UPF1 from coding sequences causes its enrichment in 3' UTRs. *Nat. Struct. Mol. Biol.* **20**, 936–943 (2013).
7. Hurt, J. A., Robertson, A. D. & Burge, C. B. Global analyses of UPF1 binding and function reveal expanded scope of nonsense-mediated mRNA decay. *Genome Res.* **23**, 1636–1650 (2013).
8. Kashima, I. et al. Binding of a novel SMG-1-Upf1-eRF1-eRF3 complex (SURF) to the exon junction complex triggers Upf1 phosphorylation and nonsense-mediated mRNA decay. *Genes Dev.* **20**, 355–367 (2006).
9. Ivanov, P. V., Gehring, N. H., Kunz, J. B., Hentze, M. W. & Kulozik, A. E. Interactions between UPF1, eRFs, PABP and the exon junction complex suggest an integrated model for mammalian NMD pathways. *EMBO J.* **27**, 736–747 (2008).
10. Silva, A. L., Ribeiro, P., Inácio, A., Liebhaber, S. A. & Romão, L. Proximity of the poly(A)-binding protein to a premature termination codon inhibits mammalian nonsense-mediated mRNA decay. *RNA* **14**, 563–576 (2008).
11. Czaplinski, K. et al. The surveillance complex interacts with the translation release factors to enhance termination and degrade aberrant mRNAs. *Genes Dev.* **12**, 1665–1677 (1998).
12. Toma, K. G., Rebbapragada, I., Durand, S. & Lykke-Andersen, J. Identification of elements in human long 3' UTRs that inhibit nonsense-mediated decay. *RNA* **21,** 887-897 (2015).
13. Lindeboom, R. G. H., Supek, F. & Lehner, B. The rules and impact of nonsense-mediated mRNA decay in human cancers. *Nat. Genet.* **48**, 1112–1118 (2016).
14. Martin, L. et al. Identification and characterization of small molecules that inhibit nonsense-mediated RNA decay and suppress nonsense p53 mutations. *Cancer Res.* **74**, 3104–3113 (2014).
15. Mendell, J. T., Sharifi, N. A., Meyers, J. L., Martinez-Murillo, F. & Dietz, H. C. Nonsense surveillance regulates expression of diverse classes of mammalian transcripts and mutes genomic noise. *Nat. Genet.* **36**, 1073–1078 (2004).
16. Buhler, M., Paillusson, A. & Muhlemann, O. Efficient downregulation of immunoglobulin mu mRNA with premature translation-termination codons requires the 5'-half of the VDJ exon. *Nucleic Acids Res.* **32**, 3304–3315 (2004).
17. Eberle, A. B., Stalder, L., Mathys, H., Orozco, R. Z. & Muhlemann, O. Posttranscriptional gene regulation by spatial rearrangement of the 3' untranslated region. *PLoS Biol.* **6**, e92 (2008).
18. Hansen, K. D. et al. Genome-wide identification of alternative splice forms down-regulated by nonsense-mediated mRNA decay in Drosophila. *PLoS Genet.* **5**, e1000525 (2009).
19. Singh, G., Rebbapragada, I. & Lykke-Andersen, J. A competition between stimulators and antagonists of Upf complex recruitment governs human nonsense-mediated mRNA decay. *PLoS Biol.* **6**, e111 (2008).
20. Chamieh, H., Ballut, L., Bonneau, F. & Le Hir, H. NMD factors UPF2 and UPF3 bridge UPF1 to the exon junction complex and stimulate its RNA helicase activity. *Nat. Struct. Mol. Biol.* **15**, 85–93 (2008).
21. Chakrabarti, S. et al. Molecular mechanisms for the RNA-dependent ATPase activity of Upf1 and its regulation by Upf2. *Mol. Cell* **41**, 693–703 (2011).
22. Fiorini, F., Boudvillain, M. & Le Hir, H. Tight intramolecular regulation of the human Upf1 helicase by its N- and C-terminal domains. *Nucleic Acids Res.* **41**, 2404–2415 (2013).
23. Melero, R. et al. Structures of SMG1-UPFs Complexes: SMG1 Contributes to Regulate UPF2-Dependent Activation of UPF1 in NMD. *Struct. Lond. Engl.* **22**, 1105–1119 (2014).
24. Durand, S., Franks, T. M. & Lykke-Andersen, J. Hyperphosphorylation amplifies UPF1 activity to resolve stalls in nonsense-mediated mRNA decay. *Nat. Commun.* **7**, 12434 (2016).
25. Yamashita, A., Ohnishi, T., Kashima, I., Taya, Y. & Ohno, S. Human SMG-1, a novel phosphatidylinositol 3-kinase-related protein kinase, associates with components of the mRNA surveillance complex and is involved in the regulation of nonsense-mediated mRNA decay. *Genes Dev.* **15**, 2215–2228 (2001).
26. Okada-Katsuhata, Y. et al. N- and C-terminal Upf1 phosphorylations create binding platforms for SMG-6 and SMG-5:SMG-7 during NMD. *Nucleic Acids Res.* **40**, 1251–1266 (2011).
27. Cho, H., Kim, K. M. & Kim, Y. K. Human proline-rich nuclear receptor coregulatory protein 2 mediates an interaction between mRNA surveillance machinery and decapping complex. *Mol. Cell* **33**, 75–86 (2009).
28. Ohnishi, T. et al. Phosphorylation of hUPF1 induces formation of mRNA surveillance complexes containing hSMG-5 and hSMG-7. *Mol. Cell* **12**, 1187–1200 (2003).
29. Chakrabarti, S., Bonneau, F., Schüssler, S., Eppinger, E. & Conti, E. Phospho-dependent and phospho-independent interactions of the helicase UPF1 with the NMD factors SMG5-SMG7 and SMG6. *Nucleic Acids Res.* **42**, 9447–9460 (2014).
30. Franks, T. M., Singh, G. & Lykke-Andersen, J. Upf1 ATPase-dependent mRNP disassembly is required for completion of nonsense- mediated mRNA decay. *Cell* **143**, 938–950 (2010).
31. Buchwald, G. et al. Insights into the recruitment of the NMD machinery from the crystal structure of a core EJC-UPF3b complex. *Proc. Natl Acad. Sci. USA* **107**, 10050–10055 (2010).
32. Bhattacharya, A. et al. Characterization of the biochemical properties of the human Upf1 gene product that is involved in nonsense-mediated mRNA decay. *RNA* **6**, 1226–1235 (2000).
33. Fiorini, F., Bagchi, D., Le Hir, H. & Croquette, V. Human Upf1 is a highly processive RNA helicase and translocase with RNP remodelling activities. *Nat. Commun.* **6**, 7581 (2015).

34. Lee, S. R., Pratt, G. A., Martinez, F. J., Yeo, G. W. & Lykke-Andersen, J. Target discrimination in nonsense-mediated mRNA decay requires Upf1 ATPase activity. *Mol. Cell* **59**, 413–425 (2015).
35. Sun, X., Perlick, H. A., Dietz, H. C. & Maquat, L. E. A mutated human homologue to yeast Upf1 protein has a dominant-negative effect on the decay of nonsense-containing mRNAs in mammalian cells. *Proc. Natl Acad. Sci. USA* **95**, 10009–10014 (1998).
36. Clerici, M. et al. Unusual bipartite mode of interaction between the nonsense-mediated decay factors, UPF1 and UPF2. *EMBO J.* **28**, 2293–2306 (2009).
37. Balistreri, G., Bognanni, C. & Mühlemann, O. Virus escape and manipulation of cellular nonsense-mediated mRNA decay. *Viruses* **9**, 24 (2017).
38. Mocquet, V., Durand, S. & Jalinot, P. How retroviruses escape the nonsense mediated mRNA decay (NMD)? *AIDS Res. Hum. Retroviruses* **31**, 948-958 (2015).
39. Balistreri, G. et al. The host nonsense-mediated mRNA decay pathway restricts mammalian RNA virus replication. *Cell Host Microbe* **16**, 403–411 (2014).
40. Garcia, D., Garcia, S. & Voinnet, O. Nonsense-mediated decay serves as a general viral restriction mechanism in plants. *Cell Host Microbe* **16**, 391–402 (2014).
41. Mocquet, V. et al. The human T-lymphotropic virus type 1 tax protein inhibits nonsense-mediated mRNA decay by interacting with INT6/EIF3E and UPF1. *J. Virol.* **86**, 7530–7543 (2012).
42. Serquina, A. K. et al. UPF1 is crucial for the infectivity of human immunodeficiency virus type 1 progeny virions. *J. Virol.* **87**, 8853–8861 (2013).
43. Weil, J. E. & Beemon, K. L. A 3' UTR sequence stabilizes termination codons in the unspliced RNA of Rous sarcoma virus. *RNA* **12**, 102–110 (2006).
44. Arrigo, S. & Beemon, K. Regulation of Rous sarcoma virus RNA splicing and stability. *Mol. Cell Biol.* **8**, 4858–4867 (1988).
45. Weil, J. E., Hadjithomas, M. & Beemon, K. L. Structural characterization of the Rous sarcoma virus RNA stability element. *J. Virol.* **83**, 2119–2129 (2009).
46. Withers, J. B. & Beemon, K. L. Structural features in the Rous sarcoma virus RNA stability element are necessary for sensing the correct termination codon. *Retrovirology* **7**, 65 (2010).
47. Ge, Z., Quek, B. L., Beemon, K. L. & Hogg, J. R. Polypyrimidine tract binding protein 1 protects mRNAs from recognition by the nonsense-mediated mRNA decay pathway. *eLife* **5**, e11155 (2016).
48. Ajamian, L. et al. Unexpected roles for UPF1 in HIV-1 RNA metabolism and translation. *RNA* **14**, 914–927 (2008).
49. Ajamian, L. et al. HIV-1 recruits UPF1 but excludes UPF2 to promote nucleocytoplasmic export of the genomic RNA. *Biomolecules* **5**, 2808–2839 (2015).
50. Tang, X. et al. Structural basis of suppression of host translation termination by Moloney Murine Leukemia Virus. *Nat. Commun.* **7**, 12070 (2016).
51. Caputo, A. & Haseltine, W. A. Reexamination of the coding potential of the HTLV-1 pX region. *Virology* **188**, 618–627 (1992).
52. Nakano, K. et al. Viral interference with host mRNA surveillance, the nonsense-mediated mRNA decay (NMD) pathway, through a new function of HTLV-1 Rex: implications for retroviral replication. *Microbes Infect.* **15**, 491–505 (2013).
53. Chapin, A. et al. In vivo determination of direct targets of the nonsense-mediated decay pathway in Drosophila. *G3* **4**, 485–496 (2014).
54. Nelson, J. O., Moore, K. A., Chapin, A., Hollien, J. & Metzstein, M. M. Degradation of Gadd45 mRNA by nonsense-mediated decay is essential for viability. *eLife* **5**, e12876 (2016).
55. Cheng, Z., Muhlrad, D., Lim, M. K., Parker, R. & Song, H. Structural and functional insights into the human Upf1 helicase core. *EMBO J.* **26**, 253–264 (2007).
56. Rigaut, G. et al. A generic protein purification method for protein complex characterization and proteome exploration. *Nat. Biotechnol.* **17**, 1030–1032 (1999).
57. Caron, C. et al. Functional and biochemical interaction of the HTLV-I Tax1 transactivator with TBP. *EMBO J.* **12**, 4269–4278 (1993).
58. Semmes, O. J. & Jeang, K. T. HTLV-I Tax is a zinc-binding protein: role of zinc in Tax structure and function. *Virology* **188**, 754–764 (1992).
59. Leeds, P., Wood, J. M., Lee, B. S. & Culbertson, M. R. Gene products that promote mRNA turnover in Saccharomyces cerevisiae. *Mol. Cell Biol.* **12**, 2165–2177 (1992).
60. Manosas, M., Spiering, M. M., Zhuang, Z., Benkovic, S. J. & Croquette, V. Coupling DNA unwinding activity with primer synthesis in the bacteriophage T4 primosome. *Nat. Chem. Biol.* **5**, 904–912 (2009).
61. Kurosaki, T. et al. A post-translational regulatory switch on UPF1 controls targeted mRNA degradation. *Genes Dev.* **28**, 1900–1916 (2014).
62. Serdar, L. D., Whiteside, D. L. & Baker, K. E. ATP hydrolysis by UPF1 is required for efficient translation termination at premature stop codons. *Nat. Commun.* **7**, 14021 (2016).
63. Morris, C., Wittmann, J., Jack, H. M. & Jalinot, P. Human INT6/eIF3e is required for nonsense-mediated mRNA decay. *EMBO Rep.* **8**, 596–602 (2007).
64. DerseD., HillS. A., Lloyd, P. A. & Chung, Hk. & MorseB. A.. Examining human T-lymphotropic virus type 1 infection and replication by cell-free infection with recombinant virus vectors. *J. Virol.* **75**, 8461–8468 (2001).
65. Ballut, L. et al. The exon junction core complex is locked onto RNA by inhibition of eIF4AIII ATPase activity. *Nat. Struct. Mol. Biol.* **12**, 861–869 (2005).
66. Niranjanakumari, S., Lasda, E., Brazas, R. & Garcia-Blanco, M. A. Reversible cross-linking combined with immunoprecipitation to study RNA-protein interactions in vivo. *Methods* **26**, 182–190 (2002).

Acknowledgements

We would like to thank Saurabh Raj at LPS of ENS-Paris for assistance during MT data collections and Derse's lab for pCMV-HTLV-1 plasmids. We also thank Armelle Roisin, Sébastian Durand and Stéphane Rety at LBMC of ENS-Lyon for technical support and for suggestions and Christophe Guillon at MMSB-Lyon and Vincent Vanoosthuyse at LBMC-Lyon for useful comments on the manuscript. We acknowledge the contribution of SFR Biosciences (UMS3444/CNRS, US8/Inserm, ENS de Lyon, UCBL) facilities: PLATIM and PSF, in particular Véronique Senty-Ségault for help in BLItz experiments' set-up. Work in the authors' laboratory is supported by grants from foundation ARC (V. M.), from La Ligue Isere contre le Cancer (V.M.) and French Agence Nationale de Recherche sur le SIDA et les Hépatite Virales (ANRS) fellowship (F.F.).

Author contributions

Protein purifications, pulldown and enzymatic bulk assays: F.F.; protein purifications and BLItz experiments: J.-P.R.; Helicase MT assays: J.K., F.F., H.L.H. and V.C.; immuno-fluorescence assays: M.B.; pull-down assays and ex vivo experiments: V.M.; writing the manuscript: F.F., V.M. and P.J.

Additional information

Supplementary Information accompanies this paper at https://doi.org/10.1038/s41467-017-02793-6.

Competing interests: The authors declare no competing financial interests.

3. *HTLV-1 Rex hijacks UPF1 in a CRM1 dependant manner, leading to NMD inhibition and UPF1 loading in the viral particle.*

La voie d'export dépendante de CRM1 est consacrée à l'export nucléaire de protéines cargo présentant un signal d'exportation nucléaire (NES) mais affecte peu l'export des ARNm. CRM1 est essentiel pour l'homéostasie cellulaire et les défauts de sa fonction sont liés à plusieurs types de cancer. Le détournement de l'exportine CRM1 est une étape critique du cycle rétroviral. Il permet l'export cytoplasmique de l'ARN viral non épissé, nécessaire à la traduction des protéines structurale et à l'encapsidation de copies complètes du génome viral dans les virions. Ces deux événements sont indispensables à la production de virions infectieux. Lors d'une infection par HTLV-1, c'est la protéine virale Rex qui se lie à l'ARN viral non épissé et détourne CRM1. Ici, nous nous sommes demandé quelles sont les conséquences cellulaires du détournement de la voie d'exportation de CRM1 par des transporteurs rétroviraux tels que Rex. Pour mener à bien cette étude nous avons vérifié l'impact de Rex sur l'hélicase UPF1, connue pour être un cargo de CRM1.

Tout d'abord, en utilisant des immunoprécipitations, nous avons identifié que CRM1 était plus lié à UPF1 lors de l'expression de Rex, conduisant à la formation d'un complexe Rex, UPF1, CRM1. La formation de ce complexe est indépendante de la présence d'ARN viral et conduit à la rétention nucléaire d'UPF1. Nous avons également pu corréler la formation de ce complexe avec une affinité réduite d'UPF1 pour tous les ARN, y compris ses cibles NMD résultant en l'inhibition du NMD. Pour confirmer qu'il s'agit d'une conséquence du détournement de CRM1, nous avons reproduit ces observations avec Rev, l'homologue fonctionnel de Rex chez HIV. Afin de valider la pertinence physiologique de nos observations, nous avons étudié ce complexe dans les cellules chroniquement infectées par HTLV-1, où Rex se lie à l'ARN viral. En confirmant nos observations, nous avons aussi identifié que Rex charge UPF1 sur l'ARN viral de manière CRM1 dépendante, dans un contexte indépendant du NMD. Finalement, ceci aboutit à l'encapsidation d'UPF1 dans les virions.

En conclusion, notre travail révèle pour la première fois que le hijacking de CRM1 par Rex induit directement la répression d'un processus cellulaire, ici le NMD. Par la même occasion, nous avons caractérisé un nouveau mode d'inhibition du NMD par HTLV-1, impliquant donc cette fois Rex, UPF1 et l'export noyau cytoplasme CRM1 dépendant. L'analyse comparative avec Rev d'HIV prouve que ce virus est également capable d'inhiber le NMD ce qui n'avait jamais été démontré. Finalement, nous avons observé qu'en détournant CRM1 à l'avantage du virus, Rex induit également le chargement d'UPF1 sur l'ARN viral. Pour finaliser ce travail, nous recherchons actuellement si la présence d'UPF1 sur l'ARN viral peut influencer soit la traduction des protéines structurales, soit le potentiel infectieux des virions. Des quantifications de p19GAG, de production de particules virales et des essais de transmission virale sont en cours.

HTLV-1 Rex hijacks UPF1 in a CRM1 dependant manner, leading to NMD inhibition and UPF1 loading in the viral particle

Prochasson L[1], Mghezzi-Habellah M[1], Roisin A[1], Palma M[2], Robin JP[1], De Bossoreille S[1], Cluet D[1], Mouehli M[1], Decimo D[3], Réty S[1], Dutartre H[3], Lejeune F[2], Jalinot P[1], Mocquet V[1]

Introduction

The maintenance of cell homeostasis requires a strict control of the repartition of macromolecules between nucleus and cytoplasm. Pathways monitoring this shuttling are dependent on the nature of the macromolecules to be exported or imported. Notably, whereas bulk mRNA export occurs via the Nxf1/Tap1 pathway after its association with TREX complex, the exportin CRM1 (XPO1) mediates the export of proteins containing a Nuclear Export Signal (NES). These cargoes may be associated or not with a specific subset of RNA such as rRNA, snRNA and some mRNA [1,2]. The NES is characterized by a specific stretch of 4 hydrophobic amino acids with variable interspaced amino acids that influences the NES affinity to CRM1. The formation of the complex between CRM1 and the NES containing protein also requires the GTPase Ran to conformationally stabilize the NES binding groove of CRM1 [3–6]. However, the affinity of many NES substrates for CRM1 is rather low, suggesting that the formation of this trimeric transport complex is a rate-limiting step in nuclear export [7–9]. Once in the cytoplasm, Ran GAP, at the nuclear pore, catalyses the conversion of RanGTP to RanGDP, inducing the dissociation of the trimeric complex CRM1/Cargo/Ran and the release of the cargo in the cytoplasm. Ultimately, the free CRM1 re-enter the nucleus for a new round of export [10].

Among the plethora of functionally and structurally unrelated protein and RNP cargoes, the mislocalisation of several of them due to CRM1 dysfunction supports a role of CRM1 in disease: that is the case of proteins involved in the control of DNA repair, cell cycle, transcription regulation or apoptosis such as BARD1, p21, p27, p53, FOXO3, APC and Survivin (reviewed in [11,12]). In addition, CRM1 overexpression and mutations were directly correlated with multiple types of cancer, notably pancreatic cancer, ovarian cancer, glioma, osteosarcoma, acute myeloid leukemia and multiple myeloma [13–16]. As a consequence, CRM1 was considered as a valuable target for anticancer therapies. CRM1 inhibitors where shown to sensitize cancerous cells to apoptosis and several of them are currently under clinic trial [17,18].

An important subset of CRM1 cargoes includes proteins involved in RNA processing. Notably, the DNA/RNA helicase UPF1 and its partner UPF2 have been reported to shuttle between cytoplasm and nucleus via CRM1: interactions were identified by mass spectrometry and leptomycin B treatments induced their nuclear retention [19–21]. However, the impact of a shuttling perturbation on their cellular functions have never been evaluated. UPF1 works at the crossroad of multiple process for DNA and RNA maintenance and is directly involved in the post-transcriptional regulation of gene expression. Its function in Nonsense Mediated mRNA Decay (NMD) is the most described[22,23]. It is commonly accepted that NMD targets and degrades mRNA harbouring premature codons (PTC) due to the wrong accumulation of UPF1 between the stalled ribosome and a downstream Exon Junction Complex: while UPF1 binds along the length of mRNA, it is gradually displaced by the running ribosome and stabilized downstream a stop codon by its partner UPF3[24–26]. Then UPF1 assembles a NMD promoting complex with UPF2, that activates its ATPase activity and SMG1 that phosphorylates its Nter and Cter extremity [27–29]. Phosphorylated UPF1 creates a scaffold for the further recruitment of decapping enzymes as well as endo/exonucleases leading to proper RNA decay[30]. In addition to PTC containing RNA, NMD was shown to target several viral RNA, exerting an antiviral function [31–37]. In the light of this, the unspliced viral RNA from the human delta retrovirus HTLV-1 has been characterized to be destabilized in a UPF1 and UPF2 dependant manner [38,39]. To counter this threat and fully express their compact genome, virus

evolved different bypass strategies (reviewed in [40]). A well characterized example is a PTBP1 binding motif from Rous sarcoma virus, known as RNA stability element (RSE) that reduces UPF1 recruitment to viral RNA [41,42]. Alternatively, the viral protein Rev from HIV binds UPF1 during vRNA export: in silico protein-protein docking analyses suggest that this interaction occurs in a region that overlaps the UPF2 binding site protecting vRNA from NMD activation [43]. In a context of HTLV-1 infection, the viral proteins Tax and Rex were shown to trans-inhibit NMD [38,39]. Tax directly binds UPF1 and exerts a dual effect on this latter, inhibiting its ATPase activity and ultimately NMD[44]; the Nterminal domain of Rex as well as its phosphorylation were shown to be critical for Rex/UPF1 interaction. Nakano et al, also suggest that this interaction results in the incorporation of Rex in the NMD complex [45].

Interestingly, viruses also express NES containing proteins. Notably, the retroviral proteins Rex from HTLV-1 and its functional homolog Rev from HIV-1 which have been extensively studied. HTLV and HIV are two human complex retroviruses which impact on the infected cell homeostasis is different, resulting in fundamentally different diseases: HTLV is the causative agent of the Adult T cell Leukemia (ATL) a malignant lymphoproliferative syndrome established after decades of latency, or the HTLV associated myelopathy/tropical spastic paraparesis (HAM/TSP), an inflammatory disease [46,47]. To the opposite, HIV is the causative agent of the acquired immunodeficiency syndrome (AIDS), characterized by the weakening of the immune system due to the progressive destruction of infected cells [48]. However, as retroviruses, their overall replication cycle share common features. Notably, both viruses export unspliced viral RNA (vRNA) molecules to the cytoplasm. To do so, they rely on viral transporters that interfere with the host splicing machinery, stabilize unspliced RNA over spliced isoforms and hijack the cellular shuttling machinery to export vRNA from the nucleus. Yet genetically divergent, these transporters, namely HTLV Rex and HIV Rev, share similar functional domains and a similar modus operandi to accomplish this task[49]: first they display a highly basic motif rich in arginine, allowing RNA binding at the the Rex/Rev responsive elements present on viral RNA (RxRE and RRE respectively)[50,51]. This RNA binding domain is partially overlapping with the Nuclear Localisation Signal (NLS), this latter being involved in their interaction with the importins. Both viral transporters also display a Nuclear Export Signal (NES) directly involved in their binding to the exportin CRM1/XPO1[52]. Rev NES is defined as a class2 while Rex NES fits a class1c. Finally, they both have a dual multimerization motif, encompassing the NLS for Rev or the NES for Rex [53,54]. After their translation, both viral transporters are translocated to the nucleus via importin b and accumulate in the nucleolus [55,56]. Rev has a strong Nucleolus localization signal (NoLS) while Rex may be driven there through interactions with the viral p30. The interaction with the nucleolar phosphoprotein B23 is another important partner controlling Rev and Rex nucleolar localization [57–59]. In the nucleolus, Rex and Rev bind the RxRE and the RRE motif of their vRNA respectively. Rev bound to vRNA then multimerizes in order to interact more efficiently with CRM1 via its NES. Concerning HTLV-1, it was proposed that Rex interacts with CRM1 and multimerizes before binding the RxRE motif of vRNA [52,60,61]. Although the sequential steps leading to the formation of an export complex with Rex are not as much described as with Rev and may diverge, both result in the formation of a viral transporter multimer interacting with vRNA and CRM1. Thus, CRM1 hijacking is a critical step that allows the cytoplasmic accumulation of unspliced vRNA. This RNA is the support of the structural polyprotein GAG translation. In addition, two copies are packaged in newly synthesized viral particles for viral transmission [62].

Unexpectedly, while the causative role of CRM1 in disease strongly stresses the importance of a correct repartition of cargoes between nucleus and cytoplasm for the proper functioning of the cell and supports the effort of developing CRM1 inhibitors for clinic, understanding the impact of CRM1 hijack by retroviral transporters on the cellular homeostasis is barely evoked in the literature. Thus, in this work, we investigated how the hijack of CRM1 by HTLV-1 Rex affects the relationship between CRM1 and the cargo UPF1 as well as this latter most described function: the NMD. We found that Rex dependent hijacking of CRM1 is the initial step of an additional UPF1 hijacking: on one side, Rex

stabilizes the UPF1/CRM1 interaction, provokes the nuclear accumulation of UPF1, and repress its association with bulk RNA. As a consequence, this inhibits NMD. On the other side, we found that Rex favours UPF1 repositioning on unspliced vRNA supporting an unexpected pro-viral role of the helicase during HTLV-1 infection.

METHODS:

Antibodies. Anti-UPF1 rabbit polyclonal (RENT1, A301-902A, Bethyl), Anti-CRM1 rabbit polyclonal (A300-469A, Bethyl), Anti-UPF2 rabbit molyclonal (A303-029A, Bethyl), Anti-HA mouse monoclonal (clone HA-7, SIGMA), Anti-FLAG mouse monoclonal (FlagM2, Sigma), Anti-HTLV-1 p19 mouse monoclonal (TP-7, Abcam), Anti-Tax mouse monoclonal, Anti-Rex and Anti-Ribonucleoside-diphosphate reductase subunit M2 (RRM2) rabbit polyclonal were homemade. For immunofluorescence specifically: primary Goat UPF1 (A300-036A, Bethyl), and secondary antibodies were goat anti-mouse Alexa Fluor 488 (Thermofischer), mouse anti-Goat CFL 555 (Santa Cruz), Donkey anti-Rabbit AlexaFluor 647 (Abcam).

Mutagenesis. To construct Rex mutant plasmids, directed mutagenesis was carried out as follow: a 20 cycle PCR was done with Phusion polymerase, 2µM of complementary primers with the point mutation and 50ng of the parental plasmid (pCMV Rex WT). PCR products were digested by DpnI before XL1 blue transformation. Rex NLSmut oligos: cgatcccaaagaGATTTAccaccaacacc and ggtgttggtggTAAATCtctttgggatcg. Rex NESmut: to sequential mutagenesis were done with the following primers couples: tcagctctacagttccGGAtcccctccttcc and ggaaggaggggaTCCggaactgt agagctga; ctacagttccGGAtcccctccttccccac and gaaggaggggaTCCggaactgtagagctg. pCMVHTLV WT and Tax9Q plasmids were already described. To modify Rex, a 1kb fragment between both BlpI restriction sites was amplified (primers: 5'forward -ggacgcgttatcagctcagctctacagttccTAAtccctcg; 3' reverse atttgtcttcaggggacac). The 5' forward primer harboured the nonsense mutation L23stop in the Rex sequence. It is neutral for the Tax sequence encoded on the same RNA. The DNA fragment and retroviral backbone were digested by BlpI (NEB). Both were ligated at 16°C overnight with T4DNA ligase (NEB) before XL1 blue transformation. All mutants were validated by sanger sequencing (Genewiz).

Immunoprecipitations. ~2 × 106 293T cells were transfected as described in the figures using jet prime reagent (Polyplus). 48h post transfection, cells were washed with PBS two times and pelleted in two dry pellets: 10% of the cells were put aside and directly resuspended in Laemmli buffer (loading buffer). It is referred as the INPUT fraction. The other pellet composed of the remaining 90% cells was resuspended in 400µl of lysis buffer (50 mM Tris–Cl, pH 8, 1% Triton, 10% glycerol, 0.05% SDS, 0.1 mM EDTA, 0.1 mM GTP, 200 mM KCl, protease inhibitor (Roche)) for 30 min at 4°C. The soluble fraction obtained after centrifugation at 11,000g for 10 min was pre-cleared with sepharose beads pre-coated with tRNA and BSA-0.3% for 30 min. Supernatant was further incubated with primary antibody (5 µl) overnight at 4 °C. Protein A Sepharose® beads (Sigma) were coated with PBS + 0.3% BSA, supplemented with tRNA overnight. After re-equilibration in lysis buffer, 30 µL of beads were added to the lysate for 2h30 at 4°C before three extensive washings of 15 min in lysis buffer. The dry beads were resuspended in loading buffer for western blotting. For RNase treatment, 0.1 mg/m RNAse A was added before the washing step.

Immunofluorescence. 50 000 cells were cultivated per well into 4 well Chamber Slide™ Labtek® II in DMEM (for HeLa or 293T cells) or RPMI medium (for Jurkat, C91PL or C8166 cells) complemented with 10% SVF and Penicillin/Streptomycin. 48h after transfection (HeLa or 293T) or after 30 minutes of sedimentation at room temperature (Jurkat, C91PL, C8166 cells), cells were fixed with PFA 4% during 20 min. After extensive washing, aldehyde groups were saturated in a 0.1M PBS Glycine solution for 30 min then washed one time with PBS 1X. Cells were permeabilized with PBS-1%Triton for 5 min and then extensively washed. Saturation of non-specific sites was performed by 0.1% PBS-BSA for 30

min then extensively washed. The indicated primary antibodies were incubated for 1h30 at Room Temperature (RT) at 1/1000 (vol/vol) and further washed three times. Secondary antibodies were incubated for 50 min at 1/500 before three washes. Hoechst coloration at 1/10 000 (10 mg/ml starting concentration) were used to visualized nucleus. Fluoromount-G® from SouthernBiotech was used before recovering with cover slips 22*60 mm from Menzel Gläser.

Proximity Ligation Assay (PLA). HA Rex plasmid was transfected in 293T cells using jet Optimus. After 24h, cells were subjected to PLA using a kit and following the manufacturer indications. Dilutions of primary antibodies (vol/vol): anti-UPF1 (1/250eme) ; anti-AKT1 (1/50eme) ; anti-HA (1/500eme) ; anti-FTSJ1 (1/250eme) ; anti-eIF4E (1/250eme) ; anti-eIF5A (1/250eme). Dilutions of secondary antibodies (PLUS et MINUS): 1/5eme. Acquisition were performed with Spinning Disk at 60x oil objective (Live SR) microscope. Huygens Professional software was used for image deconvolution. ImageJ software was used to image treatment and IMARIS software to count based on 8 pictures per condition. Experiment was repeated twice.

Image acquisition, treatment and manual counting. Image acquisitions were performed with the confocal microscope LSM800 at 60x oil objective. ImageJ software (Version 2.3.0) was used to apply 'gaussian blur' filter (3.00 rad) to all images. Then colocalisation pixel was performed on 8-bit gray scale images with the function "image calculator" and "AND" command between channels of interest. Gray scale was used to identify common pixels. For UPF1 nuclear retention quantification, common pixels between UPF1 and nucleus was used to determine the proportion of nuclear UPF1 with a yes or no criteria. The detection of cytoplasmic and nucleus region of interest (ROI) was determined on the signal strength from UPF1+CRM1 channels and Hoechst+CRM1 channels respectively, then manually verified and/or adjusted. To avoid bias from disparate volumes and proximity of different cells, ROI cytoplasm was restricted to an area near ROI nuclear. Then, nuclear/cytoplasmic ratio was extracted from fluorescence intensity mean in each ROI. Graphs was obtained with R Studio (V4.1.1) (github address to add). For foci identification, detouring with ImageJ tool of CRM1 reinforced signals was performed, then UPF1 colocalization was determined based on colocalization pixel function and extracted with a Yes or No criteria. % of foci area was determined regarding the total cell area by detouring cells on transmission (direct light) images. Hela, cells were counting as n = 54 for control, n = 36 for Rex, n = 37 for Rev, n = 67 for C91PL and n = 66 for C8166 conditions. P values were calculated by performing first Fischer test then a Student's t-test (paired, two-tailed) ns: $P > 0.05$; *$P < 0.05$; **$P < 0.01$.

RNA immunoprecipitation (RIP). ~2×10^6 HeLa cells were transfected as described in the figures, harvested and resuspended in lysis buffer (50 mM Tris–Cl, pH 7.5, 1% NP-40, 0.5% sodium deoxycholate, 0.05% SDS, 1 mM EDTA, 150 mM NaCl, protease inhibitor (Roche) and RNAsin (Promega)) as previously described. Extracts obtained after centrifugation at 12,000g for 15 min were incubated with primary antibody overnight at 4 °C. Protein A and G magnetic beads (dynabeads, Life Technology; 5 µl each) were mixed and coated with PBS + 0.3% BSA, supplemented with tRNA and RNasin (Promega) overnight. After re-equilibration in lysis buffer (supplemented with tRNA), the beads were added to the lysate for 2 h at 4 °C before extensive washing in lysis buffer. The beads were resuspended in elution buffer (50 mM Tris–HCl, pH 7.0. 1 mM EDTA, 10 mM DTT and 1% SDS). Double RIP were performed as reported previously[44]: ~ 6×10^6 HeLa cells were transfected as described in the figures, harvested and fixed with 0.05% formaldehyde for 20 min at room temperature. Then, 0.25 M glycine was added for 5 min before PBS washing. The cell pellet was resuspended in lysis buffer, and the lysate was sonicated (bioruptor, diagenode). First, the HA tag was immunoprecipitated. The immunoprecipitation steps were carried out as described for simple RIP except that samples were incubated with Sepharose beads. Extensive washings were performed with 50 mM Tris–Cl, pH 7.5, 1% NP-40, 0.5% sodium deoxycholate, 0.05% SDS, 1 mM EDTA, 1 M NaCl and 1 M urea. The beads were resuspended in elution buffer (50 mM Tris–Cl, pH 8, 1% Triton, 10% glycerol, 0.05% SDS, 0.1 mM EDTA, 0.1 mM GTP, 200 mM KCl, protease inhibitor (Roche), RNAsin + HA peptide at 0.1 mg/mL)

and incubated at 4 °C for 1H, then for 10 min at 30°C to ensure elution. Finally, the elution volume was increased to 400 µl and Rex immunoprecipitation was performed. After extensive washing, the formaldehyde fixation was reversed by heating samples 45 min at 70°C. Finally, the beads were resuspended in RNAzolRT reagent for RNA extraction. RNA was quantified by qRT-PCR using the following primers: Viral unspliced RNA: forward 5'-GGCCCGAGGACACACTAATA-3', reverse 5'-CAGCGGGGAGGTCTAATAGG-3'); GADD45α (forward 5′-ACGAGGACGACGACAGAGAT-3′, reverse 5′-GCAGGATCCTTCCATTGAGA-3′); GAPDH (forward 5'-GAGTCAACGGATTTGGTCGT-3', reverse 5'-TTGATTTTGGAGGGATCTCG-3'…….) and SMG5 (forward 5′-ACAGAATGGGATGCCAGGAA-3′, reverse 5′-TCAACAC TCCAAAAGCCAGC-3′). The values represented in the graphs correspond to the mean of at least three biological replicates, and the error bars correspond to the SD. P values were calculated by performing a Student's t-test (unpaired, two-tailed) ns: P > 0.05; *P < 0.05; **P < 0.01.

RNA decay assays and qRT-PCR/RT-PCR. RNA decay assays were performed to assess the stability of mRNA expressed from a β-globin reporter minigene that was either WT (Gl-WT) or with a PTC in the second exon (Gl-PTC). For this procedure, 0.5 µg of Gl-PTC or 0. 05 µg of Gl-WT constructs were co-transfected as indicated with 0.5 µg of renilla-expressing vector (unsensitive to NMD) in 0.7×10^6 HeLa cells with jet prime reagent (polyplus). Additional plasmids were co-transfected as indicated in the figures. After 48h, the cells were treated with DRB (100 µg.ml−1) to block transcription for 0, 1, 3 or 4 h. Total mRNAs were extracted using the Macherey-Nagel RNA easy extraction kit and quantified by qRT-PCR using the QuantiTect SYBR Green qRT-PCR kit (Qiagen) and appropriate primers: GLOBIN (Globin 3′ forward 5′-TTGGGGATCTGTCCACTCC-3′, Globin 3′ reverse 5′-CACACCAGCCACCACTTTC-3′. Normalisation was carried out with respect to renilla mRNA (renilla forward primer 5′-CTAACCTCGCCCTTCTCCTT-3′, renilla reverse 5′-TCGTCCATGCTGAGAGTGTC-3′). The values represented in the graphs correspond to the mean of at least three biological replicates, and the error bars correspond to the SD. Half-lives were calculated for each replicate, and P values were calculated by performing a Student's t-test (unpaired, two-tailed) ns: P > 0.05; *P < 0.05; **P < 0.01.

Metabolic assays (SUnSET®). The SUnSET® assay was used to monitor de novo protein synthesis as described previously [63]. ~2×10^6 of HeLa cells were transfected as described in the figures. Briefly, 10 min prior harvesting the cells, puromycin was added to culture medium at 1µg/ml. As a control, cycloheximide was added at 10µg/ml, 15min before puromycin addition, resulting in complete blockade of protein synthesis. Cell extracts were then processed for Western blotting using anti-puromycin 12D10 antibody (Millipore) at 1/5000eme. Puromycin relative incorporation was calculated based on quantification of puromycin signals normalized by total protein. Total protein levels were visualized with stain free gels. Western blot signals and total protein levels were acquired on a Biorad Chemidoc imaging system before quantification with Image Lab software. The values represented in the graphs correspond to the mean of at least three biological replicates, and the error bars correspond to the SD. P values were calculated by performing a Student's t-test (unpaired, two-tailed) ns: P > 0.05; **P < 0.05; **P < 0.01

Cell fractionation. ~2×106 HeLa cells were transfected as described in the figures, harvested and resuspended in lysis buffer (Sucrose 340 mM, Glycerol 10%, HEPES pH 7.5 10mM, KCl 10mM, MgCl2 1.5mM, Triton 0.1%, DTT 1mM, Na3VO4 1mM, protease inhibitor (Roche) and RNAsin (Promega)). The cytoplasmic fraction was collected after 1300g centrifugation and conserved for further RNA extraction with RNAzolRT reagent (MRC) and subjected to qRT-PCR or for Western blotting. The isolated nucleus were washed two times with lysis buffer and further pelleted. Nucleus were resuspended in nucleus lysis buffer (EDTA 3mM, EGTA 0.2mM, Triton 0.1%, DTT 1mM, Na3VO4 1mM, protease inhibitor (Roche) and RNAsin (Promega))) and kept under rotation during 30min at 4°C. Nuclear fraction was collected after 12 000g centrifugation, were supernatant was conserved for further RNA extraction with RNAzolRT reagent (MRC) and subjected to qRT-PCR. The values represented in

the graphs correspond to the mean of at least three biological replicates, and the error bars correspond to the SD. P values were calculated by performing a Student's t-test (unpaired, two-tailed) ns: $P > 0.05$; *$P < 0.05$; **$P < 0.01$

Viral particles and biofilm harvest. ~15 x 10^6 of lymphoid cells were harvest washed in PBS and pelleted. Culture supernatant and PBS washes were subjected to centrifugation at 4000g 4°C overnight; the pellet was resuspended in loading buffer for western blot and referred as extra cellular matrix (ECM). Three dilutions of the cell lysate (4 x 10^6, 2 x 10^6, 1 x 10^6) was used to assess the specificity of UPF1 signal; RRM2 was used as a cytoplasmic cellular marker and p19 as a marker of viral particles production in the infected cells. Total protein signals were obtained as described before. Experiment was repeated at least 3 times.

Results

1. Rex interferes with CRM1-dependent export of UPF1

To address the question of the CRM1 hijacking by the retroviral protein Rex and its impact on the cell functioning, we decided to use the RNA helicase UPF1 as a model, since its nuclear export relies on CRM1. Having verified that UPF1 export effectively depends on CRM1 *(***Supplementary 1***),* we looked at the formation of protein complexes involving Rex, CRM1 and UPF1. First, we validated the conditions of interaction between Rex and CRM1: 293T cells were transfected with combinations of a plasmid coding Rex and a plasmid expressing a RNA with a Rex Responsive Element (RxRE) to mimic the viral RNA that Rex binds and exports via CRM1 [64]. Co-immunoprecipitations (coIP) followed by western blot confirmed that Rex binds endogenous CRM1 efficiently and specifically (**Fig 1A-B lane 3).** Moreover, the expression of an RNA harbouring the RxRE motif did not modify the levels of CRM1 coIP by Rex and vice versa (**1A-B, compare lanes 2 and 3**) supporting the hypothesis that Rex can hijack CRM1 before its binding to viral RNA. Second, to investigate the composition of complexes associated to UPF1, 293T cells were transfected with combinations of plasmids coding Rex and the RxRE containing RNA. UPF1 coIP were further carried out. In the context of Rex expression, the endogenous UPF1 was able to coIP CRM1 and Rex (**1C; lane 2**). Before further explorations, we wanted to confirm the interaction of Rex with UPF1 since it is reported here for the first time with endogenous UPF1. To do so, we used Proximity Ligation Assay (PLA), a 40nm resolution technique to monitor proteins-proteins colocalization. In 293T cells expressing HA-Rex, we investigated the colocalization of this latter and different endogenous proteins: FTSJ1 (ribosomal RNA methyltransferase 1) a nucleolar protein that is not described to interact with Rex was used as a negative control and eIF5A, a known partner of Rex was used as positive control. Finally, PLA between Rex and UPF1 displayed numerous foci (in par with Rex /eIF5A PLA) localized in the nucleus as well as in the cytoplasm what supports their association (**Figure 1D, S2A**). A further analysis of the UPF1 coIP experiments (**1C**) revealed that Rex expression is linked with an increase in the amounts of CRM1 associated with UPF1, comparatively to control conditions. This suggests a stabilization of the UPF1-CRM1 interaction by Rex expression (**1C panel i, compare lanes 1 and 2**). Interestingly, the co-expression of Rex and the RxRE containing RNA didn't enhance the UPF1-Rex association nor the UPF1-CRM1 stabilization (**1C panel i, lane 2,4 compared to lane 3**). Since UPF1 is a RNA binding protein, we looked at these interactions after RNAse treatment. The same profile of UPF1-CRM1 association is observed with or without RNAse treatment (**1C panel ii, lane 2,4 compared to lane 3**), indicating that the interactions between Rex, UPF1 and CRM1 are not bridged by RNA, and that the formation of a UPF1-Rex-CRM1 complex can exist independently of RNA, including the viral RNA containing the RxRE motif. To confirm the role of Rex in stabilizing UPF1-CRM1 interaction, we looked at the CRM1-UPF1 association after UPF1 immunoprecipitation when Rex is no longer able to shuttle between nucleus and cytoplasm (**1E**). We

constructed Rex shuttling mutants targeting the Nuclear Export Signal (NES) and the Nuclear Localisation Signal (NLS) of Rex: the Rex NES mutant no longer interacts with CRM1 and is functionally not able to export RNA containing a RxRE motif comparing to Rex WT (**S2B-C**); the Rex NLS mutant still interacts with CRM1 but is also greatly impaired to export RNA (**S2B-C**). UPF1 coIP experiments were then carried out in 293T cells expressing Rex WT, NES mutant or Rex NLS mutant. They revealed that the association of CRM1 with UPF1 is significantly reduced in both Rex mutants' conditions compared to Rex WT condition (**1E, lane 3, 4 compared to 2**) as confirmed by the CRM1 quantification (**S1D**). Finally, UPF1 coIP were carried out in cells expressing Rex and treated with CRM1 siRNA. Interestingly we found that Rex is less co-precipitated with UPF1 after CRM1 depletion (1F, compared lane 2 to 3). Altogether, those data are consistent with the formation of a tripartite complex UPF1/CRM1/Rex, stabilized by UPF1/CRM1 contacts, as well as Rex/CRM1 contacts and occurring during CRM1 hijack by the retroviral transporter Rex.

In order to evaluate the consequences of Rex expression on UPF1 behaviour, we first looked at the cellular localisation of endogenous CRM1 and UPF1 by confocal microscopy (**2A-B**). As illustrated in control condition, CRM1 repartition is mostly nuclear with a homogenous staining, while endogenous UPF1 is mostly cytoplasmic (**2A-B, panel (i)**). By investigating the colocalizing pixels from UPF1 and CRM1 channels only, we observed that UPF1 and CRM1 staining overlap at the nuclear periphery consistently with the CRM1-dependent export of UPF1 (**2A, panel (i)**). Strikingly, when Rex is expressed, UPF1 is significantly retained in the nucleus compared to control conditions. As shown by common pixel superposition, Rex, CRM1 and UPF1 colocalize in the nucleus and at the nuclear membrane. To assess it, we quantified in both populations of cells, the nucleo/cytoplasmic repartition of UPF1 signal as well as the proportion of cells showing a nuclear retention of UPF1(**2A-B panel (ii)**). Thus, these results demonstrate that *in cellulo,* the expression of Rex and the further formation of a UPF1-Rex-CRM1 complex, affects UPF1 cellular repartition by retaining a significant part of the UPF1 pool in the nucleus.

2. <u>CRM1 hijacking by Rex interferes with UPF1 function during NMD</u>

To test whether the modification of UPF1 export by Rex could impact its activity, we focus on one of its well described functions: the Nonsense-Mediated Decay (NMD). Since UPF1 activity in NMD is functionally linked to its RNA binding capacity, we first investigated this latter by RNA immunoprecipitation (RIP) assays. HeLa cells were transfected with a plasmid coding a NMD sensitive reporter mRNA (Globin PTC, a globin minigene with a stop codon in the second exon) as well as increasing amounts of Rex coding plasmids. UPF1 was further immunoprecipitated and the amounts of bound Globin PTC were quantified by RTqPCR. Rex expression as well as UPF1 immunoprecipitations were checked by western blot (**Fig 3A**). When Rex is expressed, the level of Globin PTC associated to UPF1 are significantly reduced compared to conditions without Rex. This effect is observed in a Rex dose-dependent manner (**3A**). In addition, to correlate this effect with the formation of the previously described UPF1/CRM1/Rex complex and Rex export function, we also carried out UPF1 RIP experiments in cells transfected with Rex NES mutant coding plasmid. Compared to Rex WT, Rex NES mutant is no longer able to interact with CRM1 and to stabilize UPF1/CRM1 interaction (**Fig1E and S2**); As expected, Rex NES mutant restored UPF1 binding capacity to globin PTC compared to Rex WT (**Fig 3B**). This recovery confirms that CRM1 hijacking by Rex leads to UPF1 decreased association to its RNA substrate.

Since NMD requires UPF1 recruitment to RNA to initiate their degradation, we checked whether we could correlate the previously identified RNA binding defect with NMD inhibition through Rex expression. To do so, we analysed the decay rate of the Globin PTC mRNA with or without Rex

expression: decay rates were performed by monitoring the evolution of RNA levels after a treatment of HeLa cells by 100µg/ml DRB for 3h. Here, Rex expression led to a statistically significant decrease in the decay rate of Glob PTC (**3C, compare red and purple bars**). To attest the specificity of this result, the decay rate of a NMD unsensitive RNA (Globin WT, a globin minigene without stop codon in the second exon) was analysed. In the absence of Rex, the decay rate of Globin WT is lower than the Globin PTC's one, as expected from a NMD unsensitive RNA (**3C, compare blue and red bars**). When Rex is expressed, the decay rate of Glob WT is unaffected (**3C, compare blue and green bars**) and is of similar value than Globin PTC's one (**3C, compare green and purple bars**). These results demonstrate that Rex specifically and efficiently inhibits NMD. Lastly, we checked the possible trans-acting effect of a RxRE containing RNA over Rex dependent NMD inhibition. As indicated in **Fig 3C**, the expression of the RxRE RNA motif did not significantly modified Rex stabilization of the Globin PTC decay rate (**3C, compare purple and orange bars**). Consistently with the UPF1 coIP (**Fig 1C**), the co-expression of Rex and the RxRE RNA motif doesn't enhance NMD inhibition comparatively to the "Rex only" condition.

NMD is a translation dependent process. To confirm that our observations are not related to a possible impact of Rex on translation, we monitored puromycin incorporation in peptides being synthesized, using sunset assay. While translation inhibition by cycloheximide treatment prevents puromycin incorporation after 30min of puromycin pulse chase (**Fig 3D compare lanes 1 and 2**), the expression of Rex does not significantly modify it (**Fig 3D compare lanes 2 and 4**).

In order to correlate this Rex dependent NMD inhibition with our previous observations, we decided to analysed the effect of the Rex NES mutant on Globin PTC mRNA half-life (as an indication of NMD efficiency). From Fig1E and 3B, Rex NES mutant was unable to stabilize the Rex/CRM1/UPF1 complex and to prevent UPF1 binding to RNA. To measure Globin PTC mRNA half-life, HeLa cells were transfected with different Rex coding plasmids and further treated with the transcription inhibitor DRB for 0, 1, 3 or 4h. Total RNA were purified and the Globin PTC mRNA was quantified by RTqPCR. Globin PTC half live was measured for each condition and compared with the Rex WT condition as indicated in **Fig 3E**. Consistently with previous results, Globin PTC half-life is significantly increased by Rex WT expression comparatively to control condition (9.9h compared to 2.9h) showing NMD inhibition. Conversely, Rex NES loss its ability to inhibit NMD as showed by the restored Globin PTC half-life (3.8h). As a control, we monitored the effect of Rex NLS mutant, that also couldn't inhibit NMD (2.3h). Interestingly, the co-expression of NES and NLS mutants didn't restored NMD inhibition (1.9h), suggesting that the presence of Rex both in nucleus and cytoplasm is not sufficient for NMD inhibition but its shuttling capacity is required.

Altogether, these results demonstrate that Rex expression and shuttling lead to a diminution of UPF1 association with RNA, which is functionally correlated to NMD inhibition.

3. Rev from HIV-1 also interferes with UPF1 cellular localization and its NMD function.

In the other pathogenic human retrovirus HIV-1, the Rev protein is the functional homolog of HTLV-1 Rex: both shuttle between cytoplasm and nucleus and hijack the CRM1 pathway to export the unspliced viral RNA. In order to reinforce our observations supporting an impact of CRM1 hijacking on UPF1 activity, we decided to investigate the impact of Rev expression as we did previously with Rex. Interestingly, a UPF1/Rev/CRM1 export complex has already been described (ref ajamian). Thus, we directly looked at the UPF1 cellular repartition under Rev expression by confocal microscopy. Rev strongly colocalizes with UPF1 and CRM1 in nucleolar compartments, as showed by a large view as well as a unique cell view (**respectively 4A and S3A-B**). Still, as for Rex, a significant nuclear retention of UPF1 can be quantified when Rev is expressed compared to control condition (**4A, quantifications in panel ii**). To pursuit the comparative analysis, we then checked whether the relocalisation of UPF1

due to Rev expression can be correlated with NMD inhibition. To evaluate NMD activity, we measured the half live of the Globin PTC reporter in HeLa cells expressing a FlagRev construction or an empty vector, as we did previously. The increased half-life of Globin PTC under Rev expression compared to control condition (4.3h for 1.6h **Fig 4B**) suggests that Rev is able to inhibit NMD and alter the stability of non-viral RNA. To exclude that this effect was related to a translation defect, we carried out a sunset assay in cells expressing or not Rev and found that global translation was not affected (**S3B**). Moreover, to confirm that our observations illustrate the inhibition of NMD specifically, we analysed the impact of Rev expression on the decay rate of the NMD unsensitive RNA reporter (Globin WT) and compared it to the NMD sensitive one (Globin PTC). As expected, the decay rate of Globin WT was not much affected due to Rev expression while the one of Globin PTC was significantly decreased (**4C**). In addition, to determine if those observations could be verified in the context of HIV-1 infection, we infected HeLa cells (pre-transfected with Globin PTC or Globin WT expression plasmids) with HIV-GFP lentiviral particles (HIV) versus GFP only expressing lentiviral particules (VLPCtr) for 48h. Decay rate were measured as previously described: while the decay rate of Globin WT was not affected by HIV infection, the one of Globin PTC was significantly reduced, indicating that HIV infection is able to inhibit NMD **(4D**). Altogether, these results demonstrate a specific NMD inhibition during HIV infection, occurring at least in a Rev-dependent manner.

In order to identify whether Rev dependent NMD inhibition can be explained by a defect in UPF1 binding to RNA as suggested with Rex, we carried out UPF1 RIP experiments in HeLa cells transfected with Globin PTC as well as with Rev or Rex or an empty vector. Protein expression as well as immunoprecipitation levels were controlled by western blot **(4E)**. Consistently with our precedent results with Rex, Rev expression is associated with a decreased association of UPF1 with the NMD sensitive reporter mRNA, Globin PTC (**4F**). The same experiment was performed in cells expressing the NMD unsensitive reporter Globin WT and showed a similar profil (**4G**). To reinforce these observations, the association of UPF1 with endogenous NMD sensitive (smg5 and gadd45a) and NMD unsensitive (gapdh) RNA was also investigated. We observed the same decrease in UPF1 association with these endogenous RNA (**4H**). These results indicate that Rev, as Rex, decreases/prevents UPF1 binding to all RNA including NMD sensitive RNA, supporting an early inhibition of NMD. Although CMR1 export essentially target protein cargos and not bulk RNA, one can hypothesize that these results illustrate a defect in RNA export rather than in UPF1 accessibility. To eliminate this possibility, we carried out fractionation of cells expressing Rex, Rev or an empty vector and quantified the Nuclear/Cytoplasmic ratio of the previously studied RNA. Viral proteins expression didn't modify the nucleo/cytoplasmic RNA repartition (**S3C**).

Here we found that HIV Rev, known to hijack the CRM1 export pathway as HTLV-1 Rex does, induces the nuclear re-localisation of UPF1. Same as Rex, Rev provokes a decrease of UPF1 recruitment to RNA that could be correlated with the inhibition of NMD. This strongly supports our previous conclusions about HTLV-1 Rex.

4. <u>CRM1 hijacking by Rex in HTLV-1 transformed cell line leads to UPF1 relocalization</u>

So far, we demonstrated that independently of the presence of viral full-length RNA, Rex can form a tripartite complex with CRM1 and UPF1, strongly stabilizing UPF1/CRM1 interaction. We correlated the formation of this complex with the nuclear retention of UPF1 and to NMD inhibition. In order to investigate this question in physiological and more relevant cellular models, we cultivated 3 HTLV-1 chronically infected CD4+ T cells: C91PL and HUT102 that express Rex protein as well as C8166 that displays a defect in Rex expression. This was attested by western blot (**5A**) as well as confocal microscopy (**supplementary 4B**). As a negative control we also used uninfected jurkat CD4+ T cells. We performed UPF1 coIP with protein extracts from each cell line. In Rex expressing cells

(C91PL and HUT102) UPF1 co-immunprecipitates Rex as well as CRM1proteins. Interestingly, in the Rex deficient cells C8166, the level of CRM1 co-immunoprecipitated by UPF1 was strikingly lower, close to the levels obtained in Jurkat coIP (**5A, compare lanes 1-2 to 3-4**). Then we looked at the localisation of UPF1 and CRM1 in C91PL and C8166 by confocal microscopy (**5B and S4B**). We found UPF1 nuclear localisation is significantly increased in C91PL compared to C8166: quantifications attest that ~75% of C91PL cells display such a profile compared to 32% of C8166 **(5B (ii)**). In addition, in more than 70% of C91PL (compared to less than 15% of C8166), we identified a higher concentration of UPF1 and CRM1 producing "super foci", suggesting that Rex induces another supplementary UPF1 retention phenotype, more focalised and associated to CRM1 (**5B, white arrow**); notably, in each cell type, more than 80% of CRM1 super foci are colocalizing with UPF1 super foci.
Here it is difficult to directly correlate those observations with an inhibition of NMD, since C8166 and C91PL cells both express the viral protein Tax, another NMD inhibitor that we characterized in the past[38,44]. The expression of Tax in these cell lines is documented and we validated it by confocal microscopy (**S4B**). In these cell lines, Tax localisation is not specifically linked to either Rex or CRM1 profiles (**S4B-C**). To evaluate NMD efficiency in a close model, we measured the half-life of the Glob PTC reporter in HeLa cells transfected with different mutated versions of a HTLV molecular clone. As expected, we found that a molecular clone deficient for Rex alone (mimicking C8166 cells) or Tax alone inhibited NMD at similar levels than a WT clone (mimicking C91PL cells) (**Supp 4D**). Noteworthy, considering the NMD activity in infected T cells, we showed in the past that NMD is effectively inhibited in C91PL compared to Jurkat [38].

5. UPF1 is addressed to vRNA and viral particules

To the contrary of HeLa and 293T cells, C91PL cells constitutively express viral RNA. Since the Rex/CRM1 complex is selectively bound to unspliced viral RNA (vRNA) to drive its nuclear export, and as we just illustrated, Rex and CRM1 can redirect endogenous UPF1 localisation and function, we wondered what that implies for UPF1 interplay with vRNA. First, we asked whether UPF1 and Rex can be found concomitantly on vRNA. To do so, we carried out double-RIP experiments. 293T cells were transfected with a replicative HTLV-1 molecular clone with or without a plasmid coding UPF1 with the HA tag. First, a RIP targeting the HA tag was performed (**Fig 5C, blue bar**). Cells without HA-UPF1 were used as a RIP control. Second, RNAs were eluted from HA-RIP and further subjected to a second RIP against Rex (**Fig 5C, green bar**) or a control immunoglobulin. RTqPCR on each RIP revealed a significant enrichment of vRNA associated to UPF1 as well as to Rex, yet in a lesser amount. Thus, we can conclude that UPF1 can be recruited on vRNA concomitantly with Rex. Then we carried out UPF1 RIP experiments in C8166 and C91PL cells, as well as in Jurkat as a negative control. Interestingly, we found that UPF1 RIP were specifically enriched in vRNA in the Rex expressing cells (**Fig5D, compare C8166 and C91PL**). To confirm that the observed UPF1 recruitment is not related to NMD activation, we carried out RIP targeting UPF2, a NMD cofactor of UPF1. We found no specific enrichment of vRNA after UPF2 RIP in C91PL compared to C8166. In addition, we performed UPF2 coIP in C91PL extracts: an interaction between UPF2 and CRM1 was found as expected since UPF2 is a known cargo of CRM1. However, no specific association between Rex and UPF2 could be found, while UPF1 efficiently binds the viral protein (**Fig5E**). Thus, the specific recruitment of UPF1 on vRNA occurs on a Rex dependent manner but independently of its NMD function. Finally, we investigated the impact of the Rex NES mutant expression on UPF1 recruitment to vRNA. RIP experiments were carried out in 293T cells transfected with the HTLV-R23L molecular clone complemented with either Rex WT or NESmut plasmids. RIP Rex experiments showed a similar enrichment of vRNA with Rex WT and NES mutant proteins. To the contrary, vRNA enrichment in UPF1 RIP was drastically reduced with the Rex NES mutant compared to Rex WT. As demonstrated previously, Rex NES mutant is unable to hijack CRM1 exportin, indicating that this function of Rex is critical for UPF1 recruitment to vRNA.

Altogether, these results indicate that in HTLV-1 infected T cells, the CRM1 hijacking by Rex induces a stabilization of the CRM1/UPF1 interaction with a nuclear retention of UPF1, and drives the loading of UPF1 onto vRNA.

As introduced before, an additional fate of vRNA is to be encapsidated in viral particle. Thus, we wonder whether UPF1 presence on viral RNA can lead to its incorporation in viral particles as well. First, we monitored the localisation of p19 and UPF1 in T cells. As expected, C8166 do not express GAG due to the absence of Rex. In C91PL, p19 is displayed as foci at the periphery of the cytoplasmic membrane supporting virions accumulation. UPF1 profile shows foci colocalizing with p19. These profiles suggest that UPF1 is present at the sites of particles budding and may be incorporated into the virions (Fi**g6A**). To address this point, we isolated the extracellular matrix (EM) containing the viral biofilm, in which HTLV-1 particles are concentrated. EM from C91PL, C8166 and Jurkat was analysed by western blot. The presence of viral particles was assessed by the presence of p19 in C91PL only. To exclude a contamination of EM by cytoplasmic proteins, we revealed the cytoplasmic protein RRM2: its absence of the EM from all cell type confirmed the quality of our preparation. Finally, UPF1 was identified in EM from C91PL only (**Fig6B**) indicating the presence of UPF1 in HTLV-1 viral biofilm and corroborating our hypothesis of UPF1 encapsidation. Thus, we demonstrated here that UPF1 can be loaded on vRNA in a Rex dependant manner and UPF1 is further loaded into the budding viral particles.

DISCUSSION:

By regulating cellular repartition of hundreds of proteins and some specific RNA species, CRM1 export pathway is part of cellular homeostasis. In line with this, CRM1 is a therapeutic target in many human diseases. As introduced earlier, complex retroviruses like HTLV-1 and HIV-1 use retroviral transporters, respectively Rex and Rev, to export their viral RNA via CRM1. While the mechanistic steps of this export are already well described, the cellular consequences of CRM1 hijacking hasn't been addressed yet. Here, we were interested in characterizing how CRM1 hijacking by Rex could affect the NMD, a well described RNA quality control and post-transcriptional process involved in cellular homeostasis, knowing that its core factor UPF1 is a CRM1 cargo.

We observed that Rex impacts CRM1-dependent UPF1 export through the formation of an UPF1-Rex-CRM1 complex. Our data support that this complex relies on the combined interactions between UPF1 and CRM1, Rex and CRM1 as well as Rex and UPF1, leading to increased levels of CRM1 associated to UPF1. Hypothesizing that we face a sequestration complex, confocal microscopy confirms that while UPF1 is usually mostly cytoplasmic due to an efficient/active nuclear export, Rex expression effectively favours UPF1 nuclear accumulation. Consistently with UPF1 improper localization [21,65] and the current model of NMD in which UPF1 binds its target in the cytoplasm, we were able to correlate the formation of this sequestration complex with a defect in UPF1 binding to RNA. Finally, the consequences of these alterations were analysed at the light of the NMD process : NMD activity was repressed under Rex expression as shown previously [39] but more interestingly, by using selected Rex mutants, we were able to correlate this inhibition with the formation of the sequestration complex and the capacity of Rex to shuttle with CRM1. The concomitant expression of a RxRE containing RNA did not change our observations, allowing us to conclude that this inhibition process can occur independently of the Rex binding to viral RNA (in accordance with previous observations suggesting that RNA binding is not indispensable to provoke the shuttling of Rex) [54]. In addition, similar results were obtained in HTLV-1 chronically infected cells, confirming their physiological relevance.

Nakano et al reported few month ago that overexpressed UPF1 can interact with Rex in the cytoplasm and pbodies and that NMD inhibition was dependant on several domains of Rex including its

Nter (ARM NLS and X domains)[45]. Our results support and complete theirs: first we report an interaction between Rex and endogenous UPF1, which is vulnerable to a mutation in the NLS domain of Rex. Interestingly, PLA experiments support that this interaction occurs in the cytoplasm as well as in the nucleus. While the cytoplasmic presence of these complexes matches with the model of Nakano et al, suggesting that Rex alters the composition of the NMD complex after its recruitment via UPF1, the existence of nuclear complexes support the accumulation of UPF1 in the nucleus under Rex control. The modification of UPF1 nuclear export fitness in a Rex dependant manner definitely reduces the ability of UPF1 to bind RNA, further preventing NMD initiation. Thus, we reveal a second model for the Rex mediated NMD inhibition, specifically based on the capacity of Rex and UPF1 to be exported by CRM1.

In order to reinforce the demonstration that CRM1 hijacking by a retroviral transporter can alter cellular pathways, we also investigated the effect of HIV Rev expression. As expected, Rev expression globally led to similar observations, although some mechanistical divergences may support slight differences in our observations: strikingly, Rev induces a stronger UPF1 nuclear retention, essentially in nucleolus, while UPF1 staining was essentially diffuse in the nucleus with Rex. Interestingly, this demonstration also points out for the first time that HIV is able to trans-inhibit NMD in a Rev dependant manner, affecting the stability of non-viral RNA. So far, in the HIV field, UPF1 was known to be involved in viral RNA export with Rev and CRM1, and UPF1 was shown not to be part of an NMD complex when bound to viral RNA, before being encapsidated with RNA [43,66]; its presence being then necessary for a further efficient viral transmission [67]. Considering HTLV-1, although the sequestration complex UPF1/CRM1/Rex can be constituted without vRNA, we found that it also led to the loading of UPF1 onto the unspliced vRNA exported by Rex, in infected cells. Ultimately, we observed that UPF1 is effectively driven into HTLV-1 viral particles, strengthening the convergence between Rex and Rev's effect towards UPF1. Although the reasons of UPF1 presence in the HTLV-1 viral particles are still unknown and will be investigated in a future work, it may imply that UPF1 can modulate retroviral transmission/replication in the next infected cell. Several viruses, including the complex retroviruses that express Rev like protein, subvert the CRM1 nucleo/cytoplasmic export to ensure a proper replicative cycle and the production of infectious virions [68–72]. In parallel, it is well described that viruses capture cellular RBP at the expense of the host mRNP, to compose their own mRNP [73–77]. In line with this, our results thus suggest that the export of unspliced vRNA by CRM1 is a critic step in the formation of the retroviral mRNP and UPF1 incorporation.

Finally, this work also reveals unexpected data on the regulation of NMD: in the past, the nuclear import of UPF1 by the importin B was stress out as a critical step of the process. Here the expression of viral proteins shows that the CRM1 dependant export also impacts the NMD, emphasizing the importance of the nucleo/cytoplasmic shuttling process as a regulation node of the NMD. To understand how the NMD can be controlled at this step without a viral infection and the "locking" effect of Rex and Rev, still need further investigations that are currently under progress.

In conclusion, this work describes how the process of CRM1 subjugation unexpectedly provokes the coordinated hijacking of UPF1, since the formation of a sequestration complex not only trans-inhibits the NMD (which constitutes a threat toward retroviral RNA), but also redirects UPF1 isolated from its NMD partner UPF2 on the viral RNA before packaging.

References

1. Okamura, M., Inose, H. & Masuda, S. RNA Export through the NPC in Eukaryotes. *Genes* **6**, 124–149 (2015).
2. Cautain, B., Hill, R., de Pedro, N. & Link, W. Components and regulation of nuclear transport processes. *FEBS J.* **282**, 445–462 (2015).
3. Fung, H. Y. J., Niesman, A. & Chook, Y. M. An update to the CRM1 cargo/NES database NESdb. *Mol. Biol. Cell* **32**, 467–469 (2021).
4. Fung, H. Y. J. & Chook, Y. M. Atomic basis of CRM1-cargo recognition, release and inhibition. *Semin. Cancer Biol.* **27**, 52–61 (2014).
5. Güttler, T. & Görlich, D. Ran-dependent nuclear export mediators: a structural perspective. *EMBO J.* **30**, 3457–3474 (2011).
6. Güttler, T. *et al.* NES consensus redefined by structures of PKI-type and Rev-type nuclear export signals bound to CRM1. *Nat. Struct. Mol. Biol.* **17**, 1367–1376 (2010).
7. Kehlenbach, R. H., Dickmanns, A. & Gerace, L. Nucleocytoplasmic shuttling factors including Ran and CRM1 mediate nuclear export of NFAT In vitro. *J. Cell Biol.* **141**, 863–874 (1998).
8. Fu, S.-C., Fung, H. Y. J., Cağatay, T., Baumhardt, J. & Chook, Y. M. Correlation of CRM1-NES affinity with nuclear export activity. *Mol. Biol. Cell* **29**, 2037–2044 (2018).
9. Engelsma, D., Bernad, R., Calafat, J. & Fornerod, M. Supraphysiological nuclear export signals bind CRM1 independently of RanGTP and arrest at Nup358. *EMBO J.* **23**, 3643–3652 (2004).
10. Zhang, X., Yamada, M., Mabuchi, N. & Shida, H. Cellular requirements for CRM1 import and export. *J. Biochem. (Tokyo)* **134**, 759–764 (2003).
11. Hill, R., Cautain, B., de Pedro, N. & Link, W. Targeting nucleocytoplasmic transport in cancer therapy. *Oncotarget* **5**, 11–28 (2014).
12. Nguyen, K. T., Holloway, M. P. & Altura, R. A. The CRM1 nuclear export protein in normal development and disease. *Int. J. Biochem. Mol. Biol.* **3**, 137–151 (2012).
13. Saulino, D. M., Younes, P. S., Bailey, J. M. & Younes, M. CRM1/XPO1 expression in pancreatic adenocarcinoma correlates with survivin expression and the proliferative activity. *Oncotarget* **9**, 21289–21295 (2018).
14. Chen, Y. *et al.* Inhibition of the Nuclear Export Receptor XPO1 as a Therapeutic Target for Platinum-Resistant Ovarian Cancer. *Clin. Cancer Res. Off. J. Am. Assoc. Cancer Res.* **23**, 1552–1563 (2017).
15. Jiang, Y. *et al.* Circ-XPO1 upregulates XPO1 expression by sponging multiple miRNAs to facilitate osteosarcoma cell progression. *Exp. Mol. Pathol.* **117**, 104553 (2020).
16. Song, P., Li, W., Xie, J., Hou, Y. & You, C. Cytokine storm induced by SARS-CoV-2. *Clin. Chim. Acta Int. J. Clin. Chem.* **509**, 280–287 (2020).
17. Ferreira, B. I., Cautain, B., Grenho, I. & Link, W. Small Molecule Inhibitors of CRM1. *Front. Pharmacol.* **11**, 625 (2020).
18. Wang, A. Y. & Liu, H. The past, present, and future of CRM1/XPO1 inhibitors. *Stem Cell Investig.* **6**, 6 (2019).
19. Kırlı, K. *et al.* A deep proteomics perspective on CRM1-mediated nuclear export and nucleocytoplasmic partitioning. *eLife* **4**, e11466 (2015).
20. Thakar, K., Karaca, S., Port, S. A., Urlaub, H. & Kehlenbach, R. H. Identification of CRM1-dependent Nuclear Export Cargos Using Quantitative Mass Spectrometry. *Mol. Cell. Proteomics MCP* **12**, 664–678 (2013).
21. Mendell, J. T., Sharifi, N. A., Meyers, J. L., Martinez-Murillo, F. & Dietz, H. C. Nonsense surveillance regulates expression of diverse classes of mammalian transcripts and mutes genomic noise. *Nat Genet* **36**, 1073–8 (2004).
22. Kurosaki, T., Popp, M. W. & Maquat, L. E. Quality and quantity control of gene expression by nonsense-mediated mRNA decay. *Nat. Rev. Mol. Cell Biol.* **20**, 406–420 (2019).
23. Karousis, E. D. & Mühlemann, O. Nonsense-Mediated mRNA Decay Begins Where Translation Ends. *Cold Spring Harb. Perspect. Biol.* **11**, (2019).

24. Hurt, J. A., Robertson, A. D. & Burge, C. B. Global analyses of UPF1 binding and function reveal expanded scope of nonsense-mediated mRNA decay. *Genome Res* **23**, 1636–1650 (2013).
25. Zund, D., Gruber, A. R., Zavolan, M. & Muhlemann, O. Translation-dependent displacement of UPF1 from coding sequences causes its enrichment in 3' UTRs. *Nat Struct Mol Biol* **20**, 936–43 (2013).
26. Neu-Yilik, G. *et al.* Dual function of UPF3B in early and late translation termination. *EMBO J.* **36**, 2968–2986 (2017).
27. Chamieh, H., Ballut, L., Bonneau, F. & Le Hir, H. NMD factors UPF2 and UPF3 bridge UPF1 to the exon junction complex and stimulate its RNA helicase activity. *Nat Struct Mol Biol* **15**, 85–93 (2008).
28. Chakrabarti, S. *et al.* Molecular mechanisms for the RNA-dependent ATPase activity of Upf1 and its regulation by Upf2. *Mol Cell* **41**, 693–703 (2011).
29. Yamashita, A., Ohnishi, T., Kashima, I., Taya, Y. & Ohno, S. Human SMG-1, a novel phosphatidylinositol 3-kinase-related protein kinase, associates with components of the mRNA surveillance complex and is involved in the regulation of nonsense-mediated mRNA decay. *Genes Dev* **15**, 2215–28 (2001).
30. Durand, S., Franks, T. M. & Lykke-Andersen, J. Hyperphosphorylation amplifies UPF1 activity to resolve stalls in nonsense-mediated mRNA decay. *Nat. Commun.* **7**, 12434 (2016).
31. Balistreri, G. *et al.* The host nonsense-mediated mRNA decay pathway restricts Mammalian RNA virus replication. *Cell Host Microbe* **16**, 403–411 (2014).
32. Hogg, J. R. & Goff, S. P. Upf1 senses 3'UTR length to potentiate mRNA decay. *Cell* **143**, 379–89 (2010).
33. LeBlanc, J. J. & Beemon, K. L. Unspliced Rous sarcoma virus genomic RNAs are translated and subjected to nonsense-mediated mRNA decay before packaging. *J. Virol.* **78**, 5139–5146 (2004).
34. Wada, M., Lokugamage, K. G., Nakagawa, K., Narayanan, K. & Makino, S. Interplay between coronavirus, a cytoplasmic RNA virus, and nonsense-mediated mRNA decay pathway. *Proc. Natl. Acad. Sci. U. S. A.* **115**, E10157–E10166 (2018).
35. Quek, B. L. & Beemon, K. Retroviral strategy to stabilize viral RNA. *Curr. Opin. Microbiol.* **18**, 78–82 (2014).
36. Garcia, D., Garcia, S. & Voinnet, O. Nonsense-mediated decay serves as a general viral restriction mechanism in plants. *Cell Host Microbe* **16**, 391–402 (2014).
37. Li, M. *et al.* Identification of antiviral roles for the exon-junction complex and nonsense-mediated decay in flaviviral infection. *Nat. Microbiol.* **4**, 985–995 (2019).
38. Mocquet, V. *et al.* The human T-lymphotropic virus type 1 tax protein inhibits nonsense-mediated mRNA decay by interacting with INT6/EIF3E and UPF1. *J Virol* **86**, 7530–43 (2012).
39. Nakano, K. *et al.* Viral interference with host mRNA surveillance, the nonsense-mediated mRNA decay (NMD) pathway, through a new function of HTLV-1 Rex: implications for retroviral replication. *Microbes Infect.* **15**, 491–505 (2013).
40. Popp, M. W.-L., Cho, H. & Maquat, L. E. Viral subversion of nonsense-mediated mRNA decay. *RNA N. Y. N* **26**, 1509–1518 (2020).
41. Weil, J. E. & Beemon, K. L. A 3' UTR sequence stabilizes termination codons in the unspliced RNA of Rous sarcoma virus. *RNA N. Y. N* **12**, 102–110 (2006).
42. Ge, Z., Quek, B. L., Beemon, K. L. & Hogg, J. R. Polypyrimidine tract binding protein 1 protects mRNAs from recognition by the nonsense-mediated mRNA decay pathway. *eLife* **5**, (2016).
43. Ajamian, L. *et al.* HIV-1 Recruits UPF1 but Excludes UPF2 to Promote Nucleocytoplasmic Export of the Genomic RNA. *Biomolecules* **5**, 2808–2839 (2015).
44. Fiorini, F. *et al.* HTLV-1 Tax plugs and freezes UPF1 helicase leading to nonsense-mediated mRNA decay inhibition. *Nat. Commun.* **9**, (2018).
45. Nakano, K. *et al.* Elucidation of the Mechanism of Host NMD Suppression by HTLV-1 Rex: Dissection of Rex to Identify the NMD Inhibitory Domain. *Viruses* **14**, 344 (2022).
46. Iwasaki, Y. Pathology of chronic myelopathy associated with HTLV-I infection (HAM/TSP). *J. Neurol. Sci.* **96**, 103–123 (1990).

47. Poiesz, B. J. *et al.* Detection and isolation of type C retrovirus particles from fresh and cultured lymphocytes of a patient with cutaneous T-cell lymphoma. *Proc. Natl. Acad. Sci. U. S. A.* **77**, 7415–7419 (1980).
48. Barré-Sinoussi, F., Ross, A. L. & Delfraissy, J.-F. Past, present and future: 30 years of HIV research. *Nat. Rev. Microbiol.* **11**, 877–883 (2013).
49. Ahmed, Y. F., Hanly, S. M., Malim, M. H., Cullen, B. R. & Greene, W. C. Structure-function analyses of the HTLV-I Rex and HIV-1 Rev RNA response elements: insights into the mechanism of Rex and Rev action. *Genes Dev.* **4**, 1014–1022 (1990).
50. Ballaun, C. *et al.* Functional analysis of human T-cell leukemia virus type I rex-response element: direct RNA binding of Rex protein correlates with in vivo activity. *J. Virol.* **65**, 4408–4413 (1991).
51. Malim, M. H. & Cullen, B. R. HIV-1 structural gene expression requires the binding of multiple Rev monomers to the viral RRE: implications for HIV-1 latency. *Cell* **65**, 241–248 (1991).
52. Shida, H. Role of Nucleocytoplasmic RNA Transport during the Life Cycle of Retroviruses. *Front. Microbiol.* **3**, 179 (2012).
53. Madore, S. J., Tiley, L. S., Malim, M. H. & Cullen, B. R. Sequence requirements for Rev multimerization in vivo. *Virology* **202**, 186–194 (1994).
54. Hakata, Y., Umemoto, T., Matsushita, S. & Shida, H. Involvement of human CRM1 (exportin 1) in the export and multimerization of the Rex protein of human T-cell leukemia virus type 1. *J. Virol.* **72**, 6602–6607 (1998).
55. Palmeri, D. & Malim, M. H. Importin beta can mediate the nuclear import of an arginine-rich nuclear localization signal in the absence of importin alpha. *Mol. Cell. Biol.* **19**, 1218–1225 (1999).
56. Henderson, B. R. & Percipalle, P. Interactions between HIV Rev and nuclear import and export factors: the Rev nuclear localisation signal mediates specific binding to human importin-beta. *J. Mol. Biol.* **274**, 693–707 (1997).
57. Adachi, Y., Copeland, T. D., Hatanaka, M. & Oroszlan, S. Nucleolar targeting signal of Rex protein of human T-cell leukemia virus type I specifically binds to nucleolar shuttle protein B-23. *J. Biol. Chem.* **268**, 13930–13934 (1993).
58. Lin, M.-H. *et al.* Nullbasic, a potent anti-HIV tat mutant, induces CRM1-dependent disruption of HIV rev trafficking. *PloS One* **7**, e51466 (2012).
59. Baydoun, H., Duc-Dodon, M., Lebrun, S., Gazzolo, L. & Bex, F. Regulation of the human T-cell leukemia virus gene expression depends on the localization of regulatory proteins Tax, Rex and p30II in specific nuclear subdomains. *Gene* **386**, 191–201 (2007).
60. Nakano, K. & Watanabe, T. HTLV-1 Rex: the courier of viral messages making use of the host vehicle. *Front. Microbiol.* **3**, 330 (2012).
61. Daelemans, D., Costes, S. V., Lockett, S. & Pavlakis, G. N. Kinetic and molecular analysis of nuclear export factor CRM1 association with its cargo in vivo. *Mol. Cell. Biol.* **25**, 728–739 (2005).
62. Nakano, K. & Watanabe, T. HTLV-1 Rex Tunes the Cellular Environment Favorable for Viral Replication. *Viruses* **8**, 58 (2016).
63. Schmidt, E. K., Clavarino, G., Ceppi, M. & Pierre, P. SUnSET, a nonradioactive method to monitor protein synthesis. *Nat. Methods* **6**, 275–277 (2009).
64. Farjot, G. *et al.* Epstein-Barr virus EB2 protein exports unspliced RNA via a Crm-1-independent pathway. *J. Virol.* **74**, 6068–6076 (2000).
65. Singh, A. K. *et al.* The RNA helicase UPF1 associates with mRNAs co-transcriptionally and is required for the release of mRNAs from gene loci. *eLife* **8**, e41444 (2019).
66. Ajamian, L. *et al.* Unexpected roles for UPF1 in HIV-1 RNA metabolism and translation. *RNA N. Y. N* **14**, 914–927 (2008).
67. Serquina, A. K. *et al.* UPF1 Is Crucial for the Infectivity of Human Immunodeficiency Virus Type 1 Progeny Virions. *J Virol* **87**, 8853–61 (2013).
68. Huang, S. *et al.* A second CRM1-dependent nuclear export signal in the influenza A virus NS2 protein contributes to the nuclear export of viral ribonucleoproteins. *J. Virol.* **87**, 767–778 (2013).

69. Rawlinson, S. M., Pryor, M. J., Wright, P. J. & Jans, D. A. CRM1-mediated nuclear export of dengue virus RNA polymerase NS5 modulates interleukin-8 induction and virus production. *J. Biol. Chem.* **284**, 15589–15597 (2009).
70. Bodendorf, U., Cziepluch, C., Jauniaux, J. C., Rommelaere, J. & Salomé, N. Nuclear export factor CRM1 interacts with nonstructural proteins NS2 from parvovirus minute virus of mice. *J. Virol.* **73**, 7769–7779 (1999).
71. Beemon, K. L. Retroviral RNA Processing. *Viruses* **14**, 1113 (2022).
72. Mathew, C. & Ghildyal, R. CRM1 Inhibitors for Antiviral Therapy. *Front. Microbiol.* **8**, 1171 (2017).
73. Knoener, R. A., Becker, J. T., Scalf, M., Sherer, N. M. & Smith, L. M. Elucidating the in vivo interactome of HIV-1 RNA by hybridization capture and mass spectrometry. *Sci. Rep.* **7**, 16965 (2017).
74. Kamel, W. *et al.* Global analysis of protein-RNA interactions in SARS-CoV-2-infected cells reveals key regulators of infection. *Mol. Cell* **81**, 2851-2867.e7 (2021).
75. Garcia-Moreno, M. *et al.* System-wide Profiling of RNA-Binding Proteins Uncovers Key Regulators of Virus Infection. *Mol. Cell* **74**, 196-211.e11 (2019).
76. Iselin, L. *et al.* Uncovering viral RNA-host cell interactions on a proteome-wide scale. *Trends Biochem. Sci.* **47**, 23–38 (2022).
77. Zhang, S. *et al.* Comparison of viral RNA-host protein interactomes across pathogenic RNA viruses informs rapid antiviral drug discovery for SARS-CoV-2. *Cell Res.* **32**, 9–23 (2022).
78. Palma, M. *et al.* A role for AKT1 in nonsense-mediated mRNA decay. *Nucleic Acids Res.* **49**, 11022–11037 (2021).

Figures

Figure 1

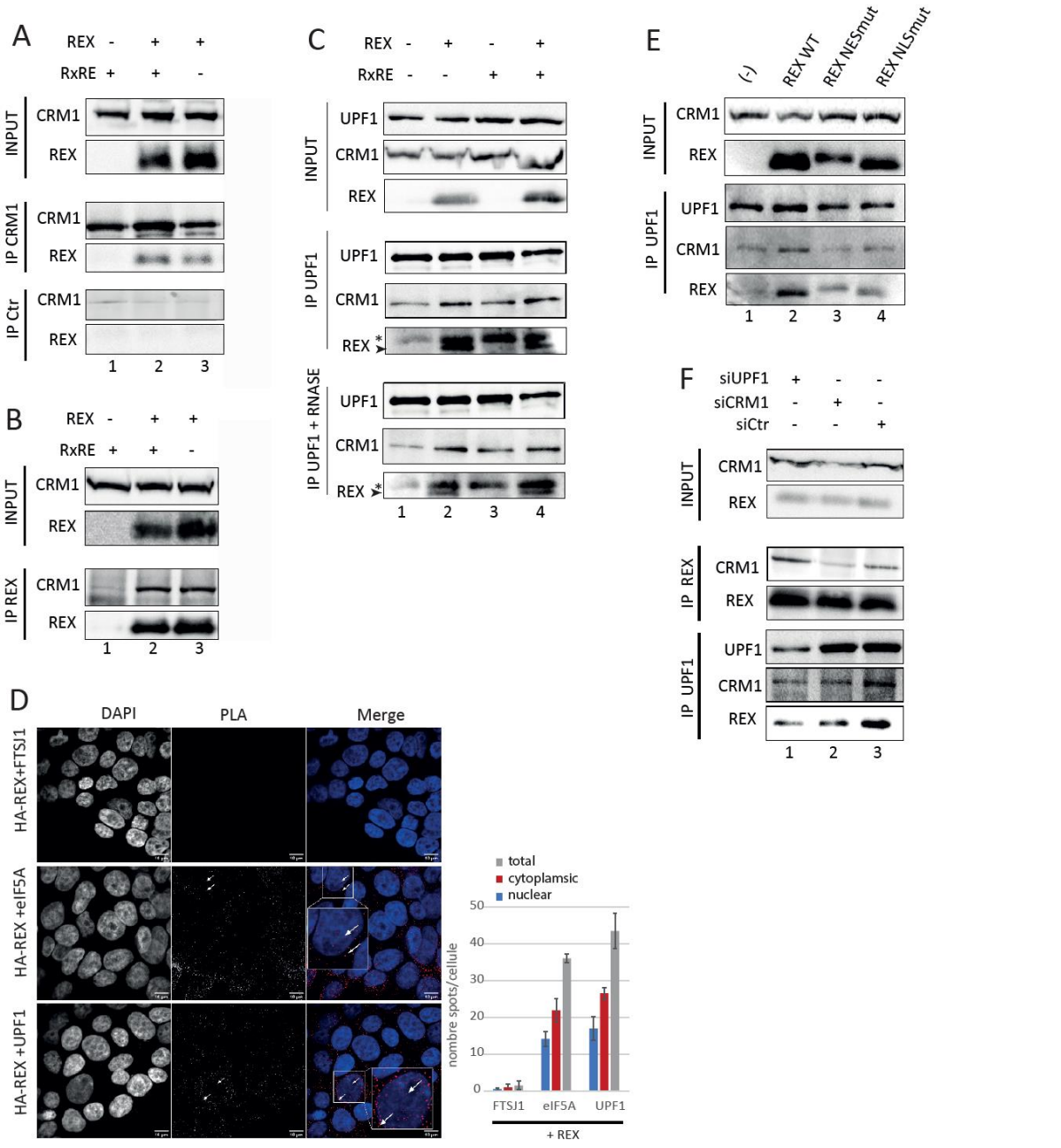

Figure 7

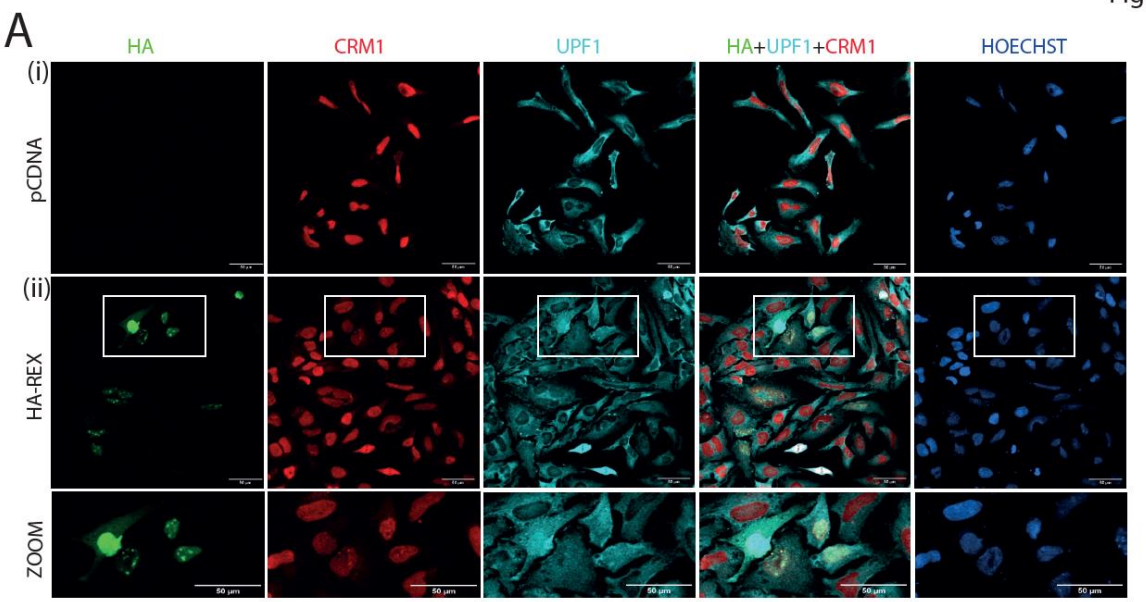
A
HA
CRM1
UPF1
HA+UPF1+CRM1
HOECHST
(i)
pCDNA
(ii)
HA-REX
ZOOM

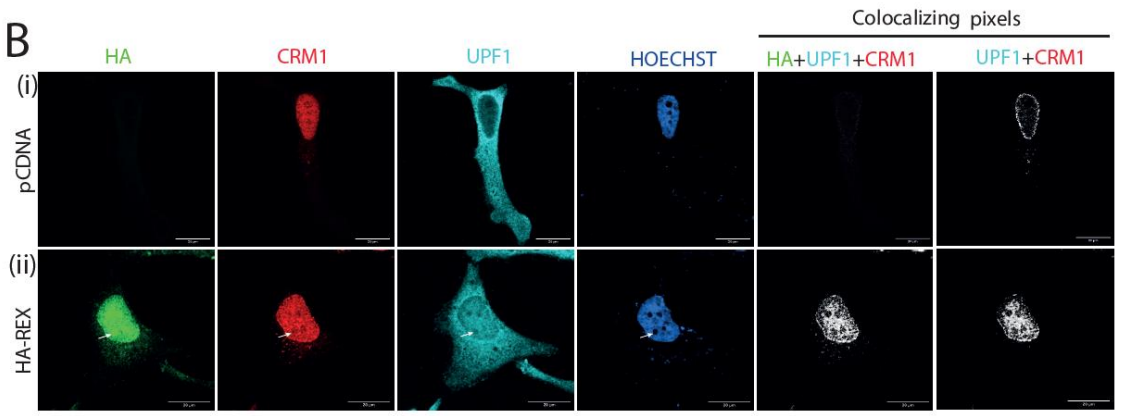
B
Colocalizing pixels
HA
CRM1
UPF1
HOECHST
HA+UPF1+CRM1
UPF1+CRM1
(i)
pCDNA
(ii)
HA-REX

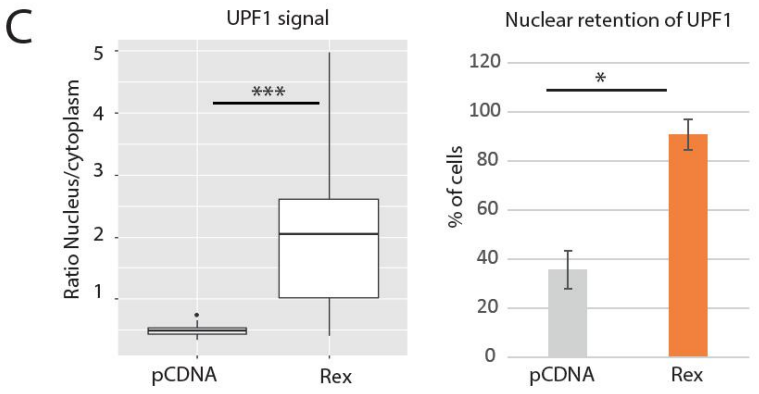
C
UPF1 signal
Ratio Nucleus/cytoplasm
5
4
3
2
1
***
pCDNA
Rex
Nuclear retention of UPF1
% of cells
120
100
80
60
40
20
0
*
pCDNA
Rex

Figure 3

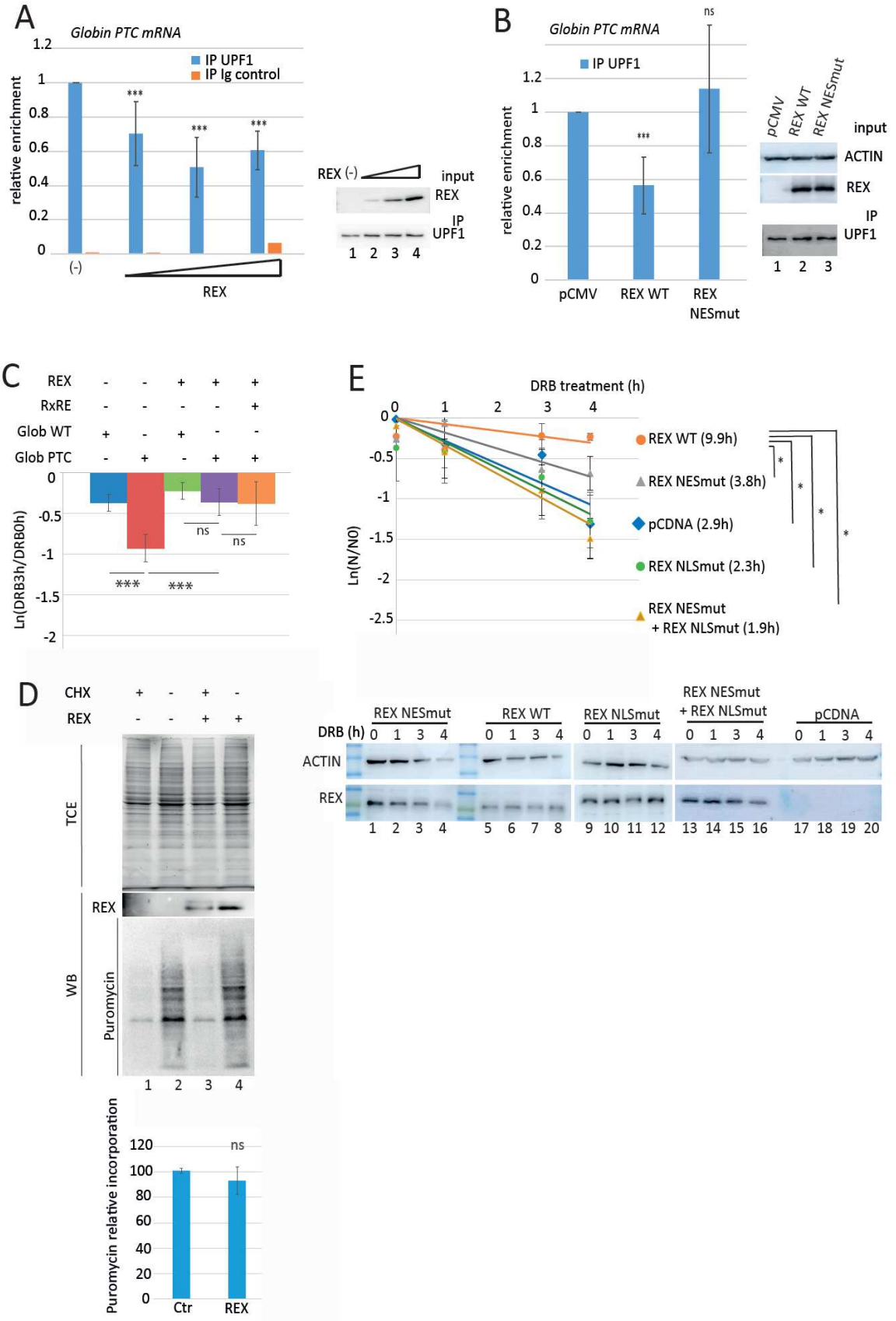
A
Globin PTC mRNA
IP UPF1
IP Ig control
relative enrichment
REX
REX (-)
input
REX
IP UPF1
B
Globin PTC mRNA
IP UPF1
relative enrichment
pCMV
REX WT
REX NESmut
ns
ACTIN
C
REX
RxRE
Glob WT
Glob PTC
Ln(DRB3h/DRB0h)
ns
D
CHX
REX
TCE
WB
Puromycin
Puromycin relative incorporation
Ctr
REX
E
DRB treatment (h)
Ln(N/N0)
REX WT (9.9h)
REX NESmut (3.8h)
pCDNA (2.9h)
REX NLSmut (2.3h)
REX NESmut
+ REX NLSmut (1.9h)
DRB (h)
ACTIN
REX

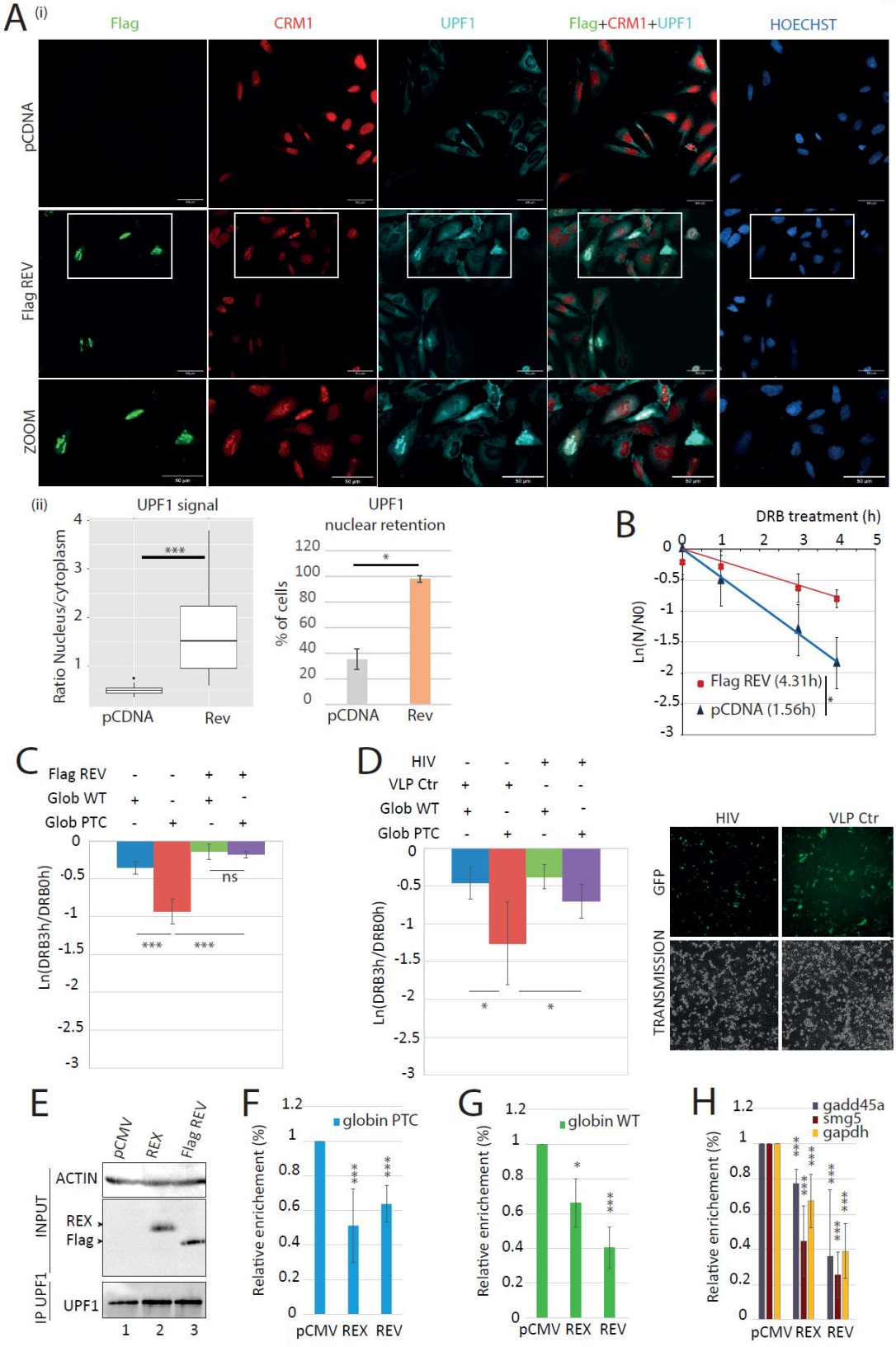
A
(i)
Flag
CRM1
UPF1
Flag+CRM1+UPF1
HOECHST
pCDNA
Flag REV
ZOOM
(ii)
UPF1 signal
Ratio Nucleus/cytoplasm
pCDNA
Rev
UPF1
nuclear retention
% of cells
B
DRB treatment (h)
Ln(N/N0)
Flag REV (4.31h)
pCDNA (1.56h)
C
Flag REV
Glob WT
Glob PTC
Ln(DRB3h/DRB0h)
ns
D
HIV
VLP Ctr
Glob WT
Glob PTC
Ln(DRB3h/DRB0h)
HIV
VLP Ctr
GFP
TRANSMISSION
E
pCMV
REX
Flag REV
ACTIN
INPUT
REX
Flag
IP UPF1
UPF1
1 2 3
F
globin PTC
Relative enrichement (%)
pCMV REX REV
G
globin WT
Relative enrichement (%)
pCMV REX REV
H
gadd45a
smg5
gapdh
Relative enrichement (%)
pCMV REX REV

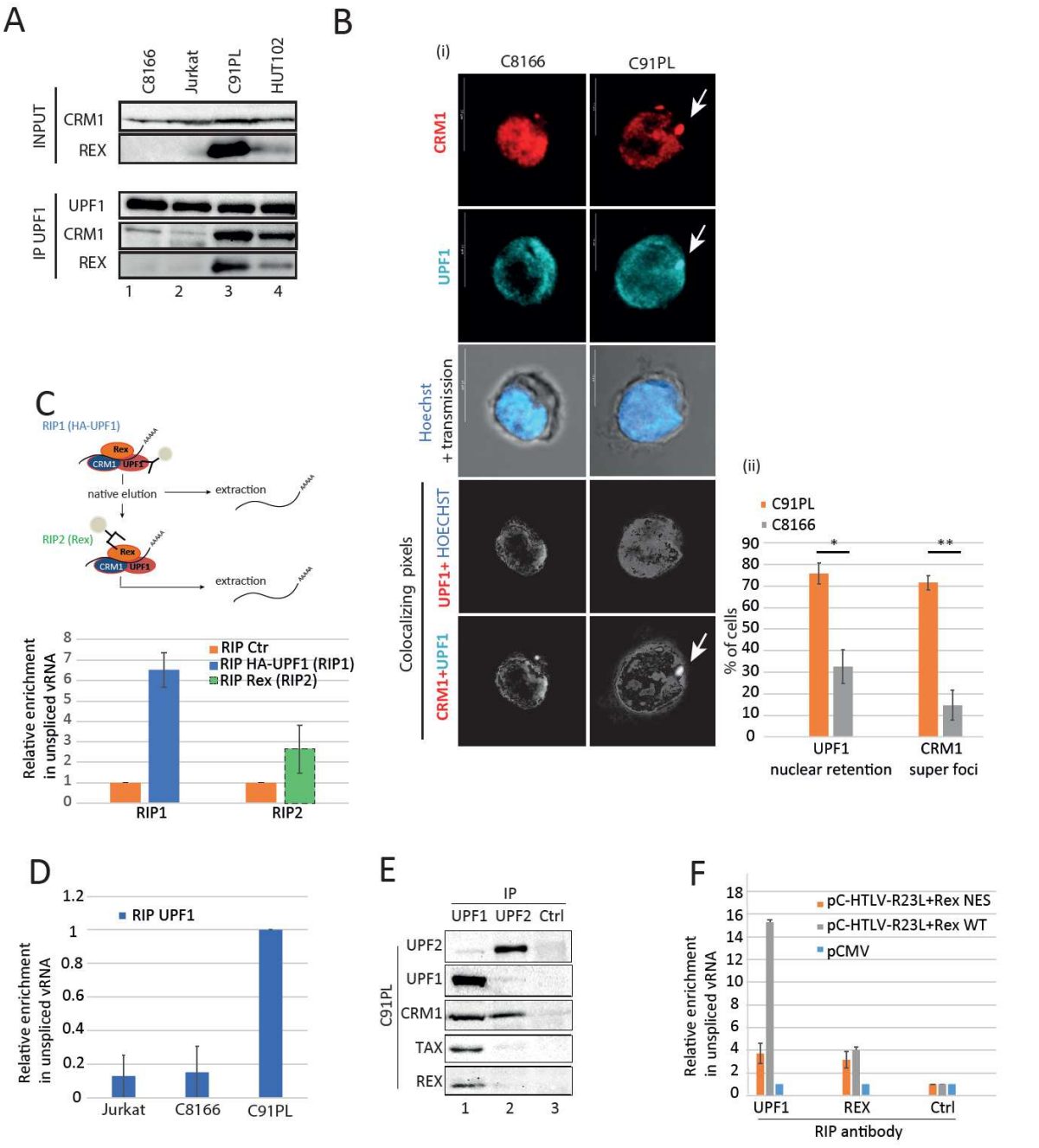
A
C8166
Jurkat
C91PL
HUT102
INPUT
CRM1
REX
IP UPF1
UPF1
CRM1
REX
1 2 3 4
B
(i)
C8166
C91PL
CRM1
UPF1
Hoechst + transmission
Colocalizing pixels
UPF1+ HOECHST
CRM1+UPF1
(ii)
C91PL
C8166
% of cells
UPF1 nuclear retention
CRM1 super foci
C
RIP1 (HA-UPF1)
Rex
CRM1
UPF1
native elution
extraction
RIP2 (Rex)
RIP Ctr
RIP HA-UPF1 (RIP1)
RIP Rex (RIP2)
Relative enrichment in unspliced vRNA
RIP1
RIP2
D
RIP UPF1
Relative enrichment in unspliced vRNA
Jurkat
C8166
C91PL
E
IP
UPF1 UPF2 Ctrl
C91PL
UPF2
UPF1
CRM1
TAX
REX
1 2 3
F
pC-HTLV-R23L+Rex NES
pC-HTLV-R23L+Rex WT
pCMV
Relative enrichment in unspliced vRNA
UPF1
REX
Ctrl
RIP antibody

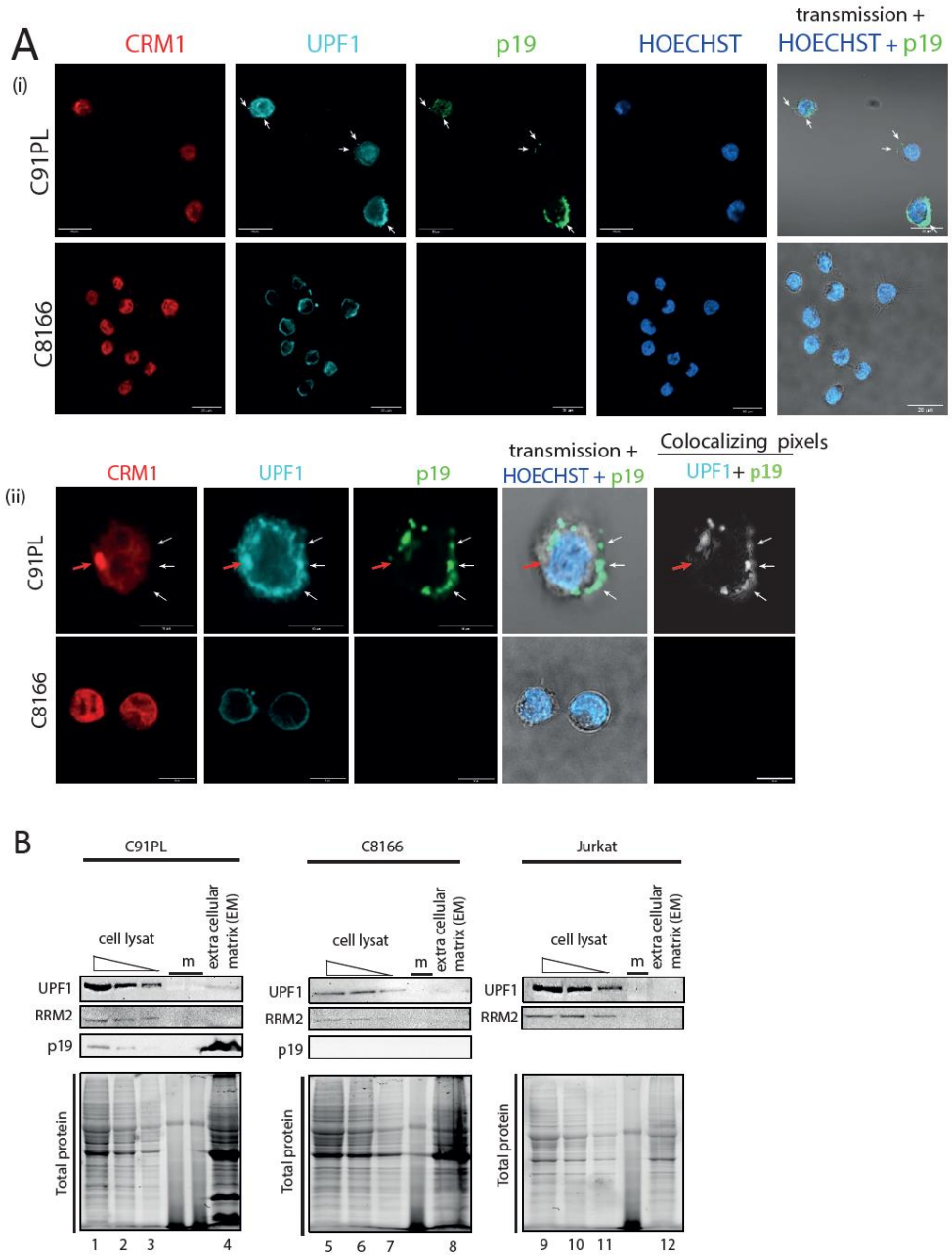
A
CRM1
UPF1
p19
HOECHST
transmission + HOECHST + p19
(i)
C91PL
C8166
(ii)
Colocalizing pixels
UPF1+ p19
B
C91PL
C8166
Jurkat
cell lysat
m
extra cellular matrix (EM)
UPF1
RRM2
p19
Total protein
1 2 3 4
5 6 7 8
9 10 11 12

Legends

Figure 1: Rex interacts with CRM1 and UPF1 to form a tripartite complex.

A) Coimmunoprecipitation (coIP) experiments on 293T cells extracts. Cells express the indicated combinations of Rex and RxRE motif containing RNA. IP were performed using rabbit polyclonal antibodies against CRM1 (middle panel) or from a pre-immune serum. Proteins revealed by western blot were indicated on the side. B) Same as A with an antibody targeting Rex. C) Same as A) with an antibody targeting UPF1. CoIP were incubated 30 min with RNAse A (0.1mg/ml) (lower panel) or not (middle panel). * indicates an aspecific signal. Rex specific signal corresponds to the lower band. D) Proximity Ligation Assay (PLA) carried out in 293T cells transiently transfected with a HA-REX coding plasmid. PLA combined antibodies specific of the HA tag and FTSJ1, eIF5A or UPF1 as indicated. Each dot corresponds to the colocalization of the indicated protein with a resolution of 40nm. Magnification of one representative cell is framed in the merge. E) coIP experiments in 293T cells transfected with plasmids coding the indicated forms of Rex and revealed by western blot. An empty vector is transfected in lane 1. IP was performed with a rabbit polyclonal antibody against UPF1. F) coIP experiments in 293T cells transfected with the indicated siRNA and revealed by western blot. IP was performed against Rex (middle panel) or UPF1 (lower panel).

Figure 2 : *Rex expression modifies UPF1 localisation.*

A) Confocal microscopy experiments were performed in HeLa cells transfected with the plasmids indicated on the left side. Rex was revealed with an antiHA tag antibody and a secondary anti mouse alexa 488. CRM1 antibody was targeted with an anti rabbit alexa 647 and the UPF1 antibody with an anti goat CFL 555. Magnification of the framed zone is shown in the lower panel (ZOOM). Images were acquired with a x20 objective. Scale: 50µm. B) same as A with a x63 objective. Scale: 20µm. Colocalizing pixels view is obtained as mentioned in the methods section and only show the pixels activated at the indicated conditions. C) Quantitative analysis of the microscopy experiments. On the left panel, UPF1 signal was quantified in the cytoplasm and in the nucleus and express as a ratio. Wilcoxon, pvalue < 0.005,***. On the right panel, the number of cells displaying nuclear retention of UPF1 is indicated. Ttest pvalue <0.05 *.

Figure 3: Rex expression leads to UPF1 diminished association to RNA, what is functionally link to NMD inhibition.

A) RNA immunoprecipitation experiment (RIP) using a rabbit polyclonal antibody targeting UPF1 or from a pre-immune serum (Ig control) were performed with HeLa cells transfected with a Globin PTC coding plasmid and increasing amounts of Rex coding plasmid. Immunoprecipitated RNA (Globin PTC) were quantified by RTqPCR. For each condition, the relative enrichment of Globin PTC RNA associated to UPF1 compared to conditions without Rex was displayed in the graph. Statistical analysis: Ttest *** $p<0.005$; ns: $p>0.05$. On the right panel, western blot controlling the levels of expressed Rex and immunoprecipitated UPF1. B) Same as A with empty vector, Rex WT or Rex NES mutant plasmids transfected as indicated. C) Decay rate analysis of Globin PTC and Globin WT RNA. Globin RNA levels were quantified after HeLa cells were treated with DRB for 0h or 3h. The rate of decay is expressed as ln (DRB3h/DRB0h). Statistical analysis: Ttest *** $p<0.005$; ns: $p>0.05$. D) Sunset assay with HeLa cells expressing or not Rex (lane 2 and 4). The level of total protein was acquired before tranfer with stainless method, Rex expression and puromycin incorporation were evaluated by western blot. Puromycin quantification was indicated on the right panel. As a negative control, cells were pre-treated with cycloheximide to inhibit translation (lane 1 and 3). Statistical analysis: Ttest ns: $p>0.05$. E) Half-life evaluation of the Glob PTC mRNA in HeLa cells transfected with the indicated forms of Rex.

mRNA half-lives (t1/2 = ln(2)/λ with λ the time constant of the decay curves) are indicated in front of their respective conditions. Statistical analysis: Ttest * $p<0.05$. The expression of Rex at each time point after DRB treatment was evaluated by WB (lower panel).

Figure 4: Rev from HIV-1 also inhibits NMD through UPF1 nuclear retention and diminished RNA association.

A) (i) Confocal microscopy experiments were performed in HeLa cells transfected with the plasmids indicated on the left side. Rev was revealed with an anti Flag tag antibody and a secondary anti-mouse alexa 488. CRM1 antibody was targeted with an anti-rabbit alexa 647 and the UPF1 antibody with an anti-goat CFL 555. Magnification of the framed zone is shown in the lower panel (ZOOM). Images were acquired with a x20 objective. Scale: 50µm. (ii) The same quantitative analysis was carried out as for Rex in Fig 2C B) Half-life evaluation of the Glob PTC mRNA in HeLa cells transfected with the indicated forms of Rev. mRNA half-lives (t1/2 = ln(2)/λ with λ the time constant of the decay curves) are indicated in front of their respective conditions. Statistical analysis: Ttest * $p<0.05$. C) Decay rate analysis of Globin PTC and Globin WT RNA. Globin RNA levels were quantified after HeLa cells were treated with DRB for 0h or 3h. The rate of decay is expressed as ln (DRB3h/DRB0h). Statistical analysis: Ttest *** $p<0.005$; ns: $p>0.05$. D) Same as C) except that HeLa cells were infected with HIV particles or control Virus Like Particles (CtrVLP) instead of being transfected with Flag Rev (left panel). GFP expressed from HIV or CtrVLP was observed with epifluorescence microscope (right panel). E) Western blot controlling the following RIP experiment: Rex and Rev proteins expression was monitored in the whole cell extract (INPUT) as well as UPF1 immunoprecipitations. F) RIP using a rabbit polyclonal antibody targeting UPF1 was performed with HeLa cells expressing Globin PTC mRNA as well as Rex or Rev as indicated. Immunoprecipitated RNA (Globin PTC) were quantified by RTqPCR. For each condition, the relative enrichment of Globin PTC RNA associated to UPF1 compared to control conditions conditions (pCMV) was displayed in the graph. Statistical analysis: Ttest *** $p<0.005$; ns: $p>0.05$. G) Same as F with cells expressing globin WT mRNA. H) same as G with the quantification of endogenous mRNA gadd45a, smg5 and gapdh.

Figure 5: Rex drives UPF1 sticking to CRM1, cellular relocalisation and loading on viral unspliced RNA

A) coIP experiments in the indicated lymphocytes cells extracts. IP were performed using rabbit polyclonal antibodies against UPF1. Proteins revealed by western blot were indicated on the side. B) (i) Confocal microscopy experiments were performed in C91PL and C8166 lymphocytes. CRM1 and UPF1 were revealed. The arrow shows a representative example of the CRM1 and UPF1 super foci (surface >= 1% total surface. Images were acquired with a x63 objective. Scale: 10µm. (ii) Quantitative analysis showing the relative number of cells with UPF1 nuclear retention (left) or with at least one CRM1 superfoci (SF). C) Schematic diagram of the double RIP experiment performed in 293T cells cotransfected with the HTLV-1 WT molecular clone and a HA-UPF1 coding plasmid (upper panel). Quantification of the relative enrichment in unspliced viral RNA (vRNA) after HA RIP targeting UPF1 (RIP1) and Rex RIP (RIP2) (lower panel) compared to RIP Ctr. D) RIP using a rabbit polyclonal antibody targeting UPF1 or UPF2 were performed with Jurkat, C91PL or C8166 lymphocytes. Immunoprecipitated RNA (vRNA) was quantified by RTqPCR. The relative enrichment of vRNA associated to UPF1 or UPF2 in C91PL was compared to Jurkat and C8166 and displayed in the graph. E) coIP experiments in the C91PL cells extracts. IP were performed against UPF1, UPF2 or using a control antibody (Ctr). Proteins revealed by western blot were indicated on the side. F) RIP targeting UPF1, Rex or using a control antibody (as indicated) were performed with 293T cells transfected with HTLV-1 R23L molecular clone complemented with either Rex NES or Rex WT (orange and grey bars respectively). As a negative control, cells were transfected with an empty vector (blue bars).

Immunoprecipitated RNA (vRNA) was quantified by RTqPCR. The relative enrichment of vRNA associated to UPF1 or Rex compared to control was displayed in the graph.

Figure 6: UPF1 controls GAG expression and is found in HTLV-1 biofilm.

A) Confocal microscopy experiments were performed in C91PL and C8166 lymphocytes. Panel (i): CRM1, UPF1 and p19 GAG were revealed. The arrow shows a representative example of p19 and UPF1 colocalization in C91PL. Images were acquired with a x20 objective. Scale: 50µm. Panel (ii): same as panel (i) with acquisitions with a x63 objective (scale 10µm). White arrows show p19 foci. Red arrow shows CRM1 superfoci. B) Extracellular matrix (EM) containing the viral biofilm was collected in C91PL, C8166 and Jurkat cells and analysed (lanes 4, 8, 12). The presence of UPF1, RRM2 and p19 was evaluated by WB and total protein was monitored with stainless procedure (upper and lower panels respectively). Corresponding cell lysates were also monitored (lanes 1-3, 5-7, 9-11).

Supplementary figure 1

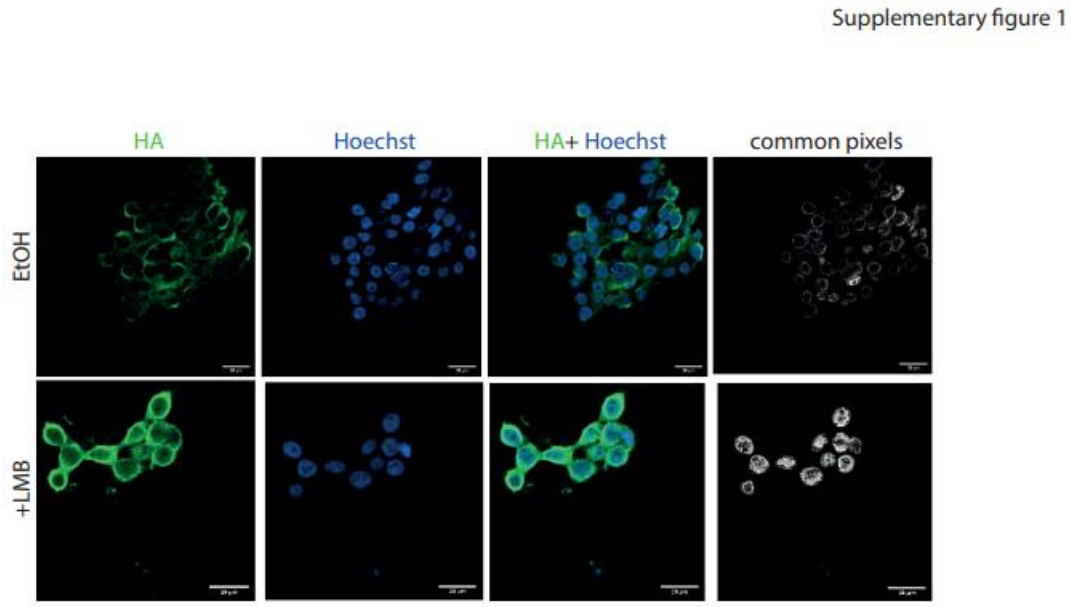

293T cells were transfected with a HA UPF1 plasmid. 12h before fixation, cells were treated with either 50nM leptomycin B (LMB) or EtOH. Cells were further stained with a anti HA antibody to localize UPF1. Nucleus were stained with Hoechst. Merge with HA and Hoechst was performed (HA+Hoechst) as well as the presentation of pixel jointly excited with anti HA and Hoechst staining (common pixels). This experiment shows a nuclear retention of HAUPF1 after LMB treatment confirming data from the literature.

Supplementary figure 2

Supplementary figure 2

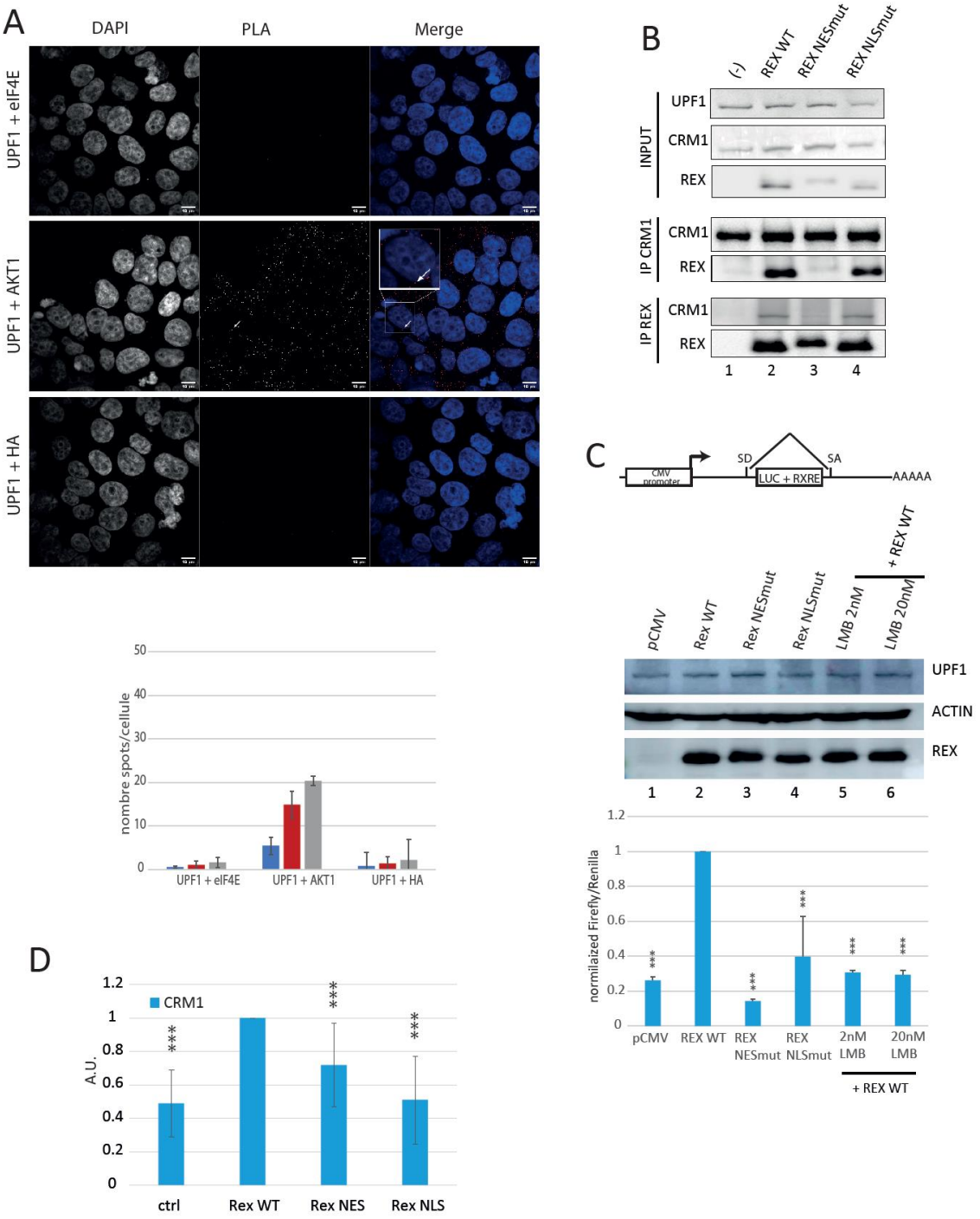

A) PLA control experiments showing UPF1 signal specificity. PLA were performed using anti UPF1 and anti eIF4E or anti HA and shows no spots, as expected of negative controls. Anti UPF1 combined with anti AKT1 generated spots as shown previously [78]. B) coIP experiment in 293T cells transfected with WT and mutant forms of Rex. Immunoprecipitations of either CRM1 or Rex show that Rex NES mutant is not able to interact with CRM1 (lane 3) while Rex NLS mutant is still able (lane 4) compared

with Rex WT (lane 2). C) An export assay was performed as previously described[64]. The Rex reporter is composed of the luciferase gene followed by the RxRE motif under the control of a pCMV promoter. The luciferase/RxRE cassette is encompassed with splicing donor and acceptor sites that provoke its splicing preventing luciferase expression (upper panel). When Rex is expressed, this latter binds the RxRE, prevents the of the Luciferase/RxRE cassette and drives its export in a CRM1 dependant manner splicing (like with vRNA), allowing luciferase expression. The luciferase expression is quantified with the "luciferase dual glo lucieferase assay" (Promega). A renilla coding plasmid is co transfected with the luc RxRE plasmid for noramlization, following the manufacturer protocol. In addition, we transfected Rex WT (positive control, lane2), Rex NES mutant (lane3), Rex NLS mutant (lane 4) or an empty vector (negative control, lane1). As controls we also treated cells that expressed Rex with LMB at the indicated concentrations for 12h (lanes 5-6). Protein level expression was controlled by western blot (middle panel). Luciferase quantification were displayed as a percentage of the Rex WT condition (lower panel, lane2). As expected, in the absence of Rex or when cells were treated with LMB, luciferase expression was strongly reduced (lower panel, compare lane1, 5, 6 and 2). The expression of Rex NES mutant or Rex NLS mutant also impaired luciferase expression, validating the export defect of both mutants (lower panel, compare lane 3-4 and 2). D) Quantification of the western blots corresponding to figure 1E. Bars represent the medium of 4 independent experiments. Co-immunoprecipitated CRM1 was quantified using imageLab (Biorad). And further normalized by the levels of immunoprecipitated UPF1(IP UPF1) and the levels of CRM1 in the total extracts (input).

Supplementary figure 3

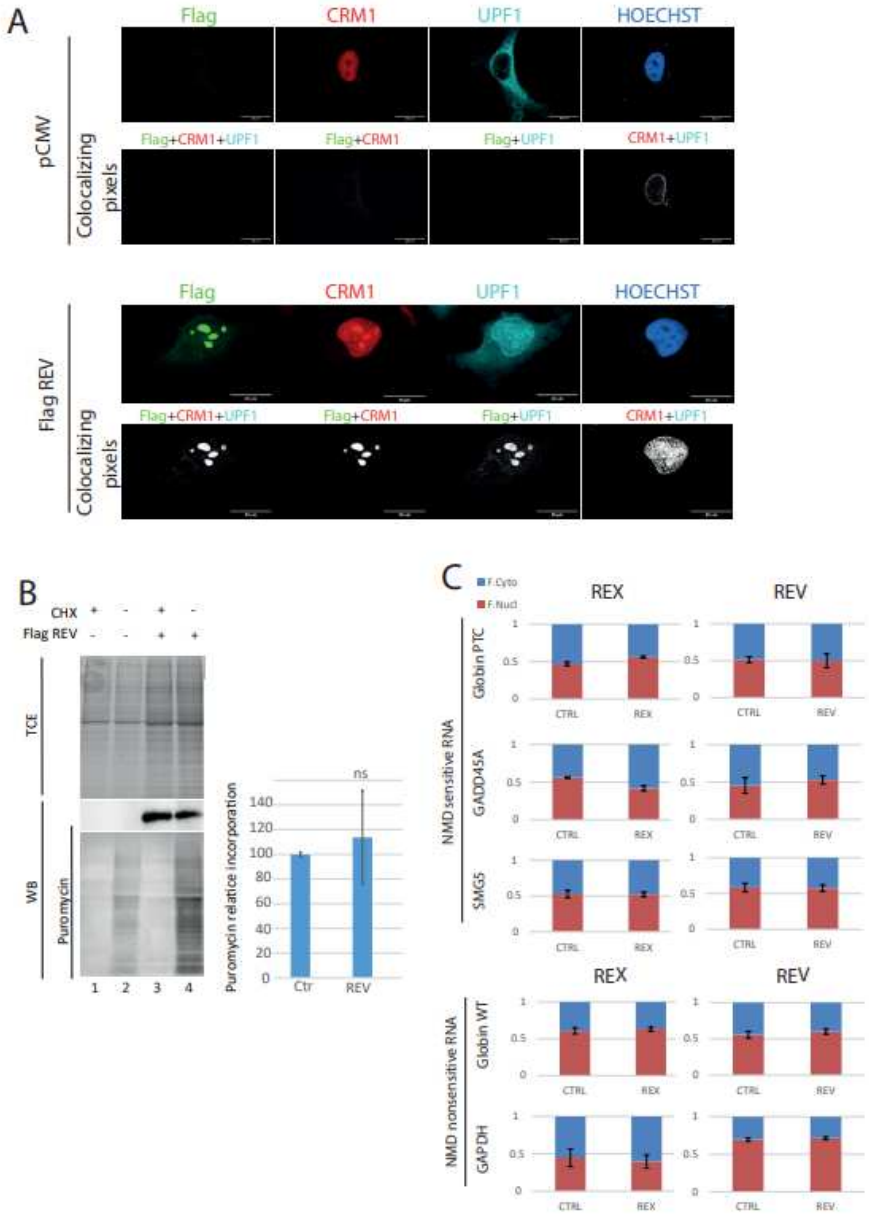

A) Confocal microscopy experiments were performed in HeLa cells transfected with the Flag-Rev plasmid. Rev was revealed with an anti-Flag tag antibody and a secondary anti-mouse alexa 488. CRM1 antibody was targeted with an anti-rabbit alexa 647 and the UPF1 antibody with an anti-goat CFL 555. Colocalizing pixels view is obtained as mentioned in the methods section and only show the pixels activated at the indicated conditions. Images were acquired with a x63 objective. Scale: 20µm. on this representative close up image, we clearly observed the nuclear localisation of UPF1 and its colocalization with Rev and CRM1. B) Sunset assay with HeLa cells expressing or not Rev (lane 2 and 4). The level of total protein was acquired before tranfer with staineless method, Rex expression and puromycin incorporation were evaluated by western blot. Puromycin quantification was indicated on the right panel. As a negative control, cells were pre-treated with cycloheximide to inhibit translation (lane 1 and 3). Statistical analysis: Ttest ns: $p>0.05$. C) Quantification of the indicated RNA in the nuclear and cytoplasmic compartments after cell fractionation. Beforehand, cells were transfected with Rex or Rev as indicated. RNA in each compartment is represented as a fraction of the total amount of RNA. No significative change in RNA repartition could be found, suggesting that Rex and Rev impact on RIP experiments (Fig 4F-H) is not due to a defect in RNA availability in each cellular compartment.

Supplementary figure 4

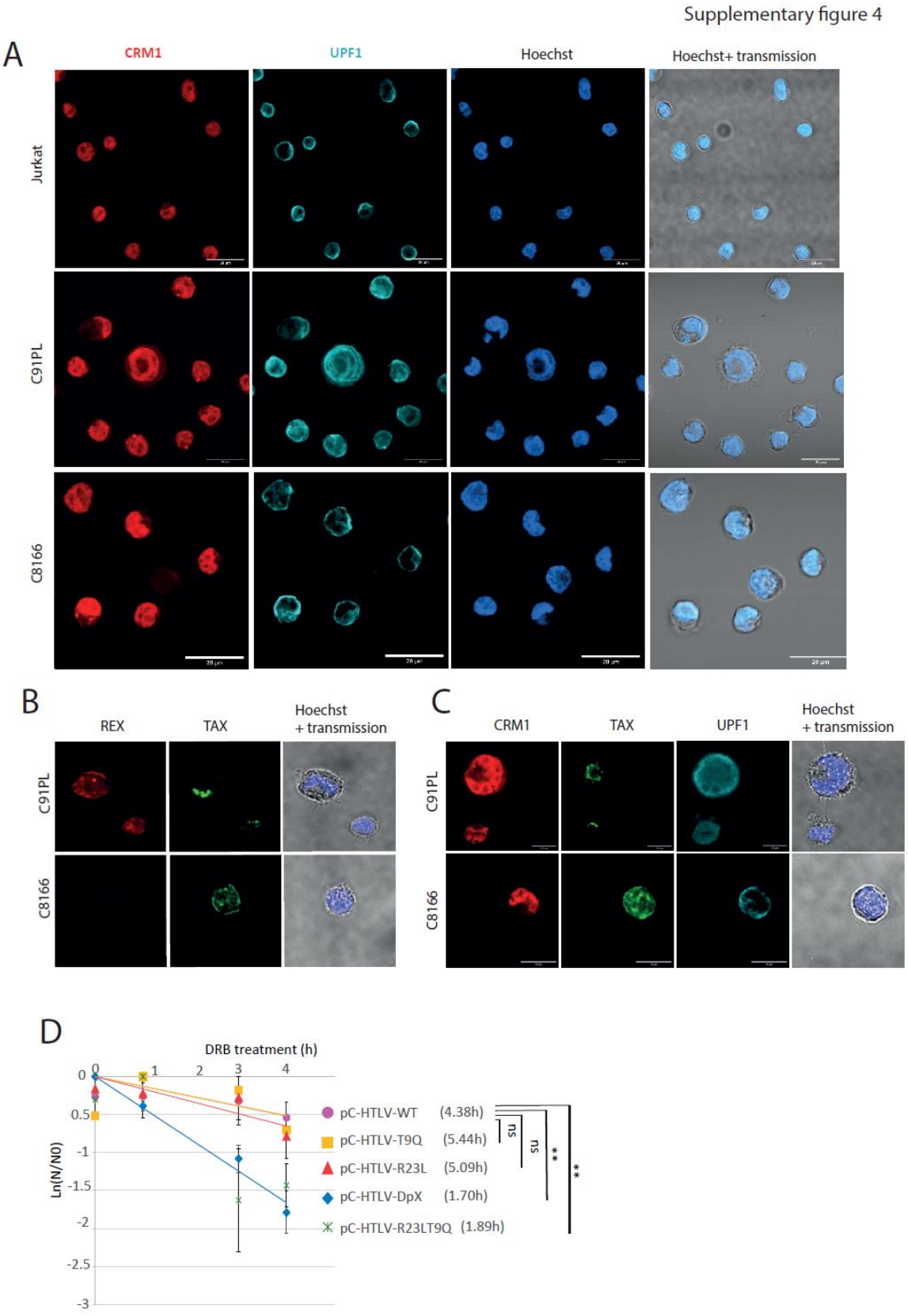

A) Wide field views of Jurkat, C91PL and C8166 lymphocytes stained for CRM1 and UPF1 and observed by confocal microscopy. Images were acquired with a x63 objective. Scale: 20µm. B) Close up view of C91PL and C8166 lymphocytes stained for Rex and Tax and observed by confocal microscopy. Images were acquired with a x63 objective. Scale: 10µm C) same as B with CRM1, Tax and UPF1 staining. D) Half-life evaluation of the Glob PTC mRNA in HeLa cells transfected with the indicated forms of HTLV-1 molecular clones:

-pC-HTLV-WT

-pC-HTLV-T9Q (extinction of Tax expression due to a point mutation inducing nonsense codon at position 9 of Tax but maintaining Rex expression)

-pC-HTLV-R23L (extinction of Rex expression due to a point mutation inducing a nonsense mutation at position 90 of Rex but maintaining Tax expression)

-pC-HTLV-R23LT9Q (extinction of Tax and Rex expression due to the combination of the 2 point mutations)

-pC-HTLV-DpX (extinction of Tax and Rex expression).

pC-HTLV-WT was previously shown to inhibit NMD while pC-HTLV-DpX couldn't[44]. Here mRNA half-lives were measured as described in Fig 3 and 4, ($t1/2 = \ln(2)/\lambda$ with λ the time constant of the decay curves) and reported in front of their respective conditions. Statistical analysis: Ttest ** $p<0.01$.

PROJETS

Les résultats présentés dans la partie précédente n'ont que partiellement répondu aux différents objectifs initialement établis. Les projets que je développerai dans un futur proche y feront donc suite.

Tout d'abord, je me concentrerai sur l'impact cellulaire de l'inhibition d'UPF1 par Tax et Rex et leur effet sur la stabilité du transcriptome cellulaire (projet 1).
Dans un second temps, j'étudierai comment ces dérégulations divergent ou convergent avec d'autres conditions d'inhibition d'UPF1. Je confronterai le modèle d'inhibition de NMD et de détournement d'UPF1 avec HTLV-1 à un autre virus, le SARS-CoV-2. Dans ce contexte, l'interaction rapportée entre UPF1 et la nucléocapside virale pourrait également suggérer que le NMD est une menace à contourner (projet 2).
Enfin, je comparerai l'inhibition du NMD par HTLV-1 à l'inhibition du NMD dans d'autres cas de cancers hors contexte viral. Je me concentrerai sur les défauts d'export via CRM1, comme suggéré par nos dernières données, pour étudier les bases moléculaires d'une modulation du NMD liée à l'export nucléaire (projet 3).

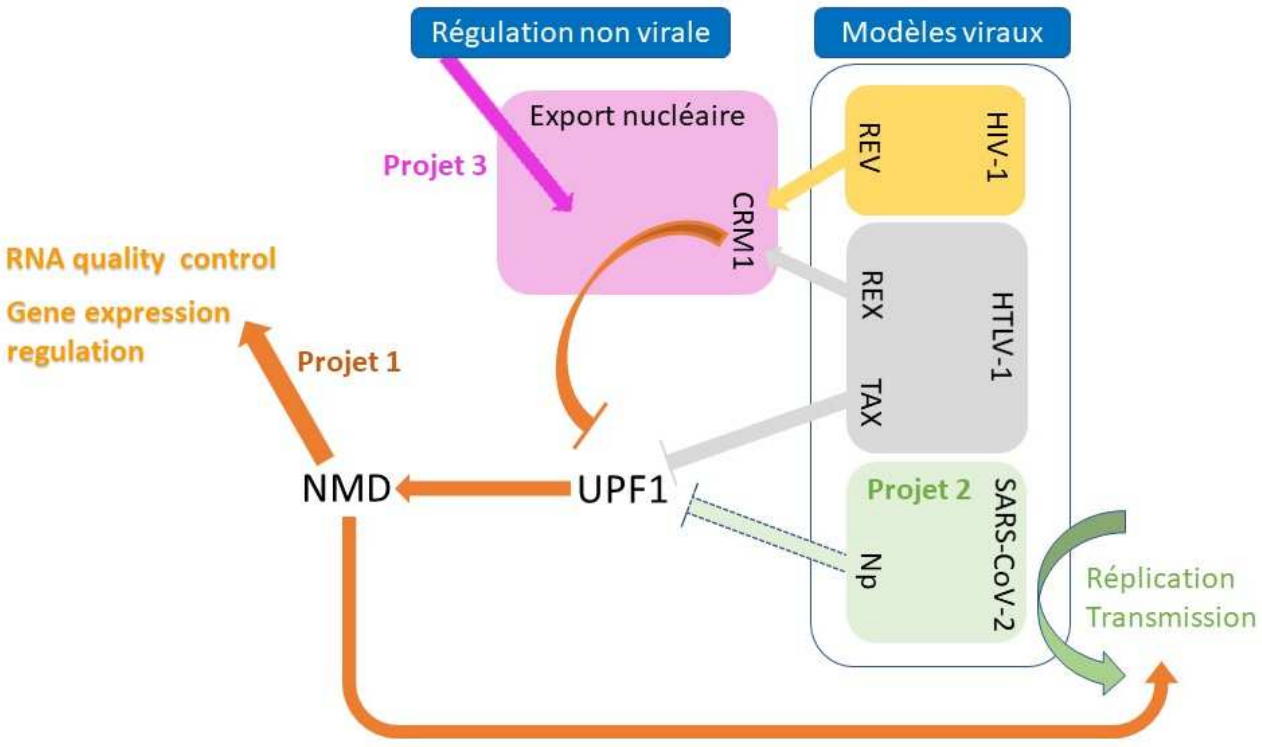

Figure 7 : Coordination des 3 projets présentés

Projet 1 : Modulation de la stabilité du transcriptome induite par HTLV-1. Evaluation et impact.

Jean-Philippe Robin, Vincent Mocquet

HYPOTHESES ET OBJECTIFS

Contribution de l'inhibition d'UPF1 et du NMD dans les dérégulations transcriptomiques induites par Tax et HTLV-1.

La plupart des impacts d'HTLV-1 et de Tax sur la cellule infectée sont décrits à la lumière de la modulation de la transcription et notre compréhension de leurs effets sur la régulation post-transcriptionnelle fait défaut. Alors que nous avons précisément décrit un mécanisme d'inhibition du NMD par Tax, impliquant l'inhibition enzymatique d'UPF1, nous n'avons validé la pertinence physiologique de cet effet que sur quelques ARNm connus pour être sensibles au NMD. Identifier l'ensemble des transcrits impliqués permettrait de clarifier le rôle et la place de l'inhibition d'UPF1 et du NMD parmi l'ensemble des transcrits modulés par Tax. Pour aborder ces points, nous prévoyons d'analyser les variations transcriptomiques des cellules exprimant la protéine virale Tax (ou le virus HTLV-1 complet) et de la comparer avec des cellules sans UPF1 (UPF1shRNA) en utilisant des approches de séquençage à haut débit.

Une fois qu'une corrélation entre les modifications transcriptomiques dues à l'expression de Tax et l'inhibition d'UPF1 sera établie, nous étudierons les conséquences de ces modifications ; Nous nous concentrerons sur les voies cellulaires modifiées. Les fonctions cellulaires altérées par Tax de manière UPF1 dépendantes conduisent-elles à des phénotypes communs décrits dans la littérature avec Tax et une infection à HTLV-1 ? Cette approche permettra peut-être d'identifier de nouvelles fonctions cellulaires impactées par Tax ? Comme discuté dans une revue récente, nous pouvons également nous demander si l'inhibition du NMD favorise les altérations associées à HTLV-1 conduisant à l'émergence de cellules leucémiques, ou à l'inverse stimulerait l'apoptose ?

Enfin, en analysant les modifications transcriptomiques, nous pourrions facilement mélanger les effets directs et indirects de l'inhibition d'UPF1. Par exemple, l'inhibition du NMD stabilise l'ARNm de SMAD7 et augmente directement son expression tandis que les gènes transactivés par SMAD7 sont indirectement régulés positivement, conduisant à une différenciation neurale[141]. Puisque notre hypothèse est qu'UPF1 est directement ciblé par Tax, une tâche importante consiste à évaluer l'impact direct de cette inhibition. Pour ce faire, nous prévoyons d'analyser la stabilité des ARN dans les cellules infectées. Appréhender les altérations transcriptomiques à la lumière de la stabilité de l'ARN au cours de l'infection par HTLV-1 est nouveau et peut révéler des processus de dérégulation inattendus.

Modèles d'inhibition de NMD par HTLV-1.

Comprendre l'inhibition de la dégradation de l'ARN dépendante d'UPF1 par l'infection à HTLV-1 soulève également le sujet important du « où » et du « quand ».

Comme décrit dans l'introduction, bien que plusieurs types de cellules sont infectés par HTLV-1 le tropisme principal est le lymphocyte T CD4+. Concernant le NMD, l'étude dans des modèles hématopoïétiques fait défaut. Des études ont été réalisées à l'origine dans les érythrocytes (avec l'identification de mutations non-sens provoquant la thalassémie B) et dans les lignées B et T pour étudier les réarrangements VDJ ainsi que les maladies génétiques associées à des mutations non-sens. Cependant, la plupart des analyses mécanistiques et à haut débit ont été effectuées dans des lignées cellulaires modèles telles que les cellules HeLa et 293T. La caractérisation récente de l'interférence entre KSHV et le NMD a été réalisée dans des lymphocytes B lymphomateuses et en est un exemple rare [142]. Sachant qu'il a été plusieurs fois décrit que la régulation du NMD dépend du type cellulaire, de l'état de différenciation et du stress cellulaire, il est nécessaire de trouver le modèle cellulaire adéquat [143]. Dans un premier temps, nous prévoyons de travailler sur des cellules Jurkat TCD4+ exprimant Tax ou un shRNA ciblant UPF1. Bien que simplifié, ce modèle reste pertinent pour l'infection par HTLV-1 et serait nouveau pour l'étude d'UPF1. Ensuite, nous élargirons notre champ d'investigation pour inclure d'autres types de cellules infectées telles que les cellules T chroniquement infectées (exprimant Tax et Rex) et des cellules de patients.

Enfin, le moment de l'expression des protéines virales nous impose de bien réfléchir à la dynamique de l'inhibition du NMD au cours de l'infection. Comme décrit précédemment, bien que le provirus soit intégré dans le génome de l'hôte, la transactivation du LTR est réprimée au fil du temps en raison de la répression épigénétique et/ou des altérations génomiques. Il en résulte l'absence de transcription du brin (+) dans la plupart des cellules ATL. Au mieux, les protéines virales sous contrôle de LTR 5' comme Tax et Rex sont exprimées par bursts. En conséquence, nous nous demandons si l'inhibition d'UPF1 par HTLV-1 a le même impact dans les premières étapes de l'infection et dans les cellules leucémiques. Intégrer l'inhibition d'UPF1 en tant que processus dynamique peut aider à en identifier l'effet précis pendant l'infection. Pour étudier ces points, nous prévoyons d'utiliser un modèle de souris humanisée. Les souris immunodéficientes NOD-SCID-IL2Rγ-/- (NSG) avec un système hémato-lymphoïde humain (après greffe de cellules souches hématopoïétiques humaines CD34+) développent des leucémies similaires à celles survenant chez l'homme 2 à 5 mois après l'infection par la HTLV-1. Ce modèle animal nous permettra de récupérer des cellules humaines infectées à différents temps et ainsi de suivre précisément les transcriptomes de cellules infectées du stade asymptomatique aux stades avancés de la leucémie dans un contexte *in vivo* [144–146]

METHODOLOGIE ET RESULTATS PRELIMINAIRES

Mise en place de l'analyse de la dégradation des ARN par Tax.

L'analyse des ARN sensibles à UPF1 par séquençage à haut débit est généralement extrapolée à partir de l'analyse différentielle de l'expression des transcrits après traitement par un siRNA contre UPF1(siUPF1) (sans inhibition de la transcription) dans des modèles cellulaires tels que les cellules HeLa et 293T. Ici, nous avons décidé de mettre en place nos conditions expérimentales dans des cellules Jurkat. Nous avons également décidé d'analyser la stabilité de l'ARN stricto sensu en plus de l'expression différentielle des gènes, pour dissocier les effets transcriptionnels des effets de dégradation de l'ARN. Pour ce faire, des cellules exprimant Tax (ou un contrôle) ou knockdown pour UPF1 (ou un contrôle) seront cultivées entre 0 et 3h avec de la triptolide (tpl), un inhibiteur de la transcription. La quantification des transcrits à ces 2 temps permettra le calcul d'un index, indicatif de la stabilité des transcrits. En plus de cette analyse quantitative, une analyse qualitative caractérisera les transcrits en y recherchant notamment les déterminants du NMD (longueur du 3'UTR, %GC, introns dans le 3'UTR, uORF, etc…). L'approche bioinformatique permettant ces analyses s'effectuera en collaboration avec Emiliano Ricci et son équipe (LBMC, Lyon) et le biocomputing hub de LBMC.

Différents systèmes ont été étudiés pour y exprimer la protéine Tax et supprimer UPF1 dans les Jurkat :

1) Tout d'abord en collaboration avec Philippe Mangeot (CIRI, ENS lyon) nous avons essayé de transférer directement la protéine virale entière en pensant pouvoir mieux contrôler les niveaux de protéine virale intracellulaire. Cependant, nous n'avons pas pu obtenir un rendement suffisant.

2) En deuxième option, nous avons électroporé Tax ou un plasmide d'expression contrôle ou un siRNA UPF1 en utilisant le système Invitrogen NEON. Ce faisant, nous avons obtenu respectivement une forte expression de Tax et une forte diminution d'UPF1 mais nous étions limités par le nombre de cellules.

3) Comme troisième option, nous avons utilisé un système d'expression inductible de Tax transduit stablement dans des cellules Jurkat. En contrôle, des jurkat exprimant des YFP inductibles ont également été établis. Ces lignées cellulaires ont été obtenues en collaboration avec JC Twizere (Institut GIGA, Belgique). Nous avons également conçu des lignées cellulaires Jurkat stables avec une expression inductible de shRNA ciblant UPF1 (Dharmacon). Avec cette option, l'expression de Tax était limitée et le knock-down UPF1 moyen, mais nous n'étions pas limités par le nombre de cellules à récolter contrairement à l'option d'électroporation.

Nous avons donc décidé d'utiliser cette troisième option. Une expérience RNAseq est actuellement en cours d'analyse. En parallèle, pour confirmer ces observations, nous nous sommes concentrés sur la caractérisation d'un mutant de Tax, incapable d'inhiber les fonctions UPF1.

Caractérisation d'un mutant Tax PA pour l'inhibition du NMD.

- Homologie domaine Tax/CH.

Il est décrit qu'au sein de la protéine UPF1, le domaine CH en Nter peut réprimer l'activité ATPase du domaine hélicase en interagissant avec et autour de la F809 du domaine hélicase. Dans des expériences de molécule unique, le domaine CH empêche alors la translocation de domaine hélicase sur son substrat. Pour concevoir un mutant Tax incapable d'inhiber UPF1, nous avons tiré parti de nos précédentes expériences en molécule unique. Dans ces expériences, Tax pouvait induire un blocage de la translocation du domaine hélicase d'UPF1. Nous suggérions que ce blocage pourrait être dû à une perte de flexibilité de ce domaine. Sur cette base, nous avons émis l'hypothèse que Tax pourrait inhiber l'activité d'UPF1 en imitant la

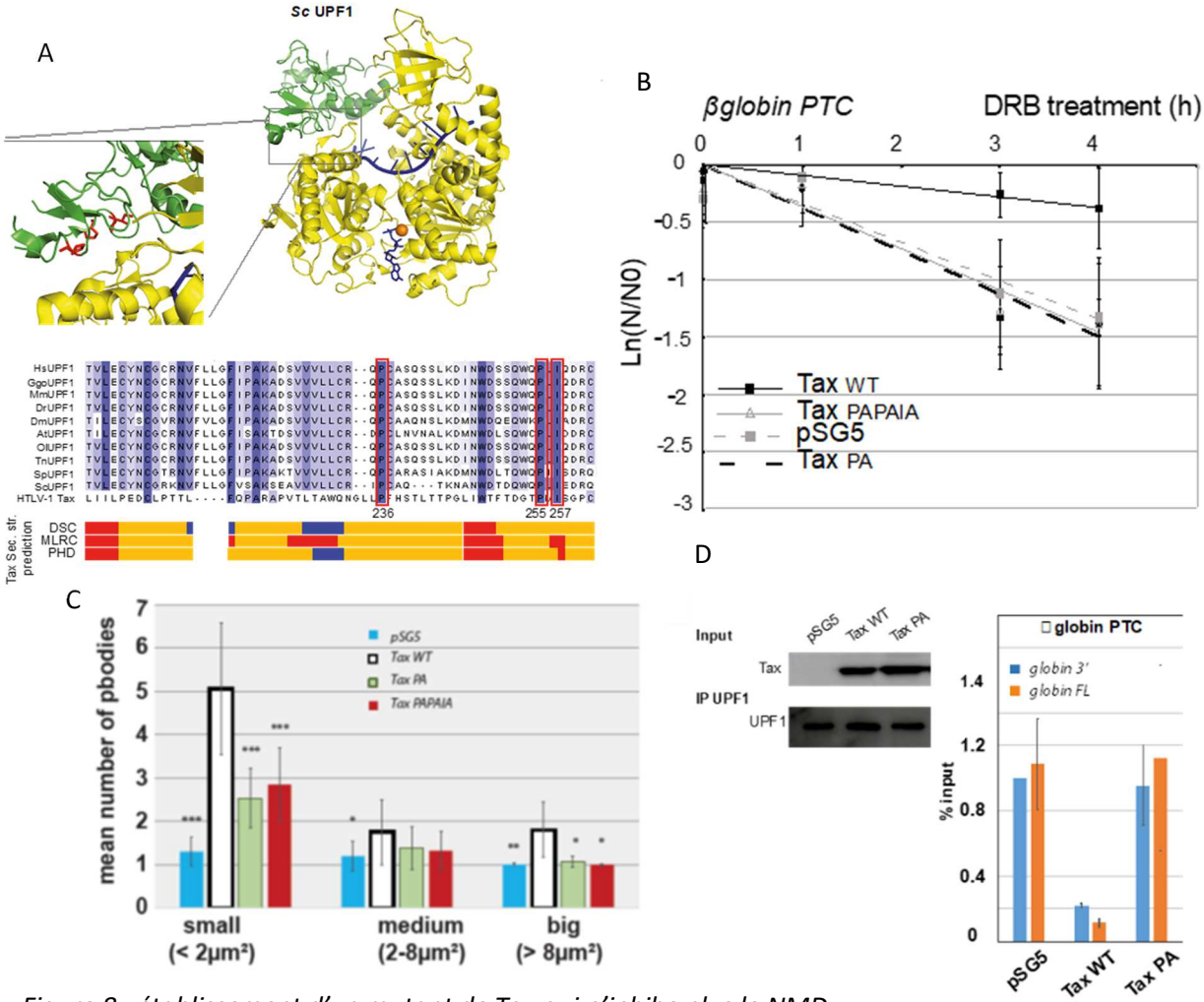

Figure 8 : établissement d'un mutant de Tax qui n'inhibe plus le NMD

A) Représentation structurale de l'interaction entre les domaines CH (vert) et HD (jaune) d'UPF1. En rouge sur le grossissement apparaissent les 3 acides aminés identifiés par l'alignement de séquence entre Tax et CH (P236 I255 et P257 dans Tax). B) Mesure de la stabilité d'un ARN rapporteur sensible au NMD avec Tax$_{wt}$, control pSG5, le triple mutant (PAPAIA) et un mutant simple (P236A : Tax PA). C) Quantification du nombre de pbodies en fonction de leur taille dans des cellules Hela exprimant Tax WT ou les 2 mutants. D) Immunoprecpitations de l'ARN rapporteur du NMD par UPF1 après expression de Tax WT et Tax PA. Les ARN sont quantifiés par 2 oligos différents (en aval du PTC (3') ou de part et d'autre du PTC (FL)).

régulation intramoléculaire par le domaine CH. L'alignement des séquences de Tax et du domaine CH nous a permis d'identifier 3 acides aminés candidats dans Tax (Figure 8A).

- La mutation PA restaure NMD

La mutagenèse dirigée a conduit à la production de 3 mutants différents de Tax avec diverses combinaisons de mutations. Ces mutants ont été testés en mesurant la demi-vie d'un ARN rapporteur (sensibles ou non au NMD) ainsi qu'une cible NMD endogène. Alors que l'ARN rapporteur sensible au NMD était stabilisé par Tax WT, les mutants de Tax n'étaient pas (ou moins) capables de modifier la demi-vie du rapporteur. Nous avons également montré que ces mutants ont une capacité réduite à modifier les profils de pbodies favorisant une inhibition réduite du NMD. Nous avons identifié qu'une seule mutation est suffisante pour atteindre ce résultat (Tax PA). Enfin, les immunoprécipitations d'UPF1 ont montré que les mutants de Tax conservaient leur liaison à UPF1 mais ne pouvaient plus empêcher UPF1 de se lier à l'ARN contrairement à Tax WT (Figure 8B-D).

- Electroporation de siRNA et plasmide Taxpa en Jurkat pour validation du RNAseq.

Sur la base de l'identification de Tax PA, incapable d'inhiber le NMD, nous mettrons en place une nouvelle analyse de la dégradation de l'ARN incluant l'expression de Tax PA. Nous électroporerons des cellules Jurkat avec Tax WT, Tax PA ou un plasmide d'expression contrôle. D'autres cellules seront électroporées avec des siRNA UPF1 ou des siRNA Ctr. Pour chaque condition, les cellules seront traitées avec du tpl ou du DMSO pour évaluer la dégradation de l'ARN comme décrit précédemment. Nous prévoyons (1) de valider les résultats obtenus dans le RNAseq décrit précédemment et (2) d'observer des dérégulations dépendantes d'UPF1 plus faibles/absentes en présence de la mutation Tax PA par rapport au Tax WT.

Projet 2 : La relation HTLV-1/UPF1 comme modèle pour d'autres virus ? Inhibition d'UPF1 par la nucléocapside du SARS-Cov-2.

Makram Mghezzi, Armelle Roisin

CONTEXTE

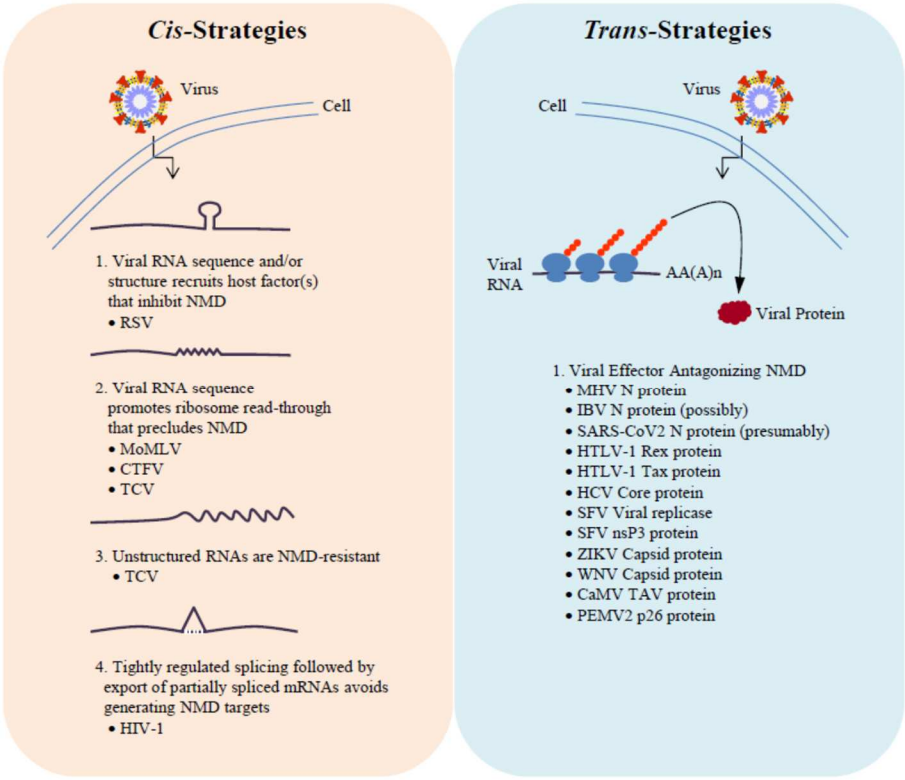

Figure 9 : différentes stratégies virales anti NMD compilées dans Popp et al [147]

Suite à nos travaux sur HTLV-1, la sensibilité de l'ARN viral au NMD a été rapportée pour plusieurs virus, présentant le NMD comme un processus antiviral. En général, la stratégie de réplication ainsi que la pression sélective pour maximiser la capacité de codage d'un ARNv sans augmenter la taille de son génome ont introduit des caractéristiques dans les ARNv qui peuvent le rendre sensible au NMD. Par exemple, chez les plantes, le NMD contrôle la stabilité des virus à ARN à brin positif des familles Alphaflexiviridae et Tombusviridae. Chez les mammifères, le NMD limite la réplication de deux alphavirus de la famille des Togaviridae tels que le Semliki Forest Virus et le Sindbis Virus, et de trois Flaviviridae tels que le West Nile Virus, le Zika et le Hepatitis C Virus. Les travaux de Nakano et al, ainsi que les nôtres ont également été démontré la sensiblité d'HTLV au NMD [130,148] et revu dans [149]. Dans ce cas, un 3´UTR long est suspecté d'être le déterminant du NMD : alors que les 3´UTR humains d'au moins 1 kb se sont révélés suffisants pour déclencher le NMD, les ARN génomiques rétroviraux ont un 3´UTR d'environ 6 kb, et les Togavirus à ARN à brin (+) jusqu'à 4 kb. Au contraire, le génome à ARN à brin (–) et segmenté du virus de la

grippe présente des 3´UTR plus courts de seulement quelques centaines de bases et s'est récemment révélé insensible au NMD [150]. Au total, ces données indiquent que le NMD cible les ARN de plusieurs virus, y compris HTLV-1, révélant ainsi une fonction du NMD dans la protection de l'hôte contre les agents pathogènes.
Cependant, la persistance de ces infections virales suggère qu'ils réussissent tous à contourner le NMD, au moins partiellement, de la même manière que d'autres processus antiviraux. Deux stratégies principales ont été décrites jusqu'à présent [151–162] (figure 9):

-Cis-inhibition avec incorporation de motifs ou caractéristiques spécifiques de l'ARN viral : par exemple le motif spécifique du RSV en aval du codon STOP de l'ARNm codant gag. Il existe aussi des séquences de bypass du codon stop (readthrough) qui empêchent l'accumulation d'UPF1 dans le 3'UTR ou bien des 3'UTR particulièrement non structurées qui ont été démontrées comme empêchant le NMD.

-Trans-inhibition ; il a été démontré que plusieurs effecteurs viraux antagonisent le NMD en ciblant UPF1 ou d'autres acteurs cellulaires de cette voie. Tax de HTLV-1 étant le premier à être identifié par notre équipe.

Dans ce projet, nous suggérons qu'un équilibre similaire puisse exister entre le SARS-Cov-2 et le NMD. Nous suggérons qu'en le modulant, nous pouvons moduler le fitness de la réplication virale.

HYPOTHESES ET OBJECTIFS

Evaluer la sensibilité de l'ARNv du SARS-CoV-2 au NMD.

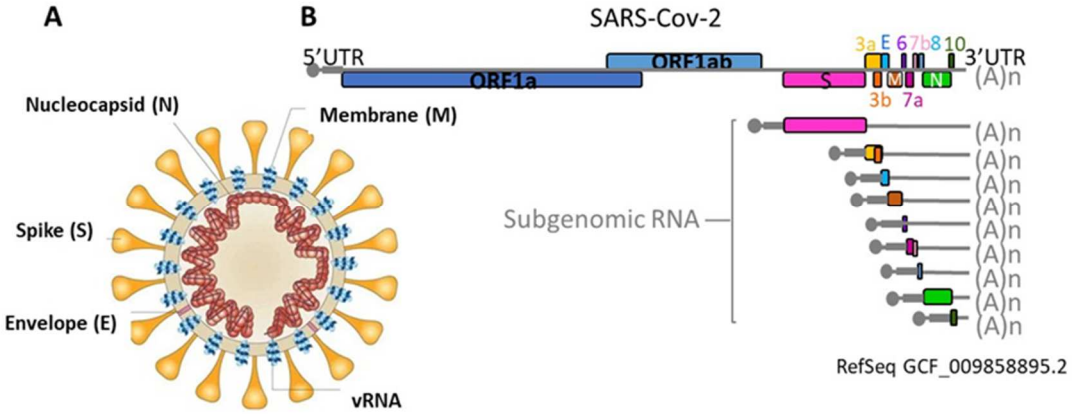

Figure 10 : organisation du de la particule virale (A) et du génome du SARS CoV 2 (B). la séquence codant la nucléocapside est représentée en vert issu de ***Kim et al*** [163]

L'ARNv de plusieurs virus à ARN (+) présente des caractéristiques qui en font potentiellement un substrat pour le NMD. Le SARS-CoV-2 partage la même organisation génomique que ces virus sensibles au NMD, dont le MHV, un membre prototypique des betacoronaviridae. La sensibilité au NMD peut être due à leur long 3´ UTR et ferait de la plupart des ARN du SARS-CoV-2 des cibles potentielles pour le

NMD, à l'exception de Np et ORF10 (figure 10). Cependant, la longueur globale du 3´UTR n'est pas tout ce qui compte : des motifs d'ARN spécifiques du côté 5´du 3´UTR peuvent également être critiques [162,164,165]. De façon intéressante, il a été démontré qu'UPF1 interagissait directement avec l'ARNv dans une étude d'interactome ARN-protéine du SARS-CoV-2 dans des cellules humaines infectées[166]. Cependant, UPF1 se lie de manière indistincte à tous les ARN, cible ou non du NMD [37,38]. Ainsi, afin de caractériser la relation entre NMD et SARS-CoV-2, nous nous concentrerons d'abord sur la sensibilité de l'ARNv au NMD et identifierons les déterminants de son initiation. Pour cela nous répondrons aux questions suivantes : L'ARNv est-il dégradé par le NMD ? En conséquence de cette sensibilité, le NMD limite-t-il la réplication du SARS-CoV-2 ? Cette répression est-elle active aux premiers stades de l'infection ou est-elle conservée dans le temps ? Quel codon stop viral peut initier la dégradation de l'ARNv ? Y a-t-il un élément en aval de l'ARNv conduit à la stabilisation d'un mRNP NMD ? Les méthodes actuelles telles que CLIPseq ou RIPseq qui sont basées sur le séquençage de reads courts ne fournissent pas d'informations fiables sur l'organisation des mRNP en aval de la protéine immunoprécipitée, car elles reposent sur le réassemblage de petits fragments après le séquençage. L'analyse est encore plus compliquée lorsque l'on considère des séquences chevauchantes, telles que les séquences virales. Pour répondre à nos questions et surmonter ces obstacles, nous devrons développer un nouvel outil plus efficace. Nous développerons un protocole de séquençage de longs fragments utilisant le Nanopore, qui devrait permettre le séquençage de la molécule d'ARN complète, de la queue polyA jusqu'au site de clivage de l'endonucléase, en cartographiant pour chaque ARNv sensible au NMD, son extrémité 5' proche du codon stop initiateur du NMD ainsi que le 3´UTR correspondant et complet.

De plus, en supposant que l'ARNv du SARS-CoV-2 soit sensible au NMD, nous nous demandons si les cellules prétraitées avec des médicaments modulant le NMD peuvent modifier leur sensibilité à l'infection et à la réplication du virus. Par exemple, plusieurs publications ont précédemment montré que l'extinction du NMD avant l'infection (par knockdown d'un facteur NMD ou en utilisant des médicaments spécifiques) facilite l'expression virale et/ou la production de virions [142,152,159]. Indépendamment des infections virales, plusieurs études ont recherché des composés à petites molécules ayant un effet modulateur NMD. La plupart d'entre eux sont des traitements déjà approuvés cliniquement. En conséquence, le fait que de tels traitements puissent moduler l'efficacité du NMD augmente le risque qu'ils puissent également améliorer la réplication virale. Au contraire, les composés stimulants du NMD peuvent-ils réduire la réplication du virus et sa propagation ? Notamment, la plupart des molécules en jeu ici n'ont pas été testées ou n'ont pas été documentées comme ayant un effet sur la COVID-19. Une exception est le nitazoxanide : ce médicament antiparasitaire, cliniquement approuvé, s'est avéré avoir une activité antivirale à large spectre bien que le mécanisme ne soit pas connu. Il pourrait inhiber la réplication du SRAS-CoV-2 à de faibles concentrations micromolaires en culture cellulaire [167]. L'effet convergent de « stimulation NMD » et de « répression de la réplication virale » du nitazoxanide peut soutenir notre hypothèse selon laquelle un traitement en cours d'exécution pourrait moduler le NMD et, en retour, modifier de

manière significative le fitness de la réplication virale. Pour ces raisons, un autre aspect de ce projet est de tester in cellulo l'impact de ces molécules modulant le NMD sur la réplication virale.

La nucléocapside (Np) du SARS-CoV-2 peut -elle cibler UPF1 et inhiber le NMD ?

Chaque virus est engagé dans une course aux armements avec son hôte pour contrecarrer les processus antiviraux intrinsèques, innés et adaptatifs et favoriser sa réplication. L'évolution rapide du SARS-CoV-2 et l'émergence de multiples variants en témoignent. Le NMD ne fait pas exception : la plupart du temps, la preuve d'une sensibilité virale au NMD a été suggérée par l'identification de mécanismes viraux inhibant le NMD. Dans le cas du SARS-CoV-2, nous émettons l'hypothèse que le virus est capable d'inhiber partiellement NMD afin de se répliquer et que cette inhibition est dépendante d'une interaction entre Np et l'hélicase à ARN NMD UPF1. Cette hypothèse s'appuie sur des données convergentes récentes : d'abord Gorgon et al. UPF1 a été identifié comme partenaire de Np par spectrométrie de masse [168]. Il n'est pas rare que UPF1 soit réprimé par des protéines de structure virale ; Np du virus du syndrome reproducteur et respiratoire porcin (PRRSV) 2 CoV et du virus de la bronchite infectieuse (IBV) sont des partenaires de l'UPF1[169]**.** Deuxièmement, nous savons que le Np du MHV peut inhiber le NMD peu de temps après l'infection [159]. Ainsi, nous chercherons d'abord à établir que Np de SARS-CoV-2 peut inhiber le NMD via UPF1. On peut alors se demander quel est le mécanisme sous-jascent. Np est-il le seul inhibiteur viral du NMD ? Le Np libre se lie-t-il à UPF1 ou UPF1 est-il piégé sur un ARNv déjà recouvert de Np ? Np empêche-t-il la formation d'un complexe NMD en séquestrant UPF1, en gênant le recrutement de son partenaire ou en induisant sa dégradation ? L'interaction avec Np inhibe-t-elle les activités enzymatiques d'UPF1 ? Notre objectif est de décrypter finement ce mécanisme inhibiteur au niveau moléculaire, comme nous avons pu le faire précédemment avec Tax d'HTLV-1.

Enfin, nous étudierons l'impact de l'inhibition du NMD par le virus sur le transcriptome de l'hôte infecté : nous nous demandons si l'inhibition du NMD par le virus est dédiée uniquement à l'ARNv ou aux cibles NMD de l'hôte dans les cellules infectées également. L'infection par le SARS-CoV-2 entraîne une modification spécifique de la signature transcriptomique de l'hôte. Il a été rapporté que Np se lie à l'ARN cellulaire. Cela induit-il un contrôle spécifique de leur sensibilité au NMD ? Notre objectif est d'évaluer la convergence entre le transcriptome lié à Np et les transcrits régulés par UPF1 et leur corrélation avec les modifications transcriptomiques dues à l'expression du SARS-CoV-2. Une telle convergence révélerait que l'interaction Np/UPF1 est un moyen pour le virus de contrôler spécifiquement l'expression de certains gènes.

METHODOLOGIE ET RESULTATS PRELIMINAIRES

Contrôle de la réplication virale par le NMD

Pour identifier la sensibilité du virus au NMD, une collaboration avec Andrea Cimarelli (CIRI, Lyon) a été établie. D'une part, des infections seront effectuées dans

des cellules où le NMD est inhibé par le knockdown d'UPF1 (ou activé si possible par la surexpression d'UPF1). Les infections seront réalisées à différentes multiplicités d'infection (MOI) avec le virus WT ou un virus SARS-CoV-2 modifié portant un rapporteur fluorescent à la place de l'ORF7 (qui s'est avéré non indispensable pour la réplication virale ex vivo[170]. La stabilité des ARN génomiques et subgénomiques sera évaluée par RT-qPCR à différents temps post-infection. Pour corréler l'impact du NMD sur la stabilité de l'ARNv avec une modification du fitness réplicatif, la réplication virale sera elle-même évaluée aux mêmes temps post-infection par dosage de plaque ou par cytométrie en flux (pour le SARS CoV 2 modifié avec un rapporteur fluorescent). A l'instar de l'infection par le MHV, nous pourrions observer que le knockdown d'UPF1 favorise la réplication virale dans les premières heures post-infection.
En complément de la modulation du NMD par le knockdown d'UPF1, l'utilisation de molécules chimiques contrôlant l'efficacité du NMD sera testée par des traitements en amont de l'infection. Le Nitazoxanide en est un exemple (décrit ci-dessus) mais d'autres molécules comme le Diflunisal (anti inflammatoire), le Tranilast (anti-allergique), le Docetaxel (traitement anti cancéreux) la Phenelzine (anxyolitique), la Mephentermine (stimulant cardiaque) ont aussi été montrés pour stimuler le NMD [66].

Développement d'une approche technique pour identifier les déterminants transcrits viraux sensibles au NMD.

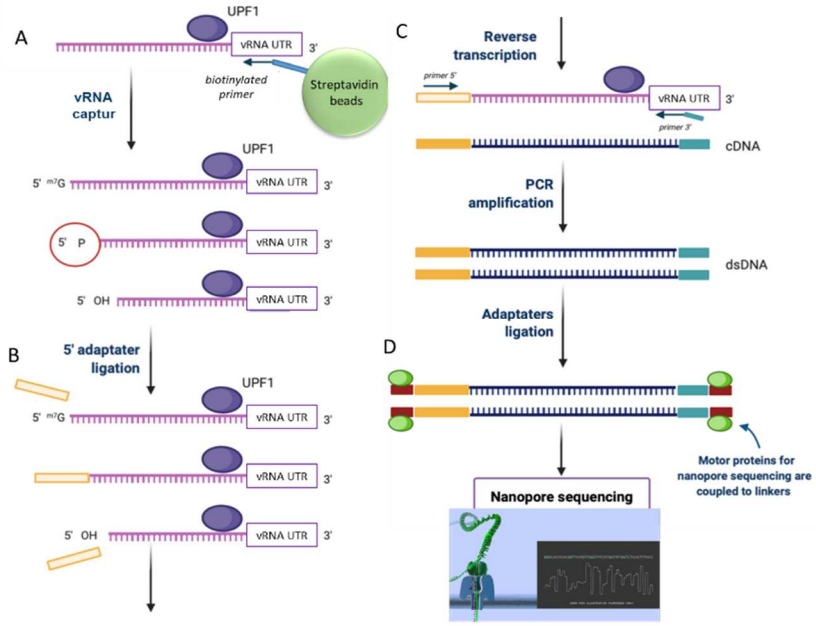

Figure 11 : schéma récapitulatif du protocole permettant d'identifier les déterminants viraux du NMD. A) l'Arn viral est capturé par un RIP pUPF1 puis par une hybridation avec des sondes spécifiques de l'ARN viral. B) Les formes 5'p sont sélectionnées par ligation d'un adaptateur ARN en 5'. C) l'ARN viral est reverse transcrit en utilisant un primer spécifique de l'ARN viral. D) La banque et le séquençage sont réalisés avec le système Nanopore.

Afin de sélectionner les ARN viraux sensibles au NMD, nous prevoyons une double capture en amont de la préparation des banques de séquençage Nanopore.
Contrairement à la forme hypophosphorylée d'UPF1 qui se lie à tous les ARN, y compris ceux insensibles au NMD, la forme hyperphosphoprylée (pUPF1) est spécifiquement associée aux ARN sensibles. Les ARN viraux en cours de dégradation seront donc immunoprécipités par un anticorps spécifique de pUPF1, après traitement des cellules avec de l'acide Okadaïc (un inhibiteur de la phosphatase PP2A ciblant

UPF1). Afin d'enrichir l'échantillon en ARN viral, nous réaliserons ensuite seconde capture d'ARN, à l'aide d'oligonucléotides biotinylés présentant des séquences virales complémentaires. Dans un second temps, comme les extrémités 5' des ARN clivés par les endo- et exonucléases du NMD sont toujours phoshporylées (l'identification des sites de clivage SMG6 par PAREseq [47] nous y liguerons directement un oligo ARN. Finalement des librairies seront construites (Oxford Nanopore). Ce protocole est adapté aux transcrits très longs comme l'ARN du SARS-CoV-2. Les résultats de séquençage indiqueront le clivage 5', spécifiquement marqué avec l'oligo d'ARN. Après alignement avec la séquence génomique, le codon stop le plus proche en amont du site de clivage sera considéré comme le codon stop responsable de l'initiation du NMD. Pour réduire l'activité de la nucléase XRN1 qui suit le clivage de SMG6 et raccourcirait l'extrémité 5' de l'ARNv, les cellules seront traitées avec des siRNA contre XRN1 (figure 11).

Inhibition du NMD par la nucléocapside du SARS CoV2

Afin d'identifier la capacité de Np à inhiber le NMD, nous avons testé l'efficacité du NMD comme décrit précédemment : des lignées stables exprimant ou non Np ont été établies puis transfectées avec des plasmides exprimant soit un rapporteur sensible (glob PTC) soit un rapporteur non sensible (glob WT) au NMD. Ces expériences préliminaires ont été réalisées dans des cellules HeLa et la quantification des transcrits par RTqPCR montre une up-régulation du transcrit sensible par rapport au transcrit non sensible. Ces résultats valident donc que l'expression de la Np est capable d'inhiber le NMD (figure 12).

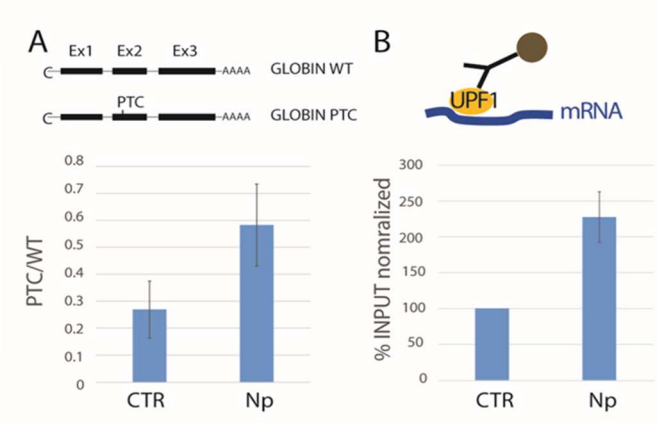

Figure 12 : A) Mesure des niveaux d'ARN sensibles et non sensible au NMD dans des cellules exprimant Np ou non. B) RIP UPF1 dans des cellules exprimant ou non Np. L'ARN quantifié est la globine PTC, sensible au NMD.

Pour décrypter ce mécanisme d'inhibition, nous suivront la même logique que celle utilisée avec Tax d'HTLV-1. En collaboration avec Francesca Fiorini (IBCP, Lyon), une analyse biochimique et structurale de l'interaction entre les différents domaines d'UPF1 et Np est en cours de réalisation.
En parallèle, nous confrontons ces résultats avec des analyses in cellulo : RIP, interaction entre UPF1 et ses partenaires, etc…). Notamment, des RIP UPF1 suggèrent que l'expression de Np modifie significativement la capacité d'UPF1 à se lier à l'ARN.

Projet 3 : la relation HTLV-1/UPF1 comme modèle pour d'autres cancers ? Export CRM1 dépendant et inhibition d'UPF1.

Léa Prochasson, Makram Mghezzi, Stéphane Réty, Jean Philippe Robin,

CONTEXTE

L'exportin chromosome region maintenance 1 (CRM1) (Xpo1 chez S. cerevisiae) assure l'export d'une multitude de protéines (aussi appelées cargos) et de certains RNP fonctionnellement et structurellement indépendants. CRM1 est essentiel dans tous les organismes testés jusqu'à présent. Par exemple, CRM1 empêche l'accumulation nucléaire de plusieurs protéines, comme l'adaptateur snurportin1 (SPN1)[171] des sous-unités pré-ribosomiques, des facteurs d'initiation et de terminaison de la traduction eucaryote [172]. L'export dépendant de CRM1 est également essentiel pour plusieurs protéines impliquées dans la dégradation de l'ARN telles que le complexe de décapping, les protéines LSM, les exonucléases 5'-3', les sous-unités du complexe CCR4 NOT. Plusieurs composants des Pbodies et des granules de stress sont également exportés du noyau par CMR1[173].

Alors que l'export de la majorité des ARNm se produit via la voie Nxf1/Tap1, seul un sous-ensemble de transcrits endogènes est exporté via CRM1. Par exemple, CRM1 assure l'export des ARNv non épissés ou partiellement épissés de VIH et HTLV via des protéines adaptatrices, respectivement Rev et Rex [174,175]. CRM1 ne lie pas directement l'ARN et doit donc utiliser une RBP cellulaire intermédiaire pour exporter certains ARNm endogènes spécifiques, comme il le fait pour les transcrits du VIH. Certains de ces cargos ont été décrits, notamment HuR pour l'export des ARNm Cd83 et Fos, et le facteur d'initiation de la traduction eucaryote 4E (eIF4e) pour l'ARNm de la cycline D1 dans les cellules humaines[176–178]. Cependant, les cargos spécifiques d'autres transcrits exportés par Crm1 n'ont pas encore été particulièrement caractérisés.

Ces cargos lient généralement CRM1 via un signal d'exportation nucléaire (NES). Le NES est une courte séquence linéaire d'acides aminés comprenant 4 à 5 résidus hydrophobes critiques avec un espacement spécifique. De plus, l'export CRM1 dépendant est alimenté par le système RanGTPase. Les cycles de shuttling noyau/cytoplasme comprennent non seulement l'hydrolyse du GTP associé à RAN en GDP, mais également un cycle de transfert de Ran entre le noyau et le cytoplasme. En conclusion, CRM1 lie ses cargos en coopération avec RanGTP à l'intérieur du noyau, les transporte sous forme de complexes trimériques RanGTP·exportine·cargo vers le cytoplasme, où l'hydrolyse du GTP déclenche la libération des cargos et de Ran. L'exportine libre peut alors ré-entrer dans le noyau et exporter la cargaison suivante. (revue dans [172])

Des mutations dans CRM1/XPO1 ont été rapportées dans plusieurs types de cancers [179] mais l'implication fonctionnelle de l'export dans le processus oncogénique n'est pas bien démontrée. Une étude approfondie récente, basée sur le séquençage de l'exome

de 42793 patients, a identifié 3 acides aminés mutés de façon récurrente dans CRM1 : E571, R749 et D624. De plus, la substitution E571K était récurrente dans la leucémie lymphoïde chronique, le lymphome de Hodgkin et le carcinome de l'œsophage[180,181]. Ce travail suggère également que la mutation E571K, proche de la poche de liaison NES, pourrait augmenter l'affinité de CRM1 pour le NES du facteur transcriptionnel Mek1 [182]. Dans le même temps, cette mutation diminuerait l'affinité pour d'autres domaines NES tels que celui d'eIF4E.

HYPOTHESES ET OBJECTIFS

Localisation d'UPF1 et efficacité du NMD

Sur la base de nos derniers résultats concernant l'inhibition de NMD par Rex et l'export CRM1 dépendant, l'objectif principal de ce 3ème projet est d'explorer comment CRM1 régule la localisation d'UPF1 et son lien avec l'efficacité du NMD.

Nous étudierons si un stress de l'export nucléaire peut avoir un impact sur les fonctions cytoplasmiques d'UPF1 et nous en décrypterons les mécanismes sous-jacents. UPF1 a des fonctions cytoplasmiques et nucléaires spécifiques. Bien que l'import nucléaire UPF1 soit gouverné par l'importB[183], sa localisation est essentiellement cytoplasmique ce qui suggère un export très efficace par CRM1 ; l'impact de son export sur ses fonctions n'a pourtant pas vraiment été abordé. Des expériences d'immunofluorescence ont montré que lorsque son export nucléaire est affecté, UPF1 s'accumule dans le noyau mais sa fraction cytoplasmique absolue ne semble pas significativement appauvrie bien que cela reste à quantifier. Dans ce contexte, aborder le lien entre l'export UPF1 et l'efficacité du NMD est tout à fait pertinent et nécessite une investigation précise. Après avoir vérifié que l'efficacité du NMD est liée à l'export d'UPF1 et à la voie CRM1, nous essaierons ensuite de décrire plus précisément la cause de cette inhibition.

Un point majeur à aborder est de caractériser si l'inhibition du NMD via CRM1 dépend uniquement du ciblage UPF1 ou si elle dépend de l'impact cumulé de plusieurs cargos : comme introduit précédemment, CRM1 contrôle l'export de plusieurs facteurs impliqués dans la dégradation de l'ARN (notamment les protéines NMD telles que les protéines UPF1, UPF2, UPF3b, DCP1 et SMG…)[173]. Il faut donc caractériser l'interaction entre UPF1 et CRM1 et donc en premier lieu le domaine NES d'UPF1 qui n'est pas encore identifié. Créer des mutants d'UPF1 et de CRM1 induisant une perte d'affinité ou un gain d'affinité l'un pour l'autre serait particulièrement intéressant et complémentaire à l'utilisation de facteurs tels que HTLV-1 Rex et HIV Rev dont nous avons déjà décrit l'effet « verrouillant » sur le complexe CRM1/UPF1. De façon intéressante, la mutation CRM1E571K identifiée dans les cancers liés à CRM1 est décrite comme une mutation « gain d'affinité » : elle pourrait entraîner une libération réduite d'UPF1 dans le cytoplasme et pourrait justement imiter l'effet observé avec Rex. Si cette hypothèse est fausse, nous étudierons les autres cargos de CRM1

impliquées dans la dégradation médiée par UPF1 et comment la modification de leur export impacte le NMD.

Contrôle de la mobilité d'UPF1 et impact fonctionnel

Parmi les différents paramètres qui seront évalués (voir section suivante), nous porterons une attention particulière à la mobilité d'UPF1, en faisant l'hypothèse qu'en tant que processus dynamique, le NMD peut être affecté par ce paramètre. D'un côté nous supposons que moduler l'export par CRM1 pourrait affecter la capacité d'UPF1 à contacter ses partenaires et d'un autre côté que cela pourrait induire une modification locale de sa concentration, affectant potentiellement ses propriétés biophysiques. Supportant ces hypothèses, **Jia et al**[70] a montré l'importance du cytosquelette dans le contrôle des fonctions d'UPF1. De plus, nos résultats précédents montrent que l'inhibition du NMD due à l'expression de Rex serait causée par la formation d'un complexe UPF1/CRM1 plus stable qu'en l'absence de Rex. On peut également considérer que cette inhibition est due à un défaut de dissociation de UPF1/CRM1, ce qui est conforté par la colocalisation d'UPF1 et de CRM1 en super foyers dans les cellules infectées. Dans les cellules Hela exprimant Rex, nous avons observé une rétention nucléaire d'UPF1, suggérant une modification de la dynamique d'export nucléaire, couplée à un défaut d'association d'UPF1 à l'ARN.

METHODOLOGIE ET RESULTATS PRELIMINAIRES

1. Impact de l'export d'UPF1 pendant le NMD

Sur la base de nos résultats précédents, nous évaluerons le mécanisme précis corrélant l'export d'UPF1 et le fonctionnement du NMD. Pour ce faire, nous étudierons différentes approches complémentaires pour modifier l'export UPF1. Tout d'abord, pour établir la preuve de concept que l'efficacité du NMD est liée à l'export d'UPF1 et à la voie CRM1, nous avons directement ciblé CRM1 en utilisant des siRNA. La mesure de la ½ vie d'un ARN rapporteur sensible au NMD a montré que l'extinction de CRM1 induit une inhibition du NMD. Étant donné que CRM1 est un acteur primordial de l'export de la machinerie de traduction, nous avons validé que la stabilisation de l'ARN observée n'était pas due à une altération de la traduction : les incorporations de puromycine (sunset assay) révèlent que dans nos conditions, la traduction n'est pas affectée par les traitements siCRM1. De plus, les expériences de RIP ont montré une diminution de l'association UPF1 à l'ARN sensible au NMD. La localisation sub-cellulaire d'UPF1 a été évaluée par fractionnement combiné à un western blot et supporte une rétention nucléaire d'UPF1 (figure 13). Ces résultats seront confirmés par microscopie confocale. Dans l'ensemble, ces données ont établi la preuve de concept que NMD peut être modulé de manière CRM1 dépendante hors infection

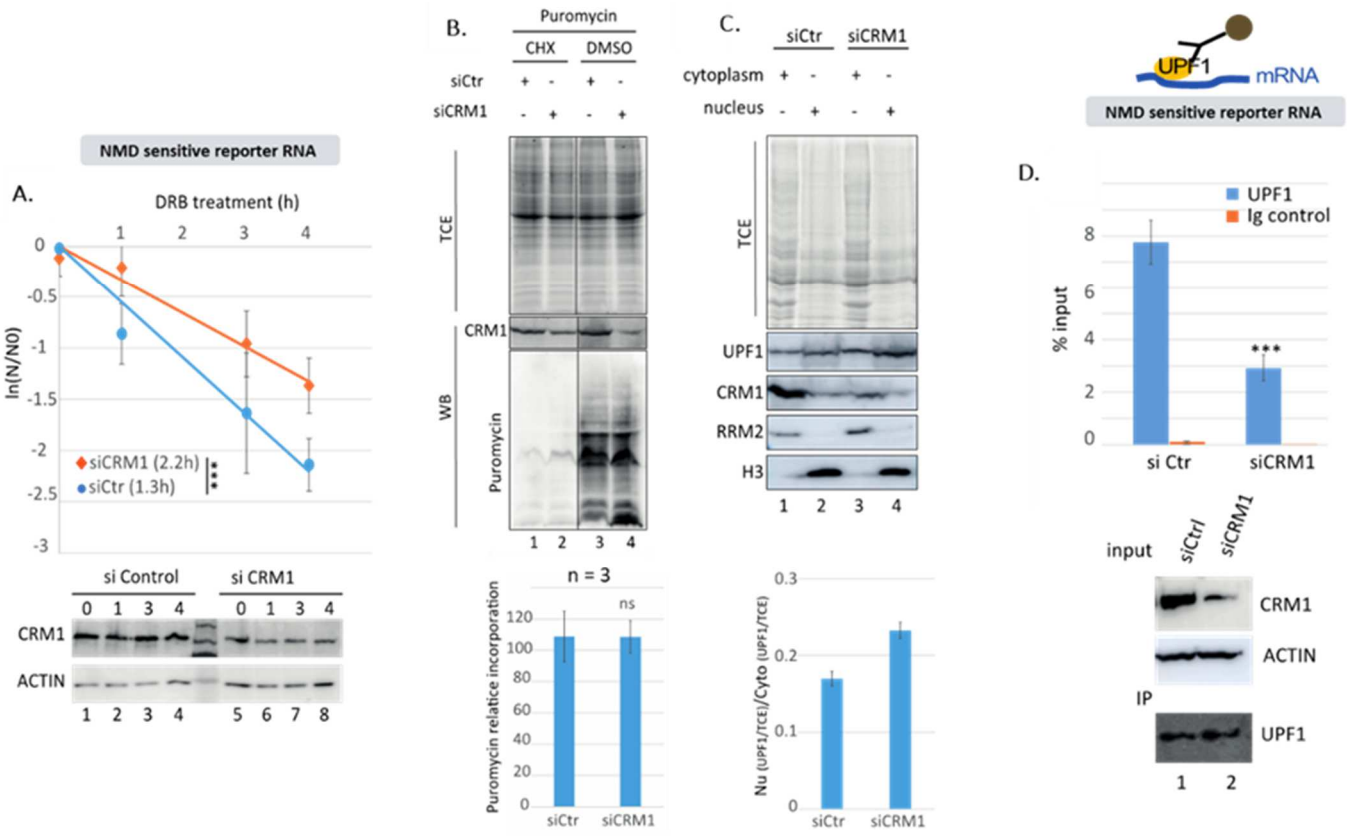

Figure 13 : A) Mesure de la stabilité de l'ARN sensibles (globin PTC) dans des cellules traitées avec un si RNAcontre CRM1 ou non. B) sunset assay évaluant la traduction par la néoincorporation de puromycin. Les niveaux de puromycin sont révélés par western Blot et rapportés à la quantité de protéine totale (évaluée par avec des gels stain free (TCE)). C Fractionnement cellulaire révélant les niveaux d'UPF1 après traitement de cellules HeLa avec des siCRM1. D RIP UPF1 dans des cellules traitées avec des siCRM1. L'ARN quantifié est la globine PTC, sensible au NMD.

virale. Ensuite, nous créerons des mutants UPF1 et CRM1 induisant une perte ou un gain d'affinité l'un pour l'autre. En collaboration avec Stéphane Réty chercheur structuraliste de l'équipe, nous modélisons l'interface d'interaction entre CRM1 et le domaine NES d'UPF1. Concernant UPF1, le domaine NES n'a pas encore été caractérisé. A l'aide d'outils bioinformatiques, nous avons identifié un motif consensus, créé un mutant et validé un défaut de localisation de ce mutant. Son activité sera vérifiée in cellulo pour déterminer si la seule rétention nucléaire d'UPF1 est suffisante pour inhiber le NMD (figure 14).

Les séquences NES sont caractérisées par 4 acides aminés hydrophobes ; les acides aminés intercalés sont variables et influencent également l'affinité du NES pour CRM1. Par exemple, la substitution CRM1E547K, a été précédemment caractérisée pour son affinité de liaison avec 10 séquences NES cellulaires[182] : elle a montré une affinité 14 fois accrue pour la NES MEK1 par rapport à la séquence WT de CRM1, tandis que son affinité pour la NES de eIF4E est diminuée 10 fois. Sur la base de la modélisation structurelle de l'interface CRM1/NES réalisée pour caractériser le NES d'UPF1, nous définirons de nouvelles mutations d'intérêt dans CRM1 et UPF1 conduisant à un gain

ou à une perte d'affinité. De plus, les formes mutantes de CRM1 identifiées chez les patients atteints de cancer seront inclues dans l'étude. Ces mutants seront testés in vitro pour évaluer leurs constantes d'affinité en utilisant l'interférométrie BioLayer (BLI) comme nous l'avons fait précédemment. In cellulo, nous caractériserons leur impact sur le NMD avec des tests NMD, l'immunoprécipitation des ARN par UPF1 et la distribution cellulaire comme nous l'avons fait précédemment dans les expériences préliminaires avec le siCRM1. De plus, de petits composés chimiques inhibant

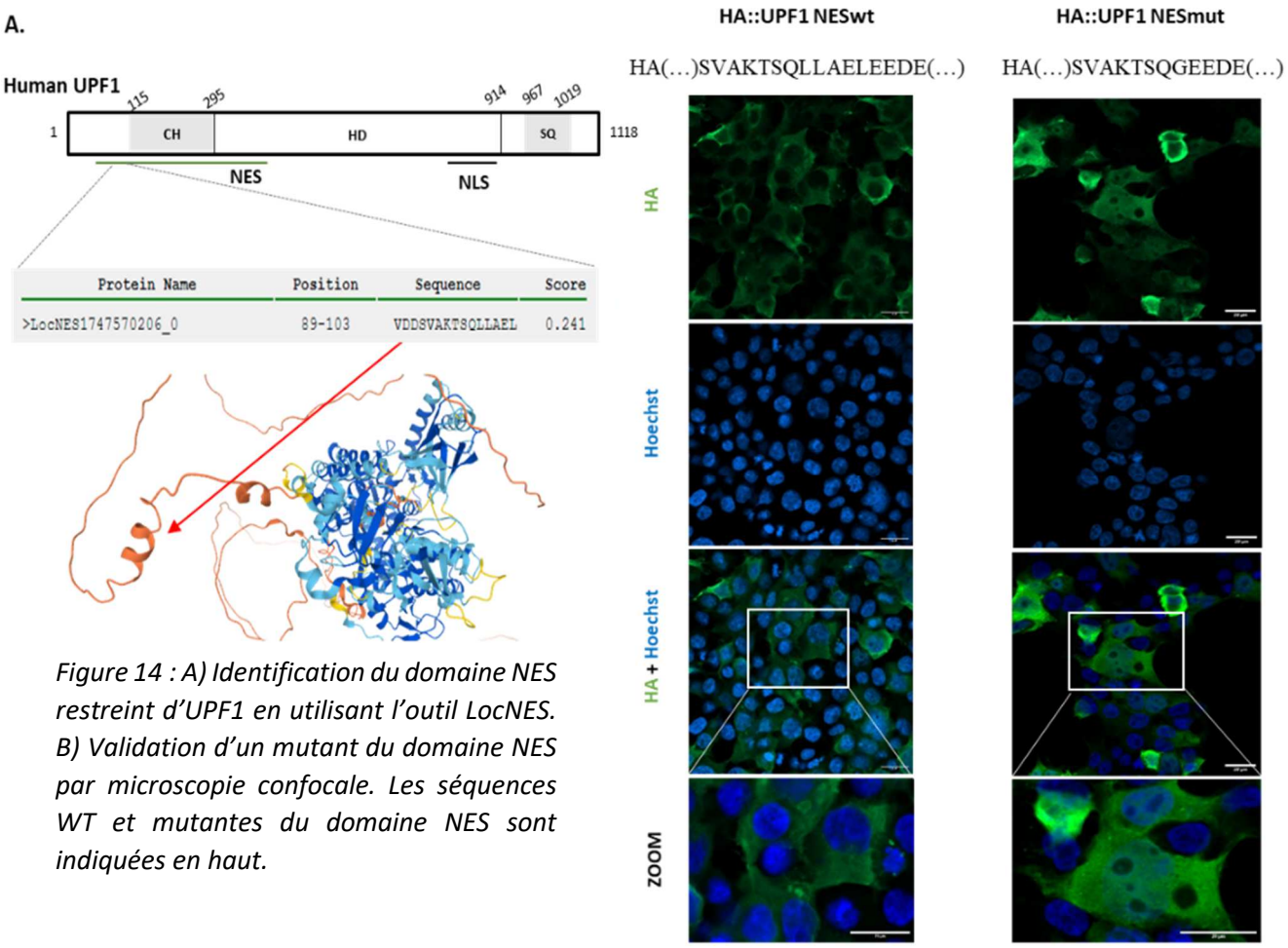

Figure 14 : A) Identification du domaine NES restreint d'UPF1 en utilisant l'outil LocNES. B) Validation d'un mutant du domaine NES par microscopie confocale. Les séquences WT et mutantes du domaine NES sont indiquées en haut.

l'association CRM1 aux NES, tels que la leptomycine B, pourront être utilisés.

Comme indiqué précédemment, 3 sites de mutations récurrente de CRM1 sont associés au développement de cancers. L'établissement d'un lien entre ces mutations et la modulation du NMD pourrait soutenir une enquête plus approfondie entre la régulation NMD, CRM1 et le cancer.

2. Mobilité d'UPF1

Afin d'évaluer l'efficacité du NMD, plusieurs paramètres vont être analysés comme décrit ci-dessus. En plus, nous prévoyons d'analyser la mobilité d'UPF1 au sein de la cellule, et de déterminer si les conditions de formation du complexe CMR1/UPF1

peuvent induire des modifications de la mobilité d'UPF1 et comment cette mobilité peut être corrélée à des défauts d'export et de NMD.
Dans un premier temps, l'aspect dynamique de l'interaction UPF1/CRM1 sera abordé in cellulo avec des approches de microscopie appelées Fluorescence Recovery After Photobleaching (FRAP) et Fluorescence Loss In Photobleaching (FLIP). Avec ces approches complémentaires, nous évaluerons la mobilité d'UPF1 entre le noyau et le cytoplasme ainsi que dans les domaines intranucléaires et intra-cytoplasmiques. Nous nous intéresserons notamment à la mobilité des molécules d'UPF1 à la périphérie du noyau. Ces expériences sont particulièrement intéressantes dans les conditions d'expression de HTLV-1 Rex : Rex augmente l'association UPF1/CRM1 et modifie la localisation subcellulaire d'UPF1 avec la formation de superfoyers UPF1/CRM1 dans les cellules T. Nous suivrons spécifiquement si Rex ralentit les déplacements d'UPF1.

3. Analyse de l'exportome de CRM1 pendant l'inhibition NMD

Dans la partie précédente, le décryptage du lien entre export CRM1 et inhibition de NMD repose sur la comparaison de différentes approches complémentaires (extinction de CRM1, modification de l'affinité de CMR1 pour la NES, expression d'un facteur exogène modifiant la formation et la localisation du complexe UPF1/CRM1), avec un accent particulier sur l'interaction entre CRM1 et UPF1. Cependant, de telles approches n'excluent pas un effet cumulatif de CRM1 sur plusieurs cargos (dont UPF1). Par exemple, le traitement par siCRM1 dans nos résultats préliminaires a induit un arrêt complet de l'export et concerne l'ensemble des cargos de CRM1. De même, les mutations de CRM1 que nous prévoyons de réaliser peuvent affecter sa liaison à d'autres NES que celui d'UPF1. Finalement, la formation d'un complexe entre Rex/CRM1 et d'autres cargos n'a jamais été explorée. Les effets observés pourraient alors être dus à des défauts de répartition de multiples facteurs impliquant des partenaires NMD tels que UPF2, UPF3b, SMG6, etc…

Afin d'aborder ce point, nous analyserons la répartition de l'exportome de CRM1 par spectrométrie de masse à haute résolution. Les différentes conditions capables d'inhiber le NMD et identifiées dans la partie précédente seront combinées ici avec un fractionnement cellulaire suivi de spectrométrie de masse. Nous étudierons ainsi l'effet des traitements siCRM1 vs siCTR, l'expression de WT CRM1 vs certains mutants CRM1, l'expression des protéines virales Rex et Rev (dont nous avons démontré qu'elles inhibent NMD de manière dépendante de CRM1) vs conditions de contrôle.

CONCLUSION

Les résultats que j'ai présentés ici ont permis de caractériser une nouvelle fonction du NMD : une fonction antivirale qui se traduit par le fait que l'hélicase UPF1 contrôle les niveaux des différents ARN viraux d'HTLV-1. Le risque que représente le NMD a été confirmé par l'existence de contre-mesures : nous avons identifié 2 protéines virales inhibitrices (Tax et Rex) ciblant l'hélicase UPF1 et réprimant le NMD. Cette redondance renforce l'idée que le NMD constitue une menace importante pour le virus, d'autant plus que des observations similaires sont retrouvés chez d'autres virus. Nous avons identifié Rev d'HIV et la Np de SarsCov2 (en cours de caractérisation - ***projet 2***).
Identifier les transcrits cellulaires également affectés par cette inhibition comme nous l'avons prévu (***projet 1***) devrait permettre de comprendre s'il s'agit uniquement pour le virus de se protéger d'UPF1 ou s'il modèle activement le transcriptome cellulaire en fonction de ses besoins. De tels résultats mettraient en évidence un nouvel aspect de la régulation post-transcriptionnelle lors de l'infection par HTLV-1.
Le projet concernant le SARS CoV2 (***projet 2***), s'il a pour vocation de comprendre les spécificités et convergences de la relation entre UPF1 et différents virus, va nous amener à développer des outils qui seront aussi utilisés avec le modèle HTLV-1 : L'identification des déterminants du NMD sur les ARN HTLV n'a pas encore été clairement établie ; l'approche Nanopore y sera utile. De même, nous prévoyons d'évaluer l'impact du NMD sur la transmission du SARS-CoV-2 en modulant son efficacité par différentes approches. Nos dernières données avec Rex d'HTLV-1 nous amènent également à questionner l'effet de cette inhibition sur la transmission d'HTLV-1. Ces mises au point présentent donc aussi un intérêt dans ce modèle rétroviral.
Dans le cadre de notre dernier travail, nous avons identifié que la séquestration d'UPF1 au cours de son export par la protéine virale Rex était une étape critique de l'inhibition du NMD Rex dépendante. Ces résultats nous ont amené à comprendre que l'export de l'ARN viral constituait une étape critique dans la formation de la mRNP virale et l'incorporation d'UPF1. Si la fonction d'UPF1 y reste inconnue pour HTLV-1 (mais pourrait ressembler à ce qui est décrit pour HIV), elle a cependant permis de mettre en avant de façon inattendue que l'export noyau cytoplasme serait un point de régulation du NMD. En comprendre le mécanisme est l'objet du ***projet 3***. De façon intéressante, cette étude pourrait permettre d'appréhender un nouveau paramètre encore peu étudié de la biologie d'UPF1 : sa mobilité. A ce nouvel aspect s'ajoute le fait que des défauts d'export par CRM1 sont fortement corrélés au développement du cancer. Analyser comment les dérégulations dépendantes d'UPF1 et observées dans les lignées HTLV-1 (***projet 1***) corrèleraient avec de possibles dérégulations dans les lignées mutées pour CRM1 pourrait aussi apporter de nouvelles données sur la façon dont l'inhibition du NMD peut influencer le développement cancéreux.

REFERENCES

1. Subba Rao, K. Mechanisms of disease: DNA repair defects and neurological disease. *Nat. Clin. Pract. Neurol.* **3**, 162–172 (2007).
2. Hoeijmakers, J. H. Genome maintenance mechanisms for preventing cancer. *Nature* **411**, 366–374 (2001).
3. Gillet, L. C. & Scharer, O. D. Molecular mechanisms of mammalian global genome nucleotide excision repair. *Chem Rev* **106**, 253–76 (2006).
4. Berneburg, M. & Lehmann, A. R. Xeroderma pigmentosum and related disorders: defects in DNA repair and transcription. *Adv. Genet.* **43**, 71–102 (2001).
5. Kraemer, K. H. *et al.* Xeroderma pigmentosum, trichothiodystrophy and Cockayne syndrome: a complex genotype-phenotype relationship. *Neuroscience* **145**, 1388–1396 (2007).
6. van der Weegen, Y. *et al.* The cooperative action of CSB, CSA, and UVSSA target TFIIH to DNA damage-stalled RNA polymerase II. *Nat. Commun.* **11**, 2104 (2020).
7. Sugasawa, K., Akagi, J., Nishi, R., Iwai, S. & Hanaoka, F. Two-step recognition of DNA damage for mammalian nucleotide excision repair: Directional binding of the XPC complex and DNA strand scanning. *Mol. Cell* **36**, 642–653 (2009).
8. Sugasawa, K. *et al.* Xeroderma pigmentosum group C protein complex is the initiator of global genome nucleotide excision repair. *Mol. Cell* **2**, 223–232 (1998).
9. Riedl, T., Hanaoka, F. & Egly, J. M. The comings and goings of nucleotide excision repair factors on damaged DNA. *Embo J* **22**, 5293–303 (2003).
10. Shivji, K. K., Kenny, M. K. & Wood, R. D. Proliferating cell nuclear antigen is required for DNA excision repair. *Cell* **69**, 367–74 (1992).
11. Shivji, M. K., Podust, V. N., Hubscher, U. & Wood, R. D. Nucleotide excision repair DNA synthesis by DNA polymerase epsilon in the presence of PCNA, RFC, and RPA. *Biochemistry* **34**, 5011–7 (1995).
12. Geacintov, N. E. & Broyde, S. Repair-Resistant DNA Lesions. *Chem. Res. Toxicol.* **30**, 1517–1548 (2017).
13. Tapias, A. *et al.* Ordered conformational changes in damaged DNA induced by nucleotide excision repair factors. *J. Biol. Chem.* **279**, 19074–19083 (2004).
14. Schultz, P. *et al.* Molecular structure of human TFIIH. *Cell* **102**, 599–607 (2000).
15. Coin, F. *et al.* p8/TTD-A as a repair-specific TFIIH subunit. *Mol Cell* **21**, 215–26 (2006).
16. Li, C.-L. *et al.* Tripartite DNA Lesion Recognition and Verification by XPC, TFIIH, and XPA in Nucleotide Excision Repair. *Mol. Cell* **59**, 1025–1034 (2015).
17. Oksenych, V., Bernardes de Jesus, B., Zhovmer, A., Egly, J.-M. & Coin, F. Molecular insights into the recruitment of TFIIH to sites of DNA damage. *EMBO J.* **28**, 2971–2980 (2009).
18. Aboussekhra, A. *et al.* Mammalian DNA nucleotide excision repair reconstituted with purified protein components. *Cell* **80**, 859–68 (1995).
19. Paul-Konietzko, K., Thomale, J., Arakawa, H. & Iliakis, G. DNA Ligases I and III Support Nucleotide Excision Repair in DT40 Cells with Similar Efficiency. *Photochem. Photobiol.* **91**, 1173–1180 (2015).
20. Ogi, T. *et al.* Three DNA polymerases, recruited by different mechanisms, carry out NER repair synthesis in human cells. *Mol. Cell* **37**, 714–727 (2010).
21. Wolin, S. L. & Maquat, L. E. Cellular RNA surveillance in health and disease. *Science* **366**, 822–827 (2019).

22. Jiao, X., Chang, J. H., Kilic, T., Tong, L. & Kiledjian, M. A Mammalian Pre-mRNA 5' End Capping Quality Control Mechanism and an Unexpected Link of Capping to Pre-mRNA Processing. *Mol. Cell* **50**, 104–115 (2013).
23. Saulière, J. *et al.* The exon junction complex differentially marks spliced junctions. *Nat. Struct. Mol. Biol.* **17**, 1269–1271 (2010).
24. Woodward, L. A., Mabin, J. W., Gangras, P. & Singh, G. The exon junction complex: a lifelong guardian of mRNA fate. *Wiley Interdiscip. Rev. RNA* **8**, (2017).
25. Simms, C. L., Yan, L. L. & Zaher, H. S. Ribosome Collision Is Critical for Quality Control during No-Go Decay. *Mol. Cell* **68**, 361-373.e5 (2017).
26. Tsuboi, T. *et al.* Dom34:hbs1 plays a general role in quality-control systems by dissociation of a stalled ribosome at the 3' end of aberrant mRNA. *Mol. Cell* **46**, 518–529 (2012).
27. Morris, C., Cluet, D. & Ricci, E. P. Ribosome dynamics and mRNA turnover, a complex relationship under constant cellular scrutiny. *Wiley Interdiscip. Rev. RNA* **12**, e1658 (2021).
28. Salas-Marco, J. & Bedwell, D. M. GTP hydrolysis by eRF3 facilitates stop codon decoding during eukaryotic translation termination. *Mol. Cell. Biol.* **24**, 7769–7778 (2004).
29. Brown, A., Shao, S., Murray, J., Hegde, R. S. & Ramakrishnan, V. Structural basis for stop codon recognition in eukaryotes. *Nature* **524**, 493–496 (2015).
30. Pisarev, A. V. *et al.* The role of ABCE1 in eukaryotic posttermination ribosomal recycling. *Mol. Cell* **37**, 196–210 (2010).
31. Ivanov, A. *et al.* PABP enhances release factor recruitment and stop codon recognition during translation termination. *Nucleic Acids Res.* **44**, 7766–7776 (2016).
32. Ivanov, P. V., Gehring, N. H., Kunz, J. B., Hentze, M. W. & Kulozik, A. E. Interactions between UPF1, eRFs, PABP and the exon junction complex suggest an integrated model for mammalian NMD pathways. *EMBO J.* **27**, 736–747 (2008).
33. Singh, G., Rebbapragada, I. & Lykke-Andersen, J. A competition between stimulators and antagonists of Upf complex recruitment governs human nonsense-mediated mRNA decay. *PLoS Biol* **6**, e111 (2008).
34. Behm-Ansmant, I. & Izaurralde, E. Quality control of gene expression: a stepwise assembly pathway for the surveillance complex that triggers nonsense-mediated mRNA decay. *Genes Dev* **20**, 391–8 (2006).
35. Eberle, A. B., Stalder, L., Mathys, H., Orozco, R. Z. & Muhlemann, O. Posttranscriptional gene regulation by spatial rearrangement of the 3' untranslated region. *PLoS Biol* **6**, e92 (2008).
36. Fiorini, F., Bagchi, D., Le Hir, H. & Croquette, V. Human Upf1 is a highly processive RNA helicase and translocase with RNP remodelling activities. *Nat. Commun.* **6**, 7581 (2015).
37. Hurt, J. A., Robertson, A. D. & Burge, C. B. Global analyses of UPF1 binding and function reveal expanded scope of nonsense-mediated mRNA decay. *Genome Res* **23**, 1636–1650 (2013).
38. Zund, D., Gruber, A. R., Zavolan, M. & Muhlemann, O. Translation-dependent displacement of UPF1 from coding sequences causes its enrichment in 3' UTRs. *Nat Struct Mol Biol* **20**, 936–43 (2013).
39. Yamashita, A. *et al.* SMG-8 and SMG-9, two novel subunits of the SMG-1 complex, regulate remodeling of the mRNA surveillance complex during nonsense-mediated mRNA decay. *Genes Dev* **23**, 1091–105 (2009).
40. Yamashita, A., Kashima, I. & Ohno, S. The role of SMG-1 in nonsense-mediated mRNA decay. *Biochim Biophys Acta* **1754**, 305–15 (2005).
41. Yamashita, A., Ohnishi, T., Kashima, I., Taya, Y. & Ohno, S. Human SMG-1, a novel phosphatidylinositol 3-kinase-related protein kinase, associates with components of the mRNA surveillance complex and is involved in the regulation of nonsense-mediated mRNA decay. *Genes Dev* **15**, 2215–28 (2001).
42. Kashima, I. *et al.* Binding of a novel SMG-1-Upf1-eRF1-eRF3 complex (SURF) to the exon junction complex triggers Upf1 phosphorylation and nonsense-mediated mRNA decay. *Genes Dev* **20**, 355–67 (2006).

43. Melero, R. *et al.* Structures of SMG1-UPFs Complexes: SMG1 Contributes to Regulate UPF2-Dependent Activation of UPF1 in NMD. *Struct. Lond. Engl. 1993* **22**, 1105–1119 (2014).
44. Hug, N. & Cáceres, J. F. The RNA helicase DHX34 activates NMD by promoting a transition from the surveillance to the decay-inducing complex. *Cell Rep.* **8**, 1845–1856 (2014).
45. Chakrabarti, S. *et al.* Molecular mechanisms for the RNA-dependent ATPase activity of Upf1 and its regulation by Upf2. *Mol Cell* **41**, 693–703 (2011).
46. Durand, S., Franks, T. M. & Lykke-Andersen, J. Hyperphosphorylation amplifies UPF1 activity to resolve stalls in nonsense-mediated mRNA decay. *Nat. Commun.* **7**, 12434 (2016).
47. Schmidt, S. A. *et al.* Identification of SMG6 cleavage sites and a preferred RNA cleavage motif by global analysis of endogenous NMD targets in human cells. *Nucleic Acids Res.* **43**, 309–323 (2015).
48. Unterholzner, L. & Izaurralde, E. SMG7 acts as a molecular link between mRNA surveillance and mRNA decay. *Mol Cell* **16**, 587–96 (2004).
49. Loh, B., Jonas, S. & Izaurralde, E. The SMG5-SMG7 heterodimer directly recruits the CCR4-NOT deadenylase complex to mRNAs containing nonsense codons via interaction with POP2. *Genes Dev.* **27**, 2125–2138 (2013).
50. Ohnishi, T. *et al.* Phosphorylation of hUPF1 induces formation of mRNA surveillance complexes containing hSMG-5 and hSMG-7. *Mol Cell* **12**, 1187–200 (2003).
51. Fiorini, F., Boudvillain, M. & Le Hir, H. Tight intramolecular regulation of the human Upf1 helicase by its N- and C-terminal domains. *Nucleic Acids Res* **41**, 2404–15 (2013).
52. Fiorini, F., Bonneau, F. & Le Hir, H. Biochemical characterization of the RNA helicase UPF1 involved in nonsense-mediated mRNA decay. *Methods Enzym.* **511**, 255–74 (2012).
53. Franks, T. M., Singh, G. & Lykke-Andersen, J. Upf1 ATPase-dependent mRNP disassembly is required for completion of nonsense- mediated mRNA decay. *Cell* **143**, 938–50 (2010).
54. Lee, S. R., Pratt, G. A., Martinez, F. J., Yeo, G. W. & Lykke-Andersen, J. Target Discrimination in Nonsense-Mediated mRNA Decay Requires Upf1 ATPase Activity. *Mol. Cell* **59**, 413–425 (2015).
55. Durand, S. *et al.* Inhibition of nonsense-mediated mRNA decay (NMD) by a new chemical molecule reveals the dynamic of NMD factors in P-bodies. *J Cell Biol* **178**, 1145–60 (2007).
56. Stalder, L. & Muhlemann, O. Processing bodies are not required for mammalian nonsense-mediated mRNA decay. *Rna* **15**, 1265–73 (2009).
57. Ge, Z., Quek, B. L., Beemon, K. L. & Hogg, J. R. Polypyrimidine tract binding protein 1 protects mRNAs from recognition by the nonsense-mediated mRNA decay pathway. *eLife* **5**, (2016).
58. Kishor, A., Ge, Z. & Hogg, J. R. hnRNP L-dependent protection of normal mRNAs from NMD subverts quality control in B cell lymphoma. *EMBO J.* **38**, e99128 (2019).
59. Karousis, E. D. & Mühlemann, O. Nonsense-Mediated mRNA Decay Begins Where Translation Ends. *Cold Spring Harb. Perspect. Biol.* **11**, (2019).
60. Kishor, A., Fritz, S. E. & Hogg, J. R. Nonsense-mediated mRNA decay: The challenge of telling right from wrong in a complex transcriptome. *Wiley Interdiscip. Rev. RNA* **10**, e1548 (2019).
61. Mabin, J. W. *et al.* The Exon Junction Complex Undergoes a Compositional Switch that Alters mRNP Structure and Nonsense-Mediated mRNA Decay Activity. *Cell Rep.* **25**, 2431-2446.e7 (2018).
62. Yi, Z., Sanjeev, M. & Singh, G. The Branched Nature of the Nonsense-Mediated mRNA Decay Pathway. *Trends Genet. TIG* **37**, 143–159 (2021).
63. Palma, M. *et al.* A role for AKT1 in nonsense-mediated mRNA decay. *Nucleic Acids Res.* **49**, 11022–11037 (2021).
64. Cho, H. *et al.* AKT constitutes a signal-promoted alternative exon-junction complex that regulates nonsense-mediated mRNA decay. *Mol. Cell* **82**, 2779-2796.e10 (2022).
65. Metze, S., Herzog, V. A., Ruepp, M.-D. & Mühlemann, O. Comparison of EJC-enhanced and EJC-independent NMD in human cells reveals two partially redundant degradation pathways. *RNA N. Y. N* **19**, 1432–1448 (2013).
66. Nickless, A. *et al.* Intracellular calcium regulates nonsense-mediated mRNA decay. *Nat. Med.* **20**, 961–966 (2014).

67. Gonzalez-Hilarion, S. *et al.* Rescue of nonsense mutations by amlexanox in human cells. *Orphanet J. Rare Dis.* **7**, 58 (2012).
68. Gopalsamy, A. *et al.* Identification of pyrimidine derivatives as hSMG-1 inhibitors. *Bioorg. Med. Chem. Lett.* **22**, 6636–6641 (2012).
69. Popp, M. W. & Maquat, L. E. Attenuation of nonsense-mediated mRNA decay facilitates the response to chemotherapeutics. *Nat. Commun.* **6**, 6632 (2015).
70. Jia, J. *et al.* Premature termination codon readthrough in human cells occurs in novel cytoplasmic foci and requires UPF proteins. *J. Cell Sci.* **130**, 3009–3022 (2017).
71. Hall, G. W. & Thein, S. Nonsense codon mutations in the terminal exon of the beta-globin gene are not associated with a reduction in beta-mRNA accumulation: a mechanism for the phenotype of dominant beta-thalassemia. *Blood* **83**, 2031–2037 (1994).
72. Thein, S. L. *et al.* Molecular basis for dominantly inherited inclusion body beta-thalassemia. *Proc. Natl. Acad. Sci. U. S. A.* **87**, 3924–3928 (1990).
73. Frischmeyer, P. A. & Dietz, H. C. Nonsense-mediated mRNA decay in health and disease. *Hum. Mol. Genet.* **8**, 1893–1900 (1999).
74. Lindeboom, R. G. H., Supek, F. & Lehner, B. The rules and impact of nonsense-mediated mRNA decay in human cancers. *Nat. Genet.* **48**, 1112–1118 (2016).
75. Hu, Z., Yau, C. & Ahmed, A. A. A pan-cancer genome-wide analysis reveals tumour dependencies by induction of nonsense-mediated decay. *Nat. Commun.* **8**, 15943 (2017).
76. Kim, Y. K. & Maquat, L. E. UPFront and center in RNA decay: UPF1 in nonsense-mediated mRNA decay and beyond. *RNA N. Y. N* **25**, 407–422 (2019).
77. Kurosaki, T., Popp, M. W. & Maquat, L. E. Quality and quantity control of gene expression by nonsense-mediated mRNA decay. *Nat. Rev. Mol. Cell Biol.* **20**, 406–420 (2019).
78. Vattem, K. M. & Wek, R. C. Reinitiation involving upstream ORFs regulates ATF4 mRNA translation in mammalian cells. *Proc Natl Acad Sci U A* **101**, 11269–74 (2004).
79. Boehm, V., Haberman, N., Ottens, F., Ule, J. & Gehring, N. H. 3' UTR length and messenger ribonucleoprotein composition determine endocleavage efficiencies at termination codons. *Cell Rep.* **9**, 555–568 (2014).
80. García-Moreno, J. F. & Romão, L. Perspective in Alternative Splicing Coupled to Nonsense-Mediated mRNA Decay. *Int. J. Mol. Sci.* **21**, 9424 (2020).
81. Ge, Y. & Porse, B. T. The functional consequences of intron retention: alternative splicing coupled to NMD as a regulator of gene expression. *BioEssays News Rev. Mol. Cell. Dev. Biol.* **36**, 236–243 (2014).
82. Saltzman, A. L. *et al.* Regulation of multiple core spliceosomal proteins by alternative splicing-coupled nonsense-mediated mRNA decay. *Mol Cell Biol* **28**, 4320–30 (2008).
83. Belew, A. T., Advani, V. M. & Dinman, J. D. Endogenous ribosomal frameshift signals operate as mRNA destabilizing elements through at least two molecular pathways in yeast. *Nucleic Acids Res* **39**, 2799–808 (2010).
84. Moriarty, P. M., Reddy, C. C. & Maquat, L. E. Selenium deficiency reduces the abundance of mRNA for Se-dependent glutathione peroxidase 1 by a UGA-dependent mechanism likely to be nonsense codon-mediated decay of cytoplasmic mRNA. *Mol Cell Biol* **18**, 2932–9 (1998).
85. Wolf, S., Vercruyssen, M. & Cook, L. HTLV-1-related adult T-cell leukemia/lymphoma: insights in early detection and management. *Curr. Opin. Oncol.* **34**, 446–453 (2022).
86. Poiesz, B. J. *et al.* Detection and isolation of type C retrovirus particles from fresh and cultured lymphocytes of a patient with cutaneous T-cell lymphoma. *Proc. Natl. Acad. Sci. U. S. A.* **77**, 7415–7419 (1980).
87. Gessain, A. *et al.* Antibodies to human T-lymphotropic virus type-I in patients with tropical spastic paraparesis. *Lancet* **2**, 407–10 (1985).
88. Uji, M., Matsushita, H., Watanabe, T. & Suzumura, T. [A human T-cell lymphotropic virus type 1 carrier presenting with Sjögren's syndrome and bronchopneumopathy]. *Nihon Kokyuki Gakkai Zasshi* **44**, 1011–1015 (2006).

89. Kamoi, K. *et al.* Horizontal transmission of HTLV-1 causing uveitis. *Lancet Infect. Dis.* **21**, 578 (2021).
90. Watanabe, T. HTLV-1-associated diseases. *Int. J. Hematol.* **66**, 257–278 (1997).
91. Martin, J. L., Maldonado, J. O., Mueller, J. D., Zhang, W. & Mansky, L. M. Molecular Studies of HTLV-1 Replication: An Update. *Viruses* **8**, E31 (2016).
92. Thulson, E. *et al.* An RNA pseudoknot stimulates HTLV-1 pro-pol programmed -1 ribosomal frameshifting. *RNA N. Y. N* **26**, 512–528 (2020).
93. Jones, K. S. *et al.* Molecular aspects of HTLV-1 entry: functional domains of the HTLV-1 surface subunit (SU) and their relationships to the entry receptors. *Viruses* **3**, 794–810 (2011).
94. Boxus, M. *et al.* The HTLV-1 Tax interactome. *Retrovirology* **5**, 76 (2008).
95. Giam, C.-Z. & Semmes, O. J. HTLV-1 Infection and Adult T-Cell Leukemia/Lymphoma-A Tale of Two Proteins: Tax and HBZ. *Viruses* **8**, (2016).
96. Ma, G. *et al.* Human retroviral antisense mRNAs are retained in the nuclei of infected cells for viral persistence. *Proc. Natl. Acad. Sci. U. S. A.* **118**, e2014783118 (2021).
97. Koyanagi, Y. *et al.* In vivo infection of human T-cell leukemia virus type I in non-T cells. *Virology* **196**, 25–33 (1993).
98. Bangham, C. R. M. CTL quality and the control of human retroviral infections. *Eur. J. Immunol.* **39**, 1700–1712 (2009).
99. Rocamonde, B., Carcone, A., Mahieux, R. & Dutartre, H. HTLV-1 infection of myeloid cells: from transmission to immune alterations. *Retrovirology* **16**, 45 (2019).
100. Pique, C. & Jones, K. S. Pathways of cell-cell transmission of HTLV-1. *Front. Microbiol.* **3**, 378 (2012).
101. Pais-Correia, A.-M. *et al.* Biofilm-like extracellular viral assemblies mediate HTLV-1 cell-to-cell transmission at virological synapses. *Nat. Med.* **16**, 83–89 (2010).
102. Igakura, T. *et al.* Spread of HTLV-I between lymphocytes by virus-induced polarization of the cytoskeleton. *Science* **299**, 1713–1716 (2003).
103. Van Prooyen, N. *et al.* Human T-cell leukemia virus type 1 p8 protein increases cellular conduits and virus transmission. *Proc. Natl. Acad. Sci. U. S. A.* **107**, 20738–20743 (2010).
104. Billman, M. R., Rueda, D. & Bangham, C. R. M. Single-cell heterogeneity and cell-cycle-related viral gene bursts in the human leukaemia virus HTLV-1. *Wellcome Open Res.* **2**, 87 (2017).
105. Kiik, H. *et al.* Time-course of host cell transcription during the HTLV-1 transcriptional burst. *PLoS Pathog.* **18**, e1010387 (2022).
106. Tanaka, A. & Matsuoka, M. HTLV-1 Alters T Cells for Viral Persistence and Transmission. *Front. Microbiol.* **9**, 461 (2018).
107. Bangham, C. R. M. Human T Cell Leukemia Virus Type 1: Persistence and Pathogenesis. *Annu. Rev. Immunol.* **36**, 43–71 (2018).
108. Thénoz, M. *et al.* HTLV-1-infected CD4+ T-cells display alternative exon usages that culminate in adult T-cell leukemia. *Retrovirology* **11**, 119 (2014).
109. Ameur, L. B. *et al.* Intragenic recruitment of NF-κB drives splicing modifications upon activation by the oncogene Tax of HTLV-1. *Nat. Commun.* **11**, 3045 (2020).
110. Vandermeulen, C. *et al.* The HTLV-1 viral oncoproteins Tax and HBZ reprogram the cellular mRNA splicing landscape. *PLoS Pathog.* **17**, e1009919 (2021).
111. Shallak, M. *et al.* The endogenous HBZ interactome in ATL leukemic cells reveals an unprecedented complexity of host interacting partners involved in RNA splicing. *Front. Immunol.* **13**, 939863 (2022).
112. Nakano, K. *et al.* Exploring New Functional Aspects of HTLV-1 RNA-Binding Protein Rex: How Does Rex Control Viral Replication? *Viruses* **14**, 407 (2022).
113. Vernin, C. *et al.* HTLV-1 bZIP factor HBZ promotes cell proliferation and genetic instability by activating OncomiRs. *Cancer Res.* **74**, 6082–6093 (2014).
114. Moles, R. & Nicot, C. The Emerging Role of miRNAs in HTLV-1 Infection and ATLL Pathogenesis. *Viruses* **7**, 4047–4074 (2015).

115. Abe, M., Suzuki, H., Nishitsuji, H., Shida, H. & Takaku, H. Interaction of human T-cell lymphotropic virus type I Rex protein with Dicer suppresses RNAi silencing. *FEBS Lett.* **584**, 4313–4318 (2010).
116. Van Duyne, R. *et al.* Localization and sub-cellular shuttling of HTLV-1 tax with the miRNA machinery. *PloS One* **7**, e40662 (2012).
117. Donzeau, M., Winnacker, E. L. & Meisterernst, M. Specific repression of Tax trans-activation by TAR RNA-binding protein TRBP. *J. Virol.* **71**, 2628–2635 (1997).
118. Kedersha, N. *et al.* Stress granules and processing bodies are dynamically linked sites of mRNP remodeling. *J Cell Biol* **169**, 871–84 (2005).
119. Kershaw, C. J. *et al.* Integrated multi-omics reveals common properties underlying stress granule and P-body formation. *RNA Biol.* **18**, 655–673 (2021).
120. Legros, S. *et al.* The HTLV-1 Tax protein inhibits formation of stress granules by interacting with histone deacetylase 6. *Oncogene* **30**, 4050–62 (2011).
121. Desbois, C., Rousset, R., Bantignies, F. & Jalinot, P. Exclusion of Int-6 from PML nuclear bodies by binding to the HTLV-I Tax oncoprotein. *Science* **273**, 951–3 (1996).
122. Twizere, J. C. *et al.* Interaction of retroviral Tax oncoproteins with tristetraprolin and regulation of tumor necrosis factor-alpha expression. *J Natl Cancer Inst* **95**, 1846–59 (2003).
123. Ahmed, Y. F., Gilmartin, G. M., Hanly, S. M., Nevins, J. R. & Greene, W. C. The HTLV-I Rex response element mediates a novel form of mRNA polyadenylation. *Cell* **64**, 727–737 (1991).
124. Ahmed, Y. F., Hanly, S. M., Malim, M. H., Cullen, B. R. & Greene, W. C. Structure-function analyses of the HTLV-I Rex and HIV-1 Rev RNA response elements: insights into the mechanism of Rex and Rev action. *Genes Dev.* **4**, 1014–1022 (1990).
125. Hanly, S. M. *et al.* Comparative analysis of the HTLV-I Rex and HIV-1 Rev trans-regulatory proteins and their RNA response elements. *Genes Dev.* **3**, 1534–1544 (1989).
126. Kress, E., Baydoun, H. H., Bex, F., Gazzolo, L. & Duc Dodon, M. Critical role of hnRNP A1 in HTLV-1 replication in human transformed T lymphocytes. *Retrovirology* **2**, 8 (2005).
127. Hakata, Y., Umemoto, T., Matsushita, S. & Shida, H. Involvement of human CRM1 (exportin 1) in the export and multimerization of the Rex protein of human T-cell leukemia virus type 1. *J. Virol.* **72**, 6602–6607 (1998).
128. Hakata, Y., Yamada, M. & Shida, H. A multifunctional domain in human CRM1 (exportin 1) mediates RanBP3 binding and multimerization of human T-cell leukemia virus type 1 Rex protein. *Mol. Cell. Biol.* **23**, 8751–8761 (2003).
129. Nakano, K. & Watanabe, T. HTLV-1 Rex Tunes the Cellular Environment Favorable for Viral Replication. *Viruses* **8**, 58 (2016).
130. Nakano, K. *et al.* Viral interference with host mRNA surveillance, the nonsense-mediated mRNA decay (NMD) pathway, through a new function of HTLV-1 Rex: implications for retroviral replication. *Microbes Infect.* **15**, 491–505 (2013).
131. Nakano, K. *et al.* Elucidation of the Mechanism of Host NMD Suppression by HTLV-1 Rex: Dissection of Rex to Identify the NMD Inhibitory Domain. *Viruses* **14**, 344 (2022).
132. Mohanty, S. & Harhaj, E. W. Mechanisms of Oncogenesis by HTLV-1 Tax. *Pathog. Basel Switz.* **9**, E543 (2020).
133. Gloggnitzer, J. *et al.* Nonsense-Mediated mRNA Decay Modulates Immune Receptor Levels to Regulate Plant Antibacterial Defense. *Cell Host Microbe* **16**, 376–390 (2014).
134. Johnson, J. L. *et al.* Inhibition of Upf2-Dependent Nonsense-Mediated Decay Leads to Behavioral and Neurophysiological Abnormalities by Activating the Immune Response. *Neuron* **104**, 665-679.e8 (2019).
135. Apcher, S. *et al.* Major source of antigenic peptides for the MHC class I pathway is produced during the pioneer round of mRNA translation. *Proc Natl Acad Sci U A* **108**, 11572–7 (2011).
136. Frischmeyer-Guerrerio, P. A. *et al.* Perturbation of thymocyte development in nonsense-mediated decay (NMD)-deficient mice. *Proc Natl Acad Sci U A* **108**, 10638–43 (2011).

137. Mendell, J. T., Sharifi, N. A., Meyers, J. L., Martinez-Murillo, F. & Dietz, H. C. Nonsense surveillance regulates expression of diverse classes of mammalian transcripts and mutes genomic noise. *Nat Genet* **36**, 1073–8 (2004).
138. Wang, D. *et al.* Inhibition of nonsense-mediated RNA decay by the tumor microenvironment promotes tumorigenesis. *Mol Cell Biol* **31**, 3670–80 (2011).
139. Gardner, L. B. Nonsense-mediated RNA decay regulation by cellular stress: implications for tumorigenesis. *Mol Cancer Res* **8**, 295–308 (2010).
140. Morris, C., Wittmann, J., Jack, H. M. & Jalinot, P. Human INT6/eIF3e is required for nonsense-mediated mRNA decay. *EMBO Rep* **8**, 596–602 (2007).
141. Lou, C. H. *et al.* Posttranscriptional control of the stem cell and neurogenic programs by the nonsense-mediated RNA decay pathway. *Cell Rep.* **6**, 748–764 (2014).
142. Zhao, Y. *et al.* The RNA quality control pathway nonsense-mediated mRNA decay targets cellular and viral RNAs to restrict KSHV. *Nat. Commun.* **11**, 3345 (2020).
143. Lejeune, F. Nonsense-Mediated mRNA Decay, a Finely Regulated Mechanism. *Biomedicines* **10**, 141 (2022).
144. Villaudy, J. *et al.* HTLV-1 propels thymic human T cell development in 'human immune system' Rag2(-)/(-) gamma c(-)/(-) mice. *PLoS Pathog* **7**, e1002231 (2010).
145. Espíndola, O. de M. *et al.* Early Effects of HTLV-1 Infection on the Activation, Exhaustion, and Differentiation of T-Cells in Humanized NSG Mice. *Cells* **10**, 2514 (2021).
146. Pérès, E. *et al.* PDZ domain-binding motif of Tax sustains T-cell proliferation in HTLV-1-infected humanized mice. *PLoS Pathog.* **14**, e1006933 (2018).
147. Popp, M. W.-L., Cho, H. & Maquat, L. E. Viral subversion of nonsense-mediated mRNA decay. *RNA N. Y. N* **26**, 1509–1518 (2020).
148. Mocquet, V. *et al.* The human T-lymphotropic virus type 1 tax protein inhibits nonsense-mediated mRNA decay by interacting with INT6/EIF3E and UPF1. *J Virol* **86**, 7530–43 (2012).
149. Prochasson, L., Jalinot, P. & Mocquet, V. The Complex Relationship between HTLV-1 and Nonsense-Mediated mRNA Decay (NMD). *Pathog. Basel Switz.* **9**, (2020).
150. Tran, G. V. Q. *et al.* Nonsense-mediated mRNA decay does not restrict influenza A virus propagation. *Cell. Microbiol.* (2021) doi:10.1111/cmi.13323.
151. Contu, L., Balistreri, G., Domanski, M., Uldry, A.-C. & Mühlemann, O. Characterisation of the Semliki Forest Virus-host cell interactome reveals the viral capsid protein as an inhibitor of nonsense-mediated mRNA decay. *PLoS Pathog.* **17**, e1009603 (2021).
152. Balistreri, G. *et al.* The host nonsense-mediated mRNA decay pathway restricts Mammalian RNA virus replication. *Cell Host Microbe* **16**, 403–411 (2014).
153. Fontaine, K. A. *et al.* The Cellular NMD Pathway Restricts Zika Virus Infection and Is Targeted by the Viral Capsid Protein. *mBio* **9**, (2018).
154. Garcia, D., Garcia, S. & Voinnet, O. Nonsense-mediated decay serves as a general viral restriction mechanism in plants. *Cell Host Microbe* **16**, 391–402 (2014).
155. Li, M. *et al.* Identification of antiviral roles for the exon-junction complex and nonsense-mediated decay in flaviviral infection. *Nat. Microbiol.* **4**, 985–995 (2019).
156. Lukhovitskaya, N. & Ryabova, L. A. Cauliflower mosaic virus transactivator protein (TAV) can suppress nonsense-mediated decay by targeting VARICOSE, a scaffold protein of the decapping complex. *Sci. Rep.* **9**, 7042 (2019).
157. May, J. P., Johnson, P. Z., Ilyas, M., Gao, F. & Simon, A. E. The Multifunctional Long-Distance Movement Protein of Pea Enation Mosaic Virus 2 Protects Viral and Host Transcripts from Nonsense-Mediated Decay. *mBio* **11**, (2020).
158. Ramage, H. R. *et al.* A combined proteomics/genomics approach links hepatitis C virus infection with nonsense-mediated mRNA decay. *Mol. Cell* **57**, 329–340 (2015).
159. Wada, M., Lokugamage, K. G., Nakagawa, K., Narayanan, K. & Makino, S. Interplay between coronavirus, a cytoplasmic RNA virus, and nonsense-mediated mRNA decay pathway. *Proc. Natl. Acad. Sci. U. S. A.* **115**, E10157–E10166 (2018).

160. Ajamian, L. *et al.* HIV-1 Recruits UPF1 but Excludes UPF2 to Promote Nucleocytoplasmic Export of the Genomic RNA. *Biomolecules* **5**, 2808–2839 (2015).
161. Tang, X. *et al.* Structural basis of suppression of host translation termination by Moloney Murine Leukemia Virus. *Nat. Commun.* **7**, 12070 (2016).
162. Weil, J. E. & Beemon, K. L. A 3' UTR sequence stabilizes termination codons in the unspliced RNA of Rous sarcoma virus. *RNA N. Y. N* **12**, 102–110 (2006).
163. Kim, D. *et al.* The Architecture of SARS-CoV-2 Transcriptome. *Cell* **181**, 914-921.e10 (2020).
164. May, J. P., Yuan, X., Sawicki, E. & Simon, A. E. RNA virus evasion of nonsense-mediated decay. *PLoS Pathog.* **14**, e1007459 (2018).
165. Toma, K. G., Rebbapragada, I., Durand, S. & Lykke-Andersen, J. Identification of elements in human long 3' UTRs that inhibit nonsense-mediated decay. *RNA* (2015) doi:10.1261/rna.048637.114.
166. Schmidt, N. *et al.* The SARS-CoV-2 RNA-protein interactome in infected human cells. *Nat. Microbiol.* **6**, 339–353 (2021).
167. Meneses Calderón, J. *et al.* Nitazoxanide against COVID-19 in three explorative scenarios. *J. Infect. Dev. Ctries.* **14**, 982–986 (2020).
168. Gordon, D. E. *et al.* A SARS-CoV-2 protein interaction map reveals targets for drug repurposing. *Nature* (2020) doi:10.1038/s41586-020-2286-9.
169. Emmott, E. *et al.* The cellular interactome of the coronavirus infectious bronchitis virus nucleocapsid protein and functional implications for virus biology. *J. Virol.* **87**, 9486–9500 (2013).
170. Xie, X. *et al.* An Infectious cDNA Clone of SARS-CoV-2. *Cell Host Microbe* **27**, 841-848.e3 (2020).
171. Paraskeva, E. *et al.* CRM1-mediated recycling of snurportin 1 to the cytoplasm. *J. Cell Biol.* **145**, 255–264 (1999).
172. Monecke, T., Dickmanns, A. & Ficner, R. Allosteric control of the exportin CRM1 unraveled by crystal structure analysis. *FEBS J.* **281**, 4179–4194 (2014).
173. Kırlı, K. *et al.* A deep proteomics perspective on CRM1-mediated nuclear export and nucleocytoplasmic partitioning. *eLife* **4**, e11466 (2015).
174. Cullen, B. R. Nuclear mRNA export: insights from virology. *Trends Biochem. Sci.* **28**, 419–424 (2003).
175. Weichselbraun, I., Farrington, G. K., Rusche, J. R., Böhnlein, E. & Hauber, J. Definition of the human immunodeficiency virus type 1 Rev and human T-cell leukemia virus type I Rex protein activation domain by functional exchange. *J. Virol.* **66**, 2583–2587 (1992).
176. Culjkovic, B., Topisirovic, I., Skrabanek, L., Ruiz-Gutierrez, M. & Borden, K. L. B. eIF4E is a central node of an RNA regulon that governs cellular proliferation. *J. Cell Biol.* **175**, 415–426 (2006).
177. Brennan, C. M., Gallouzi, I. E. & Steitz, J. A. Protein ligands to HuR modulate its interaction with target mRNAs in vivo. *J. Cell Biol.* **151**, 1–14 (2000).
178. Prechtel, A. T. *et al.* Expression of CD83 is regulated by HuR via a novel cis-active coding region RNA element. *J. Biol. Chem.* **281**, 10912–10925 (2006).
179. Taylor, J. *et al.* Altered Nuclear Export Signal Recognition as a Driver of Oncogenesis. *Cancer Discov.* **9**, 1452–1467 (2019).
180. Lin, D.-C. *et al.* Genomic and molecular characterization of esophageal squamous cell carcinoma. *Nat. Genet.* **46**, 467–473 (2014).
181. Camus, V. *et al.* Detection and prognostic value of recurrent exportin 1 mutations in tumor and cell-free circulating DNA of patients with classical Hodgkin lymphoma. *Haematologica* **101**, 1094–1101 (2016).
182. Baumhardt, J. M. *et al.* Recognition of nuclear export signals by CRM1 carrying the oncogenic E571K mutation. *Mol. Biol. Cell* **31**, 1879–1891 (2020).
183. Hu, J., Li, P., Shi, B. & Tie, J. Importin β1 mediates nuclear import of the factors associated with nonsense-mediated RNA decay. *Biochem. Biophys. Res. Commun.* **542**, 34–39 (2021).